UNIVERSITY OF BIRMINGHAM

Advancing Flavour/Fragrance Oils Microencapsulation: Exploring the Impact of Core Oil on Microcapsule Characteristics

By

Qun Huang

A thesis submitted to
the University of Birmingham
for the degree of
DOCTOR OF PHILOSOPHY

School of Chemical Engineering
University of Birmingham
December 2023

UNIVERSITY OF
BIRMINGHAM

University of Birmingham Research Archive

e-theses repository

This unpublished thesis/dissertation is copyright of the author and/or third parties. The intellectual property rights of the author or third parties in respect of this work are as defined by The Copyright Designs and Patents Act 1988 or as modified by any successor legislation.

Any use made of information contained in this thesis/dissertation must be in accordance with that legislation and must be properly acknowledged. Further distribution or reproduction in any format is prohibited without the permission of the copyright holder.

Abstract

The aim of the project is to develop simple, industrially scalable encapsulation methods to fabricate biodegradable microcapsules with desirable properties, using either natural waxes by melt dispersion or gelatine/gum arabic by complex coacervation.

L-carvone (LC) and hexyl salicylate (HS) were used as model core oils. Core oils are encapsulated based on the formation of wax microspheres, while addressing the influence of different types of waxes as well as different oil to wax ratios. HS encapsulation efficiency (EE) ranging from 75.7 ± 2.7 to 83.7 ± 1.2 % has been achieved for different types of waxes, which were comparable to those of commercially available melamine formaldehyde (MF) based microcapsules (EE, 75%), and higher than the recently developed microcapsules (EE, 47 ± 11%) using plant-based biopolymers (Chitosan and gum arabic). The Young's modulus of each wax microspheres determined by the Hertz model had a wide range of values from 28.3 ± 1.4 to 390.7 ± 16.0 MPa, suggesting the availability of wax microspheres for various industrial applications. Moreover, the desirable properties of wax microspheres could be controlled by selecting a certain oil to wax ratio.

Also, gelatine/gum arabic coacervate based microcapsules have been fabricated to encapsulate L-carvone, limonene and hexyl salicylate via complex coacervation. The highest EE (89.0 ± 1.2%) was achieved for HS loaded microcapsules. Their mean apparent Young's modulus of microcapsules was determined by the Hertz model (668 ± 165 MPa) and the intrinsic Young's modulus of microcapsules shell was determined by finite elements analysis (6.2 ± 1.0 GPa). Both the EE and mechanical properties were significantly higher than those of chitosan/gum arabic or commercially formaldehyde-based microcapsules, suggesting the feasibility of gelatine/gum arabic

to be utilised in applications for household care, laundry and textile industries. However, LC was not encapsulated well by gelatine/gum arabic microcapsules (EE, 5.0 ± 0.4 %) compared to HS (EE, 89.0 ± 1.2%), evidencing the significant influence of core oil on microcapsule characteristics.

Finally, the physical properties of core oil (linalool, L-carvone, limonene, hexyl salicylate, carvacrol and cinnamaldehyde) were examined in order to evaluate their effects on the capsule morphology and encapsulation efficiency by combining the spreading coefficient and two component surface energy theories. It was found that the spreading coefficient configurations (based solely on thermodynamic considerations) for each oil did not give an accurate prediction of capsule morphology when high molecular weight biopolymers (gelatine/gum arabic) were involved in the system. However, the predicted structural morphology for different oil microcapsules were still holistically consistent with their encapsulation efficiency, which also was found to increase with the decreasing surface polarity of the core oil.

Overall, although wax microspheres and gelatine/gum arabic coacervated microcapsules did not give satisfactory EEs for the encapsulation of LC, the performances (high EE and strong mechanical strength) of these microspheres and microcapsules containing HS looked promising. The impact of both thermodynamic spreading coefficients and surface polarity of each core oil on the formed microcapsule structural morphology and encapsulation efficiency is crucial, providing a useful insight about the engulfing mechanism for oil encapsulation both for academic research and industrial applications.

Acknowledgments

I would like to express my sincere gratitude and respect towards my principal supervisor, Prof. Zhibing Zhang, who provided me the opportunity to conduct this PhD project and gave me invaluable guidance through these years. His continuous encouragement and support, precious help and advice helped me tremendously both for my academic research and daily life. His character has set a role model for me and made me realize the true essence of actively engaging in the field of education.

I am grateful to all the members of Micromanipulation and Encapsulation Research Group, Dr Zhihua Zhang, Dr Cong Sui, Dr Yan Zhang, Dr Fanqianhui Yu, Dr Yingying Li, Dr Xiaotong Zhang, Dr Daniele Baiocco, Dr Abdullah Mustapha, Dr Gilmore Wellio, Dr Iryna Mikheenko, Dr Ana Evora, Dr Juliette Delarue, Mr Juan Alvarez Fernandez and Mr Siddhant Bhutkar for their helpful discussions and suggestions on my experimental work.

My appreciation also goes to Dr Mark Taylor, Dr Chyntol Kanhimbe, Dr Jie Chen, Dr Zhu Jiang and Ms Elaine Mitchell for their technical assistance and trainings. Thanks are extended to the administration staff in the School of Chemical Engineering: Ms Jacqueline Deans, Ms Lynn Draper and Ms Kate Sterne for their patient support.

I also would like to thank Dr Zhihua Zhang, Dr Cong Sui, Dr Rafael Kamalov and Mr Chris Finch for their friendships during my life in Birmingham. And Keyi, for her company and those sweet memories.

In the end, my deepest gratitude goes to my parents for their infinite love and care through my life. Their understanding and encouragements always motivated me to constantly challenge myself and chase my dreams.

Contents

List of Figures

List of Tables

Nomenclature

$A_{i,j}$	Interfacial area of the core with aqueous phase at state i and j
d_i	Diameter of the calculated droplets/particles
D	Diameter of the tested microcapsules
$D_{[3,2]}$	Sauter mean diameter
$D_{10\%}$, $D_{50\%}$ and $D_{90\%}$	Diameter under 10 %, 50% and 90% of the cumulative volume of the particles
E	Young's modulus of particles
EE	encapsulation efficiency
E_{in}	Intrinsic Young's modulus of microcapsule shell
E_x	Young's modulus for a certain sample
E_{wx}	Young's modulus of a certain type of pure wax microparticles
F	Compression Force
F_r	Force at rupture
g	Gravitational Constant
ΔG	Change in Gibbs Free Energy
h	Shell Thickness of Microcapsules
k	Influencing Coefficient of Payload on Young's Modulus
P	Payload
P_0	Payload of Wax Microspheres at 0 d
r_t	Retention Amount of Oil in Percentage at Time t
R	Radius of Microcapsules
R_0	Radius of the Drop Curvature
R^2	Coefficient of Determination
R_t	Released Oil in Time t
S_P, S_O and S_W	Spreading Coefficient of Polymer, Oil and Water phase
T_c	Toughness
T_r	Nominal Rupture Tension

Greek symbols

β	Shape Factor
Υ	Surface Tension
$\Upsilon^{D}$and Υ^{P}	Non-polar and Polar Component Surface Energy
Υ_i and Υ_j	Interfacial Tension between Core and Water at State i and j
$\Upsilon_{WO}, \Upsilon_{OP}$ and Υ_{WP}	Interfacial Tension between Water/Oil, Oil/Polymer and Water/Polymer
δ	Axial displacement
δ_r	Displacement at Rupture
ε	Fractional Deformation
ε_r	Fractional Deformation at Rupture
θ	Contact Angle of Liquid Droplet on Solid Surface
λ	Absorbance Wavelength
$\Delta\rho$	Density Difference between Drop and Surrounding Medium
σ_r	Nominal Rupture Stress at Rupture
υ	Poisson's ratio

Abbreviations

AFM	Atomic Force Microscopy
ATR	Attenuated Total Reflection
BW	Beeswax
CanW	Candelilla Wax
CarW	Carnauba Wax
CD	Cinnamaldehyde
CLSM	Confocal Laser Scanning Microscopy
CV	Carvacrol
FCC	Food Chemicals Codex
FG	Food Grade

FTIR	Fourier Transform Infrared Spectroscopy
GA	Gum Arabic
GC	Gas Chromatography
GE	Gelatine
GRAS	Generally Recognized As Safe materials
HPLC	High Performance Liquid Chromatography
HS	Hexyl Salicylate
LC	L-carvone
LL	Linalool
LM	Limonene
MD	Maltodextrin
pH	Potential of Hydrogen
SEM	Scanning Electron Microscopy
TEM	Transmission Electron Microscopy
TGA	Thermogravimetric Analysis
UV-Vis	Ultraviolet-Visible Spectroscopy

CHAPTER 1. Introduction

1.1. Background

There are different types of flavour/fragrance ingredients in industrial products, including naturally occurring compounds (e.g., essential oils) and synthetic aromatic oils. Essential oils are usually extracted from plants while synthetic aromas are synthesised via chemical reactions and are not present in nature. Naturally derived flavours and aromas are reported to exhibit many bioactive properties, including anti-inflammatory, anti-bacterial, antioxidant and immunomodulatory activities (Burt, 2004; Falleh et al., 2020; Mediratta et al., 2002; Mimica-Dukić et al., 2003; Silva et al., 2015) and are commonly used in the products from food and beverage, perfume and cosmetics to nutraceuticals and pharmaceuticals to enhance consumers' experience as well as the health-promoting effects of the products (Franz, 2010; Madene et al., 2006). Synthesised aroma molecules, on the other hand, are seldom used as food preservatives or additives due to the consumers' growing health awareness and preference of naturally occurring flavours and aromas (Reshna et al., 2022). Instead, they are used in personal care, perfume and cosmetics, laundry care, hand wash and detergent products to aid the consumer perception of cleanliness and freshness.

However, flavours and fragrances are highly volatile compounds, which are thermally sensitive and/or chemically reactive (Tekin et al., 2013). Thus, it is challenging to incorporate these ingredients directly into products as they are either prone to evaporating during the manufacturing and storage process or reacting with other formulated ingredients. Moreover, these oils may undergo degradation or autoxidation under harsh conditions, such as the exposure to light, heat and oxygen as well as the variations in pH and humidity (Sousa et al.,

2022). Therefore, strategies to inhibit these oils evaporation and chemical degradation in formulated products are highly desirable since this would reduce the loss of the costly ingredients and enhance the quality of products.

Microencapsulation can be an effective solution to inhibit the evaporation and/or degradation of these oils. It is a process in which a core ingredient is coated by a protective shell (wall or membrane) or entrapped within heterogeneous or homogeneous matrices, to form carrier capsules (Calvo Magro et al., 2012; Gharsallaoui et al., 2007). This process is able to maintain the functional characteristics of these oils and deliver a controlled release, by hindering their volatility and separating them from other formulated ingredients in the product. For examples, encapsulated flavours in food products have prolonged shelf life as the microcapsules provide a protective shell to hinder the evaporation of the flavours. Microcapsules rupture upon chewing, leading to the release of a core flavour oil and enhance the consumers' taste experience (Madene et al., 2006). The microcapsules can also preserve and deliver pH sensitive compounds to a target place, e.g., encapsulated essential oil can be delivered to the lower gastrointestinal tract without deterioration and exert their health-beneficial effects (Lim et al., 2023; Pedro Henrique Rodrigues do et al., 2019). Also, microcapsules for laundry applications are designed not to release the fragrance until the external mechanical forces (e.g., wearing, touching and/or friction between clothes fabrics) are applied to rupture these capsules, leading to the long-lasting freshness for consumers (Mercadé-Prieto et al., 2011). According to FMI (2024), the global encapsulated flavours and fragrances market was valued at US$ 3.99 billion in 2022. The growing demand for natural and authentic flavours/fragrances in a variety of products such as laundry detergents, the food and beverage can be credited for the market

expansion. It is thus estimated to reach an approximate valuation of US$ 7.1 billion by 2033, alongside a compound annual growth rate (CAGR) of 5.5% from 2023 to 2033.

Based on the end-used applications, the performance of microencapsulation product is strictly related to microcapsules' physical, structural and mechanical properties, which are significantly influenced by the shell materials used to encapsulate flavours and fragrances (He et al., 2018). Currently, the shell materials used for the fabrication of flavour and fragrance capsules can be broadly categorised as polymeric and inorganic materials. Although inorganic microcapsules with flavour and fragrance encapsulated were reported to have significant chemical and physical stability (Berry et al., 2017; Bollhorst et al., 2017), the relevant research focused only on particular compounds, such as SiO_2 and $CaCO_3$. Comparatively, polymeric capsules employ a natural or synthetic polymer as wall material to encapsulate flavours or fragrances. Reported synthetic shell materials have included urea formaldehyde, melamine formaldehyde, polyurea, polyamide, poly (methyl methacrylate) and polyurethane (Ghorbanzadeh Ahangari et al., 2014; Hu et al., 2018; Pan et al., 2013; Sun & Zhang, 2001; Tekin et al., 2013; Walter et al., 2000), which are relatively inexpensive and have been extensively investigated due to their efficient encapsulation. However, the aforementioned synthetic polymers are aminoplast based, and the use of these non-biodegradable polymers as microcapsule shell may lead to the accumulation of microplastics in the environment. Natural polymers including polysaccharides and proteins are hazard-free materials and can be used as the potential shell materials for the encapsulation of flavours and fragrances due to their biocompatibility, nontoxicity and wide availability (Hu et al., 2018). The commonly used natural polymers include chitosan, gum arabic, gelatine, alginate and starch and its derivations

(Eraso & Aníbal, 2014; Liu et al., 2016; Prata & Grosso, 2015; Ren et al., 2010; Soottitantawat et al., 2005).

As the most widely used encapsulation method in industry (Sousa et al., 2022), spray drying allows simple, reproducible, continuous and low-cost production of flavour/fragrance microcapsules with natural polymeric walls. However, flavours and fragrances are volatile and heat sensitive and can be readily deteriorated by evaporation or oxidation due to the high temperature involved in this process (Hogan et al., 2003; Serfert et al., 2009). In addition, the spray dried microparticles fabricated using polysaccharides and proteins as wall materials have highly porous structures, making the core oils prone to oxidation (Fang et al., 2006). In situ polymerisation can fabricate microcapsules with compact surface morphology. Microcapsules are reported to exhibit high core oil payload and encapsulation efficiency using formaldehyde-based shell materials (He et al., 2019; Long et al., 2009; Luo et al., 2022; Mercadé-Prieto et al., 2012a). Although this technique is simple and reproducible, the synthetic polymeric shells used in this method are undesirable. Freeze drying is also widely used technique for the encapsulation of flavour/fragrance. This simple process is quite useful for thermosensitive compounds since it is completed under low temperature and low pressure conditions (Zhu et al., 2012), and is reported to fabricate dry powders with high payloads and encapsulation efficiency of volatiles using natural polymers (De Araújo et al., 2020; Shahidi & Han, 1993; Yaman et al., 2023). However, the industrial applicability of freeze drying is severely restricted by its long processing time, high energy consumption and process costs (Desai & Jin Park, 2005; Fang & Bhandari, 2012). Besides, duo to the highly porous structures, the microparticles do not have very good barrier properties (Nedovic et al., 2011). Molecular

inclusion is another very common microencapsulation approach for aromas. The formed host–guest complexes are reported to effectively improve the stability and prolong the release of encapsulated fragrances and flavours (Rodríguez-López et al., 2020). Several works incorporate volatiles/inclusion complexes into natural biodegradable polymer matrix (e.g. zein or pullulan) for biomedical applications (Aytac et al., 2017; Celebioglu & Uyar, 2021; Wang et al., 2021). However, this method is not very suitable for industrial scale (Uhlemann et al., 2002; Zuidam & Shimoni, 2010), due to the high cost of cyclodextrins and their low loading capacity (Gouin, 2004). Comparatively, complex coacervation is one of the most used methodologies for the microencapsulation of flavour and fragrance oils (Bruyninckx & Dusselier, 2019). It can produce thermally stable microcapsules with high oil payload and encapsulation efficiency using natural biodegradable polymers (Napiórkowska & Kurek, 2022a). In addition, industrially scalable complex coacervation has been developed to overcome the complexity of this process (Tang et al., 2020; Timilsena et al., 2019). Considering the good performance of microcapsules obtained by complex coacervation using biopolymers as well as the potential industrial applicability of this process, complex coacervation is therefore employed in this project.

L-carvone is known for its fresh, minty aroma. It is a natural flavour and utilised in the manufacturing of food, and personal care products. Baiocco et al. (2021b) fabricated L-carvone laden microcapsules via complex coacervation by using fungal chitosan and gum arabic as wall materials, followed by spray drying. Several properties, including microcapsule morphology, size distribution, encapsulation efficiency and mechanical properties were characterised, providing a promising solution for the encapsulation of the flavour oil. However,

the payload of microcapsules was only 19 ± 3 %, with a relatively low encapsulation efficiency for the core flavour (L-carvone) at 29 ± 4 %, indicating the poor retention of this costly flavour within chitosan/gum arabic coacervates and the significant loss of L-carvone during the fabrication process. Comparatively, Pakzad et al. (2013) fabricated peppermint oil microcapsule with encapsulation efficiency up to 82% by using gelatine and gum arabic coacervates as shell material. With the same wall materials, Dong et al. (2007) also obtained high payload (90%) peppermint microcapsules by increasing the core/wall ratio to 6:1 by weight. Gelatine (GE) is an abundant protein (Napiórkowska & Kurek, 2022b), and widely used due to its good emulsifying and gelling properties (Elzoghby, 2013; Muhoza et al., 2022). The combination of gelatine and gum arabic is the most commonly used in complex coacervation (Ogilvie-Battersby et al., 2022; Shaddel et al., 2018; Yang et al., 2015). Studies based on the complex coacervation between gelatine and gum arabic to encapsulate flavours and fragrances were also extensively reported (Dong et al., 2011; Girardi et al., 2018; Lv et al., 2014; Pakzad et al., 2013; Xiao et al., 2015; Xiao et al., 2014a), focusing on the effects of various factors including core/wall ratio, wall material concentration, pH value or crosslinkers on the particle size distribution, morphology, encapsulation efficiency as well as thermal stability. However, there has been no systematic study on the effect of different types of flavour/fragrance oils on the particle size distribution, morphology, payload and encapsulation efficiency based on the complex coacervation between gum arabic and gelatine. The effectiveness of flavour/fragrance microcapsules is strictly related to their mechanical properties for the end-use applications, while little is known about the mechanical properties of gelatine/gum arabic coacervated microcapsules containing differ flavours/fragrances.

Therefore, new research is still required to investigate encapsulation of different flavour/fragrance oils using gelatine and gum arabic and to characterise various properties of the formed microcapsules.

Also, melt dispersion technique can be a feasible method for the microencapsulation of flavours/fragrances. Compared to spray drying, melt dispersion prepares microparticles at lower temperatures to reduce the loss of thermosensitive volatiles within the same experimental time scale. Besides, it is the simplest encapsulation technique and readily industrial scalable. Melt dispersion usually employ natural waxes as wall materials, and these waxes are biodegradable polymers. Ethyl vanillin is a synthetic aroma molecule with creamy sweetness odour and utilised as a substitute for vanilla in candy, cookie, chocolate and perfume products. Milanovic et al. (2010) encapsulated ethyl vanillin using carnauba wax as wall material by a melt dispersion technique. The fabricated wax microspheres were determined to have an encapsulation efficiency up to 87 % by HPLC measurement and exhibit good thermal stability. However, there has been no comprehensive study about the encapsulation and characterisation of different flavours and fragrances using waxes as wall material by melt dispersion. Investigation about the effects of different wax types and wax to oil ratios on both the physical and mechanical properties of wax microspheres still remain to be fully explored.

In addition, it is notable that different properties of microcapsules can also be significantly influenced by the encapsulated core oils. L-carvone, limonene and hexyl salicylate were reported to be encapsulated via complex coacervation using gum arabic and fungally fermented chitosan as wall materials (Baiocco et al., 2021a;2021b; Baiocco & Zhang, 2022).

The fabricated microcapsules containing each molecule exhibited significant different properties including size and size distribution, encapsulation efficiency and payload, rupture behaviour and mechanical strength. Xiao et al. (2014b) investigated the encapsulation of lavender oil by complex coacervation using gum arabic and gelatine. The oil loaded microcapsules were measured to have an encapsulation efficiency up to 66 %. However, significant variations on encapsulation efficiency were reported by Ogilvie-Battersby et al. (2022) and Manaf et al. (2018) encapsulating geraniol and citronella oil respectively by the same wall material formulations and experimental procedures. For geraniol loaded microcapsules, a range of efficiency from 68 % to 90 % were measured depending on the mixing rates, while 94% encapsulation efficiency was reported for citronella oil microcapsules. Luo et al. (2023) evaluated the effects of the chemical structure, logP, the solubility, the interfacial tension between oil and water, and the viscosity of twelve different single componential oils on the size, morphology, encapsulation efficiency as well as mechanical properties of melamine formaldehyde microcapsules, and reported that the logP influenced the encapsulation of core oil as well as the capsule size and mechanical strength. The high interfacial tension between core oil and water improved the encapsulation efficiency. However, the authors did not go further by investigating the mechanism underlying the influence of core oil on microcapsule properties from the perspective of thermodynamics.

1.2. Aim and objectives

The aim of this research is to develop biodegradable flavour/fragrance microcapsules with improved properties, including encapsulation efficiency and mechanical strength. It mainly has three objectives:

- to encapsulate L-carvone and hexyl salicylate using carnauba wax, candelilla wax and beeswax by melt dispersion and investigate the effect of formulations (including wax type, weight ratio of core oil to wax and core oil type) on the fundamental and mechanical properties of wax microspheres (Chapter 3);
- to encapsulate L-carvone, limonene and hexyl salicylate using gelatine (GE) /gum arabic (GA) coacervation followed by spray drying and investigate the influence of further treatments including spray coating by maltodextrin and wall hardening process by glutaraldehyde crosslinking on the physicochemical and mechanical properties of microcapsules (Chapter 4); and
- to study the impact of core oils on the morphology and encapsulation efficiency of GE-GA coacervated microcapsules based on the spreading coefficient and two component surface energy theory (Chapter 5).

1.3. Thesis layout

This thesis is outlined as follows:

Chapter 1 illustrates the background of this research as well as the aim and objectives of this project, followed by the thesis layout.

Chapter 2 provides a general introduction to microencapsulation and a fundamental literature review of the main encapsulation methods and the commonly used characterisation techniques for the resulting microcapsules. Particular focus is placed on the microencapsulation of flavours and fragrances, taking into consideration the significant influence of physical characteristics of core oils on the properties of microcapsules prepared using the same shell materials.

Chapter 3 describes the fabrication of wax microspheres for the encapsulation of L-carvone and hexyl salicylate via a novel melt dispersion method. Different wax types and oil/wax ratios were employed to fabricate these wax microspheres. The fundamental physical and mechanical properties of wax microspheres are characterised and extensively discussed. The possible relations between payload and Young's modulus of microspheres for each corresponding wax are also studied.

Chapter 4 focuses on investigating the encapsulation of L-carvone, limonene and hexyl salicylate based on the complex coacervation between gelatine and gum arabic, followed by spray drying/coating, with particular emphasis on the effects of different type of core oils and further treatments on gelatine/gum arabic coacervated microcapsules in terms of size, morphology, payload and encapsulation efficiency, mechanical strength and rupture behaviour.

Chapter 5 goes further by exploring the morphology and encapsulation efficiency of gelatine/gum arabic coacervated microcapsules with L-carvone, limonene, linalool, carvacrol, cinnamaldehyde or hexyl salicylate encapsulated as a core oil. The mechanism underlying the influence of core oils on both the morphology and encapsulation efficiency of the microcapsules was investigated for each coacervating system from the perspective of thermodynamics by combing spreading coefficient and two component surface energy theory.

Chapter 6 gives the overall conclusions of this project, followed by recommendations for the potential future works.

CHAPTER 2. Literature Review

2.1. Introduction

In this chapter, the literature on microencapsulation, general experimental methodologies and analytical techniques used to characterise microcapsules are presented herein. Particular emphasis is placed on the microencapsulation of different flavours and fragrances. The overall literature consists of two main parts. The first part provides an introduction of microencapsulation, with an overview on the resultant microcapsules and their typical structural configurations. The main encapsulation methods and associated analytical techniques to characterise various properties of microcapsules are also outlined. In the second part, the current development and associated challenges using various polymers as wall materials for the microencapsulation of different flavours and fragrances are presented. The basic chemical properties of different flavour and fragrance oils relevant to this project are described, and their encapsulation results using different formulations of shell material and encapsulation methods are also given. In addition, the influence of core oils on the properties of resultant microcapsules fabricated with the same shell material is reviewed.

2.2. Microencapsulation

2.2.1. Introduction

Microencapsulation is a technique to encapsulate solid, liquid or gaseous active ingredients into polymeric or nonpolymeric materials, resulting in a physical separation of active ingredients from surroundings (Dubey et al., 2009). The active ingredients to be encapsulated are referred as core materials whilst the surrounding coating is called wall (or shell)

(Sanguansri & Ann Augustin, 2010). The formed solid capsules can be spherical or irregularly shaped depending on variable factors, including physical nature of the core material, employed encapsulation method, processing parameters and material formulations (Dong et al., 2007; Nelson, 2013), which also influence the morphological structure of microcapsule, i.e., matrix, core shell, multicore shell, core multishell and irregular core shell, as shown in Figure 2-1. The sizes of capsules normally range from nanometres to millimetres and can be classified as nanocapsules (<1 μm), microcapsules (1-1000 μm) and macrocapsules (>1 mm) (Alexander & Shlomo, 2015). The pioneer work of microencapsulation was introduced in the 1950s by Green and Schleicher (1957) for the fabrication of carbonless copying paper, which was then developed rapidly for decades and nowadays the microencapsulation has been widely applied in e.g. food processing, pharmaceutical, agrochemical and cosmetic industries (Benita, 2005; Choudhury et al., 2021; Knowles, 2008; Meyer, 2005; Vilstrup, 2001).

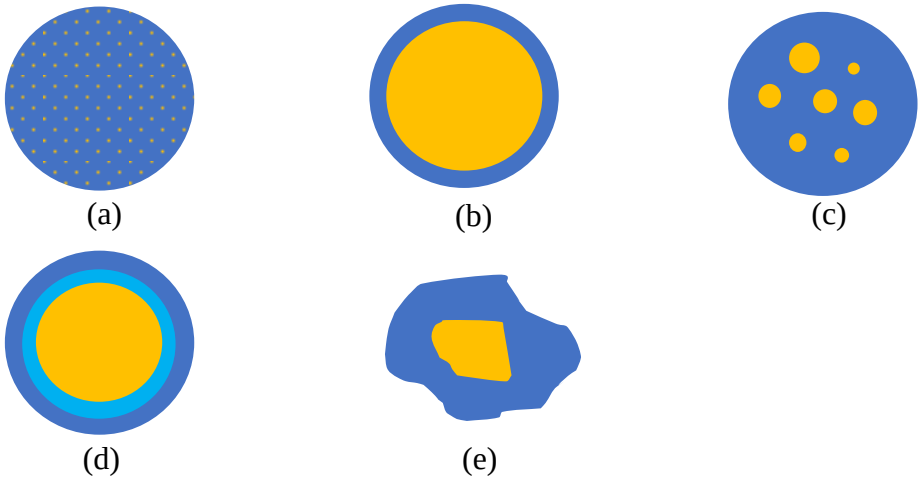

Figure 2-1 Different types of microcapsule structures: (a) microsphere (matrix), (b) core shell, (c) multicore shell, (d) core multishell and (e) irregular core shell (Choudhury et al., 2021).

2.2.2. Encapsulation techniques

The microencapsulation has been accomplished using various methods, which can be broadly divided into two different categories depending on the formation mechanism of microcapsules (see Figure 2-2) (Sousa et al., 2022). Mechanical approaches are based exclusively on physical phenomena, including spray drying, fluidized bed coating, extrusion, freeze drying etc, while physico-chemical approaches utilise chemical reactions or molecular interactions to form shell material surrounding core active ingredient, e.g., in situ polymerisation, polycondensation, coacervation, ionic gelation and molecular inclusion (Shekhar et al., 2010; Sousa et al., 2022). The selection for a specific encapsulation method can be determined by variable factors, including physical properties of core and wall materials, the compatibility between the core and wall materials, desired microcapsule properties and product end applications. The advantages and disadvantages of some widely used encapsulation methods as well as the corresponding microcapsule properties are summarised in Table 2-1. Overall, the chosen microencapsulation method has to be relatively cheap, reproducible and scalable for industrials. The following sections introduce some typical encapsulation methods in detail.

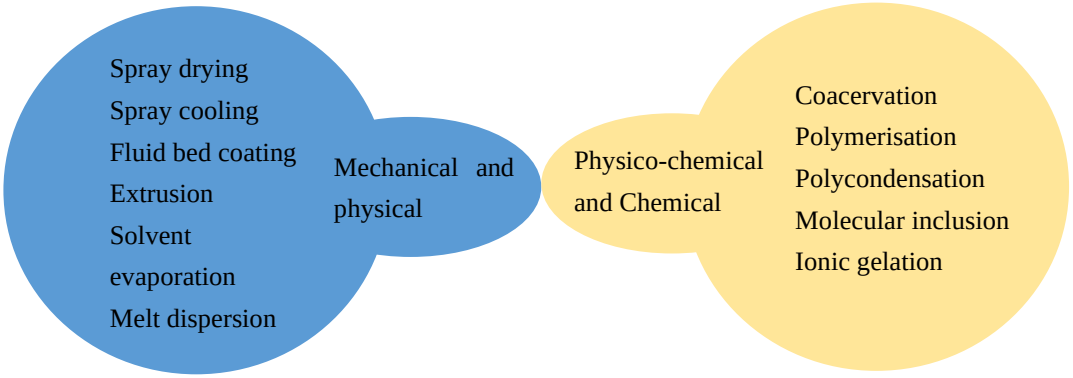

Figure 2-2. Schematic illustration of various encapsulation methods (Sousa et al., 2022).

Table 2-1. Advantages and disadvantages of each encapsulation technique and corresponding microcapsule properties (Azarpazhooh et al., 2022; Choudhury et al., 2021; Govender et al., 2015; Milanovic et al., 2010; Mittal, 2013; Sousa et al., 2022; Sri et al., 2012; Yan et al., 2022; Zuidam & Shimoni, 2010).

Type of method	Advantage	Disadvantage	Microcapsule properties		
			Size (μm)	Morphology	Porosity
In situ polymersiation	High payload, narrow size range	Non-biodegradable shell, formaldehyde toxicity	1-1000	Core-shell, spherical	Compact shell
Solvent evaporation	Low cost, water insoluble shell	Low yield, toxic solvents	0.5-1000	Matrix, spherical	Porous
Spray drying	Economical, fast, easily scaled up	Low payload, high temperature	5-5000	Matrix, irregular-spherical	Porous
Fluidized bed coating	Broad selection of coating materials, controllable shell thickness	Time consuming, large amount of shell materials needed	20-2000	Matrix, irregular-spherical	Porous
Freeze drying	Thermal sensitive core encapsulation, high yield	High cost, time consuming, limited in cell encapsulation	20-5000	Crystals, spherical	Porous

Molecular inclusion	Thermal stability, high retention efficiency	Low payload, high cost, unsuitable for industrial scale	0.01-100	Crystals	Complexation
Coacervation	High payload, reproducible, controllable particle size	Limited materials, pH sensitive	2-1200	Core-shell, Spherical	Compact shell
Melt dispersion	Simple, solvent free, low temperature	Limited shell materials	0.1-1000	Matrix, spherical	Porous

2.2.2.1. In situ polymerisation

In situ polymerisation has become one of the most commonly used methods for the preparation of microcapsules and functional fibres (Bakry et al., 2016). In an emulsion, e.g., oil-water emulsion, all the reactants including monomers or oligomers are in the continuous phase, where the polymerisations take place. The resultant polymer molecules deposit onto the surface of core material from the side of the continuous phase and form microcapsules with solid shell. The monomers used in this method include urea formaldehyde, melamine formaldehyde, urea melamine formaldehyde and melamine glutaraldehyde formaldehyde (Hwang et al., 2006; Long et al., 2010; Long et al., 2009; Luo et al., 2022; Yuan et al., 2006). Figure 2-3 demonstrates a typical in situ polymerisation process for the synthesis of melamine formaldehyde microcapsules. Herein, the monomer precondensate and copolymer were initially dissolved and precross-linked in the continuous phase (Step 1). The core oil was added into the shell solution (Step 2) and an emulsion was formed by agitation (Step 3). Melamine formaldehyde shell solidified at the dispersed oil surface by the polymerisation (Step 4) (Long et al., 2009).

In general, the microcapsules prepared via in situ polymerisation have smooth surface morphology and a compact shell thanks to the highly cross-linked copolymers, and microcapsules also display good thermal and controlled release properties (Hwang et al., 2006). This technique exhibits many advantages including being simple and reproducible. However, it brings several inevitable health and environment issues since the polymerisation reaction product is aminoplast based, making the materials non-biodegradable and/or non-biocompatible. In addition, the excess formaldehyde needs to be removed to avoid

formaldehyde toxicity.

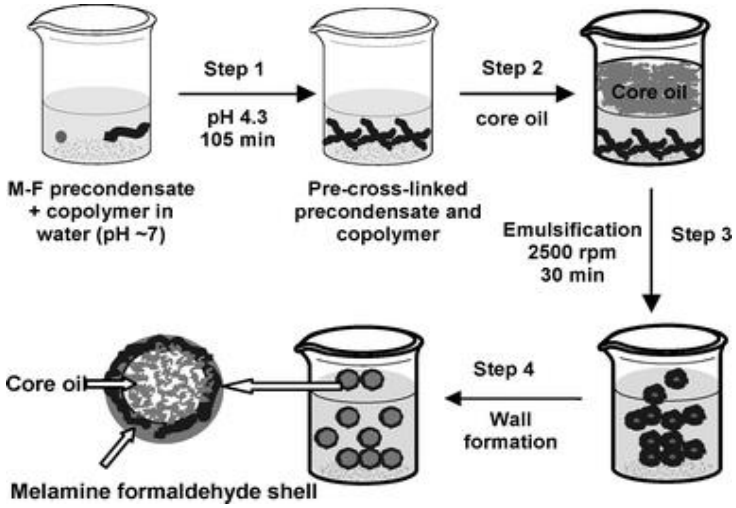

Figure 2-3. Schematic illustration of melamine formaldehyde microcapsules synthesised via in situ polymerisation (Long et al., 2009).

2.2.2.2. Solvent evaporation

Solvent evaporation is a common physical technique for the encapsulation of bio-actives in pharmaceuticals. This method consists of a few steps as shown in Figure 2-4. The coating polymer material is initially dissolved in a water immiscible volatile organic solvent, into which the active ingredient is also dissolved or dispersed. The resulting mixture solution or dispersion is then emulsified in an aqueous phase and kept with agitation until the solvent is evaporated, which results in the deposition of the coating polymer material around the core and formation of the microparticles (Dubey et al., 2009; Sri et al., 2012). The main advantages of solvent evaporation over other techniques are fast product fabrication, viable process reproducibility as well as less skills required for the operation. It also enables the use of water insoluble materials as shell materials for the microparticles. However, solvent evaporation often involves the use of toxic solvents, which limits its application for the food industry. In

addition, the encapsulation efficiency for volatile active cores by this method is inevitably low (Das et al., 2011; Tiwari & Verma, 2011).

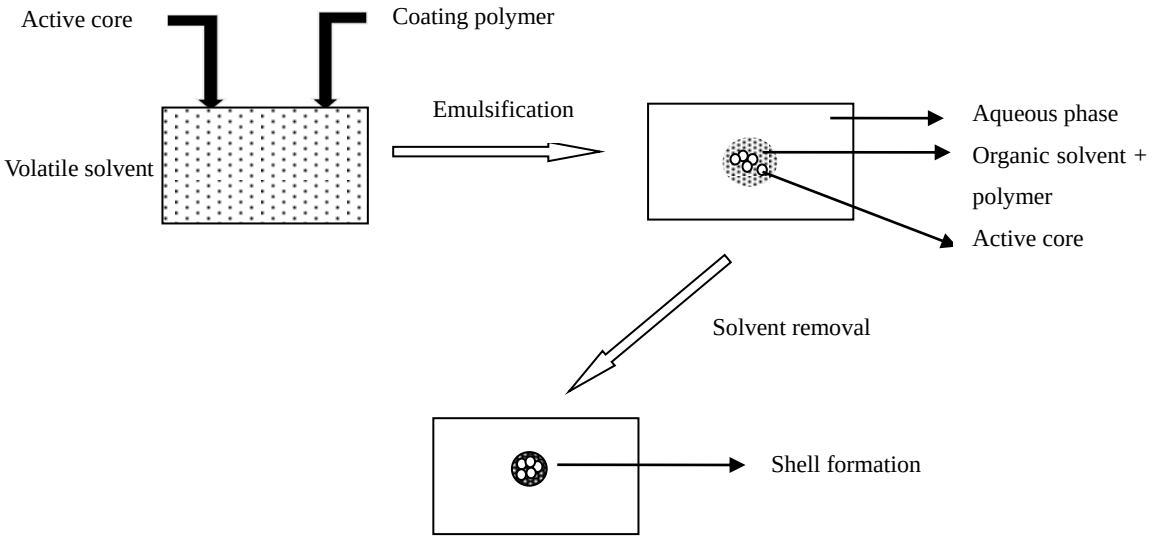

Figure 2-4. Schematic representation of microencapsulation by solvent evaporation technique (Alexander & Shlomo, 2015).

2.2.2.3. Spray drying

Spray drying is the most used microencapsulation process in the food industry, and has become widely utilised in cosmetics, pesticides and pharmaceutical industries (Estevinho et al., 2013). As shown in Figure 2-5, this technique consists of a few steps: the core ingredient is firstly emulsified or suspended in an aqueous solution containing the dissolved wall materials, then the dispersion is uniformly sprayed through a high-pressure atomising nozzle into a drying chamber, where the small liquid droplets are formed. The droplets enter the chamber with a flow of hot inlet air, which is assigned for the dehydration and solidification of wall materials onto the core ingredients via the evaporation of the water, resulting in the formation of matrix type or polynuclear microparticles. The dried particles will go through a cyclone separator with air flow and are collected in a container due to their higher density (Mohammed

et al., 2020; Tonon et al., 2011; Zuidam & Shimoni, 2010).

Thanks to the readily available equipment and high output, spray drying is a well-established microencapsulation technique commonly used on a large industrial scale, which exhibits several attractive advantages of cost-effectively producing microparticles in a relatively simple, fast, reproducible and continuous operation. Moreover, a wide variety of wall materials can be used (Liu et al., 2007; Soottitantawat et al., 2003). However, there are also a few drawbacks of this technique. Spray drying produces dried microparticles with highly porous structures, making the products more prone to oxidation (Fang et al., 2006). Heat sensitive actives or volatiles can be readily evaporated or deteriorated by oxidation due to the high temperature involved in the process (Hogan et al., 2003; Serfert et al., 2009).

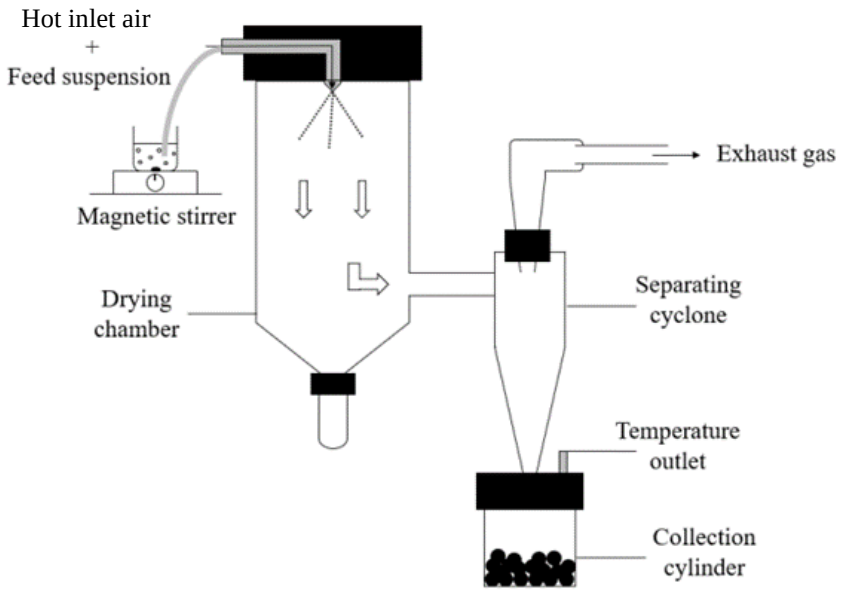

Figure 2-5. Schematic representation of spray drying process

2.2.2.4. Coacervation

Coacervation is one of the oldest and most widely used microencapsulation techniques. This technique is based on the phase separation of one or more polymeric hydrocolloids from the

initial solution followed by the subsequent agglomerated deposition of the newly formed coacervate phase around the active ingredients (Napiórkowska & Kurek, 2022b). The formation of coacervates is induced by altering temperature, pH or ionic strength depending on the physicochemical properties of the wall material (Choudhury et al., 2021). Briefly, the core material is primarily dispersed and emulsified in polymer solution to form an emulsion. The polymer then precipitates from the solution after the change of ionic strength, pH, or temperature and gradually forms coacervates, which are tiny gel solids. These coacervates will migrate and adsorb at the surface of the core droplets due to the interfacial energy balance between each phase, forming a continuous coating by coalescence, and eventually resulting in a compact shell around the core active ingredient. Finally, The shell material is hardened by chemical crosslinking with the core encapsulated (See Figure 2-6) (Sri et al., 2012). The coacervation process can be classified as simple or complex based on the number of polymers involved. In simple coacervation, only one polymer is involved and precipitated by the action of electrolytes (e.g., sodium sulfate), or desolvated by the addition of a water-miscible solvent (e.g., ethanol), or by increasing/decreasing the temperature (Gu et al., 2010; Pakzad et al., 2013). Complex coacervation is based on the phase separation caused by the molecular interactions between two or more oppositely charged water soluble polymers, which are usually proteins and polysaccharides.

The coacervation presents many advantages including high payload and encapsulation efficiency. Microcapsules prepared by coacervation have extremely low surface oil, good barrier property and shelf-life stability. The coacervation process produces microcapsules with a consistent shell, making microcapsules exhibit excellent controlled release characteristics

and heat-resistant properties (Kralovec et al., 2012; Wang et al., 2014; Xiao et al., 2011). In addition, this method is scalable, solvent-free and reproducible. However, limitations are also associated with this technique. Coacervation is a relatively complicated and long process which involves several steps, making it quite expensive. The complex coacervation occurs only within a quite narrow pH range and with certain electrolyte and colloidal solutions. Furthermore, the commonly used crosslinkers to harden wall materials (e.g., glutaraldehyde, formaldehyde) can cause toxicity.

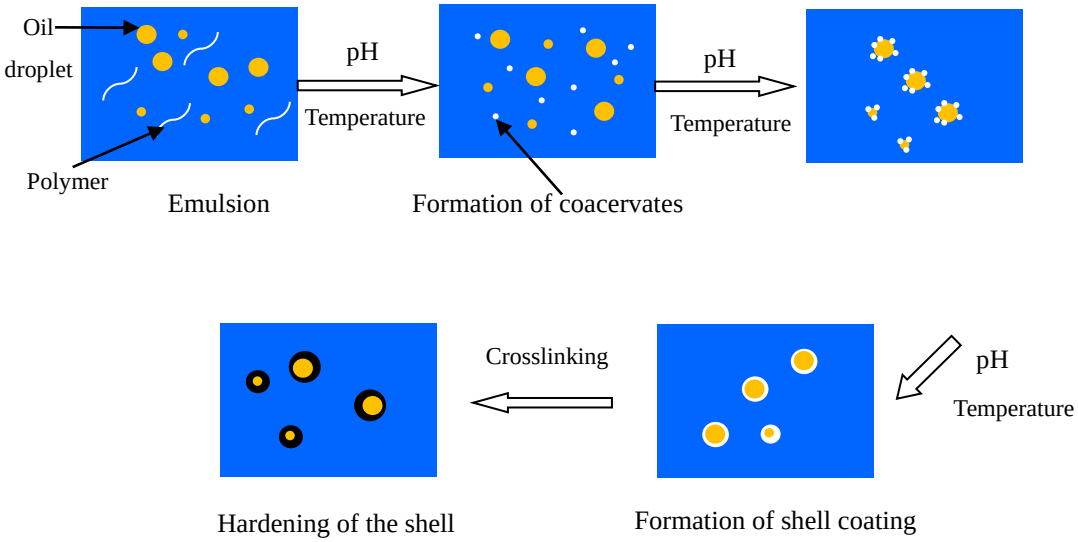

Figure 2-6. Schematic representation of the coacervation process (Sri et al., 2012).

2.2.2.4.1. Complex coacervation

As aforementioned, gelatine/gum arabic is the most common system used for complex coacervation (Ogilvie-Battersby et al., 2022; Shaddel et al., 2018; Yang et al., 2015). The mechanism of complex coacervation based on gelatine/gum arabic system is presented in Figure 2-7, that the free negatively charged carboxylic groups of gum Arabic electrostatically interact with the positively charged amino groups of gelatine to form coacervates (Rousi et al., 2019).

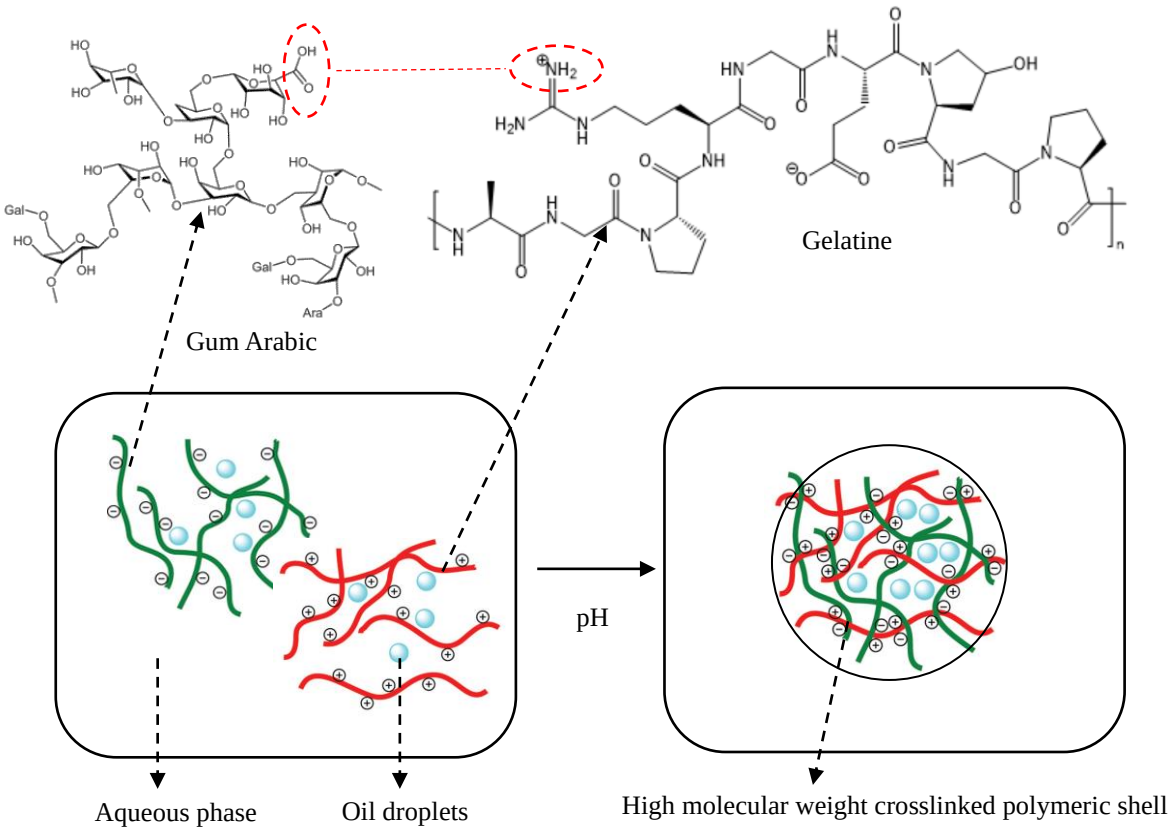

Figure 2-7. Formation mechanism of GA and GE coacervate microcapsules.

Several parameters influence the formation of coacervates (De Kruif et al., 2004). For gelatine/gum arabic system, the functional reactive branches of polymers get ionised depending on their dissociation constants (pKa), proteins' isoelectric point (PI), and the solution pH. Before complex coacervation, gelatine and gum arabic need to be dissolved at a pH where they are soluble, and enabling them to carry the same charge so that the coacervation does not initiate upon mixing (Lemetter et al., 2009; Turgeon & Laneuville, 2009). The isoelectric point of gelatine B ranges from pH 4.8-5 (Muhoza et al., 2022), and it exhibits an electrostatic switchover from a negative to positive charge by adjusting the solution from neutral to acidic. In contrast, the pKa of gum Arabic is at pH 2.0, and gum

arabic is negatively charged within solution if pH ⩾ 2 (Gulão Eda et al., 2016). Thus, coacervation occurs within this narrow pH region (pH 2-4.8) where gelatine and gum arabic are oppositely charged. According to De Kruif et al. (2004), a maximum viscosity in the coacervate phase was found at pH 4.0, indicating the strongest electrostatic interaction between polysaccharides and proteins. Several studies also adjusted the pH to 4.0 to induce the complexation between gelatine and gum arabic molecules (Aziz et al., 2014; Najafi et al., 2004; Pakzad et al., 2013; Rousi et al., 2019; Shaddel et al., 2018).

The charge density of biopolymers can be reflected by the number of charged reactive groups ionised in solution, which can be influenced by the solution pH. The net charges carried by the two biopolymers can be also influenced by the polysaccharide to protein ratio (Liu et al., 2015; Niu et al., 2015). It is demonstrated that there is an optimum polymer weight ratio to balance the net opposite charges, allowing a fully charge compensation between polysaccharide and protein molecules, and leads to the formation of electroneutral complexes (De Kruif et al., 2004; Schmitt et al., 2009). For gelatine and gum arabic system, an optimal polymer ratio of 1:1 is suggested by serveral works (Devi et al., 2023; Lv et al., 2013; Sarika et al., 2015; Yang et al., 2024).

Weinbreck et al. (2003) have also reported that coacervation can be suppressed over a critical concentration, beyond which the coacervates increase their solubility and phase separation no longer occurs. Thus, a total biopolymer concentration of 2 to 6 wt % is generally used for complex coacervation based on gelatine and gum arabic system (De Kruif et al., 2004; Lemetter et al., 2009; Schmitt, 2009; Turgeon and Laneuville, 2009).

In addition, the freshly formed gelatine/gum arabic coacervate shells are mechanically weak

(Prata et al., 2008), and the process of crosslinking enables microcapsules with better structural and mechanical properties by forming the reticulation of the shell (Burgess & Ponsart, 1998). Crosslinking can be performed via chemical or enzymatic hardening (De Kruif et al., 2004). Transglutaminase (TG) have been successfully used as crosslinkers based on the enzymatic mechanism (Motoki & Seguro, 1998; Rojas-Moreno et al., 2018). Specifically, TG is a naturally occurring enzyme that has been intensively used in food processing. it promotes proteins to bind covalently and contribute to formation of intra- and intermolecular ε-(γ-glutamyl) lysine bonds (Motoki & Seguro, 1998). However, Lv et al. (2014) have reported that the glutaraldehyde crosslinked microcapsules exhibit better barrier properties compared to TG-crosslinked ones.

Crosslinking by glutaraldehyde is a chemically induced process, the insoluble networks are formed by the reaction between the aldehyde groups and the amino groups of the protein. The newly formed networks strengthen the shell of the microcapsules, thus increasing their mechanical and barrier properties (Kelly et al., 1999). Glutaraldehyde is also considered safer than formaldehyde (Takigawa & Endo, 2006), since it is unlikely to bioaccumulate in environment, resulting in more eco-friendly wastewater (Leung, 2001).

2.2.2.5. Melt dispersion

The melt dispersion technique is a physical encapsulation method as illustrated in Figure 2-8. A molten matrix such as a wax oleogel containing dissolved hydrophobic active ingredient, is uniformly dispersed and emulsified in a hot aqueous phase by mechanical stirring or homogenisation at a maintained temperature, which is above the melting point of dispersed phase. The solidification of melt and entrapment of the active core within matrix is

accomplished through the cooling process either with the addition of cold water or transferring the batch to ice water bath (Milanovic et al., 2010; Mishra, 2015; Nandy et al., 2020). The melt dispersion technique presents several advantages in comparison with other encapsulation techniques. Firstly, it is the simplest encapsulation technique and readily scalable. Secondly, the temperature used for this method is generally significantly lower than spray drying, which is favourable in reducing the volatiles loss during the encapsulation process. In addition, unlike chemical encapsulation method, no solvent or crosslinker is required to trigger any reaction for the formation of shell materials. Instead, the encapsulation for the core ingredients is accomplished by the formation of oleogels via physical phase change.

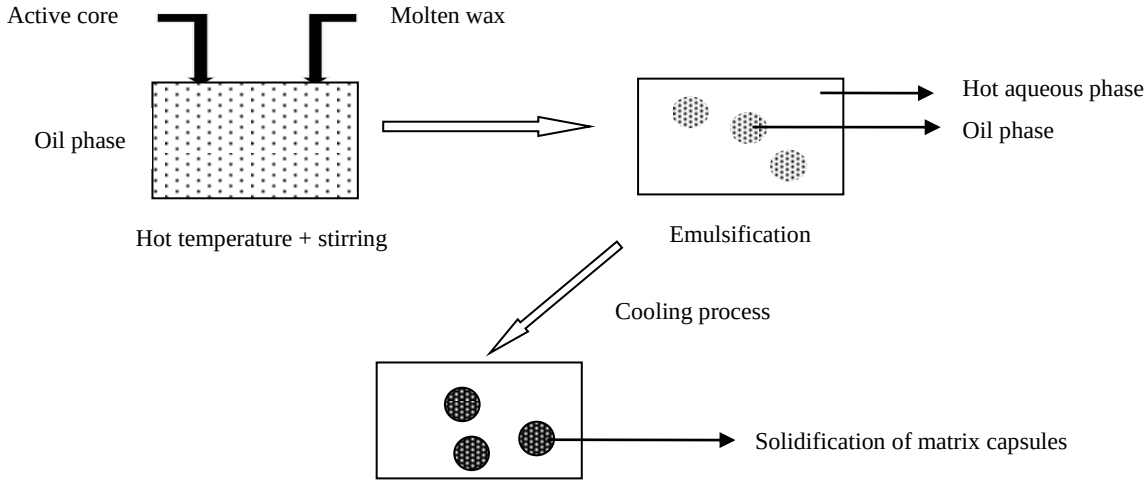

Figure 2-8. Schematic representation of melt dispersion technique (Mishra, 2015).

2.2.2.5.1. Waxes

Natural waxes are biopolymers and can be used as a promising wall material for melt dispersion technique (Mishra, 2015). Each type of wax is a complex of mixture and the major constituents usually include esters, fatty acid alcohols and hydrocarbons with different

percentages based on the wax type. The use of waxes as wall materials can provide advantages, which include good chemical and mechanical stability at different pH and moisture levels (Mishra, 2015). Waxes are usually nonpolar and hydrophobic, which makes them possible to encapsulate lipophilic materials. The melt dispersion applies a temperature higher than the melting point of wax to transform its solid state into liquid phase, and homogeneously mixing molten wax with core compounds by emulsification. The resultant wax microspheres have matrix structures, which provide a protective shell for core volatiles. The applied temperature lower than spray drying can effectively reduce the deterioration of core aromas.

The chemical compositions of waxes may vary widely depending on origins. For example, beeswax (BW) is considered an animal wax and is produced by honeybees for building honeycomb cells. It is a mixture of C_{38}-C_{52} wax esters (~71%), C_{23}-C_{31} hydrocarbons (~15%), free fatty alcohols and fatty acids (Tinto et al., 2017). Candelilla wax (CanW) is extracted from the candelilla shrub. It consists mainly of C_{29}-C_{33} hydrocarbons (~50%) and C_{34}-C_{52} wax esters (~30%) (Tinto et al., 2017). Carnauba wax (CarW) is extracted from Copernicia prunifera and consists mostly of C_{24}-C_{34} wax esters (~60%) and fatty alcohols (~31%) (Tinto et al., 2017). Waxes of different origins melt at different temperatures ranging from as low as 62 to 64 °C for BW, 68.5 to 72.5 °C for CanW and as high as 82 to 86 °C for CarW. In the European Union, BW is authorised as food additive and approved for use as a glazing agent. As carriers for flavours and colours at defined limits up to 0.1% (wt) for all food categories (EFSA, 2007), CanW and CarW are generally-recognized-as-safe (GRAS) materials, with no limitations on use levels in several food related products (EFSA, 2012a;2012b). The Physical and chemical properties of these waxes are summarised in Table 2-2.

Table 2-2. The physico-chemical properties of different waxes (Bucio et al., 2021; Mendoza-Duarte et al., 2023; Tinto et al., 2017; Zhang et al., 2016).

Properties	BW	CanW	CarW
Formula	Average chain length C_{40}	Average chain length C_{30}	Average chain length C_{50}
Molar mass (g/mol)	Average ~ 591	Average ~ 437	Average ~ 728
Density (g/cm^3) at 15°C	0.958–0.970	0.950-0.990	0.990-0.999
Melting point (°C)	62-64	68.5-72.5	82-86
Molecular structure (Main composition)	Monoesters (C_{32}-C_{52})	Hydrocarbons (C_{29}-C_{33})	Aliphatic/aromatic esters (C_{44}-C_{66})
Viscosity (mPa·s) at 85 °C	7.0	13.1	9.0

2.2.3. Characterisations of microcapsules

Research into microencapsulation focuses mainly on two categories, fabrication of microcapsules and characterisations of their properties and performances (Gray et al., 2016). In order to comprehensively understand the potential applications of the formed microcapsules, it is crucial to characterise their physicochemical, structural and mechanical properties (e.g., morphology, active core payload, encapsulation efficiency and mechanical strength) precisely since certain desirable properties can be required for a given application. For instance, for food applications, where microcapsules are used for the mask of unpleasant flavour of the core, protection of actives from oxidation or evaporation or the prolonged storage of core active, it is also desirable for microcapsules to be smaller than 100 μm in size to avoid impacting the mouthfeel negatively (Cittadini et al., 2022). In the laundry industry, microcapsules containing fragrance are expected to remain intact, to be adhesive to clothing fibres and ruptured by mechanical force after drying. Strong and optimised mechanical properties of microcapsules

are thus pivotal for the controlled release of core fragrance (He et al., 2014). Herein, various characterisation techniques for microcapsule properties are reviewed, covering size and size distribution, morphology, payload and encapsulation efficiency and mechanical properties.

2.2.3.1. Size and size distribution

Different encapsulation techniques can produce microcapsules of various sizes and size distributions, which are the fundamental physical properties, and in strong relation to other properties including flow properties, surface adhesion and mechanical properties (Gray et al., 2016). For instance, with identical wall thickness, larger sized microcapsules need greater force to be ruptured compared to the smaller sized ones (Luo et al., 2022; Mercadé-Prieto et al., 2011). Microcapsules prepared via microfluidics exhibited much narrower size distribution compared to the microcapsules generated in a stirred vessel (Ling et al., 2020). Various methods have been developed to determine the size and size distribution of microcapsules and these can broadly be classified into two categories: laser diffraction method and microscopy. Laser diffraction method, namely static light scattering, is based on the Mie Theory and is the most common method for characterising the particle size and size distribution (Merkus, 2009). It measures the variation of the light density scattered from a laser beam for a microcapsule suspension. However, identification for the refractive index values of the particle shell materials and dispersion medium is required for size measurement (Senoo & White, 2017). Microscopy is another frequently used method for size analysis. It enables the capture of microcapsules real images on individual level while inevitably it is time consuming and difficult for size distribution analysis.

2.2.3.2. Morphology

Morphology of microcapsules refers to the shape, surface roughness and external and inner structure of capsules, which dominantly depends on how the microencapsulation is achieved including microcapsules preparation techniques, wall materials as well as the physical properties of active ingredients (Choudhury et al., 2021). The morphology of microcapsules is strongly associated with other properties including payload and encapsulation efficiency, mechanical properties and core release behaviours so that undertaking the morphological characterisation for capsules is very important. Generally, optical microscopy, scanning electron microscopy (SEM), transmission electron microscopy (TEM), atomic force microscopy (AFM) and confocal laser scanning microscopy (CLSM) are the most frequently used techniques for the morphological characterisation. Optical microscopy utilises visible light as light source to obtain images while SEM and TEM use electrons with shorter wavelength to irradiate microcapsules and generate images with higher magnification. TEM enables the cross-sectional observation for microcapsules and measurement for their shell thickness. The sample needs to be entrapped uniformly inside a resin and cut into thin slices. CLSM can provide three dimensional images for the sample and is capable of offering an insight into the inner structure of microcapsules, which needs to be stained by fluorescence dyes that have different affinities to the corresponding chemical compositions. Unlike SEM or TEM, AFM does not require a high vacuum and is capable of detecting the surface roughness of microcapsules by using a probe.

2.2.3.3. Chemical composition

Fourier transform infrared spectroscopy (FTIR) is widely used to reveal the compositions of

microcapsules by detecting the characteristic wavelength of the material with specific functional groups. This technique is based on the principle that certain wavelengths of the infrared radiation will be absorbed to variable extents when passing through a specific compound, from which the absorbed radiations will be converted into rotational and/or vibrational energies, presenting a unique spectrum from 4000 to 400 cm^{-1} for the corresponding molecule. Ideally, core molecules are expected not to interact chemically with shell molecules for stable microencapsulation, and FTIR can provide information on interactions between core ingredients and shell materials on molecular level, and on whether there are new wavelengths occurring or shifting due to the formation of chemical bonds.

2.2.3.4. Encapsulation efficiency and payload

Encapsulation efficiency and payload of microcapsules are very important properties to be characterised and strongly related to other influencing factors including microcapsules morphology, physical properties of core material and wall materials, formulations, and encapsulation technique that is used to produce microcapsules. Payload is the weight ratio of encapsulated core active ingredient to the tested microcapsules while encapsulation efficiency is defined as the ratio (in percentage) of encapsulated core material to the initial core active input to the batch (Choudhury et al., 2021). Generally, UV-vis spectrophotometry, gas chromatography (GC), high-performance liquid chromatography (HPLC) and thermogravimetric analysis (TGA) are commonly used techniques for the quantitative characterisation of microcapsules payload and encapsulation efficiency. UV-vis spectrophotometry is a rapid analytical technique, which is based on quantifying the discrete wavelengths of UV or visible light that is absorbed by the compounds compared to a reference

within spectra from 180 to 750 nm. The concentration of the compound can be deduced from the absorbance value (Rakhee et al., 2018). GC is highly accurate analytical technique, which is based on the physical separation of chemical compounds due to their different boiling temperatures, vapor pressures and polarities (Stauffer et al., 2008), while HPLC separates various compounds from a mixture solution based on their different migration rate passing through a column filled with solid adsorbent particles (Seneca, 2007). Both GC and HPLC techniques can be used for the identification of compounds of interest apart from quantifying their amounts. TGA is a powerful technique for the measurement of thermal stability of materials (Ebnesajjad, 2006). This method can also be used for the quantification of active ingredient encapsulated in microcapsules by measuring the changes in their weight at different temperatures (Milanovic et al., 2010).

2.2.3.5. Mechanical properties

The requirements for good microencapsulation are to stabilise the active ingredients and achieve their controlled release. The microcapsules have to be mechanically stable during encapsulation process, subsequent processing and storage, while prone to be ruptured by mechanical force as a trigger for the release of the core, e.g. perfume microcapsules using in laundry detergents (Gray et al., 2016). Therefore, characterising the mechanical properties of microcapsules is essential to understand their behaviour during preparation, and their performance for end-use applications. The mechanical properties of the microcapsules include Young's modulus, mechanical strength parameters and viscoelastic behaviour (Zhang et al., 2009). The Young's modulus indicates the flexibility of the microcapsules under the deformation and mechanical strength parameters include rupture force, nominal rupture stress,

nominal rupture tension and toughness (Zhang et al., 2022), which along with the viscoelastic performance dominantly depend on the chemical composition of shell materials, the size and structure of microcapsules, shell thickness (Gray et al., 2016).

Numerous methods have been developed for characterising the mechanical properties of microcapsules, and they can broadly be divided into two categories: bulk methods and individual measurements. Bulk mechanical characterisation tests have focused mainly on the resistance of a population of microcapsules to mechanical forces generated by shaking, turbine rotor and bubble columns (Chen et al., 1995; Martins Dos Santos et al., 1997; Poncelet & Neufeld, 1989), and the results depend on not only the microcapsule mechanical properties but also the hydrodynamics. To eliminate the effect of the hydrodynamics, Ohtsubo et al. (1991) developed a technique involving compression of a population of microcapsules between two parallel plates. However, large experimental errors may occur since the two plates are practically difficult to be made parallel. Osmotic pressure tests were also employed for the mechanical characterisation for microcapsules with semi-permeable wall (Van Raamsdonk & Chang, 2001). However, this technique can only be used for relatively weak capsules. Regarding the characterisation of individual microcapsule, AFM and micromanipulation are the most commonly used techniques. AFM is used to determine the indentation hardness of the sample with either a sharp tip or a large colloidal probe. AFM with the sharp tip focuses on only a point on the sample surface, and the force generated is normally not great enough to cause rupture of the microcapsule. When the colloidal probe attached on the AFM cantilever is used to compress a microcapsule, there is often an alignment issue so that the microcapsule tends to slip away from the probe. Micromanipulation was firstly introduced by Zhang et al.

(1991) to investigate the rupture behaviour of individual mammalian cells. This technique was then improved to encompass a variety of biological and non-biological microparticles, as well as fabricated microcapsules (Zhang et al., 1991; Zhang et al., 1992; Zhang et al., 1999; Hu et al., 2009). In micromanipulation, individual microparticle or microcapsule is compressed between two parallel surfaces, generating a corresponding force-displacement curve, which is used to investigate the deformation behaviour and rupture strength of single microcapsules, and to determine the Young's modulus with analytical models (Yan et al., 2009) or finite element analysis (Mercadé-Prieto et al., 2011). In addition, the micromanipulation technique enables the investigation of plastic, viscoelastic and elastic-plastic properties of single microcapsules by applying compression at different speeds, repeated compression, and loading and unloading (Zhang et al., 2009). Recently, a software package was developed to simplify the data analysis procedures and allow the automatic analysis of the mechanical strength parameters of microparticles from experimental data (Zhang et al., 2022), enhancing the capability of the micromanipulation technique.

2.3. Microencapsulation of flavour/fragrance oils

2.3.1. Flavour/fragrance oils

Flavours and fragrances are complex mixtures of volatile organic compounds, which include naturally occurring (e.g., essential oils) and synthetical aromatic molecules. Flavours and fragrances are constituted by a variety of organic compound classes, including hydrocarbons, alcohols, esters, aldehydes, ketones, terpenoids and artificial ingredients that are not presented in nature (Kłosowska et al., 2023). Naturally occurring aromas are extracted from plants (Tongnuanchan & Benjakul, 2014), and characterised with many bioactive properties

including anti-inflammatory, anti-bacterial, antioxidant and immunomodulatory activities (Burt, 2004; Falleh et al., 2020; Mediratta et al., 2002; Mimica-Dukić et al., 2003; Silva et al., 2015). Synthetic aromatic molecules are synthesised via chemical reactions with scents and aromas. Flavours and fragrances are widely employed as additives in different industrial products of food, beverage, perfume, cosmetics, personal care, laundry, household care, textile as well as pharmaceuticals (Franz, 2010; Madene et al., 2006). However, there are challenges associated with the application of various flavours and fragrances, since these highly volatile compounds can be thermally unstable and/or chemically reactive (Tekin et al., 2013). Flavours and fragrances may experience evaporation or reaction with other formulated ingredients during the manufacturing and/or storage process. Degradation or autoxidation may also occur if these compounds are exposed to light, heat and oxygen, or experience the variations in pH and humidity (Sousa et al., 2022). Therefore, flavours and fragrances have often been encapsulated to maintain their functional characteristics and achieve the controlled release. Moreover, microencapsulation can also facilitate the application of these oils by transforming their liquid state to solid phase, allowing precise dosing and easy handling.

2.3.1.1. Core oils

2.3.1.1.1. Carvone

Carvone is a monoterpene ketone which is produced by plants naturally and usually present in some essential oils with other terpenoids (Morcia et al., 2016). As a monoterpene, carvone has two enantiomeric forms: S-(+)-carvone (D-carvone) and R-(−)-carvone (L-carvone) as shown in Figure 2-9. D-carvone is the main component (60%-70%) of caraway seed oil and also occurs up to 60% in dill seed oil (Putievsky, 1993), while L-carvone constitutes a major

proportion (50%–80%) in spearmint (De Carvalho & da Fonseca, 2006). Although two enantiomers of carvone have similar chemical structures, they have different characteristic smells. L-carvone presents sweetish minty aroma whereas D-carvone has a mentholated odour (Leitereg et al., 1971). Both carvones are employed in a variety of industries due for their flavours and aromas, e.g., L-carvone is extensively used in food and beverage (Morcia et al., 2016), particularly in chewing gum and sugar products. It is also a key ingredient in the fragrance formulation of personal care products, notably air fresheners, toothpaste, soaps and detergents. However, D-carvone has fewer uses in industry. Despite of being a flavouring agent, it is reported that D-carvone can be used as an anti-sprouting agent to prevent the sprouting of potatoes in agriculture (Teper-bamnolker et al., 2010). Instead of D-carvone, L-carvone is selected considering it is more widely used for industrial applications. L-carvone (LC) also exhibits multiple pharmacological properties such as antibacterial, antifungal, antioxidant, anti-inflammatory and anticancer activities (Bouyahya et al., 2021; Friedman et al., 2002; Naigre et al., 1996; Plotto et al., 2003). Moreover, LC can work as insecticide in agriculture to control insects (Franzios et al., 1997). However, LC is highly volatile, thermosensitive and reactive, besides, LC has a relatively low molecule weight and polar molecular structure. These properties attribute to the processing difficulties for its industrial applications. Although several studies have been conducted to investigate the microcapsulation of L-carvone (Baiocco et al., 2021b; Koo et al., 2014; Partanen et al., 2002), the outcomes are not satisfying either due to their low encapsulation efficiency or the employed technique being not suitable for large industrial scales. Therefore, L-carvone is used for encapsulation by either melt dispersion or complex coacervation using biopolymers in this

project.

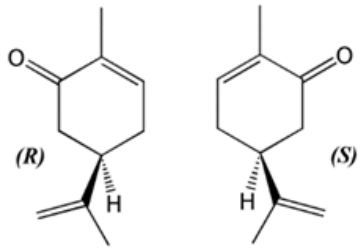

Figure 2-9. Chemical Structure of carvones.

2.3.1.1.2. Hexyl salicylate

Hexyl salicylate (HS) can be synthetically produced by esterification reactions, and employed for industrial use at a relatively cheap cost. HS is commonly used in cosmetics, fragrances, shampoos, household cleaner or detergent products due to its floral fruity character (Lapczynski et al., 2007). HS oil has an aromatic ring structurally as shown in Figure 2-10. Unlike LC, HS is a long-lasting and relatively stable fragrance material (Vecchiato et al., 2017), with its vapour pressure being less than 0.0001 mmHg at 20°C (Lapczynski et al., 2007). It is therefore chosen as a model oil to be encapsulated by melt dispersion or complex coacervation using natural biopolymers to compare the properties of LC laden microcapsules.

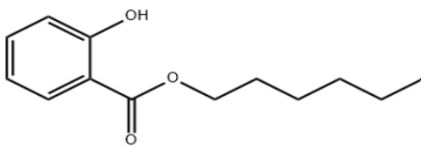

Figure 2-10. Chemical structure of hexyl salicylate.

2.3.1.2. Reference oils

2.3.1.2.1. Limonene

Limonene (LM) is a cyclic monoterpene occurring naturally in the essential oil from citrus fruit peels (Isac-García et al., 2016). It has two enantiomers: R-limonene and S-limonene, as illustrated in Figure 2-11. R-limonene has the characteristic smell of oranges while S-limonene presents a piny, turpentine-like odour (Hirai et al., 2022). This aroma has been proven harmless to human consumption and is widely used in cosmetic, food and beverage formulations (Ravichandran et al., 2018). Besides, Limonene also presents antimicrobial and anthelmintic effects, allowing this material to be used a biodegradable insecticide (Graebin et al., 2010). Similar to LC, LM is highly volatile and may easily undergo degradation when exposed to hostile conditions, such as heat, oxygen and light (Baiocco & Zhang, 2022).

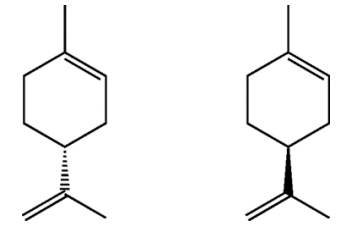

Figure 2-11. Chemical Structure of limonene.

2.3.1.2.2. Linalool

Linalool (LL) is a noncyclic monoterpenoid commonly extracted from many flowers and spice plants (Howe, 2020). It exists in two chiral enantiomers: R-linalool and S-linalool, as presented in Figure 2-12. R-linalool is perceived as a woody, lavender-like aroma naturally occurring in lavender and basil plants, whilst S-linalool exhibits sweet, floral, petitgrain-like

odour and constitutes as the major component in the essential oils of coriander (Mączka et al., 2022). This compound is widely used for commercial applications (Bickers et al., 2003), which include personal care products, fragrances, food additives as flavours and household care products. In addition, linalool also exhibits antimicrobial, antitumor, anxiolytic and cardio-protective effects (Saeed et al., 2023). Similar to LC, LL is highly sensitive to oxygen and can be readily degraded. Besides, LL has a relatively high-water solubility of 1.59 mg/mL at 25 ℃ compared to LC of 1.31 mg/mL at 25 ℃, indicating both materials are relatively polar oil molecules.

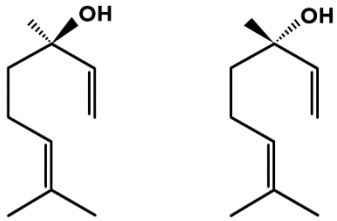

R-linalool S-linalool

Figure 2-12. Chemical Structure of linalool.

2.3.1.2.3. Carvacrol

Carvacrol (CV) is a phenolic monocyclic monoterpenoid naturally derived from aromatic plants mainly including oregano, thyme and wild bergamot (Sharifi-Rad et al., 2018). This compound exhibits more potent antimicrobial, antioxidant and anticarcinogenic properties than other essential oil components due to the presence of the hydroxyl group (Imran et al., 2022), as shown in Figure 2-13. It is also used as a preservative in food industry due to its flavour and its inhibiting ability for food borne bacterial growth.

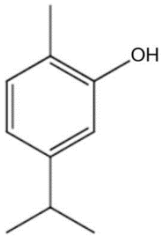

Figure 2-13. Chemical Structure of carvacrol.

2.3.1.2.4. Cinnamaldehyde

Cinnamaldehyde (CD) is a phenylpropanoid naturally biosynthesised by the shikimate pathway (Gutzeit & Ludwig-Müller, 2014), which is a multi-step metabolic process for the biosynthesis of folic acids and aromatic amino acids within bacteria, fungi, algae and plants cells (Herrmann & Weaver, 1999). This compound molecule consists of an aromatic ring attached to an unsaturated aldehyde, as shown in Figure 2-14. Cinnamic aldehyde appears as a pale-yellow viscous liquid and exhibits a sweet spicy and cinnamon-like odour, which can be extracted from the bark of cinnamon trees and other species of the genus Cinnamomum. Cinnamaldehyde presents several biological properties, including anti-inflammatory, antimicrobial, antioxidant, antitumor and immunomodulatory effects (Pandey et al., 2022) and has also been widely used in food applications (Lin et al., 2013).

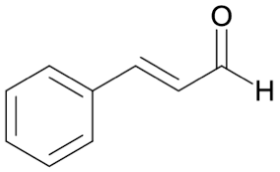

Figure 2-14. Chemical Structure of cinnamaldehyde.

2.3.1.3. Oil properties

The different physical properties of each oil are summarised in Table 2-3.

Table 2-3. The physical properties of core and reference oil (Domaraju & Lakshmi, 2012; ECHA, 2023a;2023b; Imran et al., 2022; Lapczynski et al., 2007; Li et al., 2022; Luo et al., 2023; PubChem, 2023a;2023b;2024a;2024b;2024c; sigma-Aldrich, 2023a;2023b;2023c;2023d;2023e; Wang et al., 2016).

Properties	LC	HS	LM	LL	CV	CD
Density (g/ml) at 25 °C	0.96	1.04	0.84	0.87	0.98	1.05
Molecular Weight (g/mol)	150.22	222.28	136.23	154.25	150.22	132.16
LogP	2.71	4.87	4.57	2.97	3.49	1.90
Vapour pressure (mm Hg) at 25 °C	0.115	1.98	< 0.0001	0.16	0.0296	0.0289
Viscosity (mPa.s)	4.38	10.0	0.85	4.46	28.50	22.12

2.3.2. Encapsulation of core oils

Tasker et al. (2016) encapsulated hexyl salicylate in poly (methyl methacrylate) with hexadecyltrimethylammonium bromide as an emulsifier via solvent evaporation. They focused only on the morphology of microcapsules without characterising oil encapsulation efficiency or the mechanical properties of microcapsules. The microencapsulation of hexyl salicylate, on the other hand, was extensively investigated using formaldehyde-based material as a shell via in situ polymerization (He et al., 2019; Long et al., 2009; Luo et al., 2022; Mercadé-Prieto et al., 2012a). The properties of the microcapsules such as morphology, size

and size distribution, shell thickness and permeability, mechanical strength, and encapsulation efficiency were comprehensively studied. However, these materials used for hexyl salicylate encapsulation are synthetic plastic based, which limits the universal application of this type of microcapsules. Instead, Baiocco et al. (2021a) encapsulated hexyl salicylate using biopolymers based on the complex coacervation between chitosan and gum arabic. Although the coacervated microcapsules were reported to have similar mean size and mechanical properties to melamine formaldehyde microcapsules, the encapsulation efficiency (47%) was significantly lower than the formaldehyde-based microcapsules prepared by Luo et al. (2022) and Long et al. (2009), which had an encapsulation efficiency up to 89 % and 75 % respectively.

Partanen et al. (2002) investigated the encapsulation of carvone by molecular inclusion, and found that the complexes of carvone in β-cyclodextrin exhibited good performance against core evaporation and showed superior storage property at higher relative humidities than spray dried maltodextrin-based microcapsules. However, molecular inclusion was not widely used due to the regulatory restrictions in several countries (Desai & Jin Park, 2005). Besides, the high cost of cyclodextrins and low core loading capacities due to the stoichiometry of cyclodextrin molecules are inevitable problems limiting the application of this process (Reineccius, 1989). Koo et al. (2014) encapsulated peppermint oil using a coaxial electrospray system based on the gelation between calcium ions and alginate pectin mixture. Core-shell structured microcapsules were fabricated, with core oil encapsulation efficiency varying from 27 to 85 %, which was attributed to the alginate to pectin ratio. However, such process has an inevitable drawback due to its slow rate to fabricate the microcapsules. Baiocco et al. (2021b)

encapsulated L-carvone via complex coacervation by using fungal chitosan and gum arabic as wall materials, followed by spray drying. The physical, structural, morphological, mechanical and barrier properties of the fabricated microcapsules were systematically investigated for their potential for personal care and cosmetic products. However, L-carvone encapsulation efficiency and the payload of the fabricated microcapsules were only 29 ± 4 % and 19 ± 3 % respectively. Comparatively, Pakzad et al. (2013) fabricated peppermint oil microcapsule with encapsulation efficiency up to 82% by using gelatine and gum arabic coacervates as shell material. Dong et al. (2007) investigated the effects of different peppermint oil to gelatine and gum arabic ratios on core oil loadings of the microcapsules, and obtained the highest payload (90%) using the ratio of 6:1.

Gelatine is produced by partial hydrolysis of collagen derived from skin, bones and connective tissues of animals (Napiórkowska & Kurek, 2022a; Sutaphanit & Chitprasert, 2014). It is a commonly used coacervation material due to its good emulsifying and gelling ability, biodegradability and biocompatibility, nontoxicity and low cost (Elzoghby, 2013; Muhoza et al., 2022). Gum arabic is a natural polysaccharide derived from Acacia senegal and Acacia seyal trees (Xiao et al., 2014b), and mainly consists of arabinogalactan and glycoprotein (Napiórkowska & Kurek, 2022a). It has a backbone structure of 1,3-linked β-d-galactopyranosyl units branched with galactose side chains by 1,6-linkages (Ali et al., 2009). arabic gum has high solubility in water while low viscosity in solution, making this material an effective emulsifier and good encapsulating agent (Devi et al., 2017; Napiórkowska & Kurek, 2022b). Due to the abundance, biocompatibility and biodegradability of these wall materials (Reis et al., 2022), the most common wall system used for complex coacervation is

gelatine/gum arabic (Bakry et al., 2016; Ogilvie-Battersby et al., 2022; Shaddel et al., 2018; Yang et al., 2015), which form coacervate wall by the electrostatic interactions between amino groups of protein and carboxyl groups of polysaccharides. The encapsulation of flavours and fragrances by gelatine and gum arabic microcapsules were also extensively studied by other authors (Lv et al., 2014; Ogilvie-Battersby et al., 2022; Pakzad et al., 2013; Xiao et al., 2014b; Zuanon et al., 2013). Core oils including lavender oil, jasmine essential oil, peppermint oil, geraniol and turmeric oleoresin were encapsulated with encapsulation efficiency ranging from 66% to 82%, and the microcapsules showed good thermal properties. However, no research had focused on the mechanical properties of these gelatine/gum arabic microcapsules. Yu et al. (2021) characterised the mechanical properties of gelatine/gum arabic microcapsules when encapsulating functional fish oil. The Young's modulus of whole microcapsules was determined to be 313 ± 42 MPa by the Hertz model. The rupture force increased with microcapsule diameter, with an average value of 0.58 ± 0.10 mN for the mean diameter of 10.8 ± 0.9 μm. The corresponding nominal rupture stress was 6.1± 0.6 Mpa and encapsulation efficiency was 89 ± 1 %, which are higher to chitosan-gum arabic coacervated microcapsules fabricated for L-carvone encapsulation by Baiocco et al. (2021b), which had a nominal rupture stress of 2.1 ± 0.3 Mpa and encapsulation efficiency of 29 ± 4 %. Nevertheless, gelatine is limited in its use in several food and beverage applications due to its animal origin and potential allergenic risk. However, the review of these literature works implies that gelatine and gum arabic have the potential to be more promising wall materials than chitosan and gum arabic to fabricate flavours and fragrances microcapsules with higher encapsulation efficiency and stronger mechanical properties. These gelatine/gum arabic microcapsules may still be

appliable in some products of household care, laundry or cleaning detergent instead of food and beverage. Furthermore, to the best of author's knowledge, no systematic study has been conducted to characterise the fundamental physical and mechanical properties of gelatine and gum arabic microcapsules to encapsulate flavours and fragrances. Besides, it has been reported that different types of core oil have shown significantly different morphologies, particle size distribution, encapsulation efficiency and mechanical properties of microcapsules, which had been fabricated following the same experimental procedure and material formulations (Luo et al., 2023; Zhao et al., 2021). Therefore, although the properties of gelatine/gum arabic microcapsules (fabricated for fish oil encapsulation) were characterised by Yu et al. (2021), the microencapsulation of flavours and fragrances (L-carvone and hexyl salicylate in this project) based on the coacervation between gelatine and gum arabic as well as the comprehensive characterisation of the resultant microcapsule properties still remain to be explored.

In addition, melt dispersion is also an attractive encapsulation technique to encapsulate flavours and fragrances for its possible scalability for industrial applications. Kumar et al. (2014) encapsulated Mentha piperita (peppermint) essential oil via melt dispersion using polyethylene glycol 6000 as coating material. The encapsulation efficiency of the fabricated nanoparticles was up to 83.4%, with payload of 7.46%. Differential scanning calorimetry analysis indicated the improved thermal stability of polyethylene glycol 6000 after Mentha piperita essential oil was encapsulated within nanoparticles. However, polyethylene glycol 6000 is a synthetic polymer and have been reported to have lower mechanical properties compared to natural waxes including carnauba wax and beeswax (Al-Angari et al., 1985;

Morgan et al., 2002; Zhang et al., 2016). Milanovic et al. (2010) encapsulated ethyl vanillin using carnauba wax as wall material by a novel melt dispersion technique. The fabricated microspheres were determined to have an encapsulation efficiency up to 87 % (payload at 8.7 ± 0.6 %) and exhibit good thermal stability. Different commercial flavour oils (caramel, coconut or cherry) were also encapsulated within carnauba wax carriers that presented inconsistent release behaviours under heating, suggesting the binding mechanism of the aromatic compound in the wax could possibly be influenced by the characteristics of core oil (including polarity and volatility) and the different molecule interactions between core oil and wax. Milanovic et al. (2017) mixed beeswax with carnauba wax at different ratios, investigated the effects of different waxes ratios on the thermal behaviour of ethyl vanillin laden microspheres, and demonstrated the potential feasibility of using the blend of natural waxes as shell materials for the encapsulation of flavours and fragrances. However, there is no comprehensive study of the fundamental physical, barrier and mechanical properties of wax microcapsules for encapsulation of other flavour and fragrance oils by melt dispersion. The influence of different wax types, wax to oil ratios on the properties of the wax microspheres also remains to be fully explored to understand the aroma molecule encapsulation mechanism by wax carriers.

2.3.3. Core oil influence on encapsulation

Limited works have placed emphasis on the influence of different oils on the properties of the microcapsules. Baiocco and Zhang (2022) encapsulated limonene via complex coacervation using gum arabic and fungally fermented chitosan as shell materials. The fabricated microcapsules exhibited significant different properties (including size and size distribution,

encapsulation efficiency and payload, and mechanical strength) compared to the L-carvone or hexyl salicylate laden microcapsules prepared following the identical wall material formulations and encapsulation process (Baiocco et al., 2021a;2021b). Xiao et al. (2014b) investigated the encapsulation of lavender oil by complex coacervation using gum arabic and gelatine at equal portions and a wall to core ratio of 2:1, and the fabricated microcapsules had a mean size of 77 μm and oil encapsulation efficiency of 37%. Significant variables in terms of morphology, size, encapsulation efficiency, thermal stability as well as release profiles were reported by Ogilvie-Battersby et al. (2022) and Manaf et al. (2018) using the same wall material formulations and experimental procedures for the encapsulation of geraniol and citronella oil respectively. Also, Tang et al. (2020) used gelatine and sodium alginate to encapsulate limonene and the fabricated microcapsules showed significantly different properties (including morphology, mean size and encapsulation efficiency) compared to citronella oil loaded microcapsules prepared with the same encapsulation method (De Matos et al., 2018). Besides, similar phenomena were reported for the encapsulation of cinnamaldehyde and peppermint oil using high methyl pectin and gelatine as wall materials at a ratio of 1:3 and a wall to core ratio of 1:2 (Muhoza et al., 2019).

Goubet et al. (1998) discussed the retention of various core aromas within the identical carbohydrate shell material by spray drying, which was primarily affected by the molecular weight, relative volatility and polarity of the volatile compounds. Rosenberg et al. (1990) found that ethyl hexanoate was more efficiently encapsulated than ethyl butyrate within spray dried gum arabic matrix microparticles and similar phenomena were also reported by Voilley (1995), that higher molecular weight aroma compounds had better retention performance.

Reineccius (1988) explained lower molecule weight aroma compounds diffuse through wall matrix more readily, leading to a poor retention of the encapsulated active. Bangs and Reineccius (1982) related the retention of octanol, octenol, octanone, and octanal with their corresponding relative volatility when these compounds were encapsulated within maltodextrins by spray drying, and reported that the volatile aroma compound with a higher relative volatility exhibited a lower encapsulation efficiency, which was coincident with the results reported by Saravacos and Moyer (1968) that the retention of aromas was negatively affected by the relative volatility during vacuum drying. Besides, Rosenberg and Sheu (1996) found that the retention of ethyl butyrate (which is partially water soluble due to its polarity) using whey proteins as wall materials by spray drying, was lower than ethyl caprylate that has lower polarity.

Similar to the encapsulation of volatile compounds by spray drying, Hofmeister et al. (2015) encapsulated several volatile aroma compounds via polymerisation method using acrylic copolymer. They pointed out that the Hansen parameter for hydrogen bonding (δ_H) revealed a linear relationship with encapsulation efficiency negatively, which allowed the predication of encapsulation efficiency for any core materials and enhancing the encapsulation efficiency by introducing a mediator with lower δ_H value. Zhao et al. (2021) investigated the influence of the interfacial tension between core oil and water, the relative dielectric constant, the refractive index, the viscosity and the density of nine different commercial fragrance oils on the encapsulation efficiency of microcapsules prepared using melamine formaldehyde as shell materials via in situ polymerisation. They reported that the interfacial tension between core oil and water determined whether the core oil is suitable for encapsulation. Other factors

including the relative dielectric constant, refractive index, the viscosity and the density of core oils had an auxiliary effect on the particle size and distribution of microcapsules. However, the core oils used in their study were commercial fragrance oils and their detailed compositions were not reported. Following the same encapsulation method, Luo et al. (2023) evaluate the effects of the chemical structure, logP, the solubility, the interfacial tension between core oil and water and the viscosity of twelve different single componential oils on melamine formaldehyde microcapsules in terms of size, morphology, encapsulation efficiency as well as thermal and mechanical properties. They pointed out that logP can be used as a clear determining criterion to choose core oils for successful encapsulations, which requires logP being $\geqslant$ 1.66. logP also influenced the capsule size and mechanical strength. High interfacial tension between oil and water improved the encapsulation efficiency. However, the author focused only on the melamine formaldehyde resin encapsulation system, and more wall materials and encapsulation techniques should be investigated to establish the universal applicability of the aforementioned findings. Moreover, they did not go further by investigating the mechanism underlying the influence of core oil on microcapsule properties.

Torza and Mason (1970) studied the engulfing mechanism when two immiscible phases were brought in contact in a third mutually immiscible phase, and first proposed a theory about the spreading behaviour based on the interfacial tensions between the three phases. This theory was referred as the spreading coefficient theory and it elaborated the occurring of spreading, lens or engulfing was a result of thermodynamic equilibrium determined by the spreading coefficient of each phase. In the case of encapsulation when oil, water and polymer phases are involved, the spreading coefficient theory can be used for predicting the structural

morphologies of formed capsules (Loxley & Vincent, 1998). Furthermore, the microstructural morphology of microcapsule has been reported to have a significant impact on the encapsulation efficiency (Yun et al., 2021), owing to the various inner structures and porosities of microcapsules. Therefore, the spreading coefficient theory might provide a potential perspective to investigate the mechanism underlying the influence of core oil on the properties (including morphology, encapsulation efficiency, mechanical properties or core oil release behaviour) of microcapsules fabricated using the consistent wall formulation.

2.4. Summary

This chapter provides a general introduction of microencapsulation and the resultant microcapsules with typical structural configurations. The main encapsulation methods and the analytical techniques to characterise microcapsules are also reviewed, with their own principles, merits, and drawbacks. The microencapsulation of flavours and fragrances is highlighted herein, following by literature reviews about the encapsulation of model flavour and fragrance (L-carvone and hexyl salicylate) as well as the impact of different oils on the properties of microcapsules fabricated using the same wall formulations and experimental procedure.

The current challenges in the microencapsulation of flavours and fragrances include lack of simple, universal and scalable industrial encapsulation methods to fabricate high-quality microcapsules and the fabrication of biodegradable microcapsules with desirable properties for the end-use applications. For example, spray drying is the most widely used encapsulation method in industry and it allows simple, reproducible, continuous and low-cost production of flavour/fragrance microcapsules. However, this process may cause the evaporation and/or

degradation of core materials due to the high temperature. Solvent evaporation is a fast, simple, reproducible encapsulation method, while this process usually involves the use of plastic-based synthetic polymers and fabricates flavour/fragrance capsules of low encapsulation efficiency. Polymerisation has been extensively investigated for its efficient encapsulation of flavours and fragrances, but the synthetic polymers used as microcapsule shells are usually formaldehyde-based and not biodegradable. On the contrary, melt dispersion technique is a simple, readily scalable encapsulation method for industrial applications. This process has been reported for the encapsulation of synthetic aroma with high encapsulation efficiency and good thermal stability using natural wax, making melt dispersion a promising method. Complex coacervation is an effective and well-established method for the encapsulation of flavours and fragrances using biopolymers. However, the recent development of this process based on coacervation of fungal chitosan and gum arabic did not give satisfactory encapsulation efficiency of costly flavours and fragrances (i.e., L-carvone and hexyl salicylate). On the contrary, gelatine-based microcapsules have been reported to exhibit high encapsulation efficiency, thermal stability and mechanical properties for the encapsulation of flavours and fragrances. Although gelatine is animal-sourced and unpreferred for a certain group of people, it still has potential to be used in the encapsulation of flavours and fragrances for applications in household care, laundry or cleaning detergent instead of food and beverage. Comparatively, used as coating materials via melt dispersion, natural waxes of food grade look attractive if their effective encapsulation of L-carvone and hexyl salicylate can be achieved.

To the best of author’s knowledge, no systematic study using either gelatine/gum arabic microcapsules fabricated via complex coacervation or wax microspheres prepared via melt

dispersion for the encapsulation of L-carvone and hexyl salicylate have been reported in literature. Effective encapsulation of these two model oils and characterisation of their various properties, including size distribution, encapsulation efficiency and mechanical properties (which are strictly related to their effectiveness for the end-use applications) is the primary objective of this PhD project. Another goal of this work is to investigate and understand the impact of different oils on the properties of microcapsules fabricated using the same wall formulations and experimental methods.

CHAPTER 3. Microencapsulation of L-Carvone and Hexyl Salicylate in Carnauba Wax, Candelilla Wax and Beeswax by Melt Dispersion Method

3.1. Introduction

Wax microparticles have been evaluated for encapsulation of flavours, mainly focusing on their physicochemical and structural properties, such as particle size, morphology, leakage and thermal stability (Collins et al., 2020; Milanovic et al., 2010; Stojaković et al., 2012; Yilmaztekin et al., 2019). However, little is known about the mechanical properties of oil-loaded wax microspheres. In this chapter, beeswax (BW), candelilla wax (CanW) and carnauba wax (CarW) were used to encapsulate L-carvone (LC) or hexyl salicylate (HS) with different oil and wax formulations at variable weight ratios using melt dispersion technique. Both fundamental physical properties including morphology, particle size and distribution as well as mechanical properties (nominal Young's modulus) of microspheres, oil encapsulation efficiency and its retention within wax carriers at an air-dried storage condition (60 ± 2% humidity at 25 ± 2 °C) were investigated. These experimental results not only contribute to a better understanding of oil-loaded wax microspheres from the perspective of mechanical properties but also provide guidance for their further processing for potential industrial applications.

3.2. Materials and methods

3.2.1. Materials

L-carvone (⩾97%, FCC, FG), hexyl salicylate (⩾99.0%, GC), carnauba wax (No. 1 yellow,

refined, Brazil wax), candelilla wax, beeswax (refined) and tween 60 (polysorbate 60) were all purchased from Sigma–Aldrich, UK. Reagents including absolute ethanol and 1-propanol were purchased from Sigma-Aldrich, UK, and were of analytical grade and used without further purification. All the solutions were prepared using deionised water (18.2 MΩ cm at 25 ° C).

3.2.2. Preparation of wax microspheres

The matrix microspheres were prepared by a modified melt dispersion method (Bhoyar et al., 2011; Milanovic et al., 2011; Milanovic et al., 2010). The wax (5.4 g of each type of wax) was melted in deionised water (150 ml) containing an emulsifier (0.5% w/w tween 60 (Zhang et al., 2016)) at a maintained temperature (95 °C for CarW, 75 °C for CanW, and 70 °C for BW) in a jacketed beaker of 250 ml in volume.

The core oil (L-carvone or hexyl salicylate) was added to the dispersion phase at different oil to wax ratios (1:1，1:5 and 1:10) by weight followed by homogenisation (1200 rpm) by a high shear mixer (Model L4RT, Silverson, UK) for 20 mins. During the homogenisation, the jacket beaker was covered with aluminium foil. After homogenisation, the resultant emulsion was transferred to a preheated beaker of 500 ml in volume and kept under machinal stirring at 400 rpm for 5 mins. The solidification of oil phase to encapsulate core oil and the formation of wax oleogel microspheres were accomplished by adding 300 ml cold water (0 °C) to the emulsion system and keeping stirring for further 5 min. Wax microspheres were obtained by filtration under vacuum, washed with deionised water and dried at room temperature (25 ± 2 ° C) for 24 h. As control samples, pure wax microspheres (containing no oils) were also prepared following the same procedure. The procedures of wax microsphere preparation were

illustrated in Figure 3-1.

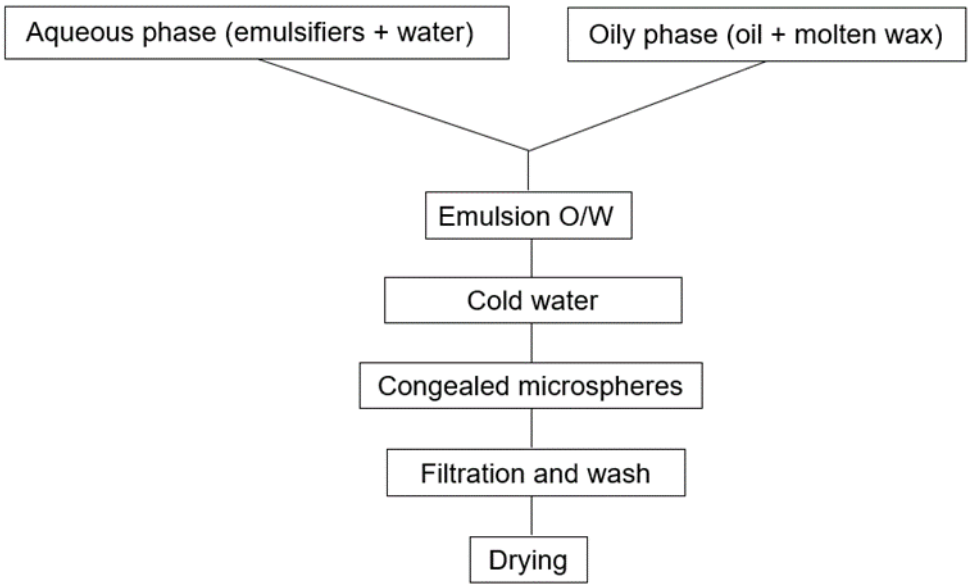

Figure 3-1. Schematic diagram of the encapsulation of core oils via melt dispersion.

Different ingredients and formulations are listed in Table 3-1. Based on the oil to wax ratios, candelilla wax, carnauba wax and beeswax microspheres are denoted by CanW, CanWLC11, CanWLC15, CanWLC110, CanWHS11, CanWHS15, CanWHS110, CarW, CarWLC11, CarWLC15, CarWLC110, CarWHS11, CarWHS15, CarWHS110, BW, BWLC11, BWLC15, BWLC110, BWHS11, BWHS15 and BWHS110 respectively. Each experiment was conducted in triplicate.

Table 3-1. The ingredients used to prepare LC and HS wax microspheres. The amount of wax was kept at 5.4 g, but different amounts of core oil (0.54-5.4 g) were used to prepare LC and HS wax microspheres.

Sample	Candelilla wax	Carnauba wax	Beeswax	Core Material	Oil/Wax ratio
Pure CanW	5.4 g	0 g	0 g	0 g	_
CanWLC11	5.4 g	0 g	0 g	LC 5.4 g	1:1
CanWLC15	5.4 g	0 g	0 g	LC 1.08 g	1:5
CanWLC110	5.4 g	0 g	0 g	LC 0.54 g	1:10
CanWHS11	5.4 g	0 g	0 g	HS 5.4 g	1:1
CanWHS15	5.4 g	0 g	0 g	HS 1.08 g	1:5
CanWHS110	5.4 g	0 g	0 g	HS 0.54 g	1:10
Empty CarW	0 g	5.4 g	0 g	0 g	_
CarWLC11	0 g	5.4 g	0 g	LC 5.4 g	1:1
CarWLC15	0 g	5.4 g	0 g	LC 1.08 g	1:5
CarWLC110	0 g	5.4 g	0 g	LC 0.54 g	1:10
CarWHS11	0 g	5.4 g	0 g	HS 5.4 g	1:1
CarWHS15	0 g	5.4 g	0 g	HS 1.08 g	1:5
CarWHS110	0 g	5.4 g	0 g	HS 0.54 g	1:10
Empty BW	0 g	0 g	5.4 g	0 g	_
BWLC11	0 g	0 g	5.4 g	LC 5.4 g	1:1
BWLC15	0 g	0 g	5.4 g	LC 1.08 g	1:5
BWLC110	0 g	0 g	5.4 g	LC 0.54 g	1:10
BWHS11	0 g	0 g	5.4 g	HS 5.4 g	1:1
BWHS15	0 g	0 g	5.4 g	HS 1.08 g	1:5
BWHS110	0 g	0 g	5.4 g	HS 0.54 g	1:10

3.2.3. Particle size analysis

Before filtration and drying, the mean size and size distribution of wax matrix microparticles

in suspension were measured by using a light scattering instrument (Mastersizer 2000, Malvern Instruments Ltd, UK) with the Mastersizer 2000 software. The measurements were aligned by a reference refractive index of 1.472 for carnauba wax, 1.454 for candelilla wax and 1.434 for beeswax microspheres respectively (Rhim & Shellhammer, 2005). The refractive index of water was set at 1.330. The mean diameter and size distribution of wax particles were measured in triplicate with a two-minute interval between each measurement. The values of Sauter mean diameter $D_{[3,2]}$ and SPAN were recorded, which are defined as follows (Pan et al., 2013),

$$D_{[3,2]} = \frac{\sum_{i=1}^{N} d_i^3}{\sum_{i=1}^{N} d_i^2} \quad (3\text{-}\mathbf{1})$$

$$SPAN = \frac{D_{90\%} - D_{10\%}}{D_{\ 50\%}} \quad (3\text{-}\mathbf{2})$$

where d_i represents the diameter of an individual particle and N is the total number of particles measured; $D_{90\%}$, $D_{50\%}$ and $D_{10\%}$ represent the diameter of particles under which the accumulative volume fraction is 90%, 50% and 10% respectively.

3.2.4. Morphological characterisation of wax microspheres

Morphological characterisations were performed by a scanning electron microscope (Hitachi TM3030 Tabletop). Each kind of dried wax microspheres were tapped on an adhesive carbon tab attached on a steel specimen stub. Wax microsphere samples were coated with platinum by using a sputter coater (Quorum SC7620) in order to make the targets electrically conductive so that high resolution images can be obtained. All the measurement were operated at an acceleration voltage of 15 kV.

3.2.5. Fourier transform infrared spectroscopy (FT-IR) of core oils, waxes and dried wax microspheres

The FT-IR analysis of LC, HS, waxes and all solid powdered wax microspheres were performed using an ATR-FTIR spectroscopy (Bruker TENSOR 27) in attenuated total reflection mode. Running at an average of 256 scans, all spectra of samples were recorded with an infrared wavelength from 4000 to 400 cm^{-1} at a resolution of 4.0 cm^{-1} with the compliance of background (blank) running at the same scanning parameters. This analysis was performed using the Bruker OPUS software.

3.2.6. Payload and encapsulation efficiency

Based on the peak absorbance wavelength of HS in 36% (w/w) 1-propanol (306 nm) and LC in absolute ethanol (319 nm), a linear standard calibration curve between UV absorbance readings (y) and oil concentrations (x) in 20 ml solvent was generated, $y = 21.286x + 0.0314$ with a coefficient of determination $R^2 = 0.9994$ for HS oil (See Figure A-1 in Appendix A) and $y = 0.2867x + 0.0075$ with a coefficient of determination $R^2 = 0.9985$ for LC oil (See Figure A-2 in Appendix A). The equations obtained from the calibration curves were further used to determine the amount of encapsulated oils in wax microspheres by a UV-Vis spectrophotometer (Cecil 1020, Cecil Instruments, UK) (Baiocco et al., 2021a).

Three types of 20 mg air-dried wax microspheres loaded with oil were firstly placed into three different screw capped glass vials, and then dispersed into 20 mL of 36% aqueous 1-propanol or absolute ethanol as the solvent for HS or LC oil. The vials were ultrasonicated in a water bath (VWR Ultrasonicator, USC100TH, UK) for 60 min to extract the core oil. The insoluble

waxy residues were removed by centrifugation (Hermle Labortechnik Z-180, Labnet, Germany, EU) at 10,000 rpm (12298 g force) for 30 mins to produce a clear supernatant containing LC or HS. The supernatant was diluted in a quartz cuvette 10 times using a solvent prior to measurement. The encapsulation efficiency (EE) and payload of wax microspheres were then calculated by the following equations:

$$Payload_{\%} = \frac{Encapsulated\ oil}{Total\ mass\ of\ particles} \times 100 \quad (3\text{-}\mathbf{3})$$

$$EE_{\%} = \frac{Encapsulated\ oil}{Total\ oil} \times 100 \quad (3\text{-}\mathbf{4})$$

Pure wax particles were also measured following the same procedures, to avoid the absorbance influence from waxes in the solvent. And the corrected absorbance (λ) of encapsulated oil was calculated by the following formula:

$$\lambda_{Encapsulated\ oil} = \lambda_{UV} - \lambda_{wax\ influence\ in\ solvent} \quad (3\text{-}\mathbf{5})$$

3.2.7. Measurement of oil retention in wax microspheres

Core oil release studies were performed within a period of 32 days, the dried wax microspheres were kept in beaker vials at 25 ± 2 °C, 60 ± 2% humidity and sampled at 0 d, 1 d, 2 d, 4 d, 8 d, 16d and 32 d respectively. Wax particles were measured following the procedures described in 3.2.6. All experiments were conducted in triplicate. The static cumulative release of oil from wax particles was determined by the following formula:

$$R_t = P_0 - r_t \quad (3\text{-}\mathbf{6})$$

where R_t represents the oil released from wax in time t, P_0 is the payload of wax microspheres at 0 d, and r_t is the retention amount of oil within the wax microspheres in percentage at time t.

3.2.8. Mechanical characterisation of wax microspheres

3.2.8.1. Micromanipulation

The mechanical properties of wax microspheres were characterised by a micromanipulation technique as shown in Figure 3-2, which was firstly developed at the University of Birmingham UK (Zhang et al., 1991; Zhang, 1999; Hu et al., 2009). A single fine glass probe about 60 μm in diameter with a polished flat end surface was glued on a force transducer (GS0-10, Sensitivity 8.674 mN V^{-1}, LLC, Temecula, CA, USA), and the probe was positioned perpendicular to the glass slide, which was mounted on the stage of a micromanipulation rig. Dried wax particles were spread on the glass slide and observed from the side view camera, which was also used to measure the diameter of selected wax particles and record the process of compression. The wax microspheres were compressed at 2 μm/s speed by the glass probe driven by the stepper motor. At least 30 wax microspheres from each sample were randomly selected for compression. Compliance tests were performed in triplicate prior to testing each wax particle sample, and their mean value was used to calculate the actual displacement of the force probe (Zhang. et al., 2022).

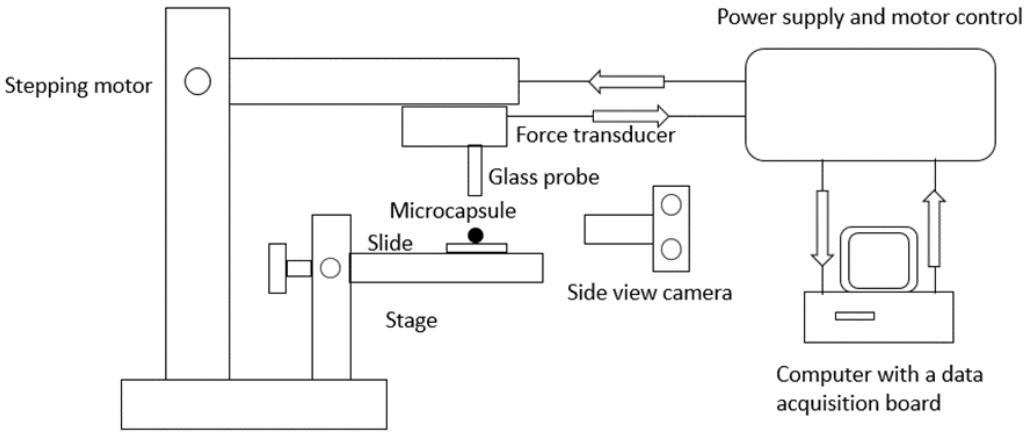

Figure 3-2. Schematic diagram of the micromanipulation rig.

Figure 3-3 presents a typical compression process for an individual wax microsphere before and after compression using a micromanipulation rig. The voltage signals generated by the force transducer due to compression were simultaneously recorded by the computer with a data acquisition card installed in it. The compression force could be calculated based on the sensitivity of force transducer and change in voltage recorded by the data acquisition card. From the curve of compression force versus displacement of glass probe, the relationship between the force and the particle deformation could be obtained using a data analysis software package as reported by Zhang et al. (2022).

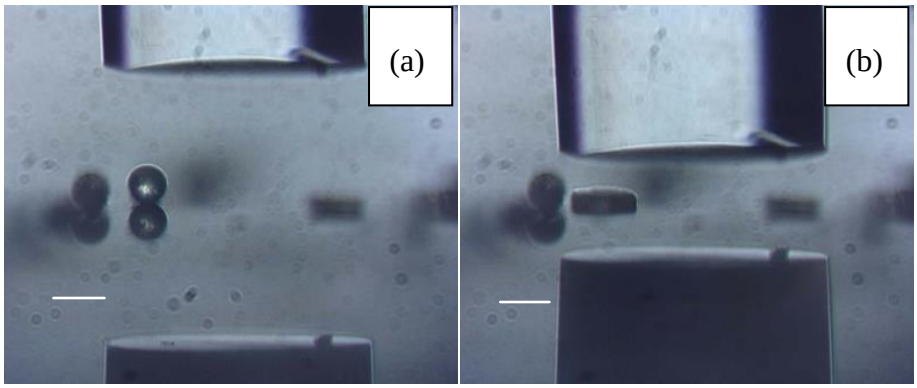

Figure 3-3. Images of a single wax microsphere (15.5 μm in diameter, CarWHS15) before compression (a) and after compression (b) (scale bar: 20 μm)

3.2.8.2. Hertz model

The Hertz model presents the relationship between the force for compressing a single linear elastic spherical particle to small deformations (usually less than nominal strain 10%) and its displacement between two rigid flat planes, and is described by Equation (3-7) (Yan et al., 2009; Zhang et al., 2009):

$$F = \frac{E\sqrt{2R}}{3(1-\upsilon^2)}\delta^{\frac{3}{2}} \qquad (3\text{-}7)$$

where F is the compression force, δ is the displacement, R is the particle radius, υ is the

Poisson's ratio, E is the Young's modulus of the wax particle. According to the model, there should be a linear relationship between F and $\delta^{\frac{3}{2}}$, and the value of Young's modulus can be determined by fitting the force-displacement data in elastic range (usually up to 10% of nominal strain) to Equation (3-7) if Poisson's ratio υ is known. In this study, the Poisson's ratios of all samples were assumed to be 0.5 since the wax microspheres were considered to be incompressible.

3.2.9. Statistical analysis

Three independent replicates for each experiment were performed. The difference among the results was expressed as mean value ± 2 × standard error (St.Err).

3.3. Results and Discussion

3.3.1. Morphology of microspheres

SEM micrographs of wax microspheres without oil encapsulated are presented in Figure 3-4. It can be observed that wax microspheres prepared by different waxes via melt dispersion are in micro-size and relatively spherical, but have variable surface smoothness. Specifically, CarW microspheres have relatively smooth surface, which are similar to the morphology of carnauba wax microspheres fabricated by Milanovic et al. (2010) for the encapsulation of ethyl vanillin. The CanW particles appear to have a scaly and nonporous surface. Microspheres prepared by BW have less smooth surface, with flaky and porous appearance as compared to those prepared by two other waxes. Similar phenomena were reported by Milanovic et al. (2017), that the surface of pure beeswax particles was rougher and had more irregularities than the surface of CarW microspheres. They explained that the difference in surface smoothness can be attributed to the slower solidification rate of molten beeswax

(melting temperature 70 °C) than carnauba wax (melting temperature 95 °C) in contact with 0 °C cold water during the formation of wax microspheres.

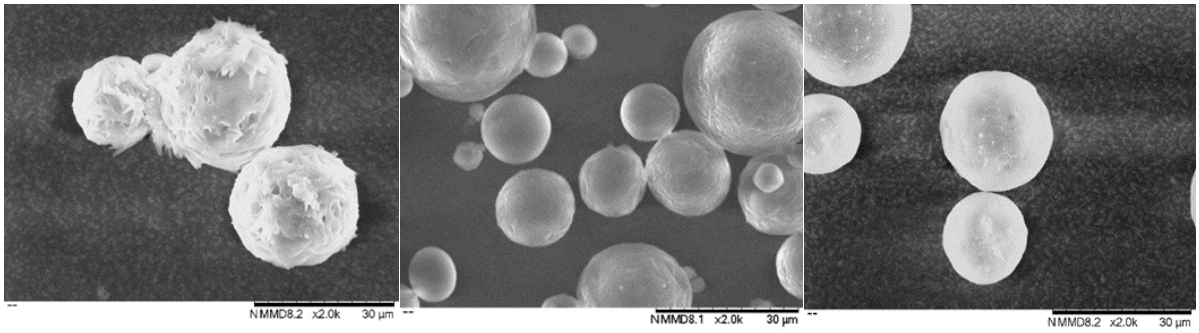

(a) (b) (c)

Figure 3-4. SEM images of wax microspheres without oil loadings (a) BW, (b) CanW, (c) CarW.

It was found that BW microspheres with various oil loadings dissolved on the adhesive carbon tab for SEM, and practically difficult for observation. Thus, only CarWHS and CarWLC samples were morphologically characterised by SEM and their images are presented in Figure 3-5. The pores on the surface of CarWHS11 microspheres can be observed while CarWHS15 and CarWHS110 have relatively smooth surface. Similar phenomena were also detected for CarWLC samples, suggesting that the surface of wax microspheres becomes rougher with the increase of oil to wax ratio. For 1:1 oil to wax ratio wax microspheres, more small holes were observed on the surface, indicating the acorn structure (see Figure 5-1), which implies that the retention of core oil by wax carriers can possibly be accomplished by the migration of small oil droplets into wax crystal networks from wax surface to its inner structure (Schubert & Müller-Goymann, 2005). This can be supported by the report of Ranjha et al. (2010). At a fixed ratio of oil to wax 1:5 or 1:10, both CarWHS and CarWLC microspheres appear to have relatively smooth surface, suggesting that the type of core oils did not have a significant

influence on particle surface compared to the parameter of oil to wax ratio.

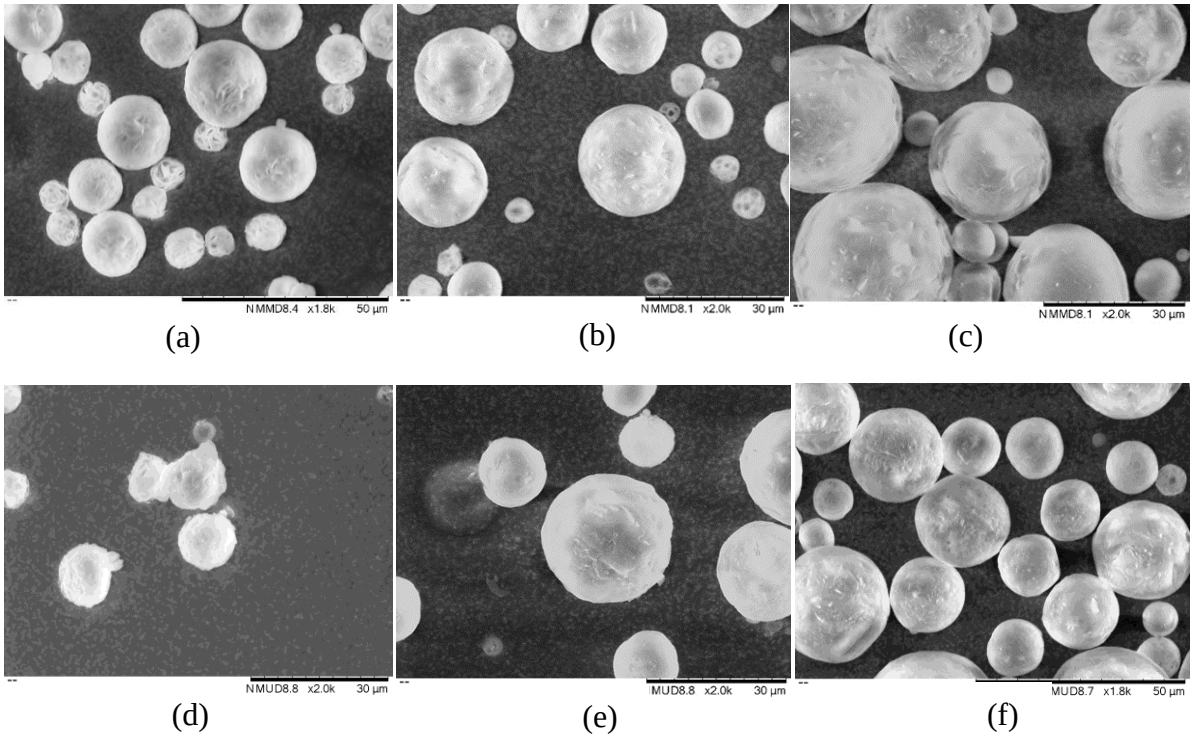

(a) (b) (c)

(d) (e) (f)

Figure 3-5. SEM images of wax particles (a) CarWHS11, (b) CarWHS15, (c) CarWHS110, (d) CarWLC11, (e) CarWLC15 and (f) CarWLC110.

3.3.2. Wax microspheres size and size distribution

To investigate the influence of core oil and the type of wax on the particle size and size distribution of wax microspheres, the values of mean size and span of each pure wax microspheres, CarWLC microspheres with each oil loading and CarWHS15 were calculated and summarised in Table 3-2.

There was no significant difference in the mean size of different pure wax particles statistically, and they all had a mean size of approximately 22 µm. Besides, they also had narrow size distributions with relatively small span values. This can be attributed to the similar interfacial tension values between each molten wax and aqueous phase, which can lead to small sized wax droplets in absence of core oil in the system and therefore narrow size distribution (Dijke

et al., 2009).

The increase of oil to wax ratios significantly reduced the size of CarWLC wax microspheres, 22.33 ± 0.25 μm for 1:10, 16.63 ± 0.14 μm for 1:5 and 15.31 ± 0.20 μm for 1:1 respectively. The decrease of particle size may be caused by the reduction of interfacial tension between the molten waxy and aqueous phase after the addition of LC. Higher concentration of oil may lower the surface tension of oily phase (molten wax and oil), thus, more readily to form smaller lipid droplets and consequently smaller microspheres (Pongpaibul et al., 1984). However, the waxy microparticles prepared by high oil to wax ratios have broader size distributions compared to those prepared by low oil ratios, which might be caused by the ease of dispersion of lower surface tension lipid droplets and the coalescence of small lipid droplets. The average particle size of CarHS15 increased to 19.79 ± 0.08 μm compared to the waxy particles using LC oil at the same ratio (16.63 ± 0.12 μm). This phenomenon revealed that not only the oil to wax ratios but also the core oil plays an important role in the process of particle formation (Silva & Pinto, 2019). This can be explained that LC has a lower interfacial tension with water than HS (see Table 5-2). At the same amount, the lipid phase mixed with LC has holistically a lower interfacial tension with aqueous continuous phase than that mixed with HS, which therefore formed smaller sized lipid droplets and wax microspheres.

Table 3-2. Mean size and span of wax microspheres (mean ± 2×St.Err)

Microspheres	BW	CanW	CarW	CarWLC 11	CarWLC 15	CarWLC 110	CarWHS 15
$D_{[3,2]}$ (μm)	22.33 ± 0.58	22.51 ± 0.06	22.15 ± 0.04	15.31 ± 0.20	16.63 ± 0.14	22.33 ± 0.25	19.79 ± 0.10
Span	0.95 ± 0.03	0.79 ± 0.01	0.89 ± 0.01	2.38 ± 0.10	1.21 ± 0.01	0.88 ± 0.02	0.98 ± 0.01

3.3.3. FT-IR analysis

The FT-IR spectra of core oils and different wax microspheres with or without oil loadings are displayed in Figure 3-6. Figure 3-6 (a) shows the peaks of LC and HS oil. The aromatic stretching vibrations of C=O from the carbonyl group can be identified at 1685 cm^{-1} for LC whereas the aliphatic stretching vibrations of C=O bonds occurs at 1725 cm^{-1} for HS oil. The peak at 1640 cm^{-1} confirms the vibrational aromatic C=C bonds for LC and similarly the peak region of 1610 and 1550 cm^{-1} for HS is observed, corresponding to the aromatic stretching of conjugated C=C bonds. The aromatic and alkyl C-H stretching can be read both for LC and HS at the region of 2954 and 2864 cm^{-1}. In addition, the peaks located in the region of 1300 and 1150 cm^{-1} are associated with the stretching vibrations of C-O-C group for HS oil. The results are consistent with the work reported by Baiocco et al. (2021a) and Elmastaş et al. (2006).

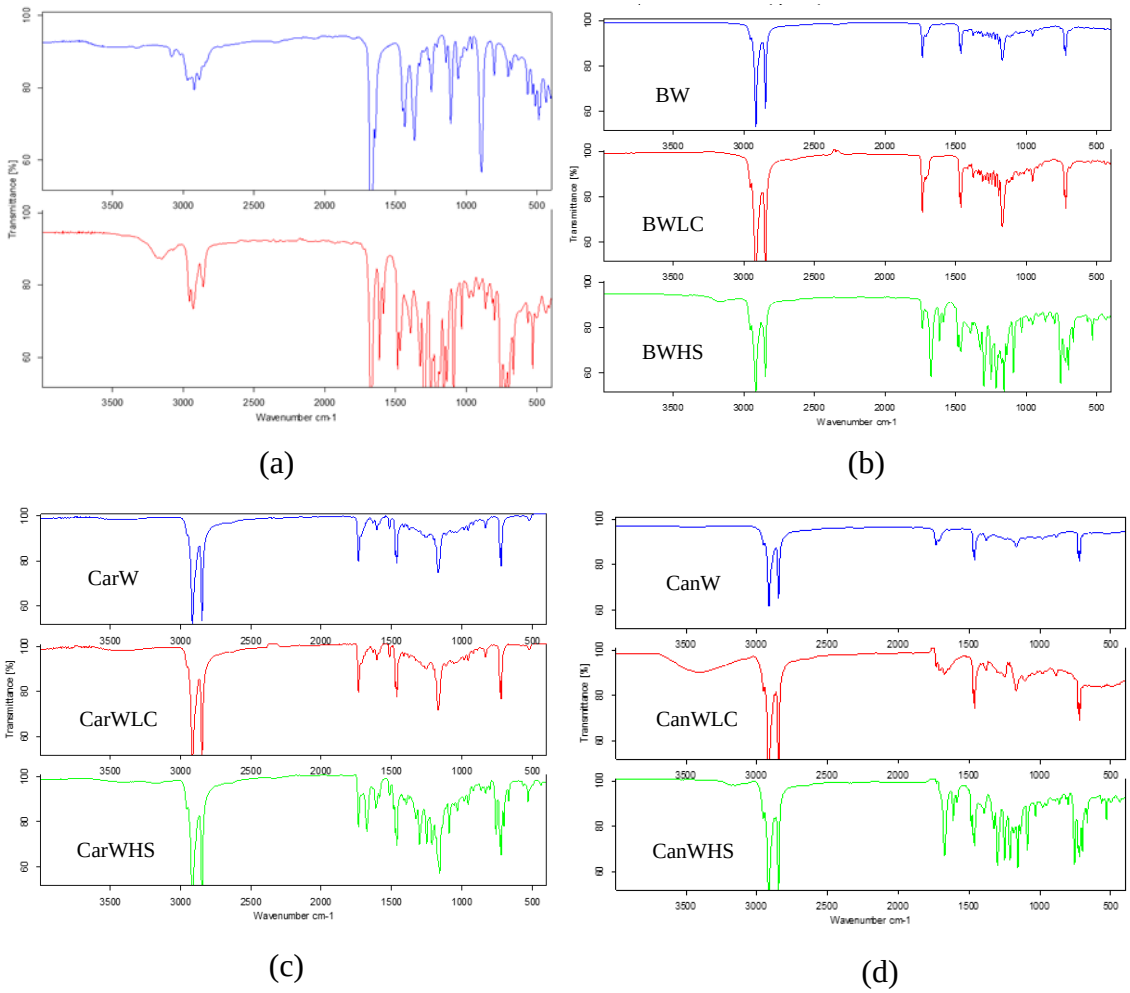

Figure 3-6. FT-IR spectra of (a) core oils, (b) BW microspheres, (c) CarW microspheres, and (d) CanW microspheres.

The blue curves in Figure 3-6 (b), (c) and (d) present the peaks of pure BW, CarW and CanW microspheres respectively. Different wax samples indicate similar spectrograms that the peaks located at the region of 2925 and 2850 cm^{-1} are related to the stretching vibrations of the C-H bonds (Meneses et al., 2019) and the peak at 720 cm^{-1} suggests the rocking vibration of CH_2 bonds. The absorbance peak occurring at 1465 cm^{-1} indicates the deformation of alkane group in long hydrocarbon chains. The absorbance peaks for all waxes occurring at 1735 cm^{-1} and 1100 cm^{-1}, indicate the stretching vibration of C=O bond from ester and alcohol groups in wax (Hacura & Zimnicka, 2006). The FT-IR spectra of waxes are consistent with the reports by

other authors (Bucio et al., 2021; Hacura & Zimnicka, 2006; Meneses et al., 2019; Shirvani et al., 2022; Trujillo-Ramírez et al., 2022; Yilmaztekin et al., 2019).

The same absorption peaks of HS oil are found in the green curves of different wax microspheres of Figure 3-6 (b), (c) and (d), suggesting the successful entrapment of HS oil in wax matrix particles. However, LC oil absorption peaks of very low intensity can be observed from the overlapping of LC laden wax microsphere spectrum shown in the red curves in Figure 3-6 (b), (c) and (d), indicating a low amount of LC oil was encapsulated. Besides, there are no new chemical bonds formed from the spectrograms of each type of wax microcapsules for both oils, evidencing their potentials to be used as wall materials.

3.3.4. Payload and encapsulation efficiency

The payload and encapsulation efficiency of different HS laden wax microspheres are summarised in Table 3-3. The payload ranges from 4.6 ± 0.2 % to 6.1 ± 0.2% at the lowest loading (oil-to-wax ratio of 1:10) and 37.9 ± 1.3 % to 41.9 ± 0.6% at the highest loading (oil-to-wax ratio of 1:1) depended on the type of wax, with the corresponding EEs of 50.8 ± 1.9 % to 66.1 ± 1.9 % at the lowest HS loading and 75.7 ± 2.7 % to 83.7 ± 1.2 % at the highest loading. CanW is observed as the most effective encapsulating wall material, compared to the corresponding encapsulation results of CarW and BW. Similar results are also reported by Blake et al. (2014) that CanW has stronger oil-binding capacity compared to CarW. The obtained EE of each type of wax microspheres at high oil loading (1:1) are higher than the HS entrapped core shell microcapsules (EE, 47 ± 11%) obtained via complex coacervation reported by Baiocco et al. (2021a). Besides, similar value of EE (86.5 ± 5.6%) is reported by Milanovic et al. (2010) using carnauba wax microspheres to encapsulate ethyl vanillin. It is

notable that both the payloads and EEs are found to increase with the increasing of oil content. Similar phenomena were also reported by Yilmaztekin et al. (2019) that Mentha piperita (peppermint) essential oil was encapsulated by carnauba wax via melt dispersion, the EE increased from 66.8 ± 4.7 to 94.2 ± 7.8 % with the increasing of weight ratios of oil to wax from 10 to 50 %. Kumar et al. (2014) reported a similar dependency of payload (3.6-7.5%) and EE (78.2-83.4%) on oil content (5-10%) when using polyethylene glycol 6000 to encapsulate Mentha piperita (peppermint) oil by melt dispersion. This phenomenon can be attributed to higher amount of oil might affect the three-dimensional wax networks, resulting in a more loading capacity for oil molecules, allowing a higher EE, while lower amount of oil has limited influence on the structural network of wax, which leads to a lower value of EE (Chen et al., 2021).

Table 3-3. Payload and corresponding encapsulation efficiency of HS-containing wax particles (mean ± 2×St.Err)

Wax microspheres	Wax to oil ratio	Payload (%)	Encapsulation efficiency (%)
BWHS11	10:10	37.9 ± 1.3	75.7 ± 2.7
BWHS15	10:2	10.5 ± 0.4	63.1 ± 2.2
BWHS110	10:1	4.6 ± 0.2	50.8 ± 1.9
CarWHS11	10:10	38.5 ± 1.0	76.9 ± 2.1
CarWHS15	10:2	11.7 ± 0.5	70.3 ± 3.1
CarWHS110	10:1	6.1 ± 0.2	66.1 ± 1.9
CanWHS11	10:10	41.9 ± 0.6	83.7 ± 1.2
CanWHS15	10:2	12.2 ± 0.4	73.1 ± 2.1
CanWHS110	10:1	6.0 ± 0.1	66.1 ± 1.3

The payloads of LC laden wax microspheres at 1:5 and 1:10 ratios are negligible low (< 1%), thus only the payloads and EEs of 1:1 oil to wax ratio particles are summarized in Table 3-4. The highest payload was 7.69 ± 0.26%, using a mass of LC equivalent to BW (EE =15.27 ± 0.32%). The CanW microspheres achieve a lower payload of 5.40 ± 1.57% while CarW oloegel particles incorporate negligible payload of 0.44 ± 0.03 %. The low values of LC payloads in wax microparticles are evidenced by the FITR spectra in Figure 3-6. Nevertheless, Baiocco et al. (2021b) obtained encapsulation efficiencies and payloads of 29 ± 4% and 19 ± 3% for LC microcapsules fabricated via complex coacervation followed by spray drying. Koo et al. (2014) reported the fabrication of peppermint oil microcapsules of 26.68% to 85.15% EE using variable alginate and pectin formulations. However, approximately 6% weight loss ascribable to the evaporation of ethyl vanillin was reported by Milanovic et al. (2010) in the thermogravimetric measurements for wax microspheres prepared by the same method

employed in this study, with the similar values to the EEs of BW (7.69 ± 0.26%) and CanW (5.40 ± 1.57%). Compared to those results, the payloads as well as EEs indicate significant loss of LC during the encapsulation preparation.

Table 3-4. Payloads and corresponding encapsulation efficiencies of BWLC11, CarWLC11 and CanWLC11 particles (mean ± 2×St.Err)

Wax microspheres	Payload (%)	Encapsulation efficiency (%)
BWLC11	7.7 ± 0.3	15.3 ± 0.3
CarWLC11	0.4 ± 0.1	0.9 ± 0.1
CanWLC11	5.4 ± 1.6	10.9 ± 3.1

3.3.5. Flavour retention in wax microspheres

Due to the low payloads of LC encapsulated in wax particles, experiments were only conducted for HS at oil to wax 1:1 ratio. It is also notable that the retention tests were carried out for a period of 32 days since HS oil in all wax samples remained constantly after 8 days storage. As can be seen in Figure 3-7, time-dependent release behaviours are observed from BWHS11, CarWHS11 and CanWHS11 samples after being exposed at ambient environment (25 ± 2 °C, 60 ± 2% humidity). CarW shows better retention capability compared to BW and CanW with only 2.1 ± 0.4 % of the original HS payload leaching out after 32 days. The highest HS loss (3.5 ± 0.4 %) occurs in CanW, followed by BW and finally CarW. As can be seen in Figure 3-4, although BW microparticles appear to have rougher and more porous surface than CanW and CarW microspheres, CanW exhibits the most rapid release performance during storage. The difference can possibly be attributed to the molecular structure of each wax (See Table 2-2). CanW consists mainly nonpolar C_{29}-C_{33} hydrocarbons, while the main compositions of CarW and BW are polar C_{44}-C_{66} aliphatic/aromatic esters and

C_{32}-C_{52} monoesters respectively. The affinity between CanW and HS molecules leads to a faster diffusion rate of core oil. In general, all wax microspheres exhibited good performance for the retention of HS oil as only less than 5% HS losses were observed for all wax samples. This might result from the good barrier properties of waxes and the strong hydrophobicity of the core active, which makes waxes very promising materials for the encapsulation of hydrophobic active ingredients.

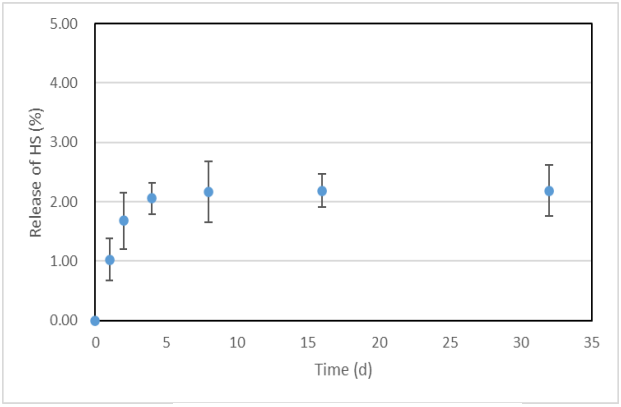

(a)

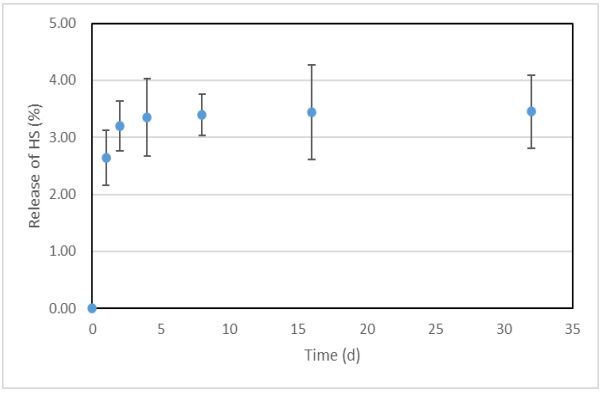

(b)

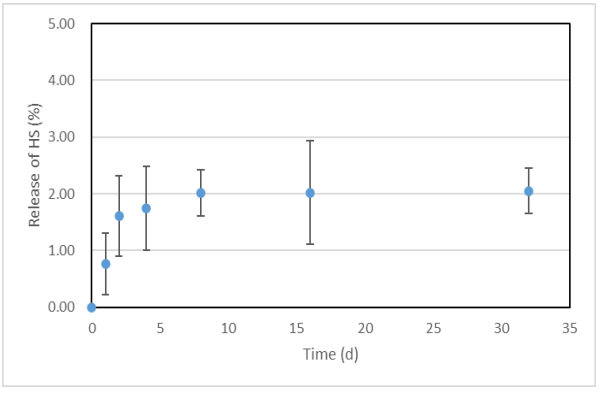

(c)

Figure 3-7. Release of HS from wax microspheres (a) BWHS11, (b) CanWHS11 and (c) CarWHS11. (mean ± 2×St.Err)

3.3.6. Mechanical properties of wax particles

3.3.6.1. Young's modulus and Hertz model fitting analysis

Young's modulus is a fundamental mechanical property that reflects the stiffness of an elastic material undergoing reversible deformations (Yu et al., 2021). Wax microspheres were considered as homogeneous matrix particles and the Hertz model was used to determine the Young's modulus of different waxy microspheres at small nominal strain (up to 10%).

Figure 3-8 (a) presents a typical force versus displacement curve obtained from the compression of a representative CarWLC110 wax microsphere. The wax microsphere did not show rupture behaviour under compression, which indicates that the wax particles have a matrix internal structure rather than core-shell structure, or too strong to be ruptured for the forces applied. Fitting the force-displacement data up to 10% nominal strain (fractional deformation) into the Hertz model described by Equation (3-**7**), the experimental and predicted force values are shown in Figure 3-8 (b). The R-squared value is 0.93, which indicates that the Hertz model can reasonably predict the mechanical behaviour of CarWLC110 well, and the Young's modulus value obtained is 330 MPa for this particle.

Figure 3-9 presents the Young's modulus versus particle diameters of some typical wax microsphere examples. Theoretically, Young's modulus is a mechanical property parameter that signifies the intrinsic stiffness of a material, which is evidenced by that the Young's modulus values for each sample do not show variable changes significantly with particle sizes in Figure 3-9. The pure BW particles have mean Young's modulus of 41 ± 2 MPa, pure CarW particles have mean Young's modulus of 271 ± 10 MPa while pure CanW microspheres have the mean Young's modulus of 434 ± 6 MPa.

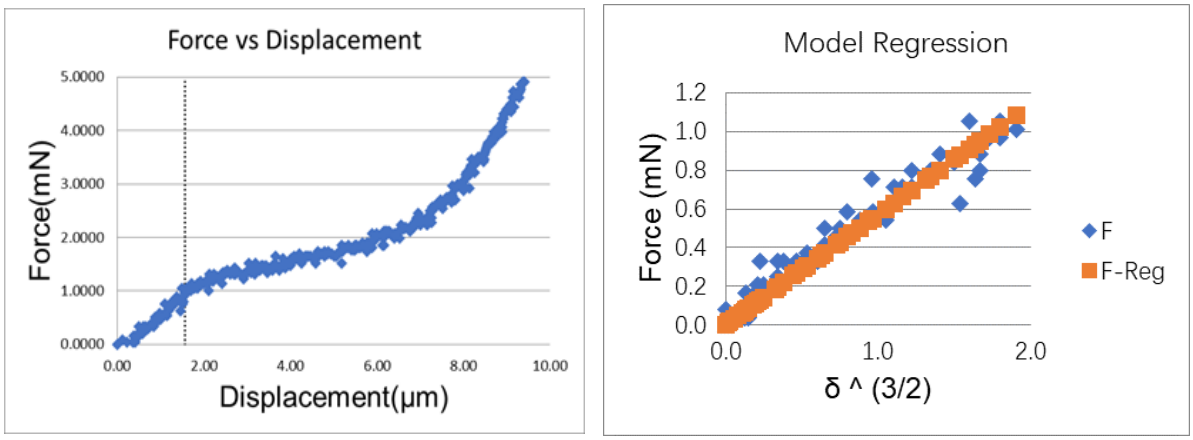

(a) (b)

Figure 3-8. Typical force versus displacement data obtained from (a) compression of an individual CarWLC110 (15.5 μm in diameter) wax microsphere, the dotted line indicates the 10% nominal strain and (b) the fitting of the experimental data using the Hertz model for the CarWLC110 particle in Figure 3-8 (a). F: experimental force. F-Reg: Predicted force.

In order to evaluate the accuracy of Young's modulus results, their mean values for each type of wax microparticle as well as the corresponding coefficient of determination (R^2) are summarised in Table 3-5. Although the values of R^2 from BW samples are significantly lower than CarW and CanW particles, the Young's modulus of BW microspheres without oil loadings (41 ± 2 MPa) calculated by the Hertz model is well consistent with the result (45 MPa) reported by Morgan et al. (2002). Lower value (271 ± 10 MPa) of Young's modulus of pure CarW is obtained compared to that of pure CanW (434 ± 6 MPa) in this study. Zhang et al. (2016) reported similar values of Young's modulus for CarW and CanW plasticised by Tween 60 from indentation and flexural measurements. The higher concertation of hydrocarbons in CanW renders the mobility of polar molecules and no sufficient polar molecules can form hydrogen bonds with hydroxyl groups in Tween 60, which contributes to less plasticising effect to CanW compared to CarW, and therefore results in higher mechanical

stiffness.

In addition, CanWHS11 microcapsules have the highest Young's modulus at 98.3 ± 2.7 MPa, followed by CarWHS11 (47.6 ± 2.1 MPa) and BWHS11 (31.3 ± 0.9 MPa). However, the Young's modulus values of these wax microparticles are inconsistent with their corresponding core oil release performances from wax matrix carriers, since CarW exhibits the highest retention capability, followed by BW and finally CanW (See Figure 3-7). It is notable that the retention tests are carried out at ambient environment (25 ± 2 °C, 60 ± 2% humidity), and there are no external forces applied for these wax microspheres. Therefore, the mechanism of HS molecule release behaviour can be primarily dominated by the molecular compositions of each wax as well as the affinity between wax and HS molecules. Notwithstanding, for some microcapsules used in laundry products or microcapsules fabricated with nondegradable shell, the release of core oil needs to be achieved using a mechanical force as a trigger for rupture and this process is significantly influenced by the mechanical properties of microcapsules (Gray et al., 2016), e.g., higher Young's modulus capsules have more capability to resist the elastic deformation of microcapsules before their ruptures.

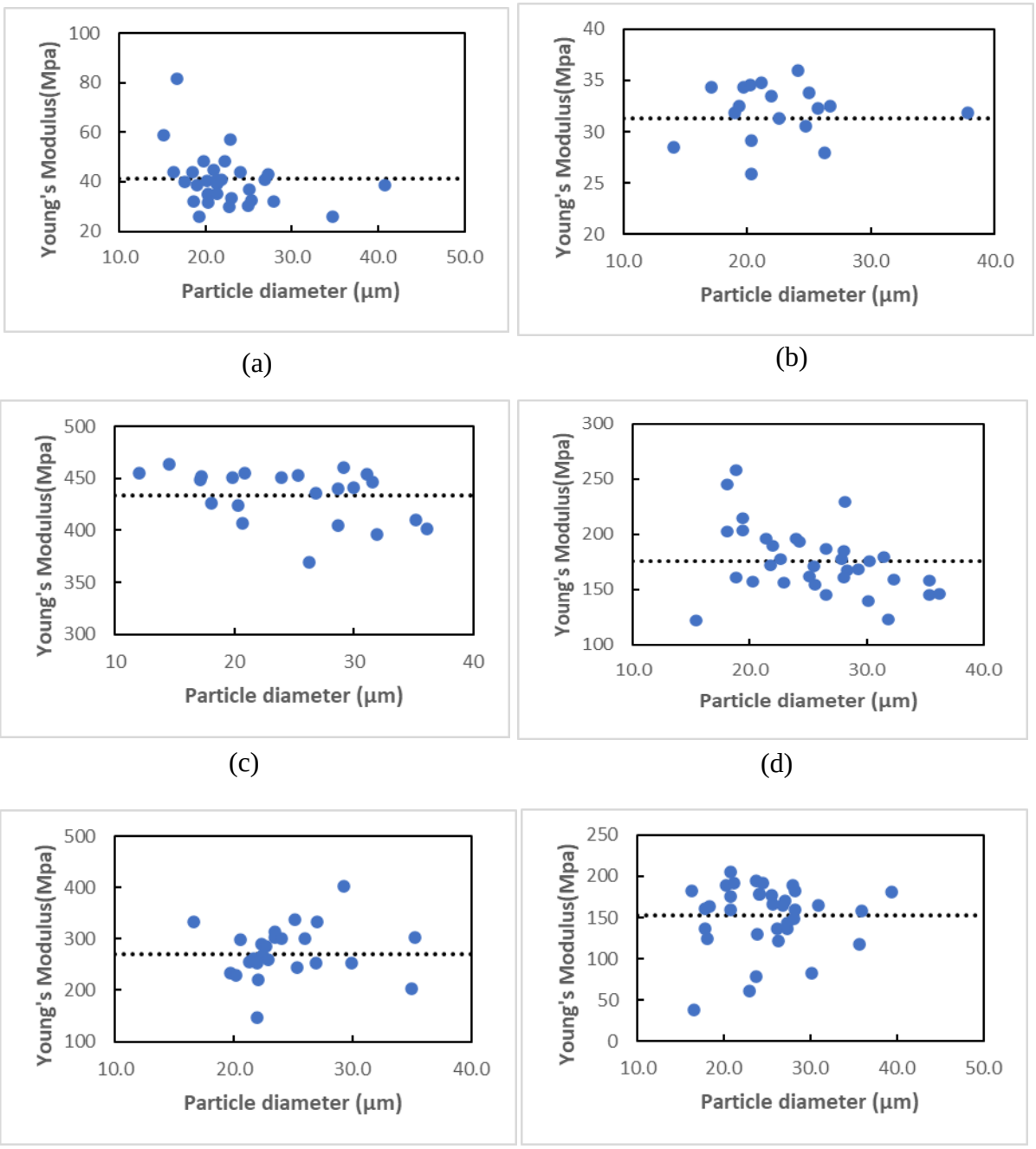

Figure 3-9. Young's modulus values of waxy microspheres versus particle size (a) BW, (b) BWHS15, (c) CanW, (d) CanWHS15, (e) CarW and (f) CarWHS15. Each dotted line indicates the mean.

3.3.6.2. Influence of oil to wax ratio on the mechanical stiffness of wax microspheres loaded with the oil

As discussed, particles prepared by the same wax should exhibit same value of Young's

modulus. However, significant different values (see Table 3-5 and Figure 3-9) are observed from different oil to wax ratios for the same wax microspheres. For instance, the Young's modulus of CarW microcapsules reduced to 229 ± 8 MPa, 153 ± 7 MPa and 48 ± 2 MPa at oil-to-wax weight ratio of 1:10, 1:5 and 1:1 respectively. In the case of LC oil, the Young's modulus at oil to wax ratio of 1:10 remained similar to that of pure CarW before decreasing to 233 ± 8 MPa and 59 ± 3 MPa at oil to wax weight ratio of 1:5 and 1:1 respectively. At the same mass loading, wax matrix particles of LC appeared to have higher Young's modulus compared to that entrapping HS oil. It is presumed that the aliphatic chain comprised in HS molecule is likely to mix with wax molecules and reduces the degree of wax crystallinity by disrupting orderly packing of wax molecules (Zhang et al., 2016), which contributes to lower Young's modulus values, while LC or other cyclic compounds are speculated to accommodate within the solid amorphous areas inside waxes. This might also explain the low values of Young's modulus at high oil contents in wax oleogels.

Table 3-5. Mean values of Young's modulus of wax microspheres and their corresponding mean values of R^2 fitted by the Hertz model (mean ± 2×St.Err)

Wax microspheres	Young's Modulus (MPa)	R^2
BW	41.7 ± 2.0	0.67 ± 0.02
BWLC11	28.3 ± 1.4	0.61 ± 0.03
BWLC15	40.3 ± 1.1	0.79 ± 0.02
BWLC110	40.7 ± 1.1	0.74 ± 0.02
BWHS11	31.3 ± 0.9	0.75 ± 0.02
BWHS15	41.0 ± 0.7	0.76 ± 0.02
BWHS110	41.3 ± 1.7	0.74 ± 0.02
CarW	271.4 ± 10.0	0.92 ± 0.01
CarWLC11	59.3 ± 2.6	0.67± 0.02
CarWLC15	233.4 ± 7.7	0.90 ± 0.01
CarWLC110	270.9 ± 7.5	0.94 ± 0.01
CarWHS11	47.6 ± 2.1	0.72 ± 0.02
CarWHS15	152.7 ± 6.7	0.91 ± 0.01
CarWHS110	228.9 ± 7.8	0.92 ± 0.01
CanW	433.7 ± 5.5	0.95 ± 0.01
CanWLC11	112.6 ± 2.8	0.75 ± 0.03
CanWLC15	188.5 ± 5.5	0.78 ± 0.03
CanWLC110	390.7 ± 16.0	0.73 ± 0.03
CanWHS11	98.3 ± 2.7	0.90 ± 0.01
CanWHS15	175.8 ± 5.4	0.89 ± 0.01
CanHS110	357.2 ± 9.4	0.86 ± 0.01

The Young's modulus of each wax microspheres was monitored for HS oils (Payloads of LC of each wax microspheres were too low) and their Young's modulus dependences on payload are described based on the following Equation (3-**8**):

$$\log_{10}\frac{E_x}{E_{wx}} = k_x \log_{10} P \qquad (3\text{-}\mathbf{8})$$

where E_x is the Young's modulus for a certain sample, E_{Wx} is the Young's modulus of the corresponding pure wax microparticles, k is a constant influencing coefficient and P is the corresponding payload. The type of sample is denoted by x.

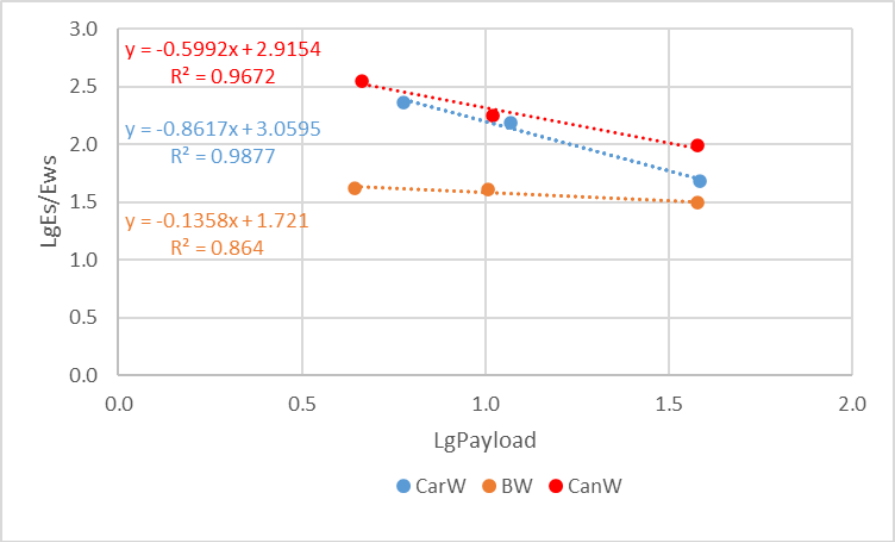

Figure 3-10. Correlation between the Young's modulus and payload using HS as a core.

The correlations between the $\log_{10}$ values of normalised Young's modulus and corresponding payload are plotted in Figure 3-10. The R^2 values obtained from each wax microspheres are in a range of 0.86-0.98, which implies the fitting is good with the proposed equation. It is assumed that the influencing coefficient k_s can reflect the intrinsic property of wax, i.e., the tendency degree of its mechanical strength to be affected by the presence of oil molecules within wax crystal networks. The lg values of normalised Young's modulus decreased with the lg payload linearly. The highest absolute value of k_{carw} is obtained (0.8617) for the CarW microspheres, followed by CanW and BW particles, indicating that CarW is the wax that can be affected the most easily on the mechanical strength after encapsulating oils. However, due

to the limited number of experimental data obtained in this study, further investigation including more wax or oil types, more sets of oil to wax ratios, should be undertaken to validate this hypothesis.

3.4. Conclusions

LC or HS loaded wax microspheres were prepared by a melt emulsification method considering its potential possibility for large-scale industrial applications and very low environmental impacts. It was found that the formed waxy microparticles have spherical shapes. The highest EE of 83.7 ± 1.2% was obtained from CanWHS11 sample, which was higher than chitosan/gum arabic coacervated microcapsules (47 ± 11%) reported by Baiocco et al. (2021a) and formaldehyde-based microcapsules (75%) prepared by Long et al. (2009). CarW shows better retention capability compared to BW and CanW during the storage tests. Mechanical characterisation of wax microparticles showed that CanWLC110 exhibited the strongest mechanical strength (390.7 ± 16.0 MPa), which was also significantly higher than that of HS laden chitosan/gum arabic microcapsules (95 ± 14 MPa) (Baiocco et al., 2023). In addition, the encapsulation efficiency was found to increase with oil to wax ratios while an inversely relation was observed for Young's modulus versus oil loading. Thus, depends on the end applications of wax microspheres, their desirable properties could be controlled by selecting a certain wax and oil to wax ratio.

CHAPTER 4. Microencapsulation of Three Different Oils (L-Carvone, Limonene And Hexyl Salicylate) in Gelatine-Gum Arabic Shell Using Complex Coacervation Followed by Spray Drying/Coating

4.1. Introduction

LC or HS laden wax microspheres prepared via melt emulsification exhibited significant variations in payload and encapsulation efficiency, which can be affected by the molecular weight and structure, polarity, volatile rate, solubility in water of core ingredients as well as their interactions with wax materials (Mehta et al., 2022). During melt emulsification, wax microspheres were prepared at the temperature with a range between 70 to 95 °C to melt waxes and maintained for 20 mins to achieve a stable system. Due to the different solubilities in water and vapour pressures between LC and HS (Lapczynski et al., 2007; Vilas-Boas et al., 2019; Yalkowsky et al., 2010), considerable LC loss might occur contributed by the oil evaporation and being unable to get encapsulated (LogP value of L-carvone is 2.71 compared to the LogP value of hexyl salicylate at 4.87 (Luo et al., 2023; PubChem, 2023b)), leading to the low payload and EE of LC wax microspheres. Also, LC is highly sensitive to temperature and its degradation can be accelerated due to the heat in the process (Napiórkowska & Kurek, 2022a). In addition, wax microspheres prepared by the melt dispersion method had an inner matrix structure instead of typical core-shell structure. The latter structure was reported to allow for a higher payload (Bennacef et al., 2023), and a better retention of the encapsulated substances with wall protection and delayed release of the core (Bennacef et al., 2021; López

de Dicastillo et al., 2023). Therefore, core-shell structured microcapsules prepared at a relatively low ambient temperature can be tentatively favourable to increase the payload and EE for the encapsulation of volatile oils. Complex coacervation has been extensively investigated for the encapsulation of essential oils in food, textile, cosmetic and pharmaceutical applications (Elkalla et al., 2023; Jyothi et al., 2010; Martins et al., 2014; Muhoza et al., 2022; Napiórkowska & Kurek, 2022a; Sousa et al., 2022; Xiao et al., 2014a; Yan et al., 2022). Microcapsules prepared via this method exhibited improved thermal stability and overall higher EE compared to other microencapsulation methods, with core-shell structure obtained (Comunian et al., 2013; Napiórkowska & Kurek, 2022a).

In this chapter, limonene was also encapsulated via complex coacervation using gum arabic and gelatine as a comparative to investigate the properties of LC microcapsules since both materials share similar aromatic molecular structures as well as physical properties. Three different oils including LC, LM and HS were encapsulated in GA-GE coacervated microcapsules and their fundamental physical, structural and mechanical properties were investigated. In addition, the effects of different type of core oils and following treatments of gelatine/gum arabic coacervated microcapsules on these properties were also studied.

4.2. Materials and methods

4.2.1. Materials

L-carvone (99%, w/w), S-limonene (95%, w/w), hexyl salicylate (98%, w/w) and glutaraldehyde (50%, w/w) were all purchased from Macklin, China. Gum arabic (GA) was purchased from Solarbio Life Sciences, China, gelatine (GE, type B, ~220 g bloom, average Mw = 500 kDa) was obtained from Shanghai Yuanye Biotechnology Co. Ltd., Shanghai,

China, and maltodextrin (MD, DE16.5–19.5) was purchased from Sigma-Aldrich, UK. Reagents including absolute ethanol and 1-propanol were purchased from Sigma-Aldrich, UK, and were of analytical grade and used without further purification. All the solutions were prepared using deionised water (18.2 MΩ cm at 25 °C).

4.2.2. Preparation of microcapsules

The GE-GA coacervated microcapsules were prepared based on the method (Yu et al., 2017; Yu et al., 2021) with some modifications. The aqueous phase was prepared by dissolving 2.5 g GE and 2.5 g GA in deionized water (200 ml) at 60 °C with magnetic stirring for 1 h. The resulting solution was continuously stirred for 12 h at 25 ± 2 °C. 2.5 g model oil (L-carvone, limonene or hexyl salicylate) was added to the GE-GA mixture solution and homogenised by a high shear mixer (Model L4RT, Silverson, UK) at 3000 rpm for 10 mins to prepare an oil in water emulsion. During the homogenisation, the beaker was covered with aluminium foil. After emulsification, the obtained emulsion was transferred into a beaker equipped with 4 standard baffles and kept under mechanical agitation at 400 rpm at room temperature (25 ± 2 °C). In the meantime, the pH of emulsion was adjusted to 4.0 by adding 10% aqueous acetic acid solution, which induced the complex coacervation occurring at the surface of oil droplets by the formation of coacervates between GE and GA due to their opposite electrostatic charges. The oil loaded GE-GA microcapsules can be obtained under continuous agitation at 400 rpm after 4 h at room temperature.

4.2.2.1. Microcapsules prepared via direct spray drying

The obtained HS-loaded microcapsule suspension was fed into a mini spray dryer YM-8000B (YUMING, Shanghai, China) to produce dry microcapsules, denoted by GG-HS. The

suspension was atomised into a cylindrical chamber through a stainless-steel nozzle (2.8 mm in diameter). The spray drying system was operated with an inlet air temperature at 180 ± 2 °C and drying air flow rate at 35 m^3/h. The emulsion was kept under stirring with a feeding flow rate of 2 mL/min into the drying chamber, and the resulting outlet air temperature was recorded to be 80 ± 5 °C. Free-flowing powders of microcapsules were collected from the bottom container and stored in glass vials for further analysis.

4.2.2.2. Microcapsules prepared with additional coating

1.5 g MD was dissolved in 100 ml deionized water at room temperature with magnetic stirring to prepare the coating solution. 50 ml obtained HS-loaded microcapsule suspension was added to the coating solution under agitation. Then the mixed suspension was fed into the spray dryer to produce double shell microcapsules following the procedure in 4.2.2.1, denoted by GG-HS-MD.

4.2.2.3. Microcapsules prepared with a crosslinker

After complex coacervation, the obtained oil-loaded microcapsule suspensions were added by 0.5 ml 50% aqueous glutaraldehyde as a crosslinker to harden GE-GA coacervated gelling shell, and the microcapsule suspension was agitated for 12 h followed by subsequent spray drying described in 4.2.2.1. Samples are donated by GG-LC-GT, GG-LM-GT and GG-HS-GT for LC, LM and HS oil respectively. As control sample, the crosslinked GE-GA microcapsules containing no oils were also prepared following the same procedures. The detailed ingredients are listed in Table 4-1 Each sample was prepared in triplicate.

Table 4-1. The ingredients to prepare GE-GA microcapsules.

Sample	GE (g)	GA (g)	MD (g)	Core oil	Oil amount (g)
GG-HS	2.5	2.5	0	HS	2.5
GG-HS-MD	2.5	2.5	1.5	HS	2.5
GG-HS-GT	2.5	2.5	0	HS	2.5
GG-LC-GT	2.5	2.5	0	LC	2.5
GG-LM-GT	2.5	2.5	0	LM	2.5

4.2.3. Particle size analysis

Before spray drying, the mean size and size distribution of the fabricated microcapsules in suspension were measured by using a light scattering instrument (Mastersizer 2000, Malvern Instruments Ltd, UK) with the Mastersizer 2000 software. The measurements were aligned by a reference refractive index of 1.505 for HS, 1.495 for LC and 1.473 for LM respectively (Baiocco et al., 2021a;2021b; Clará et al., 2009). The refractive index of water was set at 1.330 and the refractive index of GE-GA coacervates gel was tested to be 1.59 by a J357 automatic refractometer, and the value is in coincident with literatures (Rousi et al., 2019; Yang et al., 2012). The mean diameter and size distribution of microcapsules were measured by a Mastersizer following the protocols in Section 3.2.3.

4.2.4. Morphological characterisation of GG-GA coacervated microcapsules

The morphology of microcapsules was firstly observed by a Leica DMRBE optical microscope (Leica microsystems, USA) with A Moticam Pro 252B camera fitted on and the images of microspheres were captured by Motic Images Advanced 3.2 software. Secondly, further morphological characterisations were performed by a scanning electron microscope

(Hitachi TM3030 Tabletop) following the procedures described in Section 3.2.4.

4.2.5. Fourier transform infrared spectroscopy (FT-IR) of core oils, GE, GA and spray dried microcapsules

The FT-IR analyses of LC, LM, HS, GE, GA and solid powdered microcapsules with or without any oil were performed by using ATR-FTIR spectroscopy (Bruker TENSOR 27). The detailed experimental protocols are presented in Section 3.2.5. All solid samples for analysis were prepared by a 13 mm evacuable pellet die (Specac, UK) using a compression instrument (LS100 Plus, Lloyd, UK) and compressed at a maximum load (40 MPa) monitored by NEXYGEN Plus software.

4.2.6. Payloads and encapsulation efficiency

4.2.6.1. Sample preparation and calculation

Different spray dried oil loaded microcapsules were dispersed into corresponding solvent following the protocol described in Section 3.2.6.

In addition, empty GE-GA microcapsules containing no oil were also measured following the same procedures, to investigate the absorbance influence from coacervates in solvents. All the results showed that the shell coacervates did not dissolve in the solvent and did not consequently influence the UV absorption readings.

4.2.6.2. UV-Vis spectrophotometry to quantify HS

The amount of HS was quantified by UV-Vis spectroscopy, following the experimental protocols described in Section 3.2.6.

4.2.6.3. Gas-chromatography to quantify LC and LM

Since LC and LM are highly volatile and the absorption peak wavelength (218 nm) of LM

positioned within the background noise area (200 - 300 nm) of Cecil 1020 UV-Vis spectrophotometer (data not shown), the quantitative analyse of LC and LM were performed by a gas chromatography method and ethanol was used as the solvent for LC and LM. Linear standard calibration curves for LC and LM were determined based on the rising areas (y) from detection peak and oil concentrations (x) in 20 ml ethanol respectively: $y = 19.075x - 7.2779$ with a coefficient of determination $R^2 = 0.9998$ for LC (See Figure B-1 in Appendix B) and $y = 15.821x + 2.7718$ with a coefficient of determination $R^2 = 0.9994$ for LM (Figure B-2 in Appendix B). The calibration equations were further used to determine the amount of encapsulated LC or LM in dry microcapsules, using an Agilent GC 8890 system (Agilent, USA) coupled with an Agilent 7693 automatic sample injector. The supernatants prepared as described in Section 4.2.6.1 for LC or LM were transferred into 2 ml glass vials (Agilent, USA) sealed with rubber caps (Thermo scientific, UK). The GC tests were performed with an Agilent HP-5 capillary column (30 m × 0.32 mm × 0.25 µm, Agilent, USA).

Instrumental parameters for LM analysis were as follows (Baiocco & Zhang, 2022): the temperature of the injector was 250 ◦C; N^2 flow rate was 1.5 mL/min; column temperature program: initial temperature at 50 ◦C, increased to 180 ◦C at 10 ◦C/min (held for 2 min), and then increased at 5 ◦C/min to 200 ◦C (held for 1 min); the temperature of the detector was 250 ◦C. The separation time of LM was at 10.5 min based on the response of LM to the detector in the column.

Parameters for LC analysis were as follows (Elmastaş et al., 2006): the temperature of the injector was 250 ◦C; N^2 flow rate was 1.5 mL/min; column temperature program: initial temperature at 100 ◦C, increased to 230 ◦C at 10 ◦C/min (held for 5 min), and then increased at

10 ◦C/min to 240 ◦C (held for 1 min); the temperature of the detector was 250 ◦C. The separation time of LC was at 13.5 min based on the response of LC to the detector in the column.

4.2.7. Mechanical characterisation of microcapsules

4.2.7.1. Micromanipulation

The mechanical properties of GE-GA coacervated microcapsules were characterised by the micromanipulation technique as presented in Section 3.2.8.1.

Figure 4-1 presents a typical force versus displacement curve from compression of a representative GG-LM-GT microcapsule. Point a is the initial point when the probe touched the microcapsule, b is the yield point, and a-b curve corresponds to the elastic behaviour of the microcapsule. The curve of b-c shows the plastic behaviour of microcapsules and point c is the rupture point of the microcapsule (Luo et al., 2022). At point c, there was a significant instant force reduction due to the sudden burst of the microcapsule. The force increased gradually when compressing the ruptured microcapsule residue and dramatically when the force probe approached the substrate holding the sample of microcapsules. Accordingly, the values of rupture force (F_r) and displacement (δ_r) at rupture for the selected microcapsule can be determined, and the corresponding fractional deformation at rupture (ε_r), nominal rupture stress (σ_r), nominal rupture tension (T_r) and toughness (T_c) can be calculated based on the following equations (Zhang. et al., 2022):

$$\varepsilon_r = \frac{\delta_r}{D} \quad (4\text{-}\mathbf{1})$$

$$\sigma_r = \frac{4F_r}{\pi D^2} \quad (4\text{-}\mathbf{2})$$

$$T_r = \frac{F_r}{D} \quad (4\text{-}3)$$

$$T_c = \int_0^{\varepsilon_r} \sigma d\varepsilon \quad (4\text{-}4)$$

where subscript r represents the rupture point, D is the initial diameter of the tested microcapsule, σ is the nominal stress, T_r is the nominal tension, ε is the fractional deformation and T_c is toughness that corresponds to the integration of the nominal rupture stress over the fractional deformation using Equation (4-**4**).

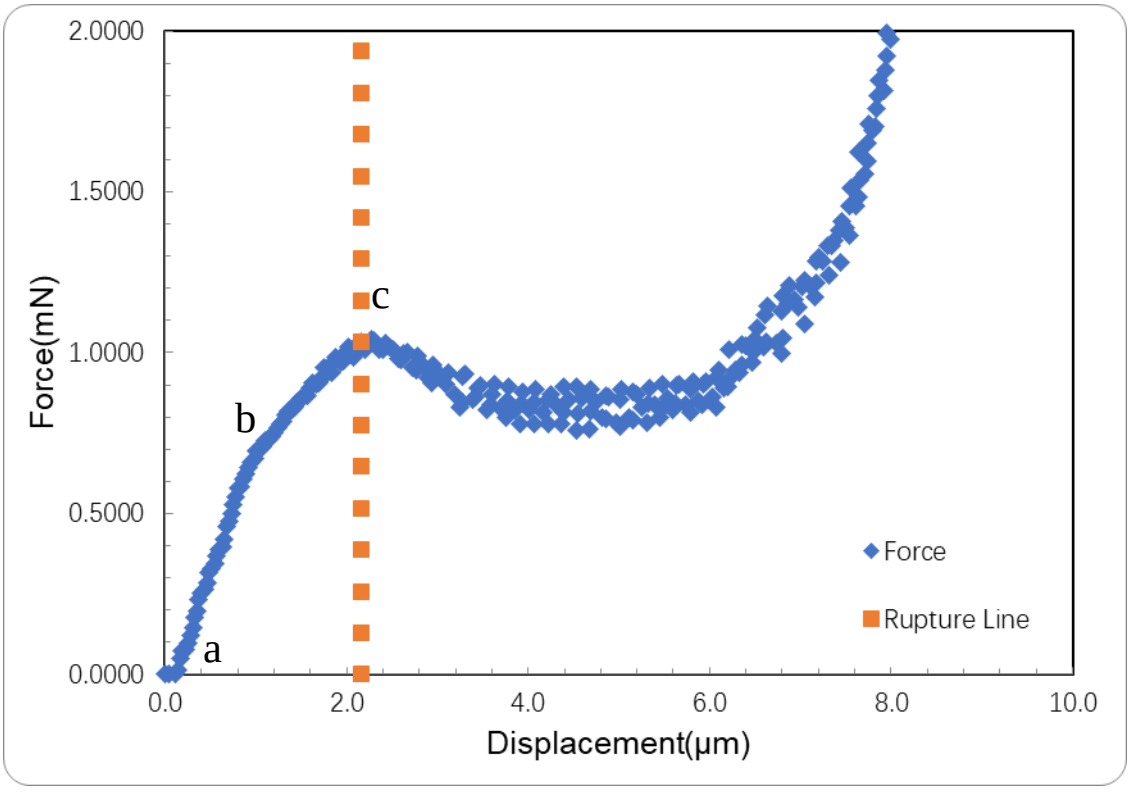

Figure 4-1. Typical force versus displacement data obtained from the compression of an individual GG-LM-GT (13.2 μm in diameter) microcapsule. The dotted line indicates the rupture of the microcapsule.

4.2.7.2. Hertz model

To further investigate the elastic behaviour of different microcapsules, the apparent Young's modulus for each type of microcapsule was characterised by fitting the force versus

displacement data corresponding to the nominal strain (factional deformation) up to 10% with the Hertz model (see Section 3.2.8.2). For each sample, more than 30 microcapsules were analysed.

4.2.8. Statistical analysis

See Section 3.2.9.

4.3. Results and Discussion

4.3.1. Morphology of microcapsules

The light microscopy images of different oil microcapsules prepared by coacervation are shown in Figure 4-2, and they display that the suspended microcapsules containing different core oils exhibit spherical shape and are in micro size. It can be clearly seen that oil droplets were encapsulated within a GA-GE coacervate shell, forming multinuclear structured microcapsules regardless of the type of core oils. Similar morphological characteristics were also reported by the previous works of GA-GE coacervated microcapsules for the encapsulation of castor oil (da Silva et al., 2015), Michelia alba D.C. extract aromas (Samakradhamrongthai et al., 2019), peppermint oil (Dong et al., 2011), paprika oleoresin (Alvim & Grosso, 2010) and ascorbic acid (Comunian et al., 2013). Dong et al. (2011) investigated the effects of core/wall weight ratio on the morphology of GA-GE coacervated microcapsules and found that higher core/wall ratios resulted in microcapsule structural transition from spherical to irregular, which is coincident with reports by Baiocco et al. (2021a;2021b) and Baiocco and Zhang (2022) when they fabricated irregular eye-shaped microcapsules with a core/wall ratio as high as 12:1, for the encapsulation of L-carvone, limonene, hexyl salicylate used in this study via complex coacervation using chitosan and gum

arabic.

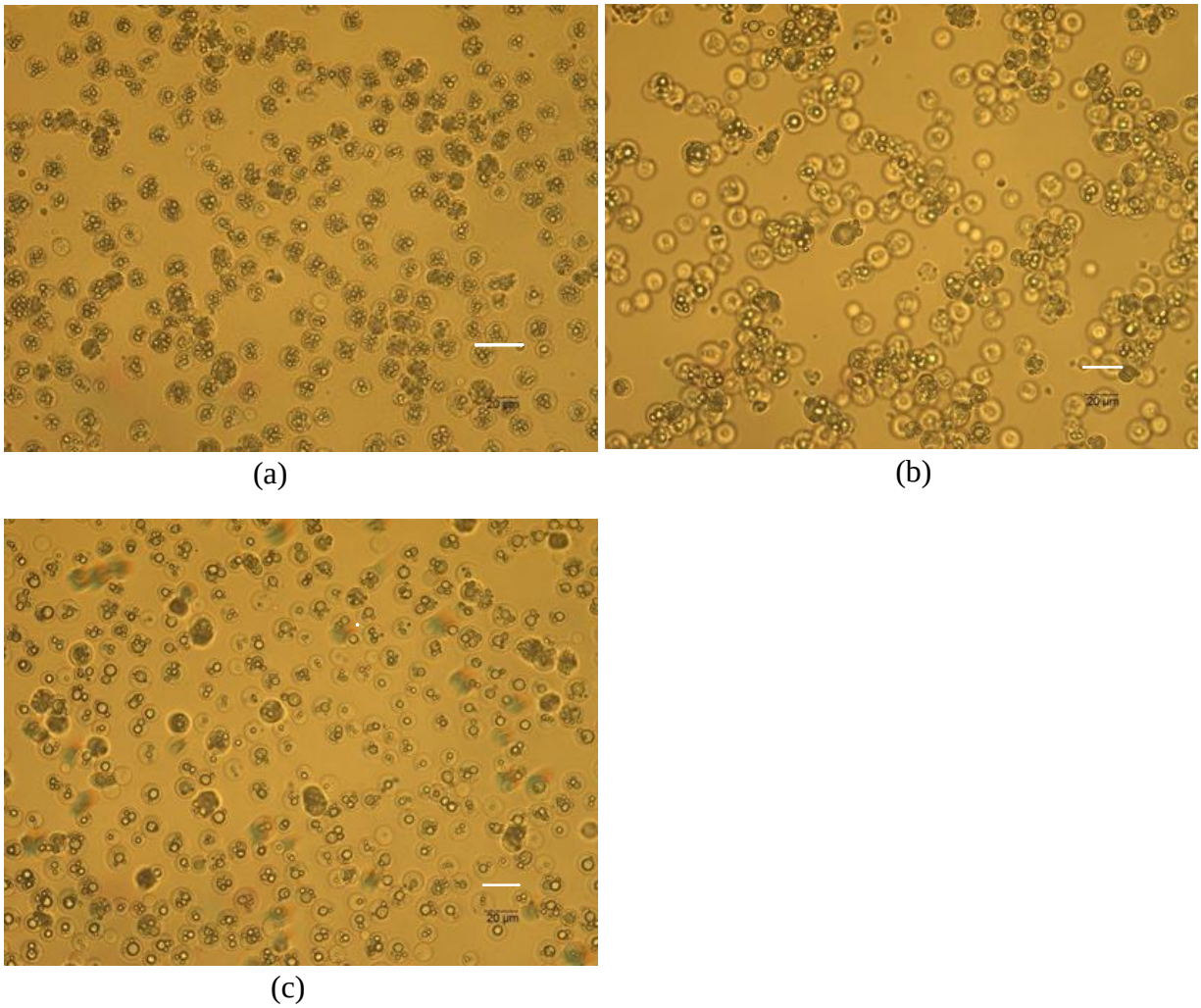

(a) (b)

(c)

Figure 4-2. Optical microscopy images of different microcapsules prior to spray drying (a) LC, (b) LM and (c) HS. Scale bars represent 20 µm.

SEM micrographs of spray dried microcapsules with different cores are presented in Figure 4-3. As can be seen in Figure 4-3 (a), (c) and (e), different oil microcapsules appear to have relatively spherical shapes and smooth surfaces, with the presence of wrinkles or concavities, which may be a consequence of the shrinkage of microcapsules due to the rapid evaporation of moisture during spray drying (Rocha et al., 2012). Similar morphological characteristics were also reported by other authors using the same wall materials when Yu et al. (2021) fabricated

microcapsules for the encapsulation of fish oil, and Dong et al. (2011) prepared peppermint oil microcapsules via GA-GE complex coacervation. In addition, similar morphologies were also observed for spray dried microcapsules using different shell materials, when orange essential oil was encapsulated by whey protein isolate and gum arabic as wall materials (Rojas-Moreno et al., 2018), β-carotene was encapsulated by modified tapioca starch (Loksuwan, 2007), and ascorbic acid was encapsulated by Capsul and maltodextrin (Finotelli & Rocha-Leão, 2005). It was further demonstrated by Sheu et al. (1998) that the formation of indentations on microcapsule surface can potentially be attributed to wall compositions and spray drying conditions. Besides, multiple minute coacervates with smooth surface were also observed at the surface of relatively larger microcapsules. Partly incomplete microcapsules with their unsealed shell can be seen in Figure 4-3 (b), (d) and (f), suggesting the core-shell inner structure for different oil microcapsules.

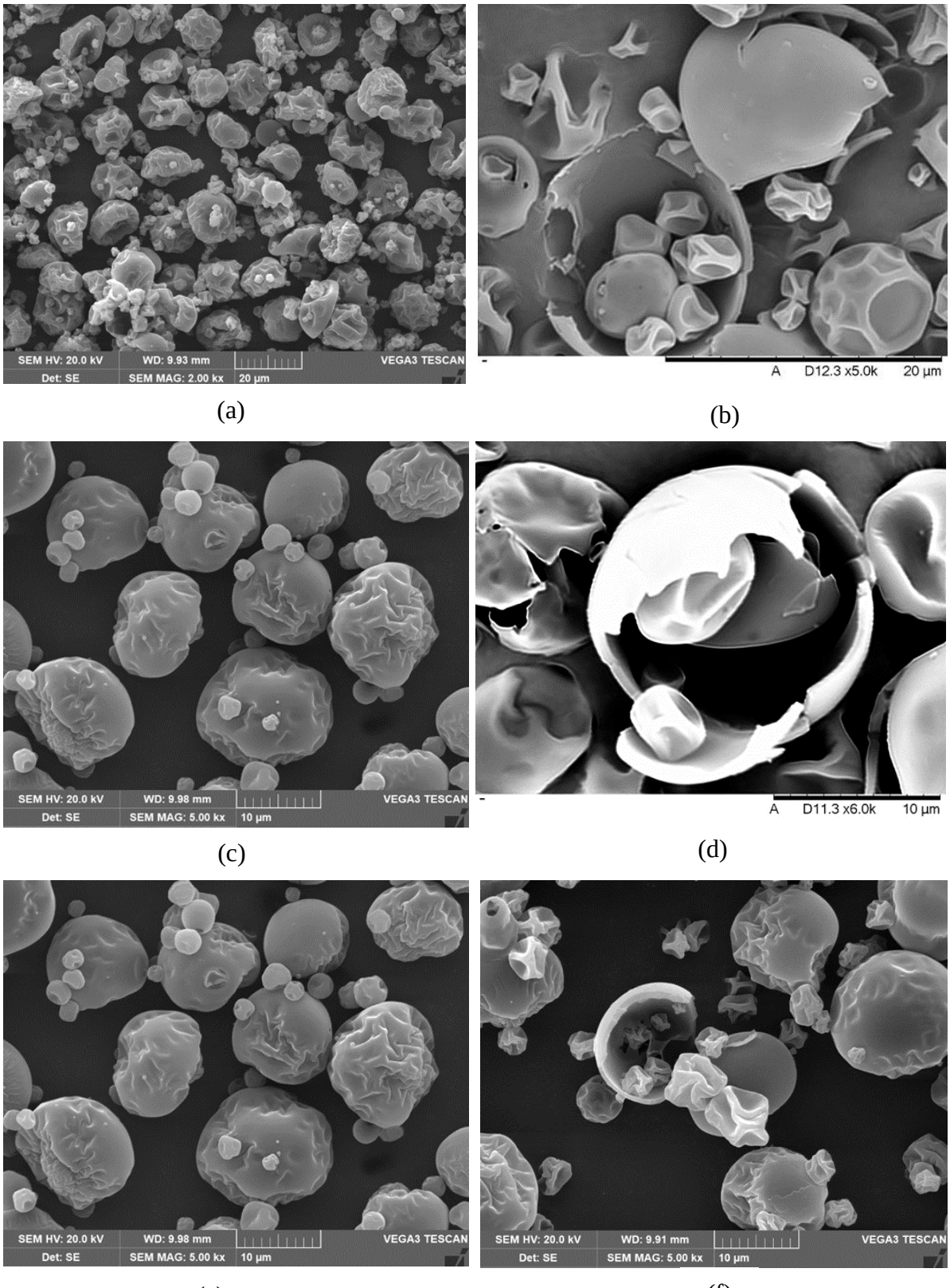

Figure 4-3. SEM images of (a) spray dried GG-LC-GT microcapsules, (b) partly incomplete GG-LC-GT microcapsules, (c) GG-LM-GT microcapsules, (d) partly incomplete GG-LM-GT microcapsules, (e) GG-HS-GT microcapsules, (f) partly incomplete GG-LM-GT microcapsules.

4.3.2. Particle size and size distribution

The size and size distribution of HS oil droplets and HS microcapsules as representatives are illustrated in Figure 4-4. The surface mean size of HS oil droplets in emulsion is approximately 3.85 ± 0.01 μm whilst HS microcapsules have an average size of 10.71 ± 0.06 μm, suggesting the possibility of successful entrapment of core oils within microcapsules, which was also evidenced by optical images (Figure 4-2).

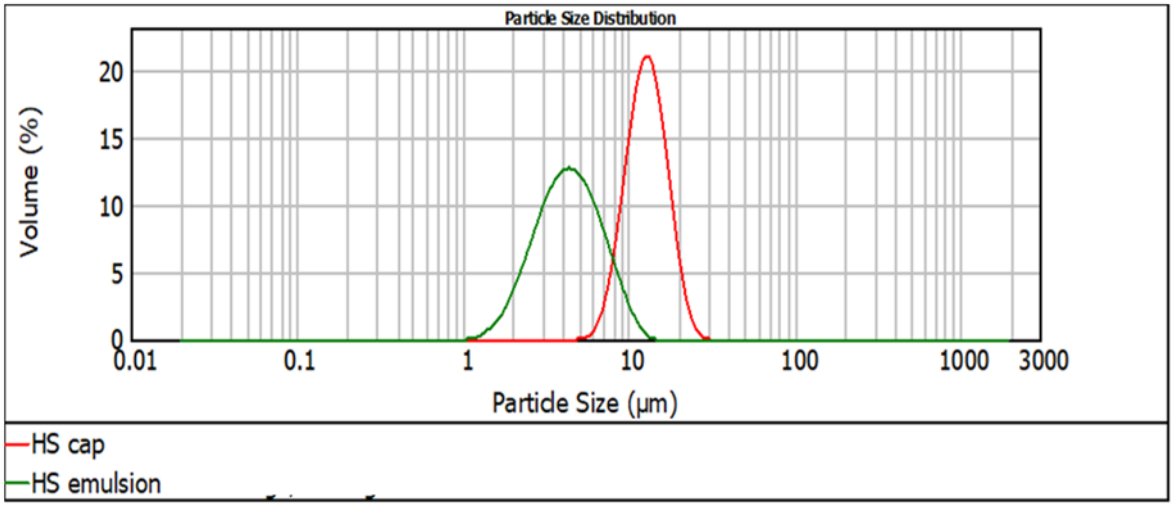

Figure 4-4. Size and size distribution of HS emulsion and HS microcapsules.

The mean size and size distribution of different oil microcapsules are displayed in Figure 4-4. There are significant statistical differences in the mean size between GG-LC-GT microcapsules (9.8 ± 0.1 μm) and GG-LM-GT and GG-HS-GT microcapsules of 11.0 ± 0.2 μm and 10.7 ± 0.1 μm respectively, suggesting the significant influence of core oils on their microcapsule sizes. Van der Graaf et al. (2004) reported that lower interfacial tension between oil and aqueous phase can lead to smaller sized emulsion droplets, which was in accordance with this work since LC has a lower interfacial tension with aqueous phase than HS and LM (see Table 5-2). In addition, all samples exhibit narrow size distributions with a relatively

small span value approximately at 0.7.

Table 4-2. Mean surface size and span of different microcapsules (mean ± 2×St. Err)

Microcapsules	GG-LC-GT	GG-LM-GT	GG-HS-GT
$D_{[3,2]}$ (μm)	9.8 ± 0.1	11.0 ± 0.2	10.7 ± 0.1
Span	0.739 ± 0.001	0.728 ± 0.001	0.778 ± 0.001

4.3.3. FT-IR analysis

The FT-IR spectra of the shell materials and different oil microcapsules are displayed in Figure 4-5. Figure 4-5 (a) shows the peaks of gum arabic, gelatine and GA-GE coacervate that was used as the shell material for oil encapsulation. The FT-IR spectrum of gum arabic reveals a broad peak at 3314 cm^{-1}, which was attributed to OH stretching vibration (Anvari & Chung, 2016; Rousi et al., 2019; Wang et al., 2021), and overlapping the peak of amino group stretching (Espinosa-Andrews et al., 2010; Shaddel et al., 2018). The peak that appears at 2909 cm^{-1} was a characteristic of OH stretching vibration, confirming the presence of carboxyl groups which are negatively charged (Comunian et al., 2013). Two strong bands at 1599 cm^{-1} and 1420 cm^{-1} can be detected, corresponding to asymmetric and symmetric stretching vibration of carboxylic acids (Espinosa-Andrews et al., 2010; Rousi et al., 2019; Wang et al., 2021). The strong peak occurring at 1020 cm^{-1} is associated with the bending vibration of the CO bonds (Espinosa-Andrews et al., 2010). The FT-IR spectrum of gelatine highlights a broad vibrational peak occurring at 3289 cm^{-1}, corresponding to amide A, which is due to the vibrations of OH and NH bonds in amino groups and positively charged in acidic medium (Jridi et al., 2014; Oliveira et al., 2019; Peng et al., 2014). Other absorption bands appearing at 1631 cm^{-1}, 1528 cm^{-1} and 1242 cm^{-1} are related to amide I (C=O and CN

stretching), amide II (mainly NH bending) and amide III (CN stretching vibrations) respectively (Anvari & Chung, 2016; Liu et al., 2012). After complex coacervation, the stretching vibrations of carboxyl groups in the GA occurring at 1599 cm^{-1} is not present in the GA-GE coacervates spectrum, and the characteristic peak at the amide I region (1631 cm^{-1}) for gelatine spectrum was shifted to a higher wavelength at 1642 cm^{-1}, indicating the involvement of GA molecules in electrostatic interactions and the carboxylic groups of GA molecules complexed with the amino groups of GE molecules upon the formation of the coacervates. Similar observations have been also reported by other authors for upshift wavenumber of amide I units after coacervation (Anvari et al., 2015; Duhoranimana et al., 2017; Mendes et al., 2018; Rousi et al., 2019). Amide I region can reflect the secondary structure of proteins, which is primarily due to the C=O bonds vibration coupled with the CN stretching (Surewicz & Mantsch, 1988). The absorption peak at 1633 cm^{-1} was considered a characteristic for the random coil structure of gelatine (Yakimets et al., 2005), and the upshift of the amide bands I from 1631 cm^{-1} to 1642 cm^{-1} suggests that gelatine might possibly undergo a structural transition from a random coil to a helical conformation attributed to the intermolecular interactions between GA and GE. Amide II is attributed to the combination of CN stretching and NH bending from peptides, and the shift of the peak in amide II to a higher wavelength suggests that hydrogen bonds were formed in the complex coacervates (Anvari et al., 2015).

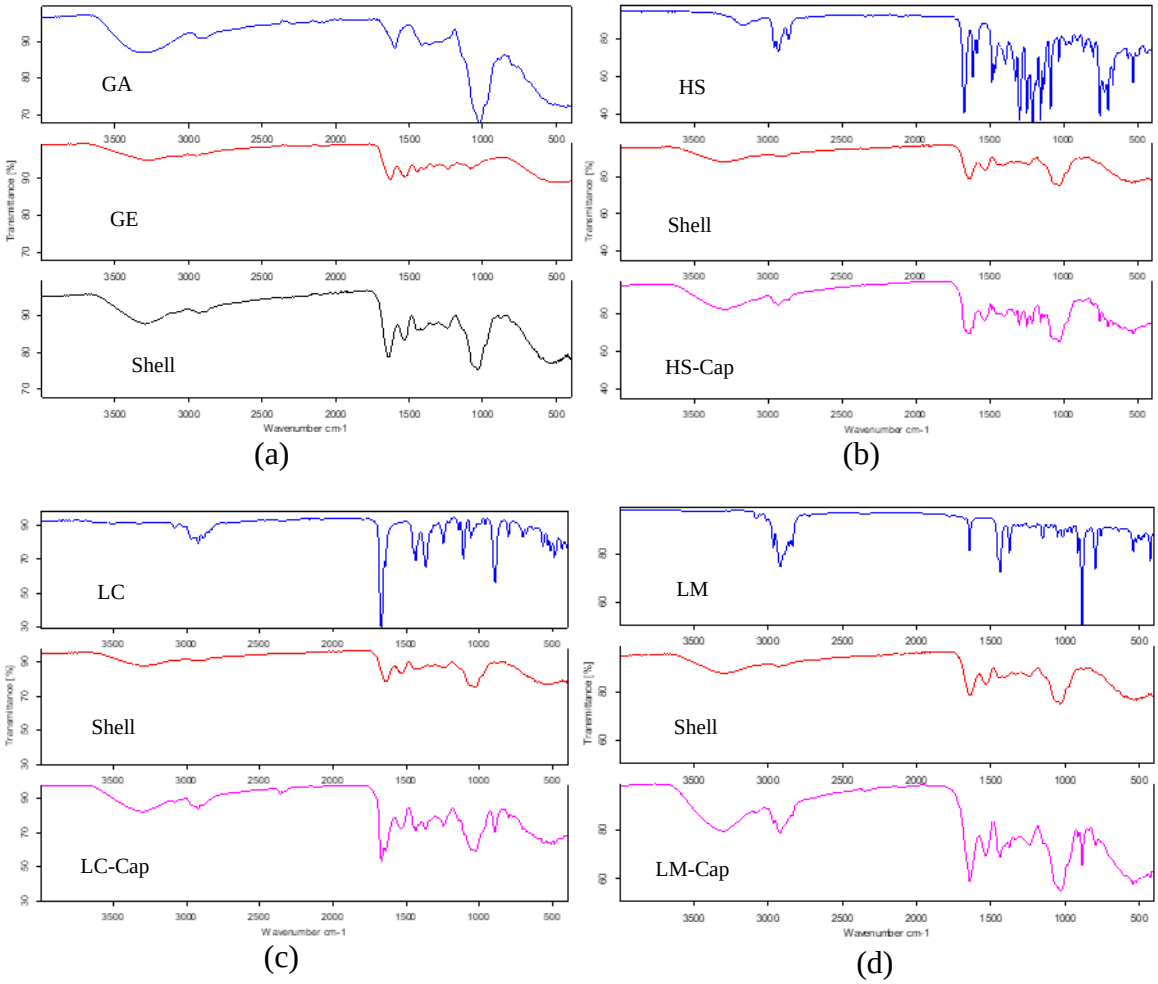

Figure 4-5. FT-IR spectra of (a) wall materials, (b) HS and HS-entrapping microcapsules, (c) LC and LC-entrapping microcapsules, and (d) LM and LM-entrapping microcapsules.

The blue curves in Figure 4-5 (b), (c) and (d) present the spectrum of HS, LC and LM respectively. The aromatic stretching vibrations of C=O from the carbonyl group can be identified at 1685 cm^{-1} for LC whereas the aliphatic stretching vibrations of C=O bonds occur at 1725 cm^{-1} for HS oil. The peak at 1640 cm^{-1} confirms the vibrational aromatic C=C bonds for LC and LM and similarly the peak region of 1610 and 1550 cm^{-1} for HS can be observed, corresponding to the aromatic stretching of conjugated C=C bonds. The aromatic and alkyl CH stretching can be read for LC, LM and HS at the region of 2954 and 2864 cm^{-1}. In

addition, the peaks located in the region of 1300 and 1150 cm^{-1} are associated with the stretching vibrations of C-O-C group for HS oil. The characteristic peak at 850 cm^{-1} was attributed to CH bending absorption for LM. The results are well in consistent with the works reported by other authors (Alipanah et al., 2021; Baiocco et al., 2021a; Elmastaş et al., 2006). The resultant microcapsule spectrum can be observed from the overlapping of each core oil absorption bonds with the shell coacervate spectrum in Figure 4-5 (b), (c) and (d) respectively, since there were no new formed peak and the specific characteristic peaks of each core oil can also be detected in its corresponding microcapsule spectrum, evidencing the successful entrapment of each core oil within GA-GE coacervates.

4.3.4. Payload and encapsulation efficiency

The payload and encapsulation efficiency of different microcapsules are summarised in Table 4-3. As can be seen, the payload and EE of GG-HS-GT were determined to be 29.7 ± 0.4% and 89.0 ± 1.2%, which are similar to the values (28.3 ± 0.7% and 89.8 ± 1.4%) of fish oil microcapsules prepared by Yu et al. (2021) following the same experimental formulations and procedures. Similar EE values were also reported for the encapsulation of other essential oils employing the coacervation between gum arabic and gelatine by other authors (Khatibi et al., 2021; Napiórkowska & Kurek, 2022b; Pakzad et al., 2013; Rungwasantisuk & Raibhu, 2020; Xiao et al., 2014b). The obtained GG-HS-GT microcapsules present superiorly to the HS entrapped microcapsules (EE, 47 ± 11%) prepared by Baiocco et al. (2021a) using chitosan and gum arabic as wall materials, indicating the superior performance of gelatine than chitosan in forming microcapsules with a higher encapsulation efficiency (Baiocco et al., 2021b; Bruyninckx & Dusselier, 2019). Besides, it is worth noting that additional treatments

to freshly coacervated microcapsules significantly improved the payload as well as EE. Similar results were also reported by Tello et al. (2016) that the EE of soy oil increased from 79.0% to 89.9% after microcapsules were crosslinked with glutaraldehyde. Liu and Jiang (2023) discussed the influence of crosslinkers on encapsulating β-Ionone, and found microcapsules crosslinked with higher concentrations of glutaraldehyde exhibited higher EE of the core material. Dinarvand et al. (2005) explained that a higher amount of glutaraldehyde increased the density of polymer through the chemical coupling of aldehyde groups with the amino groups of the gelatine (Chang et al., 2006), and thus reduced macromolecular chains mobility and finally formed stable and rigid spheres, which was conducive for better entrapment of the core material. Maltodextrin as an out layer of physical coating for coacervated microcapsules also enhanced the payload and EE of microcapsules. However, the payload and EE were significantly lower than those of GG-HS-GT, suggesting the higher permeability of maltodextrin coating than the chemical reticulation after glutaraldehyde crosslinking. In addition, it is notable that the payload of GG-HS-MD was expected to be lower than GG-HS microcapsules as 1.5 g maltodextrin was used and increased the value of total mass of particles. However, higher values of both payload and EE were obtained for GG-HS-MD, suggesting that the additional physical coating by maltodextrin significantly reduced the core loss during the spray drying process.

Table 4-3. Payload and corresponding encapsulation efficiency of different microcapsules (mean ± 2 × St. Err)

Microcapsules	Payload (%)	Encapsulation efficiency (%)
GG-HS	7.0 ± 0.1	21.1 ± 0.1
GG-HS-MD	10.1 ± 0.3	54.0 ± 2.0
GG-HS-GT	29.7 ± 0.4	89.0 ± 1.2
GG-LM-GT	9.9 ± 0.9	30.0 ± 2.6
GG-LC-GT	1.7 ± 0.1	5.0 ± 0.4

Significant variations of payload and EE were obtained for different oil microcapsules following the identical formulations of the wall materials and preparation procedures. The highest payload and EE are 29.7 ± 0.4% and 89.0 ± 1.2% for GG-HS-GT, while GG-LC-GT presents a low payload and EE at 1.7 ± 0.1% and 5.0 ± 0.4%. Such differences can be ascribable to the evaporation of volatiles during encapsulation stage and/or spray drying process. However, considering the higher values of payload and EE of GG-LM-GT compared to GG-LC-GT and their vapour pressure values (the vapour pressure of L-carvone is 0.115 mm Hg at 25 °C, compared to 1.98 mm Hg at 25 °C of limonene (PubChem, 2023a;2023b)), it is unlikely that the loss was solely due to volatile evaporation. It is presumed that the payload and EE of different oil microcapsules are associated with their inner structures and morphologies, which are dominated by the interfacial tension balance between different phases (Loxley & Vincent, 1998; Torza & Mason, 1970) since different oils have different interfacial tensions against GA-GE coacervates phase and aqueous phase. The mechanism underlying this phenomenon will be investigated and discussed in Chapter 5.

4.3.5. Mechanical properties of coacervated microcapsules

4.3.5.1. Rupture analysis

The rupture force, displacement at rupture, nominal rupture stress, toughness and nominal rupture tension as a function of diameter of different microcapsules are presented in Figure 4-6. Both the rupture force and the displacement at rupture increase with microcapsule diameter. In contrast, the nominal rupture stress and toughness decreased with the increase of microcapsule size. The nominal rupture tension was independent of diameter. These results are consistent with the previous work of microcapsules prepared with the same shell materials (Yu et al., 2021), or different wall materials (Baiocco et al., 2021a; Luo et al., 2022).

The mechanical properties of different microcapsules varied significantly when different core oils or encapsulation methods were used, as shown in Figure 4-6. In order to investigate the influence of different variables on the mechanical properties, the average values of the rupture force, displacement at rupture, nominal rupture stress, toughness and nominal rupture tension were calculated and the data are presented in Table 4-4. For microcapsules prepared with HS oil, GG-HS-MD and GG-HS-GT had similar values of toughness, which were significantly higher than that of GG-HS, indicating that microcapsules prepared with a second coating by maltodextrin or wall hardened by glutaraldehyde crosslinking were mechanically stronger than those without additional treatment. It is worth noting that a microcapsule rupturing at a relatively smaller deformation is more likely due to its higher structural brittleness. On the contrary, if a microcapsule ruptures at a larger deformation, the phenomenon is associated with its greater structural flexibility and stretchability (Baiocco & Zhang, 2022). The average rupture tension of GG-HS-MD was 175 ± 33 μN/μm, which is significantly higher than that of

GG-HS-GT (120 ± 16 μN/μm), whilst the average deformation at rupture of GG-HS-MD (12 ± 1 %) was marginally lower than GG-HS-GT (15 ± 1 %). Although both additional treatments made microcapsules mechanically stronger, the former provided a layer of dried physical coating to make the microcapsules more structurally brittle while the latter made the microcapsules more flexible to resist capsule rupture through gelatine-glutaraldehyde crosslinking. For microcapsules prepared with different core oils, although there was no significant difference in the mechanical strength parameters between GG-LM-GT and GG-HS-GT, their rupture force, nominal rupture stress, rupture tension and toughness of GG-LC-GT were significantly higher than the corresponding LM and HS microcapsules, which suggests that the influence of core oils on the mechanical strength of microcapsules is not negligible. Similar results were also reported by other authors (Baiocco & Zhang, 2022; Luo et al., 2022). Luo et al. (2022) encapsulated 2-hydroxy-3-(octanoyloxy) propyl decanoate, hexyl salicylate, lavender oil and lily oil within melamine-glutaraldehyde-formaldehyde microcapsules via an in-situ polymerization method and found stronger microcapsules were obtained when encapsulating core oils with higher hydrophobicity. Baiocco & Zhang (2022) reported that LM microcapsules were mechanically weaker than the HS microcapsules after the wall was fabricated using gum arabic and fungally fermented chitosan via complex coacervation and vacuum drying. They assumed the difference may be due to the nature of terpenic molecules (LM), which can cause a higher interfacial energy level, and possibly impair the intermolecular bonds within coacervates network, thereby affecting the overall robustness of the microcapsule.

The mechanical properties of microcapsules can be associated with their chemical

compositions, geometries and inner structures, which resulted from the interfacial energy balance between the phases in the system (Loxley & Vincent, 1998; Torza & Mason, 1970). As can be seen in Table 5-2, LC, LM and HS have different interfacial tensions against GA-GE coacervates phase and aqueous phase, microcapsules with different inner structures and morphologies can be obtained. For instance, due to the hydrophobic nature of core oils, HS and LM have higher interfacial tensions with aqueous phase than LC, which favours the movement of coacervate phase to the water/oil interface to form the microcapsules with a core-shell structure. Comparatively, the lower value of interfacial tension between LC and aqueous phase results in less core-shell structured microcapsules, i.e., more solid-like microspheres, which correspondingly results in stronger mechanical strength. The results of payloads for each oil microcapsule can possibly evidence this assumption (see Table 4-3).

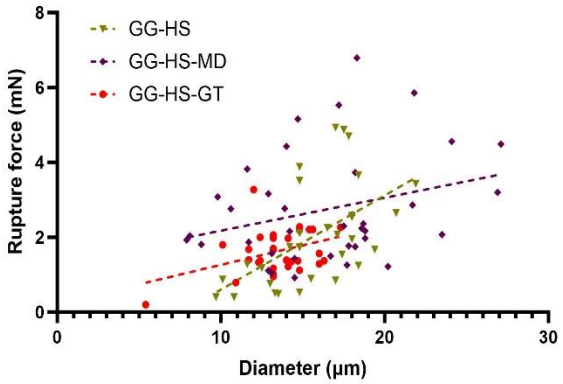
GG-HS
GG-HS-MD
GG-HS-GT
Rupture force (mN)
Diameter (μm)

(A)

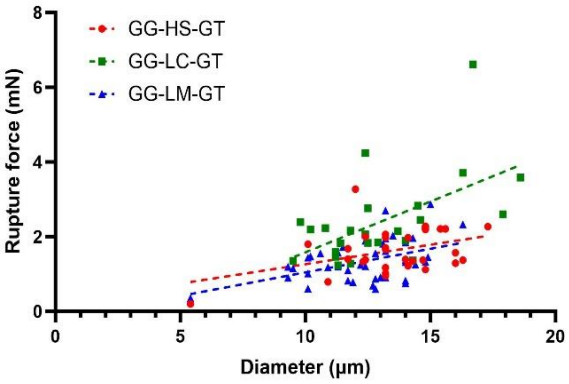
GG-HS-GT
GG-LC-GT
GG-LM-GT
Rupture force (mN)
Diameter (μm)

(a)

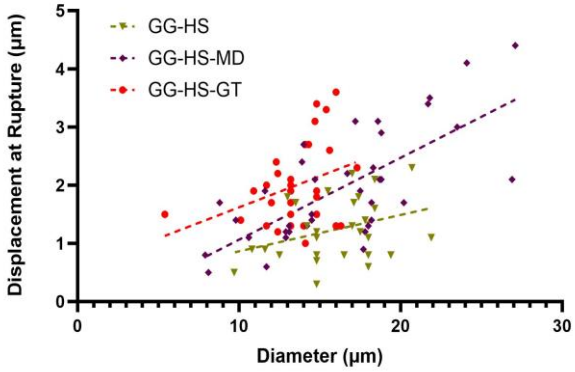
GG-HS
GG-HS-MD
GG-HS-GT
Displacement at Rupture (μm)
Diameter (μm)

(B)

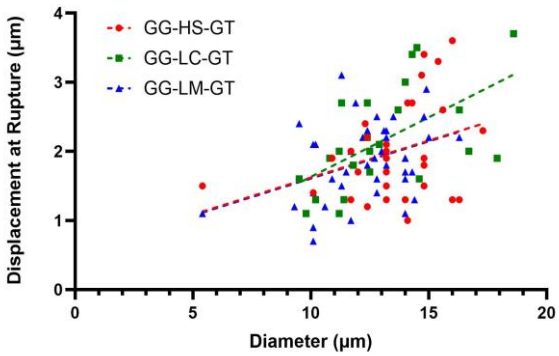
GG-HS-GT
GG-LC-GT
GG-LM-GT
Displacement at Rupture (μm)
Diameter (μm)

(b)

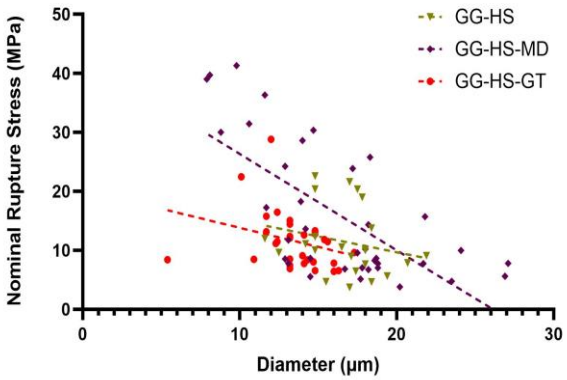
GG-HS
GG-HS-MD
GG-HS-GT
Nominal Rupture Stress (MPa)
Diameter (μm)

(C)

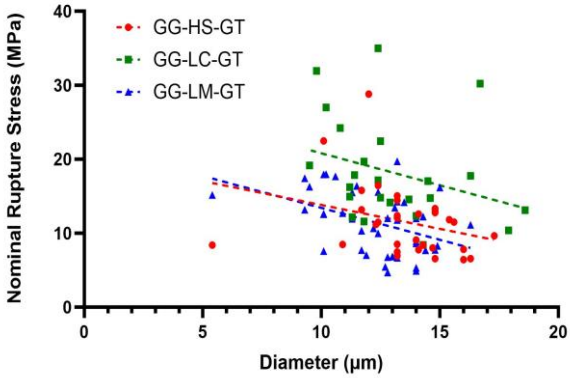
GG-HS-GT
GG-LC-GT
GG-LM-GT
Nominal Rupture Stress (MPa)
Diameter (μm)

(c)

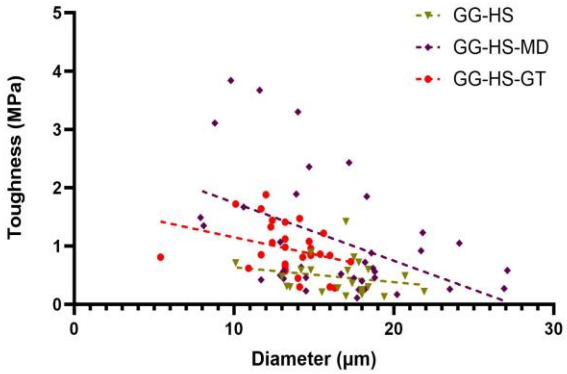
GG-HS
GG-HS-MD
GG-HS-GT
Toughness (MPa)
Diameter (μm)

(D)

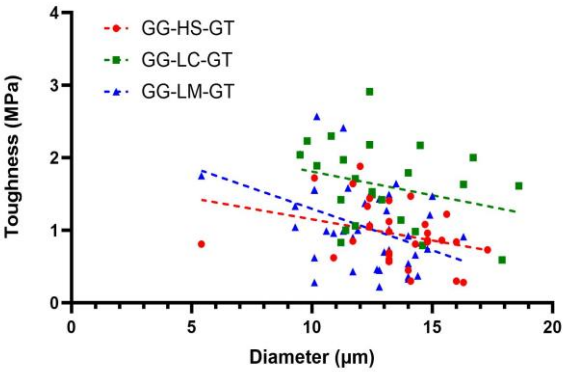
GG-HS-GT
GG-LC-GT
GG-LM-GT
Toughness (MPa)
Diameter (μm)

(d)

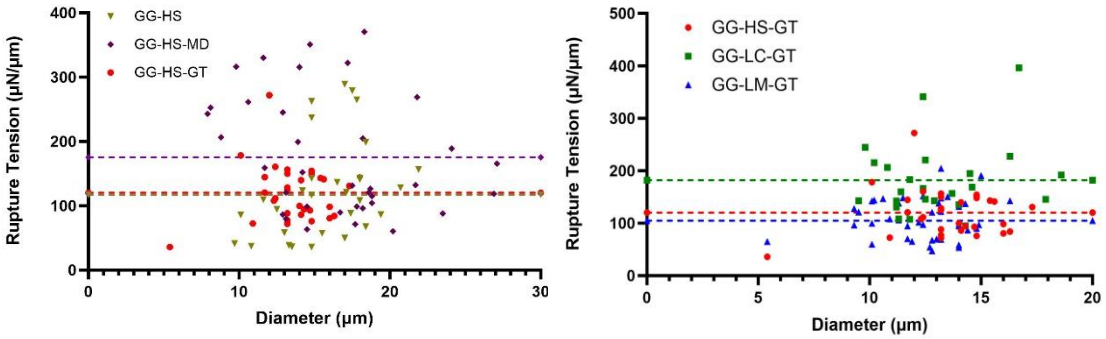

Figure 4-6. Mechanical strength parameters of microcapsules versus diameter: rupture force (A, a), displacement at rupture (B, b), nominal rupture stress (C, c), nominal toughness (D, d) and nominal rupture tension (F, f). ▼: GG-HS, ♦: GG-HS-MD, ●: GG-HS-GT, ■: GG-LC-GT, and ▲: GG-LM-GT. The dotted lines only indicate the trend or the mean value for nominal rupture tension

Table 4-4. Summary of the mechanical strength of GE-GA coacervated microcapsules (mean ± 2 × St. Err).

Microcapsules	GG-HS	GG-HS-MD	GG-HS-GT	GG-LM-GT	GG-LC-GT
Diameter (µm)	16.6 ± 2.0	16.6 ± 1.6	13.5 ± 0.8	12.5 ± 0.6	13.0 ± 1.0
Displacement at Rupture (µm)	1.5 ± 0.4	2.0 ± 0.4	2.0 ± 0.2	2.0 ± 0.2	2.2 ± 0.4
Rupture force (mN)	1.9 ± 0.5	2.7 ± 0.5	1.6 ± 0.2	1.3 ± 0.2	2.4 ± 0.5
Nominal Deformation at Rupture (%)	9 ± 2	12 ± 1	15 ± 1	15 ± 2	17 ± 2
Nominal Rupture Stress (MPa)	10 ± 2	16 ± 4	12 ± 2	11 ± 1	18 ± 3
Nominal Rupture Tension (µN/µm)	117 ± 29	175 ± 33	120 ± 16	105 ± 13	182 ± 29
Nominal Toughness (MPa)	0.4 ± 0.1	1.2 ± 0.4	1.0 ± 0.2	1.0 ± 0.2	1.6 ± 0.2

4.3.5.2. Apparent Young's modulus determined by Hertz analysis

The Hertz model fitting to the force versus displacement data of a representative GG-HS-GT microcapsule is presented in Figure 4-7, and the Young's modulus for each type of microcapsules versus diameter is shown in Figure 4-8.

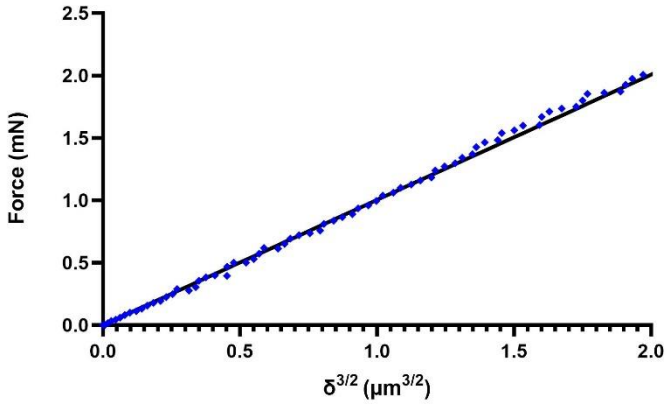

Figure 4-7. A linear fit of the Hertz model to the experimental force versus displacement data for a representative GG-HS-GT (17.5 μm) microcapsule (R^2 = 0.99). ♦: Experimental data, straight line: Hertz model fitting.

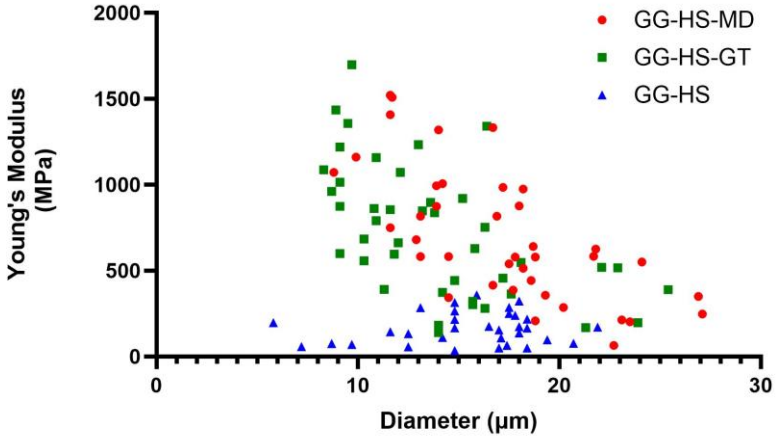

(a)

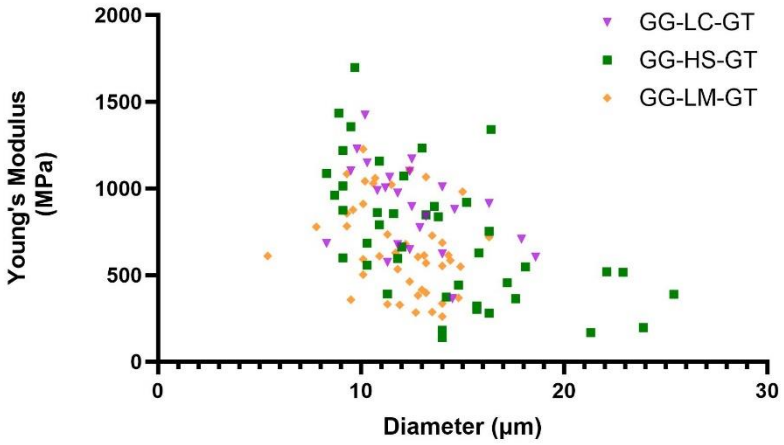

(b)

Figure 4-8. Apparent Young's modulus of different microcapsules versus diameter (a) GG-HS, GG-HS-MD and GG-HS-GT and (b) GG-HS-GT, GG-LC-GT and GG-LM-GT. ▼: GG-LC-GT, ♦: GG-LM-GT, ●: GG-HS-MD, ■: GG-HS-GT, and ▲: GG-HS.

Figure 4-8 presents the Young's modulus as a function of particle diameters for the compressed microcapsules. As can be seen in Figure 4-8 (a), the Young's modulus of GG-HS microcapsules was holistically lower than GG-HS-MD and GG-HS-GT, indicating the latter two types of microcapsules had higher elasticity. The mean values of Young's modulus for each type of microparticle as well as the corresponding coefficient of determination (R^2) are summarised in Table 4-5.

Table 4-5. Mean values of apparent Young's modulus for different microcapsules and their corresponding mean values of R^2 from using the Hertz model (mean ± 2×St.Err)

Microcapsules	Young's Modulus (MPa)	R^2
GG-HS	163 ± 33	0.86 ± 0.04
GG-HS-MD	702 ± 125	0.81 ± 0.06
GG-HS-GT	668 ± 165	0.80 ± 0.04
GG-LM-GT	663 ± 79	0.80 ± 0.04
GG-LC-GT	891 ± 104	0.91 ± 0.04

The mean R^2 values obtained from all microcapsules are in a range of 0.80-0.91, which implies the fitting is good, but not perfect. The Hertz model can normally be applied to describe the relationship between the imposed compression force and the displacement of the spherical homogenous particles at small fractional deformation (up to 10 %) (Baiocco et al., 2023; Wang et al., 2018). Herein, the calculated Young's modulus in this work is in fact the apparent young's modulus of the whole microcapsules as they contained multiple oil droplets which are considered to have no elastic performance but are able to affect the force response under compression. The value of R^2 of GG-LC-GT (0.91) is higher than those of other microcapsules, indicating that GG-LC-GT may be more homogenous and uniform, which can possibly be evidenced by the lower value of oil payload for GG-LC-GT microcapsules.

For HS microcapsules prepared by different methods, both GG-HS-MD and GG-HS-GT had significantly higher values of apparent Young's modulus than GG-HS, indicating that the further treatments towards GE-GA coacervated microcapsules improved their elastic performance. Compared with GG-HS, the crosslink of glutaraldehyde on gelatine/gum arabic resulted in a more compact shell structure for GG-HS-GT (Knaebel et al., 1997), potentially allowing higher payload of core oil. While for microcapsules prepared with identical shell

materials, the mean apparent Young's modulus of GG-LC-GT was significantly higher than GG-HS-GT and GG-LM-GT microcapsules. As aforementioned, core oils of different hydrophobicity may influence the diffusion of the coacervates from the bulk to oil/water interface or glutaraldehyde molecules and thus the crosslink reaction rate, leading to the gradient of local crosslink density and spatial distribution on capsule surface (He et al., 2008), which eventually resulted in the variation in payload and mechanical properties even with identical shell chemical compositions.

Theoretically, Young's modulus represents the intrinsic stiffness of an elastic material undergoing recoverable deformation, which is expected to be a constant value regardless of microcapsule size. However, as presented in Figure 4-8, it seems that the apparent Young's modulus of microcapsules is strongly size dependant and larger microcapsules have less Young's modulus values. As discussed above, the calculated apparent Young's modulus is the outcome of liquid core combined with the shell material and cannot fully represent the intrinsic elastic modulus value of the shell material. The deviations between the apparent and intrinsic Young's modulus become more evident especially when the microcapsules are larger for lower volume ratios of shell material to core if the shell thickness is independent of microcapsule size (Mercadé-Prieto et al., 2011). Baiocco et al. (2023) reported that gum arabic and chitosan coacervated core-shell microcapsules were firstly treated as homogenous solid spherical microspheres to estimate the apparent Young's modulus of the whole microcapsules by the Hertz model, and the intrinsic Young's modulus of shell material was also quantified via finite element analysis (FEA). They reported that the apparent Young's modulus (0.095 ± 0.014 GPa) of microcapsules was approximately one order of magnitude lower than the

intrinsic Young's modulus of the shell material (1.02 ± 0.13 GPa), suggesting that the effects of microcapsule inner structural configurations were not neglectable.

4.3.5.3. Intrinsic Young's Modulus of shell material by FEA model

Considering the bending and stretching effects of shell material under compression, Mercade-Prieto et al. (2011) developed a reliable FEA numerical model for core–shell structured microcapsules, which enables the evaluation of the intrinsic Young's modulus of shell material, as well as the determination of wall thickness to capsule radius ratio (h/R) for the corresponding microcapsule using the experimental micromanipulation data at relatively low fractional deformation ($\leqslant$ 0.1 within the elastic region), which can be expressed mathematically as:

$$F = E_{in}Rh(a\varepsilon^2 + b\varepsilon + c) \qquad (4\text{-}5)$$

where the three coefficients a, b and c are h/R dependent and correlated with polynomial functions, from which the obtained values of shell thickness (h) were further validated by Transmission Electron Microscopy (TEM) for the cross-sectional imaging for 186 microcapsules.

The fractional deformation ε can be calculated as $\frac{\delta}{2R}$, as illustrated in below,

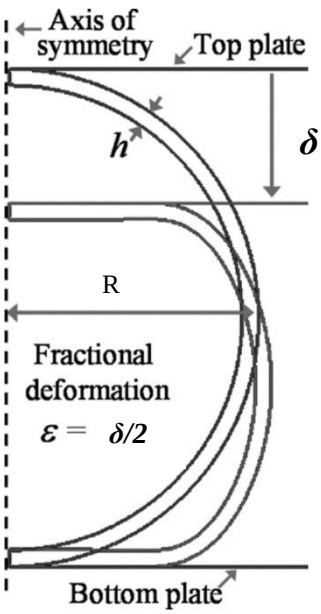

Figure 4-9. Schematic diagram of a core-shell capsule before and after a displacement δ of top plate (Mercadé-Prieto et al., 2012b).

Hence, E_{in} can be expressed using Equation (**4-5**):

$$E_{in} = \frac{F}{\frac{h}{R}\left[a\left(\frac{\delta}{2}\right)^2 + b\left(\frac{\delta}{2}\right)R + cR^2\right]} \quad (4\text{-}6)$$

where E_{in} is the intrinsic Young's modulus of the shell material of microcapsules, F is the experimental compression force measured by micromanipulation, δ is the compressive axial displacement during compression, h/R is the ratio of shell thickness to the microcapsule initial radius, a, b and c are the polynomials of h/R to determine the coefficients in Equation (**4-5**) and summarised in Table 4-6.

Table 4-6. Polynomial functions of h/R (Mercadé-Prieto et al., 2011)

Coefficients	Polynomials
a	$95071.891\times (h/R)^5 - 28426.030 \times (h/R)^4 + 2411.056 \times (h/R)^3 - 7.476 \times (h/R)^2 - 10.829 \times (h/R) + 1.52882$
b	$-318.702 \times (h/R)^4 + 120.784 \times (h/R)^3 - 11.380 \times (h/R)^2 + 2.518 \times (h/R) - 0.05792$
c	$-0.004242 \times (h/R) + 0.00107$

A typical example of the force versus fractional deformation data obtained from the compression of a representative GG-LC-GT microcapsule fitted by FEA simulation (Equation (4-**5**)) result is presented in Figure 4-10. For each sample, more than 30 microcapsules were analysed and the shell Young's modulus and h/R values were determined by the FEA model.

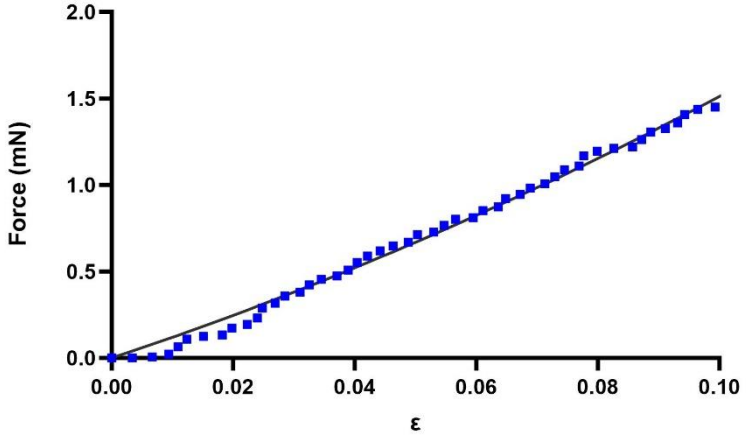

Figure 4-10. FEA simulation for a representative GG-LC-GT (10.8 µm) microcapsule (E_{in}= 10.541 GPa, h/r = 0.1035, R^2 = 0.99). ♦: Experimental force, straight line: FEA simulation regression.

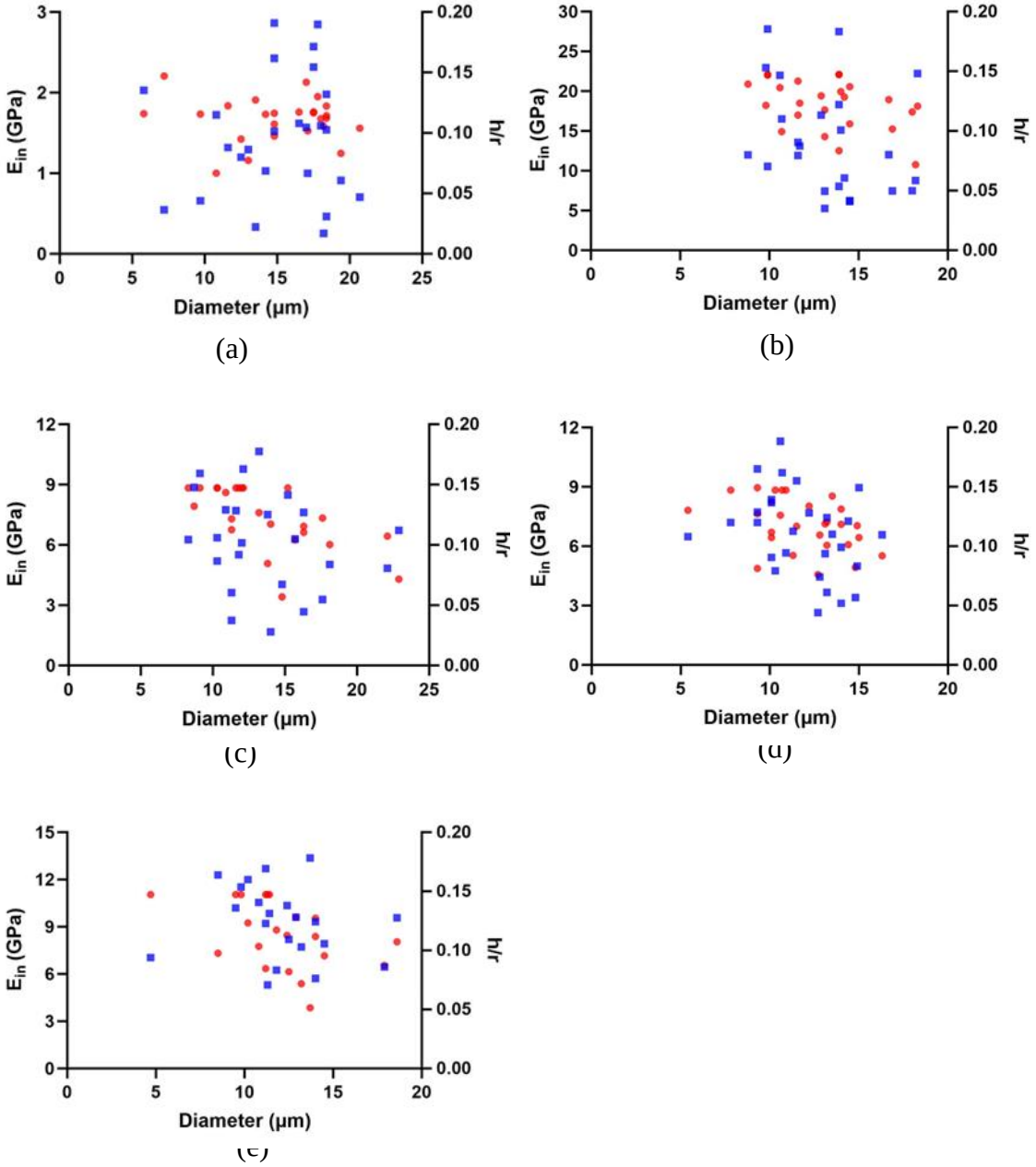

Figure 4-11. FEA-derived intrinsic Young's modulus and h/R values of different microcapsules versus diameter (a) GG-HS, (b) GG-HS-MD, (c) GG-HS-GT, (d) GG-LM-GT and (e) GG-LC-GT. ■: intrinsic shell Young's modulus, ●: h/r.

Figure 4-11 presents the FEA-derived intrinsic Young's modulus and h/r ratios versus diameter for the corresponding microcapsules. On average, the Young's modulus value by FEA for each type of microcapsule did not seem to vary with the diameter significantly, which agrees with the discussion in Section 4.3.5.2, and indicates FEA might be a more accurate model to

determine the E_{in} for core-shell structured microcapsules. The values of h/R for each sample reduced with particle size holistically, which is consistent with results of Baiocco et al. (2023). The mean E_{in} values along with the corresponding h/r as well as coefficient of determination R^2 for each sample can be seen in Table 4-7.

Table 4-7. Mean values of intrinsic Young's modulus of shell materials and h/r for different microcapsules and their corresponding mean values of R^2 derived from FEA model (mean ± 2×St.Err)

Microcapsules	Young's Modulus (GPa)	h/R	R^2
GG-HS	1.5 ± 0.3	0.111 ± 0.007	0.970 ± 0.005
GG-HS-MD	13.7 ± 2.8	0.122 ± 0.008	0.977 ± 0.005
GG-HS-GT	6.2 ± 1.0	0.115 ± 0.010	0.975 ± 0.004
GG-LM-GT	6.4 ± 0.8	0.117 ± 0.007	0.976 ± 0.004
GG-LC-GT	9.3 ± 1.1	0.114 ± 0.013	0.978 ± 0.007

The mean E_{in} value of GG-HS was determined as 1.5 ± 0.3 GPa, which was similar to the results reported by Mercadé-Prieto et al. (2011) for melamine formaldehyde microcapsules (1.6 ± 0.3 GPa), chitosan gum arabic (Ch-GA) coacervated microcapsules (1.0 ± 0.1 GPa) reported by Baiocco et al. (2023) as well as glassy polymer microspheres (0.6 -1.8 GPa) fabricated by Yap et al. (2008). Comparatively, GG-HS has slightly higher E_{in} value than Ch-GA microcapsules, which might be caused by the stronger interactions between gelatine and gum arabic and the presence of long chain polymers after complex coacervation. It is notable that E_{in} is approximately one order of magnitude higher than the value of apparent Young's modulus (163 ± 33 MPa), and other microcapsules also exhibited one order magnitude difference between their intrinsic and apparent Young's modulus values as well. The values of E/E_{in} for each sample are summarised in Table 4-8.

Table 4-8. Values of E/E_{in} for different microcapsules

Microcapsules	E/E_{in}
GG-HS	0.112534
GG-HS-MD	0.051316
GG-HS-GT	0.107573
GG-LM-GT	0.095954
GG-LC-GT	0.099617

The mean value of E/E_{in} for each sample approached to a constant value at 0.09 ± 0.02 (mean ± 2×St.Err) in this study, which is statistically similar to the coefficient 0.085 ± 0.002 established by Baiocco et al. (2023), evidencing the applicability of this model regardless of different microcapsule chemistry.

4.4. Conclusions

In this chapter, different flavour/fragrance oils including LC, LM and HS were encapsulated using gelatine and gum arabic by the complex coacervation method. Micro-size spherical microcapsules with polynuclear core shell structure were fabricated. The highest EE of 89.0 ± 1.2 % was obtained from GG-HS-GT, which was higher than wax microspheres presented in Chapter 3 and chitosan/gum arabic coacervated microcapsules reported by Baiocco et al. (2021a). Further treatments to coacervated microcapsules by spray coating with maltodextrin or glutaraldehyde crosslinking significantly improved EE and evident variations were observed for different core microcapsules with identical shell materials. Mechanical characterisations of microcapsules were undertaken using micromanipulation measurements of their rupture strength parameters and determination of the apparent Young's modulus of the whole microcapsule and the intrinsic Young's modulus of shell material by Hertz and FEA

models respectively. It was found that the apparent Young's modulus of whole microcapsules analysed by the Hertz model was approximately one order of magnitude lower than the intrinsic Young's modulus of coacervate shell derived from FEA model. Additional processing by either the maltodextrin coating or glutaraldehyde crosslinking significantly enhanced the mechanical strength of microcapsules. Future works include the investigation of the influence of core oil polarity and their interfacial tensions with aqueous phase and coacervate phase on the microcapsule morphology and corresponding EE.

CHAPTER 5. Evaluation of Gum Arabic and Gelatine Coacervated Microcapsule Morphology and Encapsulation Efficiency by Combining the Spreading Coefficient and Two Component Surface Energy Theory

5.1. Introduction

For L-carvone (LC), limonene (LM) and Hexyl salicylate (HS) oils, microcapsules prepared with complex coacervation using gum arabic (GA) and gelatine (GE) as wall materials and subsequent spray drying/coating have shown significantly different encapsulation efficiencies and payloads. Similarly, variable encapsulation efficiencies for different oils using the same preparation procedure and shell materials were also reported by other researchers. For instance, when Zuanon et al (2013) fabricated turmeric oleoresin microcapsules following GE-GA complex coacervation, the encapsulation efficiency ranged from 49 to 73%, while Kong et al (2009) found an efficiency as low as 16 % when encapsulating dodecanol using the same encapsulation procedure and shell materials. Encapsulation efficiencies as high as 90% were also reported for GE-GA coacervated microcapsules containing other oils (Chang et al., 2006; Liu et al., 2023; Yu et al., 2021; Zhang et al., 2011). Although the mechanism underlying GE-GA complex coacervation has been known for decades, the particular mechanisms about microcapsule formation with different oils in GE-GA aqueous phase still need to be investigated.

Generally, to successfully encapsulate oil into a shell by complex coacervation as well as increase its encapsulation efficiency, the deposition of complex coacervates at the oil/water

interface and its wettability are key parameters to be considered (Dardelle & Erni, 2014). The gel coacervates in aqueous phase have to spread spontaneously onto the surface of dispersed oil droplets and form the core-shell microcapsule structure. However, variable capsule morphologies can be fabricated and they are presented in Figure 5-1. In addition to a core-shell morphology where single core or multiple small cores are completely entrapped inside the carrier shell/matrix, alternative morphologies including acorn structure in which the oil is partially engulfed and dissociation where oil and water droplets are completely separated could be obtained.

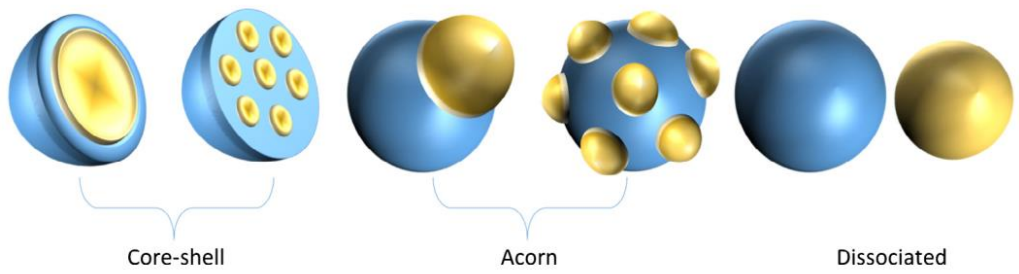

Figure 5-1. Possible final microcapsule morphologies for core microencapsulation (Tasker et al., 2016)

The microcapsule morphologies can be influenced by thermodynamic and kinetic factors of the system with different molecules (Szczotok et al., 2018). In the case of complex coacervation, the kinetics include the rate of electrostatic interaction between different molecules with opposite charges and phase separation while the thermodynamics are controlled by the interfacial tension balance of oil, the polymers as well as aqueous phases involved in the capsule formation (Dardelle & Erni, 2014). These final resultant morphologies will lead to variable encapsulation efficiencies for different oils although they are prepared under the same process conditions and with the same wall materials.

Torza and Mason (1970) studied the engulfing mechanism when two immiscible phases were brought in contact in a third mutually immiscible phase, and first proposed a theory on predicting the morphologies of capsules. Based on measuring the interfacial tensions between the three phases, which were used to determine the spreading coefficients for each phase. This theory was later expanded by Loxley and Vincent to also encompass solid polymers (Loxley & Vincent, 1998), and three spreading coefficients can be defined as follows:

$$S_P = \Upsilon_{WO} - (\Upsilon_{OP} + \Upsilon_{WP}) \quad (5\text{-}\mathbf{1})$$

$$S_O = \Upsilon_{WP} - (\Upsilon_{OP} + \Upsilon_{WO}) \quad (5\text{-}\mathbf{2})$$

$$S_W = \Upsilon_{OP} - (\Upsilon_{WP} + \Upsilon_{WO}) \quad (5\text{-}\mathbf{3})$$

where subscripts O, W and P refer to the three phases core material (oil herein), aqueous phase (here water) and polymer (here coacervates) respectively, Υ_{OP} , Υ_{WP} and Υ_{WO} are the oil/polymer, water/polymer and water/oil interfacial tensions, respectively, see Figure 5-2. S_P, for instance, is the spreading coefficient for coacervates at the water/oil interface. When S_P is positive, the balance of interfacial tensions of the three phases favours complete wetting of the water/oil interface by the polymer phase (Harkins & Feldman, 1922). It is usually assumed that $\Upsilon_{WO} > \Upsilon_{WP}$ (Bago Rodriguez et al., 2018; Dardelle & Erni, 2014; Priftis et al., 2012; Qin et al., 2014; Spruijt et al., 2010), which leads to only three possible scenarios:

$$S_O < 0;\ S_W < 0;\ S_P > 0 \quad (5\text{-}\mathbf{4})$$

$$S_O < 0;\ S_W < 0;\ S_P < 0 \quad (5\text{-}\mathbf{5})$$

$$S_O < 0;\ S_W > 0;\ S_P < 0 \quad (5\text{-}\mathbf{6})$$

For the conditions in Equation (5-**4**), the capsules adopt a core–shell morphology. When conditions in Equation (5-**5**) are satisfied, acorn-shaped capsules are formed. When the conditions in Equation (5-**6**) are fulfilled, separated droplets of oil and polymer are predicted.

The predicted capsule morphologies can be seen correspondingly in Figure 5-1.

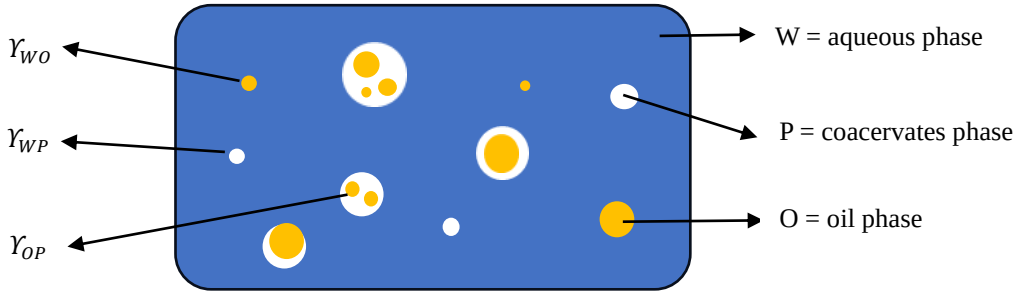

Figure 5-2. Oil phase (O) to be encapsulated by the coacervate phase (P). Empty and oil loaded coacervate droplets are dispersed in the aqueous phase (W). γ_{OP}, γ_{WP} and γ_{WO} represent the interfacial tensions between the different phases. Adapted from Thomasin et al. (1997).

Following Torza and Mason's work, several researchers have also studied the effect of spreading coefficient combinations on capsule morphology. Using solvent evaporation method, Loxley et al. (1998) encapsulated n-hexadecane in poly (methyl methacrylate), which had been dissolved in dichloromethane with different emulsifiers of poly (vinyl alcohol), poly (methacrylic acid), sodium dodecylsulfate or cetyltrimethylammonium bromide, and found that a core shell structure was predicted and experimentally observed only for poly (methacrylic acid), whilst the predictions for poly (vinyl alcohol) and its final morphology were not in agreement. Following the same encapsulation method, Tasker et al. (2016) observed that the morphology was coinciding with the predictions by using the same polymers and core while changing the surfactant chain length. Feczkó et al. (2014) investigated the encapsulation of n-hexadecane in ethyl cellulose emulsified by poly (methacrylic acid sodium salt), Tween 80 or poly (vinyl alcohol) by solvent evaporation method and found that the final capsule morphology was successfully predicted from the spreading coefficients for poly

(methacrylic acid sodium salt) but the predictions failed for using poly (vinyl alcohol) and Tween 80 as emulsifiers. Also, with solvent evaporation method employed, Pisani et al. (2008) used poly (lactide coglycolide) (which had been dissolved in dichloromethane) as a shell to encapsulate perfluorooctyl bromide, stabilised with poly (vinyl alcohol), sodium cholate or sodium taurocholate, and found the morphology was correctly predicted only for sodium cholate based on experimental determinations of the spreading coefficients. However, Shirin-Abadi et al. (2014) reported that their calculated results were in good agreement with experimental observations when fabricating n-hexadecane loaded nanocapsules using copolymers of methyl methacrylate with 2-ethylhexyl acrylate and methacrylic acid through in situ polymerization. On the contrary, Szczotok et al. (2018) found significant discrepancy between the predicted morphology and experimental observations when investigating the encapsulation of Rubitherm (RT27) using copolymer of styrene crosslinked with divinylbenzene as a shell, suspended by hexa (methacryloylethylenedioxy) cyclotriphosphazene, sodium dodecylsulfate, gum arabic or poly (vinyl pyrrolidone) through suspension polymerization method.

There have been limited works attempting to utilise complex coacervation within the theoretical framework of three-phase thermodynamics. Thomasin et al. (1997) investigated the encapsulation of bovine serum albumin powders and aqueous bovine serum albumin solution by the complexes from poly (D, L-lactic acid) and poly (D, L-lactic-co-glycolic acid) at various weight ratios, which had been dissolved in either dichloromethane or ethyl acetate, and observed core-shell structure with multicores for all samples, evidencing the morphology predictions are coinciding with the spreading coefficients. In the study conducted by Bago

Rodriguez et al. (2018), the coacervates of poly (acrylic acid) sodium salt and poly (diallyl dimethylammonium chloride) were used as stabilisers for oil in water emulsions. Complete engulfing of oil droplets within coacervates were only detected for dodecane and toluene, while the predicted core shell morphology was not observed for isopropyl myristate and squalene. They suggested that the viscosity of the aqueous phase with coacervates formed affects the kinetics of spreading, which is not accounted for the theory on predicting the morphologies of microcapsules. Similarly, by employing in situ mini-emulsion polymerization method, Van Zyl et al. (2003) and Cho & Lee (1985) also pointed out that the capsule morphology was significantly influenced by kinetic factors (surface anchoring effects, polymer chain mobility, viscosity) apart from thermodynamic considerations. It was further demonstrated by Dardelle and Erni (2014) that the equilibrium spreading coefficient theory is the basis to understand three phases wetting in terms of coacervate/oil/water systems, the fluid rheology and even actual flow process in the system can be additional factors influencing the resulting morphologies.

Furthermore, using different types of surfactants and initiators, Van Zyl et al. (2003) investigated the anchoring of entering radicals at the oil/water interface, where the anchoring effects can hinder the diffusion of radicals, thereby causing the engulfing of core oil by polymer and thus the formation of the capsules with core-shell structured morphologies. Sundberg et al. (1990; 1993) reported that different morphologies (hemispherical, sandwich, multiple lobes) were observed to be coexisting at the same time within a single emulsion after replacing low molecular weight polymers that diffuse readily by high molecular weight ones, which provided evidence of the kinetic influence in terms of polymer chain mobility as

reported by Van Zyl et al. (2003) and Cho & Lee (1985). Considering the work of Torza and Mason (1970) focusing only on thermodynamics, an alternative model was developed by Sundberg et al. (1990) and Waters (1994) based on the free energy changes at the interfaces of a three-phase system,

$$\Delta G = \Upsilon_i A_i - \Upsilon_j A_j \qquad (5\text{-}7)$$

where G is the Gibbs free energy. A_i refers to the initial interfacial area of the core in contact with the aqueous phase containing polymers, and Υ_i is its interfacial tension. A_j is the interfacial area of core dispersed into the coacervate phase during capsule formation and Υ_j is the corresponding interfacial tension. In thermodynamic terms, each specific morphological configuration has a certain value for ΔG, and the configuration with the minimal free energy is thermodynamically favoured.

Capsule morphology and core encapsulation efficiency can also be dependent on the surface energy of the two components of dispersed and continuous phases (Szczotok et al., 2018). Based on the theory of Girifalco and Good (1957), Fowkes (1962;1964) suggested that the surface tension of liquids or the surface free energy of solids per unit area is the sum of contributions from the dispersive (Υ^D) and polar components (Υ^P):

$$\Upsilon = \Upsilon^D + \Upsilon^P \qquad (5\text{-}8)$$

where Υ^D is the component surface tension induced from dispersion interactions of London-van der Waals forces and Υ^P is contributed by the intermolecular interactions like dipole-dipole interactions, hydrogen bonding, π bonding and electrostatic interactions (Fernández & Khayet, 2015; Jańczuk et al., 1989). According to Fowkes (1964), dispersive interactions of the molecules of two phases at the interface prevailed among other interaction forces, see

Figure 5-3.

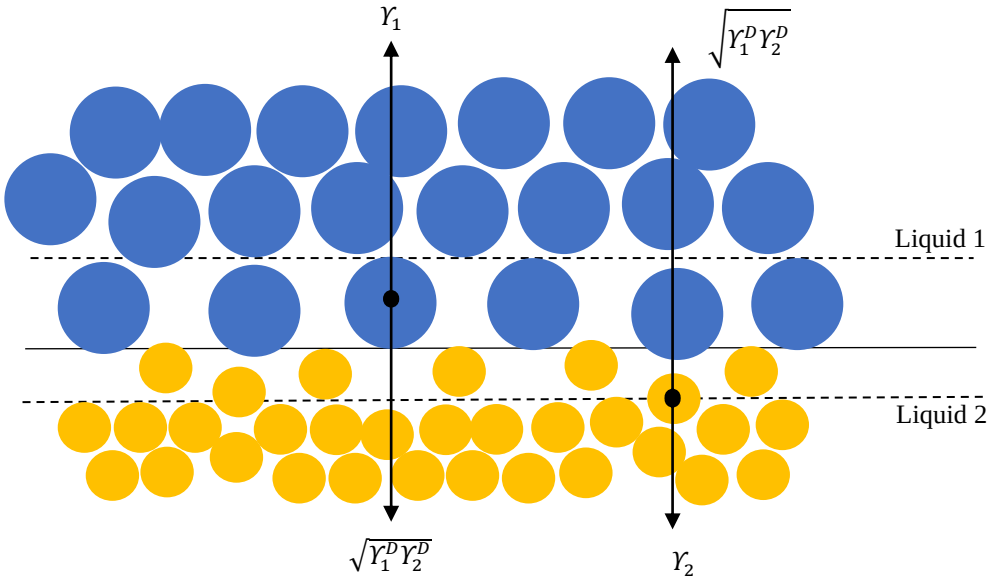

Figure 5-3. At the interface between two liquids, the molecules at interface are subject to the attractive forces in each phase (Fowkes, 1964).

The interfacial tension between liquid and solid as a function of the geometric mean of the dispersive interactions can be expressed as:

$$\gamma_{LS} = \gamma_L + \gamma_S - 2\sqrt{\gamma_L^D \gamma_S^D} \qquad (5\text{-}\mathbf{9})$$

where γ_L and γ_S, γ_L^D and γ_S^D, γ_{LS} are the surface tension of liquid and solid, their dispersion components and the interfacial tension between two phases, respectively. Based on the Young equation (Young, 1805), an expression for the liquid on the solid surface interacting with dispersion forces is as follows:

$$\gamma_L(1 + \cos\theta) = 2\sqrt{\gamma_L^D \gamma_S^D} \qquad (5\text{-}\mathbf{10})$$

where θ is the contact angle of the liquid droplet on the solid surface.

Equation (5-**10**) was further expanded by Owens and Wendt (1969) to include the contributions from non-dispersion interfacial interactions:

$$\Upsilon_L(1+\cos\theta) = 2\sqrt{\Upsilon_L^D \Upsilon_S^D} + 2\sqrt{\Upsilon_L^P \Upsilon_S^P} \qquad (5\text{-}\mathbf{11})$$

where Υ_L^P and Υ_S^P denote the polar components of liquid and solid due to their polar intermolecular interactions.

The polar surface tension component Υ_L^P can be calculated by $\Upsilon_L^P = \Upsilon_L - \Upsilon_L^D$. Surface polarity of liquid can be calculated as 100% Υ_L^P/Υ_L and polar surface energy components for polymer can be calculated as 100%Υ_S^P/Υ_S.

In this chapter, the aim is to ascertain whether it is possible to justify the morphology and oil encapsulation efficiency of spray dried microcapsules by combing spreading coefficient and two component surface energy theory. A range of flavour oils including L-carvone, limonene, hexyl salicylate, cinnamaldehyde, carvacrol and linalool were encapsulated into gum arabic and gelatine coacervates shell via complex coacervation. Surface tensions of core materials, interfacial tensions between each core and aqueous phase, contact angle of cores and a standard reference liquid on gelatine/gum arabic coacervated polymer surface as well as contact angle of cores on the standard reference solid surface were measured. The equilibrium configurations between the three phases for each oil were given through the calculations of the three spreading coefficients and compared with the experimental morphology of microcapsules. Different values of polar surface energy components of the continuous and dispersed phases were collected and investigated in order to understand the effects of type of core oils as well as their polarity on the morphology of the formed microcapsules and the corresponding on encapsulation efficiency.

5.2. Materials and methods

5.2.1. Materials

L-carvone (99%), S-limonene (95%), hexyl salicylate (98%), cinnamaldehyde (98%) and carvacrol (99%) were all purchased from Macklin, China. Linalool (98%, 154.25 MW) was purchased from Aladdin Bio-Chem Technology Co. Ltd., Shanghai, China. Gum arabic (GA) was purchased from Solarbio life sciences, China and gelatine (GE, type B, ~220 g bloom, average Mw = 500 kDa) was obtained from Shanghai Yuanye Biotechnology Co. Ltd., Shanghai, China. Reagents including absolute ethanol,1-propanol and hexane were purchased from Sigma-Aldrich, UK, and were of analytical grade and used without further purification. All the solutions were prepared using deionised water (18.2 MΩ cm at 25 °C).

5.2.2. Preparation and characterisation of microcapsules

5.2.2.1. Microcapsules prepared via coacervation followed by spraying drying

The GE-GA coacervated microcapsules containing core oil (LC, LM, HS, CD, CV or LL) were prepared following the protocol described in Section 4.2.2 and Section 4.2.2.1.

Gum arabic and gelatine coacervated microcapsules containing no oils were also prepared following the same procedure to investigate the influence of shell materials in solvent on UV tests and for the preparation of polymer shell tablets in contact angle measurements.

5.2.2.2. Morphological characterisation of microcapsules

Morphological characterisations of microcapsules with a different core oil were performed by a scanning electron microscope (Hitachi TM3030 Tabletop) (see Section 3.2.4).

5.2.2.3. Encapsulation efficiency

5.2.2.3.1. Sample preparation and calculation

Three batches of 50 mg oil loaded microcapsules were firstly placed into three different screw capped glass vials, and then dispersed into 10 mL solvent (36% 1-propanol for HS, ethanol for for LC, LM and LL, hexane for CD and CV). The vials were ultrasonicated and centrifugated following the procedures detailed in Section 3.2.6.

5.2.2.3.2. UV-Vis spectrophotometer

The amount of HS in microcapsules was measured by the UV-Vis spectrophotometer, whose details were described in Section 3.2.6.

Pure GA-GE coacervates without any oil were also measured following the same procedures, to avoid the absorbance influence from coacervates in the solvents. All the results showed the shell coacervates neither dissolve in the solvent nor influence the UV absorption readings.

5.2.2.3.3. Gas-chromatography

The quantitative analysis of LC and LM were detailed in Section 4.2.6.3. The amount of CV, CD and LL were also measured using a gas chromatography method. Ethanol was used as solvent for LC, LM and LL while hexane was selected as the solvents for CD and CV (Abu-Lafi et al., 2008; Baiocco & Zhang, 2022; Elmastaş et al., 2006; Lim et al., 2014; Yang et al., 2016). Linear standard calibration curves for different oils were determined based on the rising areas (y) from detection peak and oil concentrations (x) in 10 ml solvent:

$y = 15.850x + 0.256$ with a coefficient of determination R^2 = 0.9997 for LL (Figure D-1 in Appendix D),

$y = 13.229x - 5.453$ with a coefficient of determination R^2 = 0.9994 for CV (Figure D-2 in

Appendix D),

and $y = 19.987x + 2.145$ with a coefficient of determination $R^2 = 0.9999$ for CD (Figure D-3 in Appendix D) were generated.

The obtained calibration equations were further used to determine the amount of encapsulated oils in dry microcapsules measured by gas chromatography using an Agilent GC 8890 system (Agilent, USA) coupled with an Agilent 7693 automatic sample injector. The supernatants prepared from Section 5.2.2.3.1 for different oils were transferred into 2 ml glass vials (Agilent, USA) sealed with rubber caps (Thermo scientific, UK). The GC tests were performed with an Agilent HP-5 capillary column (30 m × 0.32 mm × 0.25 µm, Agilent, USA), the temperature of the injector was 250 ◦C and the N^2 flow rate was set at 1.5 mL/min. The column temperature programs for each oil were referenced from literatures (Abu-Lafi et al., 2008; Baiocco & Zhang, 2022; Elmastaş et al., 2006; Lim et al., 2014; Yang et al., 2016) with modifications and summarised in Table C-1 in Appendix C.

The separation time of LM, LC, LL, CV and CD each was at 10.5, 13.5, 12.7, 16.3 and 17.2 min respectively based on their response to the detector in the column. Experiments for each oil were conducted in triplicate.

5.2.3. Surface and interfacial tension measurement

The surface and interfacial tension measurements were conducted using a drop shape analyser (DSA30, Kruss) via a pendant drop method. For surface tension measurements, individual oil and water that contains dissolved GA (1 wt%) and GE (1 wt%) were generated into droplets of 12 ± 1 µl in the surrounding air phase respectively by a glass syringe (SY20) with a 1.8 mm stainless steel needle tip (NE45). To ensure accurate measurements, the droplet was set at a

volume nearly detached from the needle tip (Berry et al., 2015). For interfacial tension measurements, polymer solution was added in an optical quartz cuvette (SC02). Depends on the density of sample oil, J-shaped needle (2.001 mm, NE73) or a straight needle (NE45) was selected to generate oil droplet immersed in the aqueous polymer phase. All measurements were conducted for 6 h for reaching surface or interfacial tension equilibrium at 25 °C, and each measurement was performed in triplicate.

The surface and interfacial tension values were calculated by analysing the recorded drop shape profiles according to the Young-Laplace equation by KRÜSS ADVANCE software:

$$\Upsilon = \Delta\rho g \frac{R_0^2}{\beta} \qquad (5\text{-}\mathbf{12})$$

where Υ is the surface or interfacial tension, Δρ is the density difference between the drop and the surrounding medium, g is the gravitational constant, R_0 is the radius of the drop curvature at the vertex and β is the shape factor (Tasker et al., 2016). The density for each oil at 25 °C was summarised in Table 5-1 (Imran et al., 2022; sigma-Aldrich, 2023a;2023b;2023c;2023d;2023e).

Table 5-1. Density of each oil at 25 °C.

Core oil	LM	LC	LL	CV	HS	CD
Density (g/ml)	0.84	0.96	0.87	0.98	1.04	1.05

5.2.4. Contact angle measurement

The GA-GE coacervated shell polymer tablets with flat surface were prepared by a 13 mm evacuable pellet die (Specac, UK) using a compression instrument (LS100 Plus, Lloyd, UK), and compressed at a maximum load (50 MPa) monitored by NEXYGEN Plus software.

The sessile drop method was employed for contact angle measurements. Drops of different oil, water or diiodomethane was deposited onto the surface of a polymer tablet in air surrounding phase using the glass syringe (SY20) connected with a 0.5 mm stainless steel needle (NE44), see Figure 5-4. At least 5 different drops were measured for each sample. The tests were maintained for 1 min to achieve the equilibrium contact angle between samples and polymer surface.

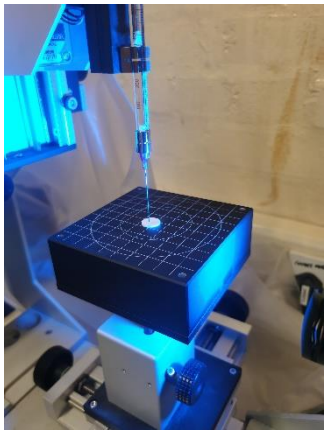

Figure 5-4. Experimental setup of oil droplet on polymer tablet surface (contact angle test).

5.2.5. Statistical analysis

See Section 3.2.9.

5.3. Results and Discussion

The microcapsules with various oils as core and gum arabic and gelatine coacervates as shell material were prepared by complex coacervation. The capsule morphology and encapsulation efficiency for different core oils were determined. The relationship between the capsule morphology and relevant spreading coefficients was investigated, combining with the effect of polarity of core oil on its encapsulation efficiency within GA-GE polymeric complexes.

5.3.1. Calculation of spreading coefficients

Based on Fowkes theory (Fowkes, 1964; Rulison, 2000), diiodomethane and water were used to determine the value of surface free energy of solid shell polymer. Diiodomethane was tested as a probe liquid, as its surface tension is attributed to its dispersive component only, which means $\Upsilon_L = \Upsilon_L^D$, and $\Upsilon_L^P = 0$ mN/m. The surface tension of diiodomethane was tested to be 50.8 mN/m, which was combined with Equation (5-**11**) to obtain:

$$\Upsilon_S^D = (\Upsilon_L/4)(cos\,\theta + 1)^2 \qquad (5\text{-}\mathbf{13})$$

The contact angle of diiodomethane on the shell polymer surface was tested to be 34.96 °, thus the dispersive component Υ_S^D of the solid polymer material can be calculated by Equation (5-**13**) as 42.05 mN/m.

Water (Υ_w^D=26.4 mN/m, and Υ_w^P=46.4 mN/m (Rulison, 2000)) was used as a testing liquid since its surface tension is contributed by both its polar and dispersive components. The contact angle of water on the polymer surface was measured to be 53.33 °, thus Υ_S^P can be calculated after Υ_S^D (42.05 mN/m), Υ_w^D (26.4 mN/m), Υ_w^P (46.4 mN/m) and Υ_W (72.8 mN/m) were substituted into Equation (5-**11**): $72.8 \times (1 + \cos 53.33°) = 2\sqrt{26.4 \times 42.05} + 2\sqrt{46.4 \times \Upsilon_S^P}$, obtaining $\Upsilon_S^P = 13.28$ mN/m.

The overall surface tension of the GA-GE coacervates, Υ_P can therefore be calculated based on Equation (5-**11**) as $\Upsilon_P = \Upsilon_P^P + \Upsilon_P^D = 42.05 + 13.28 = 55.33$ mN/m.

The interfacial tension between oil/polymer or water/polymer was calculated based on Young's equation (Young, 1805):

$$\Upsilon_{OP} = \Upsilon_P - \Upsilon_{OA}\,cos\,\theta \qquad (5\text{-}\mathbf{14})$$

$$\Upsilon_{WP} = \Upsilon_P - \Upsilon_{WA}\,cos\,\theta \qquad (5\text{-}\mathbf{15})$$

where Υ_{OP} or Υ_{WP} correspond to the interfacial tension between liquids (oil or water phase)

and the solid shell, Υ_{OA} and Υ_{WA} refer to the surface tension of the liquids, Υ_P and Θ are the surface tension of the polymer and the contact angle of liquids on solid shell respectively (Szczotok et al., 2018). A liquid drop on the polymer tablet surface is sketched in Figure 5-5.

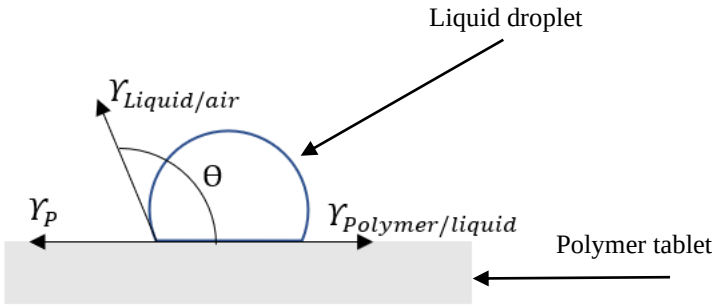

Figure 5-5. Schematic diagram of drop deposition onto polymer surface

The accepted standard reference surface is Polytetrafluoroethylene (PTFE). Untreated PTFE is assumed not to be capable of polar interactions with water, which means $\Upsilon_S = \Upsilon_S^D$, and $\Upsilon_S^P = 0$ mJ/m^2 (Rulison, 2000). The contact angle of water on PFTE surface was tested to be 105.22°. As the Υ_W^D of water is 26.4 mN/m and surface tension of water Υ_W is 72.8 mN/m, substituting these values into Equation (5-**11**): $72.8 \times (1 + \cos 105.22°) = 2\sqrt{26.4 \times \Upsilon_S^D} + 2\sqrt{\Upsilon_L^P \times 0}$, obtaining $\Upsilon_S^D = \Upsilon_S = 27.30$ mJ/m^2 for PTFE used in this work.

This leads to $\Upsilon_L(1 + \cos\Theta) = 2\sqrt{\Upsilon_L^D \times 27.30} + 2\sqrt{\Upsilon_L^P \times 0}$ based on Equation (5-**11**) and finally Equation (5-**16**) can be obtained:

$$\Upsilon_L^D = (\Upsilon_L{}^2/109.2)(cos\,\Theta + 1)^2 \qquad (5\text{-}\mathbf{16})$$

Equation (5-**16**) can be used to calculate the dispersive surface tension component Υ_L^D of different oils based on the results of surface tension of oils (Υ_L) and their contact angles (Θ) with PTFE.

5.3.2. Comparing morphology predictions and experimental observations

The interfacial tensions between different oils and aqueous phase, surface tensions of each oil and water were measured by the pendant drop method, contact angles of each oil and water on the polymer surface were determined by the sessile drop method, the value for γ_W of water was obtained from literature and was taken as 72.8 mN/m (Rulison, 2000), the calculation of surface energy of solid shell polymer is illustrated in Section 5.3.1 and the results are summarised in Table 5-2.

Table 5-2. Calculated surface tension of solid polymer per unit area and measured interfacial (IFT) and surface (SFT) tension of different oils and their contact angle on GA-GE coacervates surface. (mean ± 2× St.Err)

Material	LC	LM	HS	LL	CD	CV	Solid polymer	Water
IFT (mN/m)	14.9 ± 0.3	15.3 ± 0.7	34.3 ± 1.5	12.8 ± 0.3	44.3 ± 0.6	13.4 ± 0.9	-	-
SFT (mN/m)	33.0 ± 0.3	28.7 ± 1.3	35.4 ± 1.1	29.4 ± 1.6	47.8 ± 2.3	33.0 ± 1.5	55.33	72.8 (Rulison, 2000)
Contact Angle (°)	11.67 °	8.09 °	18.79 °	9.67 °	23.77 °	11.98 °	-	53.33 °

A contact angle below 90° (53.33° herein) for pure water on a flat GA-GE coacervates surface was obtained, suggesting that the polymer is relatively hydrophilic. Compared with HS and CD (18.79 ° and 23.77 °), the other oils (LC, LM, LL and CV) have lower contact angle on polymer surface (11.67 °, 8.09 °, 9.67 °, and 11.98 ° respectively), indicating LC, LM, LL and CV are more polar.

The highest interfacial tension was observed for CD in aqueous phase (44.3 ± 0.6 mN/m), followed by HS at 34.3 ± 1.5 mN/m, the interfacial tension between oil and water (γ_{WO}) decreased dramatically for LC, LM, LL and CV, which are similar to each other at around 14

mN/m. From a thermodynamical perspective, it was CD or HS with higher oil/aqueous interfacial tension theoretically promoted the formation of core shell structure (Eriksson et al., 2020).

The interfacial tension between oil/polymer or water/polymer can be obtained by calculations with Equation (5-**14**) and (5-**15**), based on the given data summarised in Table 5-2, from where the spreading coefficients for each oil have been calculated and their values are presented in Table 5-3. In addition, graphical representation of the spreading coefficient values and consequent predicted morphologies for each oil are presented in Figure 5-6.

Table 5-3. Spreading coefficients of each oil and corresponding morphology prediction

Material	γ_{WO} **(mN/m)**	γ_{OP} **(mN/m)**	γ_{WP} **(mN/m)**	S_o	S_W	S_P	**Predicted**
LC	14.9	23.0	11.9	-26.0	-3.8	-20.0	Acorn
LM	15.3	26.9	11.9	-30.3	-0.3	-23.5	Acorn
HS	34.3	21.9	11.9	-44.3	-24.3	0.5	Core-shell
CD	44.3	11.6	11.9	-44.0	-44.6	20.8	Core-shell
CV	13.4	23.1	11.9	-24.6	-2.2	-21.6	Acorn
LL	12.8	26.4	11.9	-27.3	1.7	-25.5	Dissociated

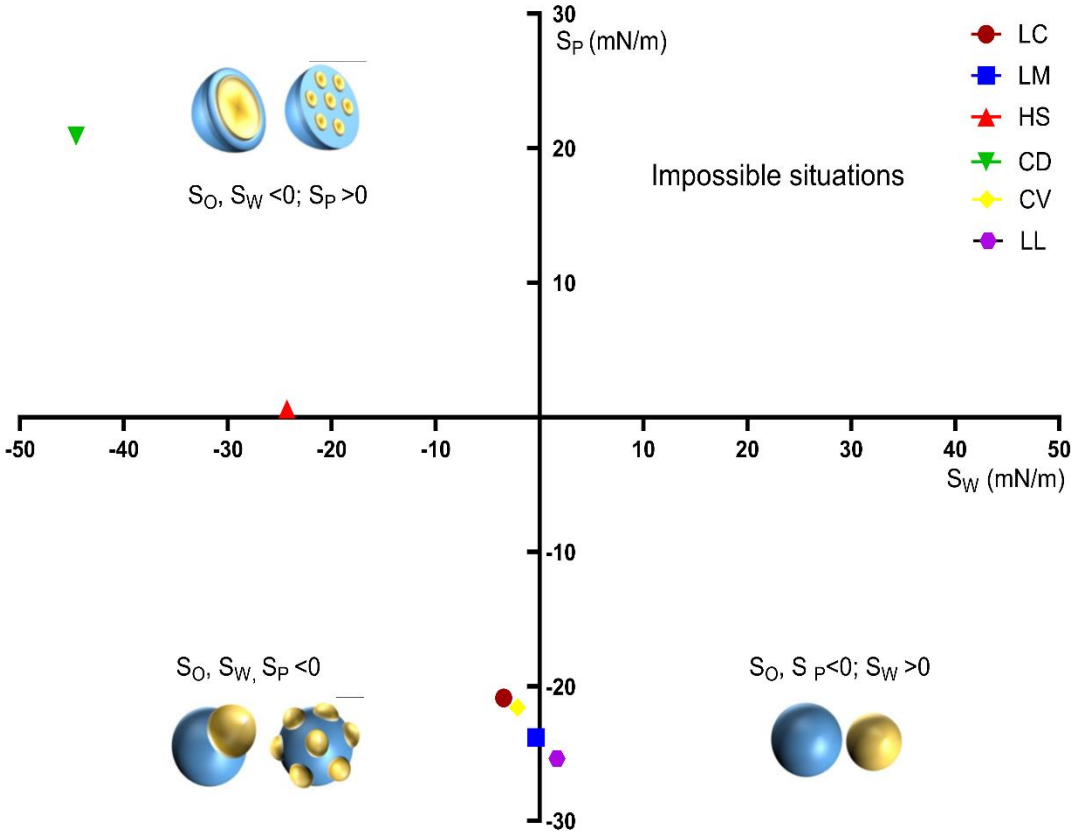

Figure 5-6. Graphical representation of spreading coefficients and predicted morphologies of capsules for each oil.

By solving Equation (5-**15**) with the given data, Υ_{WP} = 11.85 mN/m, which confirms the assumption that $\Upsilon_{WO} > \Upsilon_{WP}$ (Bago Rodriguez et al., 2018; Priftis et al., 2012; Qin et al., 2014; Spruijt et al., 2010). It is also notable that the contact angle measurement for each oil on polymer surface and calculation of Υ_{OP} in this study are based on the dried coacervated polymer solid tablets, which may possess a different surface energy compared to that of a hydrated one formed in situ within the aqueous phase. Tasker et al. (2016) discussed the influence of polymer form on the values of Υ_{OP} using two different methods. In the first method, Υ_{OP} was calculated by the data obtained from contact angle measurements using hexadecane on dry polymer flat surface. In the second method, Υ_{OP} was directly measured using an aqueous phase with polymer (poly (methyl methacrylate)) dissolved in the solvent

(dichloromethane). They reported that solid form polymer gave predictions that were more consistent to the observed morphologies, which was due to the absence of solvent influence, possibly leading to more accurate predictions.

The spreading coefficient of the polymer S_P varied greatly depending on the type of core oils. Only in the cases of HS and CD, the interfacial tensions between the oil and aqueous phase were high enough to ensure positive values of S_P. For the other oils, the oil/water interfacial tensions were relatively low so that their S_P values were negative. Consequently, acorn structure is predicted for the fabricated microcapsules using LC, LM or CV as core, whilst the predicted morphology should be core shell for HS and CD microcapsules. The positive value S_W of LL indicates that the aqueous phase is able to spread at oil/coacervate interface, and non-engulfing is expected for LL oil. Compared to LC, LM, CV and LL, HS and CD are relatively nonpolar compounds that increase the interfacial tension between the oil phase and the polymer aqueous phase, which leads to a complete engulfing of the core to form core shell morphology (Shirin-Abadi et al., 2014).

The capsule morphology was preliminarily observed under optical light microscopy with fluorescence. HS was firstly stained with Nile red and microcapsules were prepared following the procedure described in Section 5.2.2.1. Fluorescence observations were performed with a blue light excitation peaking around λ = 460 nm using a CoolLED pE-300 LED illumination system. The microcapsule suspension resulting from agitation for 4 h for complex coacervation are presented in Figure 5-7.

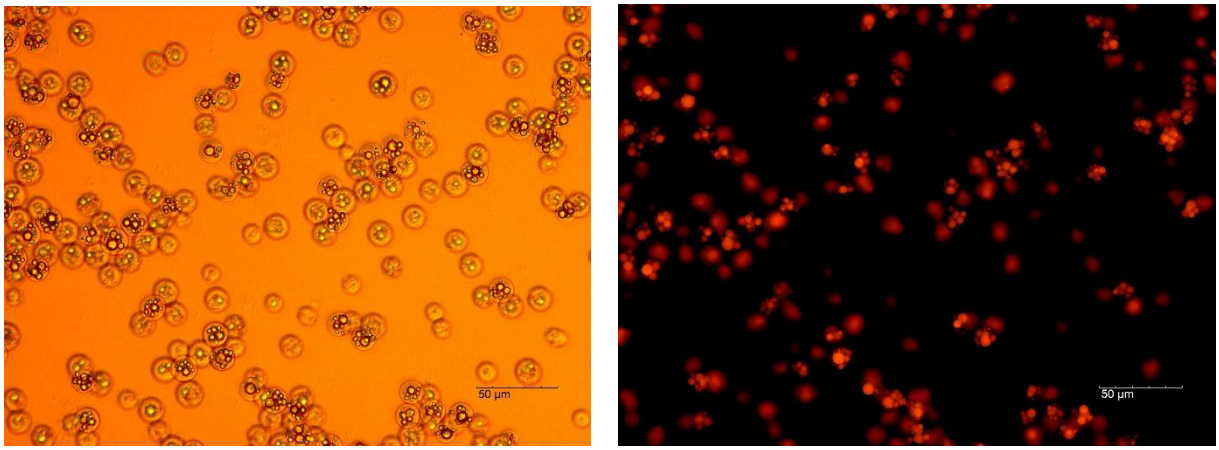

(a) (b)

Figure 5-7. Optical and fluorescence microscopy images of HS microcapsules after complex coacervation for 4 h. HS is stained with Nile red and seen in red under exposure to a filtered lamp (λmax = 460 nm) in situ (a) Optical image of the microcapsules, (b) Fluorescence image. Both scale bars represent 50 µm.

Core-shell structured microcapsules were observed for HS, which fulfils the spreading coefficient configurations for core shell morphology prediction. In order to check the validity of the spreading coefficients in predicting the morphology and inner structures of the microcapsules for each oil, they were compared with their corresponding SEM images, see Figure 5-8. The hollow pores on the surface of microcapsules can be observed in Figure 5-8 (A) (a), (B) (b) and (E) (e), which indicate partially engulfing of LC, LM or CV within the polymer shell. The pores on the capsule surface might be formed after partially engulfed oil droplets evaporated from the coacervated polymer shell during the drying process for SEM. Figure 5-8 (C) (c), (D) (d) and (F) (f) show that microcapsules prepared with HS, CD and LL oils are relatively spherical and have smooth surface, from which HS and CD microcapsules have core-shell structures while LL have solid filled structure which was caused by the separation of oil and solid shell, as indicated by its spreading coefficients. It is notable that

although acorn structures are predicted from the thermodynamic perspective for LC, LM and CV oils, different morphologies (core-shell structure and acorn structured microcapsules) were found to coexist at the same time.

Torza and Mason (1970) found the agreement between morphology predictions and experimental observations using a variety of low molecular weight polymers in aqueous phases, which are able to diffuse readily and achieve the lowest interfacial energy for the equilibrium morphology within the time frame of the experiment. However, high molecular weight of polymers of gelatine and gum arabic were used in this work. The diffusions of GA and GE complexed molecules are much slower compared to the polymers of lower molecular weight, and the decreased mobility of these biopolymers can hinder upon their molecular bindings (Turgeon et al., 2007), suggesting the difficulty to achieve the thermodynamics equilibrium by considering the time scale of coacervation. As discussed by Van Zyl et al. (2003), the rate of morphological change of microcapsules is dependent on the diffusional resistance, which is related to polymer chain mobility. The mobility of the polymer chains can be enhanced in aqueous phase with low viscosity (low molecular weight polymer solution), whilst for highly viscous aqueous phase (high molecular weight polymer solution), polymer chain diffusion will be hindered, leading to a decreased deposition on the oil surface. Thus, Torza and Mason's theory can be considered to be applicable to low molecular polymers from the thermodynamic perspective, but the kinetic factor should also be considered for high molecular weight polymer encapsulating systems.

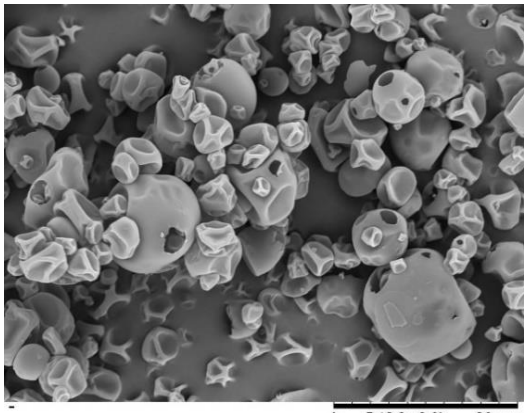
A D12.3 x2.0k 30 µm

(A)

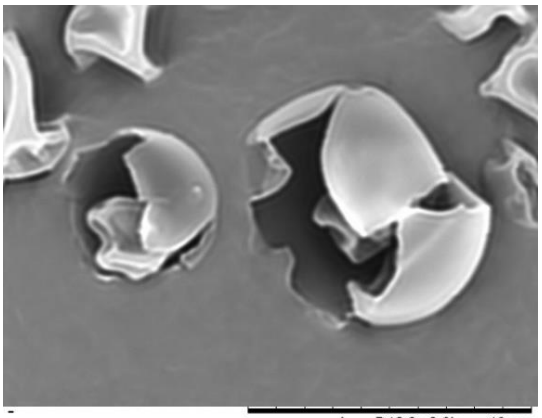
A D12.3 x9.0k 10 µm

(a)

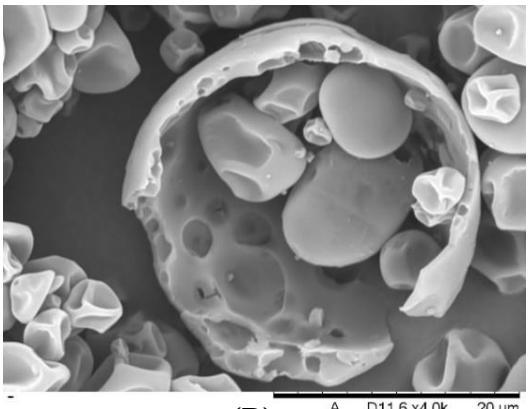
A D11.6 x4.0k 20 µm

(B)

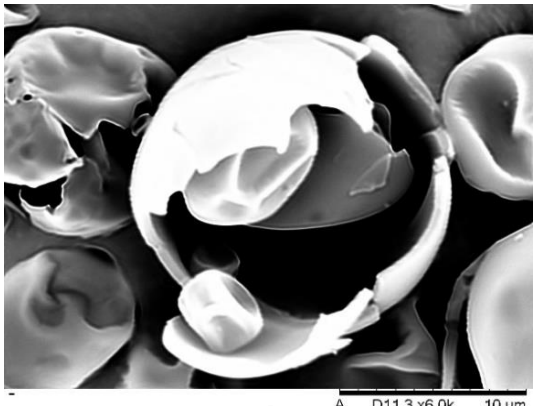
A D11.3 x6.0k 10 µm

(b)

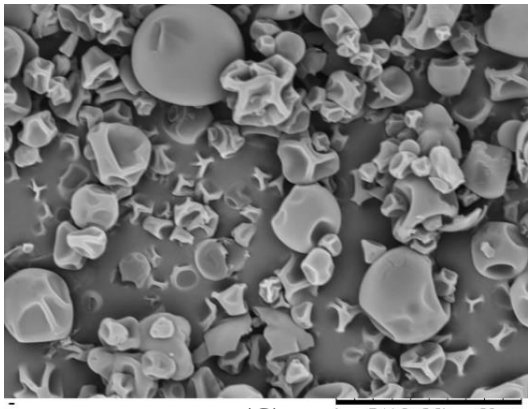
A D11.9 x2.0k 30 µm

(C)

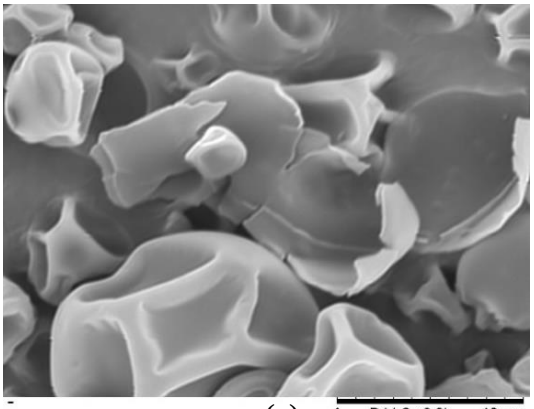
A D11.9 x6.0k 10 µm

(c)

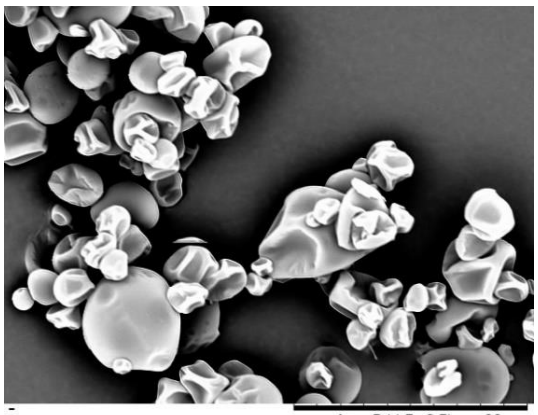
A D11.5 x2.5k 30 µm

(D)

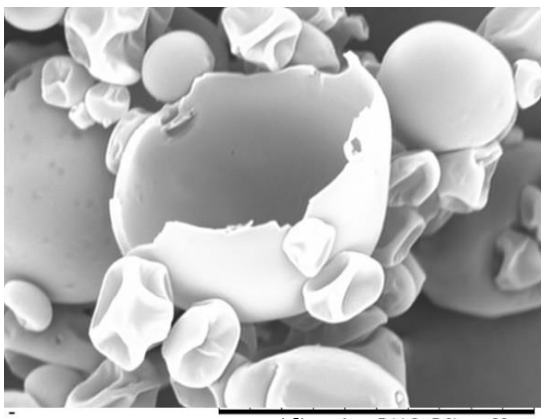
A D11.3 x5.0k 20 µm

(d)

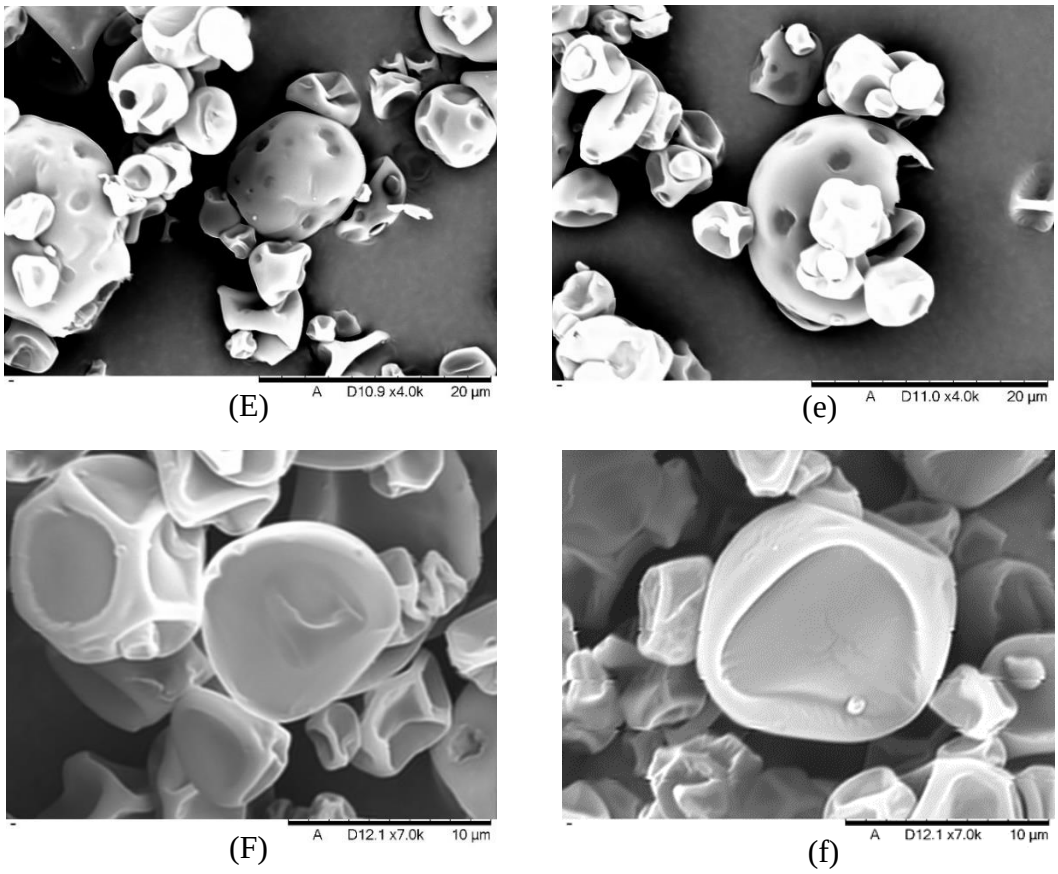

(E) (e)

(F) (f)

Figure 5-8. SEM images of (A) LC microcapsules, (a) broken LC microcapsules, (B) LM microcapsules, (b) broken LM microcapsules, (C) HS microcapsules, (c) broken HS microcapsules, (D) CD microcapsules, (d) broken CD microcapsules, (E) CV microcapsules, (e) broken CV microcapsules, (F) LL microcapsules, (f) broken LL microcapsules.

In this study, high molecular weight of polymers of gelatine and gum arabic coacervates were used as the wall material. The SEM experimental observations for LC, LM and CV were not in agreement with their predicted morphology based solely on the spreading coefficient configurations, whilst the predicted morphologies of HS, CD and LL microcapsules were in consistent with their corresponding SEM observations. However, it is notable that the microcapsule morphological characterisation by SEM was based only on the selected individual microcapsule, which cannot represent for the whole population. Therefore, the

encapsulation efficiency for each oil was also measured to validate the microcapsule morphology predictions, since the predicted dissociation (between core and aqueous phase) and acorn morphology will lead to an oil encapsulation efficiency of 0%, and core-shell morphology (with core oil encapsulated) can result in an encapsulation efficiency that is much higher.

5.3.3. Encapsulation efficiency and polarity

The encapsulation efficiency for each oil is summarised in Table 5-4. The EEs range from 2.64 % for LL to 46.61 % for HS, although each oil was encapsulated into the same shell materials.

Table 5-4. Encapsulation efficiency of each oil in GA-GE coacervates shell (mean ± 2×St.Err)

Oil	LC	LM	HS	LL	CD	CV
Encapsulation efficiency (%)	5.4 ± 0.1	18.7 ± 1.6	46.6 ± 2.2	2.6 ± 0.2	18.11± 1.8	5.8 ± 1.8

The polarity of the core oil was reported significantly related to the polymer engulfing behaviour (Lashgari et al., 2017), thus the relation between the efficiency of oil encapsulation into GA-GE coacervates shell and its corresponding polarity is also investigated. The contact angle of each oil and water on the surface of untreated PTFE are presented in Table 5-5.

Table 5-5. Contact angle of pure material on PTFE

Material	LC	LM	HS	LL	CD	CV	GG	Water
Contact Angle (m)	63.57 °	34.15 °	44.40 °	49.65 °	67.59 °	64.07 °	91.98 °	105.22 °

Surface polarity of liquid (100% Υ_L^P/Υ_L) or polymer (100%Υ_P^P/Υ_P) can be calculated by

substituting the surface tension of each molecule in Table 5-2 and its contact angle on PTFE in Table 5-5 based on Equation (5-**16**), and Table 5-6 can be obtained.

Table 5-6. Percent surface polarity and their corresponding EEs

Material	γ_L (mN/m)	γ_L^P (mN/m)	γ_P (mJ/m)	γ_P^P (mJ/m)	Polarity (%)	EE (%)
LC	33.0	12.2	-	-	36.9	5.4
LM	28.7	3.5	-	-	12.2	18.7
HS	35.4	1.7	-	-	4.8	46.6
CD	47.8	7.9	-	-	16.5	18.1
CV	33.0	12.4	-	-	38.0	5.8
LL	29.4	7.9	-	-	26.9	2.6
GA-GE mixture solution	44.0	27.5	-	-	62.5	-
Solid coacervates	-	-	55.3	13.3	24.0	-
Water	72.8	46.4	-	-	63.7	-

The aqueous GA-GE mixture solution had similar polarity with water. HS is the most non-polar oil and CV is the most polar oil, the relation between their surface polarity and corresponding encapsulation efficiency is presented in Figure 5-9.

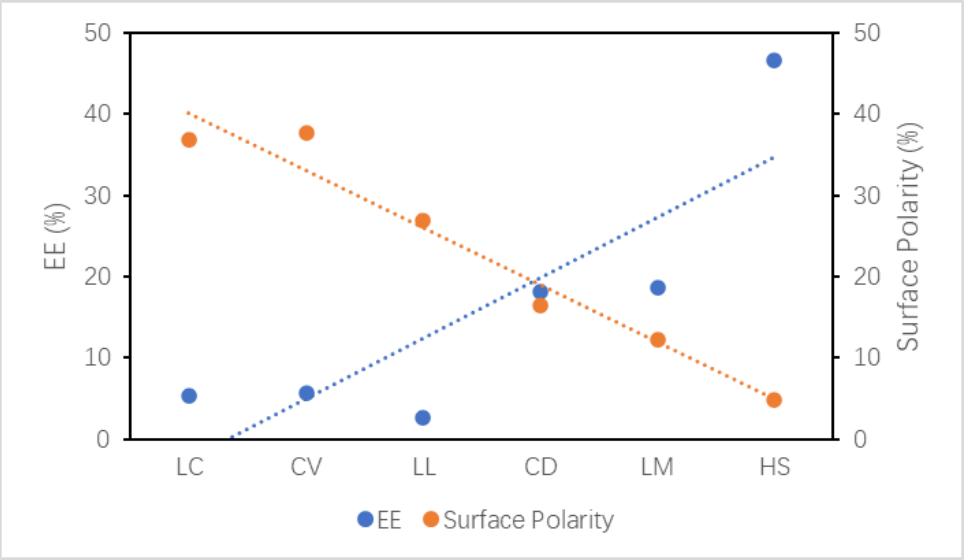

Figure 5-9. Relation between each oil surface polarity and its corresponding encapsulation efficiency within the GA-GE coacervated shell.

The results reveal that the encapsulation efficiency decreases with the increasing surface polarity of the core oil on average. Although all oils are hydrophobic, the cores with high polarity closer to water are more relatively hydrophilic and compatible with GA-GE mixture solution (surface polarity 62.45%). The affinity between them can cause increased oil solubility in the aqueous phase, droplet coalescence and phase separation (Chanamai et al., 2002), and therefore leading to difficulties in core-shell formation and ultimately low encapsulation efficiency (Szczotok et al., 2018). From the thermodynamic perspective, core oil with a lower polarity will result in a higher interfacial tension with polar continuous phase, causing an increase in the total free energy in the system, thus the complete engulfing of nonpolar cores within polymer is able to achieve a reduction in the free energy for the system and therefore favourable to encapsulation (Rulison, 2000; Szczotok et al., 2018). In addition, it is worth noting that LL is an exception as LL has the lowest encapsulation efficiency (2.64 %) while its surface polarity (26.94%) is lower than LC (36.92 %) and CV (37.96 %). Such exception can be attributed to the morphology of LL microcapsules, which is predicted as dissociation where LL and aqueous phase are completely separated based on the spreading coefficient theory. Notwithstanding, the encapsulation efficiency of LL is 2.64 %, indicating some amounts of LL were still encapsulated, which is not fully consistent with the predicted dissociation. Similar discrepancies were also found for LC, LM and CV as acorn structure were predicted for their microcapsules based on the spreading coefficient theory, for which the encapsulation efficiency should also be 0 %, while 5.35%, 18.68% and 5.77% encapsulation efficiencies were obtained for LC, LM and CV respectively, evidencing the presence of some core-shell structured microcapsules. The higher encapsulation efficiency of LM can be

attributed to the lower value of surface polarity (12.23%) compared to LC (36.92%) and CV (37.96%). CD is predicted to have core-shell structured microcapsules, while its encapsulation efficiency (18.11%) is similar to LM microcapsules with a predicted acorn structure (18.68%), which can be due to its higher surface polarity (16.54%) compared to that of LM (12.23%).

The results of all the core oil encapsulation efficiency data suggest that the spreading coefficient theory did not give an exactly accurate prediction for the GE-GA coacervated microcapsule morphology. However, it still provides an insight for the engulfing behaviour of coacervates to core oil in aqueous phase, as the predicted microcapsule morphologies correspond with their actual ones holistically, which can be reflected by the values of each oil encapsulation efficiency (i.e., core-shell morphology is predicted for HS and CD, with relatively higher EE at 46.61% and 18.11%; acorn morphology is predicted for LC, LM and CV, with the corresponding EE at 5.35%, 18.68% and 5.77% respectively; dissociation morphology is predicted for LL, with the lowest EE at 2.64 %). Therefore, in order to have a better understanding of whether different oils can be encapsulated using the same process and shell material, the impacts of both the thermodynamic spreading coefficients theory and the surface polarity of each core oil on the formed microcapsule morphology and encapsulation efficiency should be considered.

5.4. Conclusions

Microcapsules containing various flavour/fragrance oils with different surface polarities were fabricated using GA and GE by complex coacervation. The physical properties (including surface polarity and the spreading coefficients) of core oils were examined in order to evaluate their effects on the capsule morphology and encapsulation efficiency. By both SEM

experimental observations and encapsulation efficiency measurements for each oil microcapsules, the thermodynamic spreading coefficients theory did not give an exactly accurate prediction for capsule morphology using high molecular weight biopolymer coacervates as the wall material in this work. Notwithstanding, the morphology predictions for different oil microcapsules are holistically consistent with their real encapsulation efficiency. The microcapsules with the predicted core-shell morphology had relatively high values of experimental EE (HS at 46.61%, CD at 18.11%), while the microcapsules with the predicted dissociation morphology had the lowest value of EE (LL at 2.64%), and those with the predicted acorn morphology capsule had the EE in between (LC at 5.35%, LM at 18.68% and CV at 5.77%). Since the EE of core oil can be significantly influenced by the structural morphology of microcapsules, the spreading coefficients theory can be still used for the evaluation of capsule morphology. Also, it has been found that the encapsulation efficiency increased with the decreasing surface polarity of the core oil holistically.

Overall, the effects of both the thermodynamic spreading coefficients theory and the surface polarity of each core oil on the formed microcapsule morphology and encapsulation efficiency are all important, and should be simultaneously taken into consideration to determine whether different oils can be encapsulated successfully for a given encapsulation technique and same shell material to be used.

CHAPTER 6. Overall Conclusions and Future work

Flavour/fragrance oils often required to be encapsulated into microcapsules/microspheres to maintain their functional properties and achieve controlled release for industrial applications. However, the microencapsulation of these materials is challenging since there are lacks of biodegradable microcapsules with desirable properties for various end-use applications, and simple, cheap and scalable encapsulation methods to fabricate high-quality microcapsules.

Although spray drying is the most widely used encapsulation method in industry, this method can readily lead to the evaporation and/or deterioration of core ingredients. Other approaches (e.g., solvent evaporation, polymerisation and complex coacervation) often raised some concerns about either the safety of some shell polymers and their non-biodegradability or the resulting microcapsules from relatively safe materials do not possess all the desirable properties for a given industrial application.

This project aimed at developing novel microencapsulation techniques for different flavours and fragrances using wax melt dispersion and gelatine-gum arabic coacervation followed by spray drying/coating respectively, and systematically charactering their physical, mechanical and structural properties, as well as exploring the impact of core oils on resulting microcapsule characteristics. In this chapter, the work that was conducted to meet these objectives in this PhD project is summarised and recommendations for future work are also given.

6.1. Overall conclusions

6.1.1. Fabrication and characterisation of wax microspheres by melt dispersion

Natural waxes are biodegradable and exhibit good chemical and mechanical stability at

different pH and moisture levels. Due to their chemical compositions, they can readily encapsulate hydrophobic materials when waxes are at liquid phase under heating. The temperature required for melting wax is lower than that normally used for spray drying, which can effectively reduce the deterioration of core ingredients. Wax microspheres were prepared by a simple melt dispersion method due to its readily availability for large industrial scales and very low environmental impacts, using L-carvone and hexyl salicylate as model flavour and fragrance compounds. Three different types of waxes (i.e., carnauba wax, candelilla wax and beeswax) as well as different oil to wax ratios (i.e., 1:1, 1:5 and 1:10 wt/wt) were investigated. It was found that the highest encapsulation efficiency (83.7 ± 1.2%) was obtained from candelilla wax encapsulating hexyl salicylate at 1:1 oil to wax ratio, which is similar to the value previously reported by Milanovic et al. (2010) using carnauba wax encapsulating ethyl vanillin (86.5 ± 5.6%), and higher than the reported encapsulation efficiency (47 ± 11%) by Baiocco et al. (2021a) using fungal chitosan and gum arabic coacervates as shell materials. It is notable that the highest encapsulation efficiency of beeswax microspheres and carnauba wax microspheres are 75.7 ± 2.7% and 76.9 ± 2.1% respectively, which are similar to the result obtained from formaldehyde-based microcapsules (75%) (Long et al., 2009). Notwithstanding, the retention of L-carvone using each wax by melt dispersion was relatively low, with EE ranging from 15.3 ± 0.3 % for beeswax at 1:1 oil to wax ratio and < 1% for carnauba wax at all oil loadings, which could be resulted from the poor barrier property of wax for low molecule aromas as well as the evaporation of L-carvone due to the heating during preparation of microspheres. Due to the low payload of L-carvone within each type of wax microspheres, the core leakage tests were conducted only for wax microspheres

containing hexyl salicylate in a dry state, which did not show any significant leakage over 30 days. The micromanipulation studies revealed that there was no typical rupture behaviour for wax microspheres under compression for the experimental conditions investigated. The Young's modulus for each wax microspheres was determined by the Hertz model, ranging from 28.3 ± 1.4 to 40.2 ± 1.1 MPa for LC and 31.3 ± 0.9 to 41.3 ± 1.7 MPa for HS in beeswax microspheres, 59.3 ± 2.6 to 270.9 ± 7.5 MPa for LC and 47.6 ± 2.1 to 228.93 ± 7.76 MPa for HS in carnauba wax microspheres and 112.6 ± 2.8 to 390.7 ± 15.9 MPa for LC and 98.3 ± 2.7 to 357.23 ± 9.43 MPa for HS in candelilla wax microspheres, which depended on the oil to wax ratios. Except beeswax microspheres, the Young's modules values of the other microspheres can be similar to that of gelatine-gum arabic based microcapsules (287 ± 38 to 390 ± 41 MPa) (Yu et al., 2021) and higher than that of chitosan/gum arabic microcapsules (95 ± 41 MPa) (Baiocco et al., 2023). The Young's modulus of wax microspheres was also found to decrease with increasing of oil to wax ratios regardless of core oil types or wax types. Thus, depending on the end applications of wax microspheres, the desirable properties could be controlled by selecting a certain oil to wax ratio. Overall, although each type of wax microspheres did not give satisfactory EEs for the encapsulation of LC, the performances of HS laden wax microspheres looked promising.

6.1.2. Fabrication and characterisation of flavour/fragrance microcapsules using complex coacervation followed by spray drying/coating

L-carvone is highly volatile and was poorly encapsulated by waxes using the melt dispersion method. Baiocco et al. (2021b) fabricated L-carvone laden microcapsules based on the complex coacervation between fungal chitosan and gum arabic, and achieved 29 ± 4 %

encapsulation efficiency. Such coacervating system also demonstrated the feasibility of encapsulating another flavour oil limonene (Baiocco & Zhang, 2022) and fragrance oil hexyl salicylate (Baiocco et al., 2021a). However, this process based on coacervation of fungal chitosan and gum arabic still did not give satisfactory encapsulation efficiency of costly flavours and fragrances. Comparatively, gelatine is 1/5 cheaper than chitosan (Ji et al., 2020), and has good emulsifying and gelling properties. Gelatine-gum arabic coacervated microcapsules to encapsulate fish oil were reported to have high EE and good mechanical properties (Yu et al., 2021). In the current project, gelatine-gum arabic coacervated microcapsules were prepared using complex coacervation followed by spray drying, with L-carvone, limonene or hexyl salicylate encapsulated as a model flavour or fragrance oil. The influences of different types of core oil and further treatments including maltodextrin coating or glutaraldehyde crosslinking on size, morphology, payload, encapsulation efficiency and mechanical strength of the resulting microcapsules were investigated. It was observed that micro-size spherical microcapsules were obtained and they had polynuclear core-shell structure, with an average size of 10.7 ± 0.1 μm. The encapsulation efficiency ranged from 5.0 ± 0.4 to 89.0 ± 1.2% for different core oils and 21.1 ± 0.1 to 89.0 ± 1.2 % after the further treatments to freshly coacervated microcapsules. The highest EE of 89.0 ± 1.2 % was obtained for encapsulating hexyl salicylate with a harden process by glutaraldehyde crosslinking, which was higher than that of chitosan/gum arabic microcapsules (47 ± 11%) (Baiocco et al., 2021a) or formaldehyde-based microcapsules (75 %) (Long et al., 2009). However, L-carvone laden microcapsules exhibited a lower encapsulation efficiency of 5.0 ± 0.4%, compared to 29 ± 4 % EE of chitosan/gum arabic microcapsules (Baiocco et al., 2021b). The difference in EE might

be attributed to their differences in coacervation conditions including pH adopted interactions between the coacervate (fungal chitosan and gelatine) and the oil. Micromanipulation tests revealed that gelatine-gum arabic microcapsules exhibited typical rupture behaviours under compression. The rupture force increased with microcapsule diameter, with an average value of 2.0 ± 0.6 mN for the mean diameter of 14.4 ± 2.0 μm. The nominal rupture stress and toughness decreased with the increase of microcapsule size, and the nominal rupture tension was independent of diameter, which were consistent with chitosan-gum arabic based microcapsules (Baiocco et al., 2021a), gelatine-gum arabic based microcapsules (Yu et al., 2021) and melamine formaldehyde-based microcapsules (Long et al., 2009). The apparent Young's modulus of whole microcapsules was determined by the Hertz model. The mean Young's modulus of GG-HS-GT was 668 ± 165 MPa, which was significantly higher than that of HS laden chitosan/gum arabic microcapsules (95 ± 14 MPa) (Baiocco et al., 2023). The intrinsic Young's modulus of shell was determined by finite elements analysis and the mean value of GG-HS-GT was 6.2 ± 1.0 GPa (with the corresponding mean h/r of 0.132 ± 0.009), which was also significantly higher than that reported by Mercadé-Prieto et al. (2011) for melamine formaldehyde shell (1.6 ± 0.3 GPa), chitosan-gum arabic coacervated shell (1.0 ± 0.1 GPa) reported by Baiocco et al. (2023) and glassy polymer shell (0.6 -1.8 GPa) reported by Yap et al. (2008), indicating gelatine and gum arabic coacervates crosslinked by glutaraldehyde had greater mechanical strength. Nevertheless, the ratio of the apparent Young's modulus of the whole microcapsules to the intrinsic Young's modulus of gelatine/gum arabic coacervate shell was 0.09 ± 0.02, which was statistically similar to the coefficient 0.085 ± 0.002 reported by Baiocco et al. (2023) for chitosan/gum arabic

coacervated capsules. Besides, the additional processing by either the maltodextrin coating or glutaraldehyde crosslinking significantly enhanced the mechanical strength of the microcapsule shell. The core oil also played an important role in affecting the mechanical properties of microcapsules.

6.1.3. Impact of core oils on microcapsule morphology and encapsulation efficiency

L-carvone and hexyl salicylate were encapsulated by either a wax melt dispersion systems or gelatine-gum arabic coacervating system. It was found that their encapsulation efficiencies and the corresponding microcapsules payloads varied significantly although they were prepared following the same experimental procedure and material formulations. The effect of core oil type on encapsulation efficiency was also reported for chitosan-gum arabic coacervated microcapsules and melamine-glutaraldehyde-formaldehyde microcapsules (Baiocco & Zhang, 2022; Luo et al., 2022). In this work, the morphology and encapsulation efficiency of gelatine/gum arabic coacervated microcapsules with L-carvone, limonene, linalool, carvacrol, cinnamaldehyde or hexyl salicylate encapsulated as a core were investigated by combining the spreading coefficient and two component surface energy theory. Surface tensions of core oils, interfacial tensions between each core oil and aqueous phase, contact angles of cores and a standard reference liquid (diiodomethane) on flat surface of dry gelatine/gum arabic coacervates as well as contact angles of cores on the standard reference solid (polytetrafluoroethylene) surface were firstly measured. The equilibrium spreading coefficient configurations of the three phases (oil phase, aqueous phase and gelatine/gum arabic coacervated polymer) for each oil were then calculated which were compared with the corresponding experimental morphologies. It was found that the thermodynamic spreading

coefficients theory did not give an exactly accurate prediction of capsule morphology using gelatine and gum arabic coacervates as shell. The discrepancy between the predicted and experimental morphologies may be attributed to the high molecular weight biopolymers (gelatine and gum arabic) used in this work, and consequently the thermodynamic equilibrium was difficult to be realised due to the decreased mobility of GA and GE complexed molecules upon interaction bonding. Nevertheless, the morphology predictions for different oil microcapsules are holistically consistent with their encapsulation efficiency. The microcapsules with the predicted core-shell morphology had relatively high values of experimental EE (HS at 46.61%, CD at 18.11%), while the microcapsules with the predicted dissociation morphology had the lowest value of EE (LL at 2.64%), and those with the predicted acorn morphology capsules had the EE in between (LC at 5.35%, LM at 18.68% and CV at 5.77%), supporting the feasibility of using the spreading coefficients theory to evaluate capsule morphology. In addition, it was found that the encapsulation efficiency increased with the decreasing surface polarity of the core oil holistically. The core oils with high surface polarity are relatively hydrophilic and the affinity between these oils and aqueous phase can lead to higher oil solubility in the aqueous phase. This, in turn, speeds up the migration of the oil molecules to the aqueous phase, ultimately resulting in low encapsulation efficiency. In contrast, core oils with lower surface polarity result in relatively higher interfacial tensions with polar aqueous phase, and the complete engulfing of the core oil by the coacervate phase is thermodynamically favourable to reduce the total free energy in the system. Overall, the effects of both the thermodynamic spreading coefficients theory and the surface polarity of each core oil on the formed microcapsule morphology and encapsulation efficiency are all

important, and should be simultaneously taken into consideration to determine whether different oils can be encapsulated successfully using a given encapsulation technique and same shell material.

6.2. Future work

Wax microspheres or gelatine-gum arabic coacervated microcapsules exhibited high encapsulation efficiency and strong mechanical properties compared to chitosan/gum arabic or formaldehyde-based microcapsules when encapsulating hexyl salicylate. Nevertheless, the encapsulation of L-carvone by either wax melt dispersion systems or gelatine-gum arabic coacervating system had relatively low encapsulation efficiency. Since FTIR results elucidated there was no chemical interactions between L-carvone molecules and GE/GA complexes or waxes molecules, this phenomenon can be attributed to the physical properties (e.g., volatility, chemical structure, molecular weight, solubility in water) of L-carvone or the poor barrier properties of waxes and gelatine/gum arabic coacervates for the small molecule compounds.

Seeing the promising results obtained with β-cyclodextrin (Partanen et al., 2002), it may be helpful to initially form the complexes of L-carvone in β-cyclodextrin, and subsequently encapsulated them within waxes or gelatine/gum arabic coacervates, where the complexes will have a decreased mobility, and ultimately an improved retention of L-carvone molecules. It was also highlighted in Chapter 4 that adding an extra layer of maltodextrin (MD, DE16.5–19.5) coating significantly enhanced the encapsulation efficiency of hexyl salicylate from 21.1 ± 0.1 to 54.0 ± 2.0 %. Besides, improved encapsulation efficiency and lower particle porosity were also reported using starch (tapioca starch) as a filler for the encapsulation of essential oil (Cortés-Camargo et al., 2023; Lozano-Vazquez et al., 2015). Therefore, treatments including

an initial molecular inclusion of L-carvone by cyclodextrin and/or further layer-by-layer coating to the freshly fabricated wax microspheres or gelatine/gum arabic microcapsules using water soluble biopolymer (e.g., maltodextrin, pectin, starch derivatives, tamarind seed mucilage) could have a good potential to improve the encapsulation efficiency for L-carvone.

Baiocco et al. (2021b) reported an encapsulation efficiency of 29 ± 4 % for L-carvone using fungal chitosan and gum arabic coacervates, which was higher than the reported encapsulation efficiency (5.0 ± 0.4 %) using gelatine and gum arabic coacervates as shell. Gelatine used in this work has a molecule weight of 500 kDa, compared to the fungal chitosan (150 kDa) used in the work of Baiocco et al. (2021b). The results indicated that the lower molecule weight of wall material can be more efficient when encapsulating small molecule core material (L-carvone, 150.22 g/mol; hexyl salicylate, 222.28 g/mol). If this speculation can be validated, other polymers (including gelatine (Kim et al., 2021), pea proteins (Archut et al., 2023), soy proteins (Nishinari et al., 2014), lentil (Saricaoglu, 2020) or wheat proteins (Voci et al., 2021)) of low molecule weight can be used as wall material in order to improve the encapsulation efficiency of L-carvone.

Besides, for each type of wax microspheres, the oil encapsulation efficiency and payload were found to increase with the increasing of oil weight ratios, further investigation about the molecular structural binding between oil and wax after crystallisation might offer an insight to understand the encapsulation mechanism of these oils using matrix carriers. In addition, the relation between the Young's model of each type of wax microspheres and their payloads was investigated based on a proposed equation using the lg values of normalised Young's modulus and lg payload. However, the experimental samples were limited in numbers, further

investigation including more wax or oil types, more sets of oil to wax ratios, should be undertaken to validate the dependency of Young's modulus on payload. Also, wax microspheres were characterised, and they showed good barrier properties for HS during storage. It would also be helpful to carry out the release tests for HS laden wax microspheres in aqueous medium. Additional studies addressing both the storage stability and the release profiles of core oil from GE/GE coacervate in an aqueous medium would be useful to investigate the quality and performance of these microcapsules for such end-use applications.

Finally, although the equilibrium spreading coefficient configurations of the three phases (oil phase, aqueous phase and gelatine/gum arabic coacervated polymer) calculated for each oil did not give an exactly accurate evaluation of the resulting microcapsule morphology, the predicted morphologies for different oil microcapsules were holistically consistent with their encapsulation efficiency. Hofmeister et al. (2015) mixed a pinene (low surface polarity) with β-damascone or ionone at 1:1 (weight ratio) respectively, and found the encapsulation efficiency of β-damascone was increased from 57 to 80% and that of ionone from 46 to 69%. A similar approach can be taken by introducing a mediator to the core oil, which can either decrease the surface polarity of core oil or alternatively maintain a relatively high positive value of polymer spreading coefficient to confirm the general applicability of the theories reported in Chapter 5. In addition, the investigation of core oil impact on microcapsule morphology and encapsulation efficiency by combining the spreading coefficient and two component surface energy theories focused on only gum arabic and gelatine coacervating system, future works including synthetic polymers (e.g. melamine formaldehyde) as a shell prepared by polymerisation, chitosan/gum arabic polymers prepared by complex coacervation

as well as wax systems by melt dispersion can be utilised to examine the applicability of this evaluation with different wall material chemistries. Core oils (including functional oils, vegetable oils) apart from flavour/fragrance oils can also be tested for their influences on microcapsules characteristics. It was also notable that the encapsulation efficiency of hexyl salicylate using gelatine/gum arabic (89.0 ± 1.2%) as wall material was higher than that of chitosan/gum arabic coacervate shell (47 ± 11%) (Baiocco et al., 2021a), suggesting a higher retention efficiency of HS by gelatine/gum arabic coacervate molecules, even gelatine has a higher molecule weight than fungal chitosan and theoretically diffuse more slowly than the latter. Exploring the kinetic impact, including the underlying mechanism governing the retention of core molecules by polymer molecules of varying sizes with different diffusion rates, would be valuable in understanding the influence of polymers on microcapsule morphology and encapsulation efficiency. It would be useful to further investigate the kinetic influence of polymer molecules with different molecular weights on the resultant microcapsule morphology and encapsulation efficiency, including the mechanism underlying the retention of core molecules by the polymers.

References

Abu-Lafi, S., Odeh, I., Dewik, H., Qabajah, M., Hanuš, L. O., & Dembitsky, V. M. (2008). Thymol and carvacrol production from leaves of wild Palestinian Majorana syriaca. *Bioresource Technology, 99*(9), 3914-3918. doi:https://doi.org/10.1016/j.biortech.2007.07.042

Al-Angari, A. A., Kennerley, J. W., & Newton, J. M. (1985). The compaction properties of polyethylene glycols. *J Pharm Pharmacol, 37*(3), 151-153. doi:10.1111/j.2042-7158.1985.tb05030.x

Alexander, K., & Shlomo, M. (2015). Microencapsulation. In *Encyclopedia of Surface and Colloid Science, Third Edition*: CRC Press.

Ali, B. H., Ziada, A., & Blunden, G. (2009). Biological effects of gum arabic: A review of some recent research. *Food and Chemical Toxicology, 47*(1), 1-8. doi:https://doi.org/10.1016/j.fct.2008.07.001

Alipanah, H., Farjam, M., Zarenezhad, E., Roozitalab, G., & Osanloo, M. (2021). Chitosan nanoparticles containing limonene and limonene-rich essential oils: potential phytotherapy agents for the treatment of melanoma and breast cancers. *BMC Complementary Medicine and Therapies, 21*(1), 186. doi:10.1186/s12906-021-03362-7

Alvim, I. D., & Grosso, C. R. F. (2010). Microparticles obtained by complex coacervation: influence of the type of reticulation and the drying process on the release of the core material. *Food Science and Technology, 30*.

Anvari, M., & Chung, D. (2016). Dynamic rheological and structural characterization of fish gelatin – Gum arabic coacervate gels cross-linked by tannic acid. *Food Hydrocolloids, 60*, 516-524. doi:https://doi.org/10.1016/j.foodhyd.2016.04.028

Anvari, M., Pan, C.-H., Yoon, W.-B., & Chung, D. (2015). Characterization of fish gelatin–gum arabic complex coacervates as influenced by phase separation temperature. *International Journal of Biological Macromolecules, 79*, 894-902. doi:https://doi.org/10.1016/j.ijbiomac.2015.06.004

Archut, A., Klost, M., Drusch, S., & Kastner, H. (2023). Complex coacervation of pea protein and pectin: Contribution of different protein fractions to turbidity. *Food Hydrocolloids, 134*, 108032. doi:https://doi.org/10.1016/j.foodhyd.2022.108032

Aytac, Z., Ipek, S., Durgun, E., Tekinay, T., & Uyar, T. (2017). Antibacterial electrospun zein nanofibrous web encapsulating thymol/cyclodextrin-inclusion complex for food packaging. Food Chem, 233, 117-124. doi:10.1016/j.foodchem.2017.04.095

Azarpazhooh, E., Sharayei, P., Rui, X., Gharibi-Tehrani, M., & Ramaswamy, H. S. (2022). Optimization of Wall Material of Freeze-Dried High-Bioactive Microcapsules with Yellow Onion Rejects Using Simplex Centroid Mixture Design Approach Based on Whey Protein Isolate, Pectin, and Sodium Caseinate as Incorporated Variables. Molecules, 27(23). doi:10.3390/molecules27238509

Aziz, S., Gill, J., Dutilleul, P., Neufeld, R., & Kermasha, S. (2014). Microencapsulation of krill oil using complex coacervation. Journal of Microencapsulation, 31. doi:10.3109/02652048.2014.932028

Bago Rodriguez, A. M., Binks, B. P., & Sekine, T. (2018). Emulsion stabilisation by complexes of oppositely charged synthetic polyelectrolytes. *Soft Matter, 14*(2), 239-

254. doi:10.1039/C7SM01845B

Baiocco, D., Preece, J. A., & Zhang, Z. (2021a). Encapsulation of hexylsalicylate in an animal-free chitosan-gum Arabic shell by complex coacervation. *Colloids and Surfaces A: Physicochemical and Engineering Aspects, 625*, 126861. doi:https://doi.org/10.1016/j.colsurfa.2021.126861

Baiocco, D., Preece, J. A., & Zhang, Z. (2021b). Microcapsules with a fungal chitosan-gum Arabic-maltodextrin shell to encapsulate health-beneficial peppermint oil. *Food Hydrocolloids for Health, 1*, 100016. doi:https://doi.org/10.1016/j.fhfh.2021.100016

Baiocco, D., & Zhang, Z. (2022). Microplastic-Free Microcapsules to Encapsulate Health-Promoting Limonene Oil. *Molecules, 27*(21), 7215. Retrieved from https://www.mdpi.com/1420-3049/27/21/7215

Baiocco, D., Zhang, Z., He, Y., & Zhang, Z. (2023). Relationship between the Young's Moduli of Whole Microcapsules and Their Shell Material Established by Micromanipulation Measurements Based on Diametric Compression between Two Parallel Surfaces and Numerical Modelling. *Micromachines (Basel), 14*(1). doi:10.3390/mi14010123

Bakry, A. M., Abbas, S., Ali, B., Majeed, H., Abouelwafa, M. Y., Mousa, A., & Liang, L. (2016). Microencapsulation of Oils: A Comprehensive Review of Benefits, Techniques, and Applications. *Compr Rev Food Sci Food Saf, 15*(1), 143-182. doi:10.1111/1541-4337.12179

Bangs, W. E., & Reineccius, G. A. (1982). Influence of Dryer Infeed Matrices on the Retention of Volatile Flavor Compounds During Spray Drying. *Journal of Food Science, 47*(1), 254-259. doi:https://doi.org/10.1111/j.1365-2621.1982.tb11072.x

Benita, S. (2005). *Microencapsulation: methods and industrial applications*: Crc Press.

Bennacef, C., Desobry-Banon, S., Linder, M., Khanji, A. N., Probst, L., & Desobry, S. (2021). Study and optimization of core-shell capsules produced by annular jet breaking coextrusion. *Colloids and Surfaces A: Physicochemical and Engineering Aspects, 629*, 127475. doi:https://doi.org/10.1016/j.colsurfa.2021.127475

Bennacef, C., Desobry, S., Probst, L., & Desobry-Banon, S. (2023). Alginate Based Core Shell Capsules Production through Coextrusion Methods: Recent Applications. *Foods, 12*(9), 1788. Retrieved from https://www.mdpi.com/2304-8158/12/9/1788

Berry, J. D., Mettu, S., & Dagastine, R. R. (2017). Precise measurements of capsule mechanical properties using indentation. *Soft Matter, 13*(10), 1943-1947. doi:10.1039/C6SM02841A

Berry, J. D., Neeson, M. J., Dagastine, R. R., Chan, D. Y. C., & Tabor, R. F. (2015). Measurement of surface and interfacial tension using pendant drop tensiometry. *Journal of Colloid and Interface Science, 454*, 226-237. doi:https://doi.org/10.1016/j.jcis.2015.05.012

Bhoyar, P., Morani, D., Biyani, D., Umekar, M., Mahure, J., & Amgaonkar, Y. M. (2011). Encapsulation of Naproxen in Lipid-Based Matrix Microspheres: Characterization and Release Kinetics. *Journal of young pharmacists : JYP, 3*, 105-111. doi:10.4103/0975-1483.80293

Bickers, D., Calow, P., Greim, H., Hanifin, J. M., Rogers, A. E., Saurat, J. H., & Tagami, H. (2003). A toxicologic and dermatologic assessment of linalool and related esters when used as fragrance ingredients. *Food and Chemical Toxicology, 41*(7), 919-942.

doi:https://doi.org/10.1016/S0278-6915(03)00016-4

Blake, A. I., Co, E. D., & Marangoni, A. G. (2014). Structure and Physical Properties of Plant Wax Crystal Networks and Their Relationship to Oil Binding Capacity. *Journal of the American Oil Chemists' Society, 91*(6), 885-903. doi:10.1007/s11746-014-2435-0

Bollhorst, T., Rezwan, K., & Maas, M. (2017). Colloidal capsules: nano- and microcapsules with colloidal particle shells. *Chemical Society Reviews, 46*(8), 2091-2126. doi:10.1039/C6CS00632A

Bouyahya, A., Mechchate, H., Benali, T., Ghchime, R., Charfi, S., Balahbib, A., . . . Omari, N. E. (2021). Health Benefits and Pharmacological Properties of Carvone. Biomolecules, 11(12). doi:10.3390/biom11121803

Bruyninckx, K., & Dusselier, M. (2019). Sustainable Chemistry Considerations for the Encapsulation of Volatile Compounds in Laundry-Type Applications. *ACS Sustainable Chemistry & Engineering, 7*. doi:10.1021/acssuschemeng.9b00677

Bucio, A., Moreno-Tovar, R., Bucio, L., Espinosa-Dávila, J., & Anguebes-Franceschi, F. (2021). Characterization of Beeswax, Candelilla Wax and Paraffin Wax for Coating Cheeses. *Coatings, 11*(3). doi:10.3390/coatings11030261

Burgess, D. J., & Ponsart, S. (1998). Beta-Glucuronidase activity following complex coacervation and spray drying microencapsulation. J Microencapsul, 15(5), 569-579. doi:10.3109/02652049809008241

Burt, S. (2004). Essential oils: their antibacterial properties and potential applications in foods--a review. *Int J Food Microbiol, 94*(3), 223-253. doi:10.1016/j.ijfoodmicro.2004.03.022

Calvo Magro, P., Castaño, Á., Lozano, M., & Gonzalez-Gomez, D. (2012). Influence of the microencapsulation on the quality parameters and shelf-life of extra-virgin olive oil encapsulated in the presence of BHT and different capsule wall components. *Food Research International, 45*, 256–261. doi:10.1016/j.foodres.2011.10.036

Celebioglu, A., & Uyar, T. (2021). Electrohydrodynamic encapsulation of eugenol-cyclodextrin complexes in pullulan nanofibers. Food Hydrocolloids, 111, 106264. doi:https://doi.org/10.1016/j.foodhyd.2020.106264

Chanamai, R., Horn, G., & McClements, D. J. (2002). Influence of Oil Polarity on Droplet Growth in Oil-in-Water Emulsions Stabilized by a Weakly Adsorbing Biopolymer or a Nonionic Surfactant. *Journal of Colloid and Interface Science, 247*(1), 167-176. doi:https://doi.org/10.1006/jcis.2001.8110

Chang, C. P., Leung, T. K., Lin, S. M., & Hsu, C. C. (2006). Release properties on gelatin-gum arabic microcapsules containing camphor oil with added polystyrene. *Colloids Surf B Biointerfaces, 50*(2), 136-140. doi:10.1016/j.colsurfb.2006.04.008

Chen, J., Jo, S., & Park, K. (1995). Polysaccharide hydrogels for protein drug delivery. *Carbohydrate Polymers, 28*(1), 69-76. doi:https://doi.org/10.1016/0144-8617(95)00080-1

Chen, X., Sun, G., Liu, D., Zhang, H., Zhang, H., Li, C., & Zhao, Z. (2021). Two effects of wax crystals on stabilizing water-in-oil emulsions. *Colloids and Surfaces A: Physicochemical and Engineering Aspects, 625*, 126884. doi:https://doi.org/10.1016/j.colsurfa.2021.126884

Cho, I., & Lee, K.-W. (1985). Morphology of latex particles formed by poly(methyl

methacrylate)-seeded emulsion polymerization of styrene. *Journal of Applied Polymer Science, 30*(5), 1903-1926. doi:https://doi.org/10.1002/app.1985.070300510

Choudhury, N., Meghwal, M., & Das, K. (2021). Microencapsulation: An overview on concepts, methods, properties and applications in foods. *Food Frontiers, 2*(4), 426-442. doi:https://doi.org/10.1002/fft2.94

Cittadini, A., Munekata, P., Pateiro, M., Sarriés, M., Domínguez, R., & Lorenzo, J. M. (2022). Encapsulation techniques to increase lipid stability. In (pp. 413-459).

Clará, R. A., Marigliano, A. C. G., & Sólimo, H. N. (2009). Density, Viscosity, and Refractive Index in the Range (283.15 to 353.15) K and Vapor Pressure of α-Pinene, d-Limonene, (±)-Linalool, and Citral Over the Pressure Range 1.0 kPa Atmospheric Pressure. *Journal of Chemical & Engineering Data, 54*(3), 1087-1090. doi:10.1021/je8007414

Collins, S., York, D. W., Kazmi, S., & Mohammed, A. K. (2020). Formation of wax walled microcapsules via double emulsion using cross membrane emulsification at elevated temperatures. *Journal of Food Engineering, 269*, 109739. doi:https://doi.org/10.1016/j.jfoodeng.2019.109739

Comunian, Thomazini, M., Alves, A. J. G., de Matos Junior, F. E., de Carvalho Balieiro, J. C., & Favaro-Trindade, C. S. (2013). Microencapsulation of ascorbic acid by complex coacervation: Protection and controlled release. *Food Research International, 52*(1), 373-379. doi:https://doi.org/10.1016/j.foodres.2013.03.028

Cortés-Camargo, S., Román-Guerrero, A., Alvarez-Ramirez, J., Alpizar-Reyes, E., Velázquez-Gutiérrez, S. K., & Pérez-Alonso, C. (2023). Microstructural influence on physical properties and release profiles of sesame oil encapsulated into sodium alginate-tamarind mucilage hydrogel beads. *Carbohydrate Polymer Technologies and Applications, 5*, 100302. doi:https://doi.org/10.1016/j.carpta.2023.100302

Da Silva, B. C., de Oliveira, M., Ferreira, J. G. L., Sierakowski, M. R., Simas-Tosin, F. F., Orth, E. S., & Riegel-Vidotti, I. C. (2015). Polyelectrolyte complexes from gum arabic and gelatin: Optimal complexation pH as a key parameter to obtain reproducible microcapsules. *Food Hydrocolloids, 46*, 201-207. doi:https://doi.org/10.1016/j.foodhyd.2014.12.022

Dardelle, G., & Erni, P. (2014). Three-phase interactions and interfacial transport phenomena in coacervate/oil/water systems. *Advances in Colloid and Interface Science, 206*, 79-91. doi:https://doi.org/10.1016/j.cis.2013.10.001

Das, S., David, S., Rajabalaya, R., Mukhopadhyay, H., Halder, T., Palanisamy, M., Nanda, A. (2011). Microencapsulation techniques and its practices. *International Journal of Pharmaceutical Science and Technology, 6*, 1-23.

De Araújo, J. S. F., de Souza, E. L., Oliveira, J. R., Gomes, A. C. A., Kotzebue, L. R. V., da Silva Agostini, D. L., Cavalcanti, M. T. (2020). Microencapsulation of sweet orange essential oil (Citrus aurantium var. dulcis) by liophylization using maltodextrin and maltodextrin/gelatin mixtures: Preparation, characterization, antimicrobial and antioxidant activities. Int J Biol Macromol, 143, 991-999. doi:10.1016/j.ijbiomac.2019.09.160

De Carvalho, C. C. C. R., & Da Fonseca, M. M. R. (2006). Carvone: Why and how should one bother to produce this terpene. *Food Chemistry, 95*(3), 413-422. doi:https://doi.org/10.1016/j.foodchem.2005.01.003

De Kruif, C. G., Weinbreck, F., & de Vries, R. (2004). Complex coacervation of proteins and anionic polysaccharides. Current Opinion in Colloid & Interface Science, 9(5), 340-349. doi:https://doi.org/10.1016/j.cocis.2004.09.006

De Matos, E. F., Scopel, B. S., & Dettmer, A. (2018). Citronella essential oil microencapsulation by complex coacervation with leather waste gelatin and sodium alginate. *Journal of Environmental Chemical Engineering, 6*(2), 1989-1994. doi:https://doi.org/10.1016/j.jece.2018.03.002

Desai, K. G. H., & Jin Park, H. (2005). Recent Developments in Microencapsulation of Food Ingredients. *DRYING TECHNOLOGY, 23*(7), 1361-1394. doi:10.1081/DRT-200063478

Devi, L. M., Das, A. B., & Badwaik, L. S. (2023). Effect of gelatin and acacia gum on anthocyanin coacervated microcapsules using double emulsion and its characterization. Int J Biol Macromol, 235, 123896. doi:10.1016/j.ijbiomac.2023.123896

Devi, N., Sarmah, M., Khatun, B., & Maji, T. K. (2017). Encapsulation of active ingredients in polysaccharide-protein complex coacervates. *Adv Colloid Interface Sci, 239*, 136-145. doi:10.1016/j.cis.2016.05.009

Dijke, K., Kobayashi, I., Schroën, K., Uemura, K., Nakajima, M., & Boom, R. (2009). Effect of viscosities of dispersed and continuous phases in microchannel oil-in-water emulsification. *Microfluidics and Nanofluidics, 9*, 77-85. doi:10.1007/s10404-009-0521-7

Dinarvand, R., Mahmoodi, S., Farboud, E., Salehi, M., & Atyabi, F. (2005). Preparation of gelatin microspheres containing lactic acid--effect of cross-linking on drug release. *Acta Pharm, 55*(1), 57-67.

Domaraju, P., & Lakshmi, P. (2012). Terpenes: Effect of lipophilicity in enhancing transdermal delivery of alfuzosin hydrochloride. Journal of advanced pharmaceutical technology & research, 3, 216-223. doi:10.4103/2231-4040.104712

Dong, Z., Ma, Y., Hayat, K., Jia, C., Xia, S., & Zhang, X. (2011). Morphology and release profile of microcapsules encapsulating peppermint oil by complex coacervation. *Journal of Food Engineering, 104*(3), 455-460. doi:https://doi.org/10.1016/j.jfoodeng.2011.01.011

Dong, Z. J., Touré, A., Jia, C. S., Zhang, X. M., & Xu, S. Y. (2007). Effect of processing parameters on the formation of spherical multinuclear microcapsules encapsulating peppermint oil by coacervation. *Journal of Microencapsulation, 24*(7), 634-646. doi:10.1080/02652040701500632

Dubey, R., Shami, T. C., & Rao, K. U. (2009). Microencapsulation Technology and Applications. *Defence Science Journal, 59*, 82-95. doi:10.14429/dsj.59.1489

Duhoranimana, E., Karangwa, E., Lai, L., Xu, X., Yu, J., Xia, S., & Habinshuti, I. (2017). Effect of sodium carboxymethyl cellulose on complex coacervates formation with gelatin: Coacervates characterization, stabilization and formation mechanism. *Food Hydrocolloids, 69*, 111-120. doi:https://doi.org/10.1016/j.foodhyd.2017.01.035

Ebnesajjad, S. (2006). 4 - Surface and Material Characterization Techniques. In S. Ebnesajjad (Ed.), *Surface Treatment of Materials for Adhesion Bonding* (pp. 43-75). Norwich, NY: William Andrew Publishing.

ECHA. (2023a). Hexyl salicylate. Retrieved from https://echa.europa.eu/registration-dossier/-

/registered-dossier/14766/4/23
ECHA. (2023b). (R)-p-mentha-1,8-diene. Retrieved from https://echa.europa.eu/registration-dossier/-/registered dossier/15256/4/23#:~:text=The%20dynamic%20viscosity%20of%20(%2D),determined%20to%20be%200.8462%20mPa
EFSA. (2007). Beeswax (E 901) as a glazing agent and as carrier for flavours - Scientific Opinion of the Panel on Food additives, Flavourings, Processing aids and Materials in Contact with Food (AFC). *EFSA Journal, 5*(12). doi:10.2903/j.efsa.2007.615
EFSA. (2012a). Scientific Opinion on the re-evaluation of candelilla wax (E 902) as a food additive. *EFSA Journal, 10*(11). doi:10.2903/j.efsa.2012.2946
EFSA. (2012b). Scientific Opinion on the re-evaluation of carnauba wax (E 903) as a food additive. *EFSA Journal, 10*(10), 2880. doi:https://doi.org/10.2903/j.efsa.2012.2880
Elkalla, E., Khizar, S., Tarhini, M., Lebaz, N., Zine, N., Jaffrezic-Renault, N., & Elaissari, A. (2023). Core-shell micro/nanocapsules: from encapsulation to applications. *Journal of Microencapsulation, 40*(3), 125-156. doi:10.1080/02652048.2023.2178538
Elmastaş, M., Demirtas, I., & Isildak, O. (2006). Antioxidant Activity of S-Carvone Isolated from Spearmint (Mentha Spicata L. Fam Lamiaceae). *Journal of Liquid Chromatography & Related Technologies - J LIQ CHROMATOGR RELAT TECHNO, 29*, 1465-1475. doi:10.1080/10826070600674893
Elzoghby, A. O. (2013). Gelatin-based nanoparticles as drug and gene delivery systems: reviewing three decades of research. *J Control Release, 172*(3), 1075-1091. doi:10.1016/j.jconrel.2013.09.019
Eraso, M. O., & Aníbal, H. (2014). Use of Starches and Milk Proteins in Microencapsulation. *International Journal of Vegetable Science, 20*(4), 289-304. doi:10.1080/19315260.2013.803181
Eriksson, V., Andersson Trojer, M., Vavra, S., Hulander, M., & Nordstierna, L. (2020). Formulation of polyphthalaldehyde microcapsules for immediate UV-light triggered release. *Journal of Colloid and Interface Science, 579*, 645-653. doi:https://doi.org/10.1016/j.jcis.2020.06.024
Espinosa-Andrews, H., Sandoval-Castilla, O., Vázquez-Torres, H., Vernon-Carter, E. J., & Lobato-Calleros, C. (2010). Determination of the gum Arabic–chitosan interactions by Fourier Transform Infrared Spectroscopy and characterization of the microstructure and rheological features of their coacervates. *Carbohydrate Polymers, 79*(3), 541-546. doi:https://doi.org/10.1016/j.carbpol.2009.08.040
Estevinho, B. N., Rocha, F., Santos, L., & Alves, A. (2013). Microencapsulation with chitosan by spray drying for industry applications – A review. *Trends in Food Science & Technology, 31*(2), 138-155. doi:https://doi.org/10.1016/j.tifs.2013.04.001
Falleh, H., Ben Jemaa, M., Saada, M., & Ksouri, R. (2020). Essential oils: A promising eco-friendly food preservative. *Food Chem, 330*, 127268. doi:10.1016/j.foodchem.2020.127268
Fang, X., Kikuchi, S., Shima, M., Kadata, M., Tsuno, T., & Adachi, S. (2006). Suppressive effect of alkyl ferulate on the oxidation of microencapsulated linoleic acid. *European Journal of Lipid Science and Technology - EUR J LIPID SCI TECHNOL, 108*, 97-102. doi:10.1002/ejlt.200500258

Fang, Z., & Bhandari, B. (2012). 4 - Spray drying, freeze drying and related processes for food ingredient and nutraceutical encapsulation. In N. Garti & D. J. McClements (Eds.), Encapsulation Technologies and Delivery Systems for Food Ingredients and Nutraceuticals (pp. 73-109): Woodhead Publishing.

Feczkó, T., Kardos, A. F., Németh, B., Trif, L., & Gyenis, J. (2014). Microencapsulation of n-hexadecane phase change material by ethyl cellulose polymer. *Polymer Bulletin, 71*(12), 3289-3304. doi:10.1007/s00289-014-1250-y

Fernández, V., & Khayet, M. (2015). Evaluation of the surface free energy of plant surfaces: toward standardizing the procedure. *Front Plant Sci, 6*, 510. doi:10.3389/fpls.2015.00510

Finotelli, P. V., & Rocha-Leão, M. H. (2005). *Microencapsulation of ascorbic acid in maltodextrin and capsul using spray-drying.* Paper presented at the Anais do 4◦ Mercosur Congress on Process Systems Engineering.

FMI. (2024). Global Encapsulated Flavors and Fragrances Market Snapshot (2023 to 2033). Retrieved from https://www.futuremarketinsights.com/reports/encapsulated-flavors-and-fragrances-market

Fowkes, F. M. (1962). Determination of interfacial tensions, contact angles, and dispersion forces in surfaces by assuming additivity of intermolecular interactions in surfaces. *The Journal of Physical Chemistry, 66*(2), 382-382. doi:10.1021/j100808a524

Fowkes, F. M. (1964). Attractive forces at interfaces. *Industrial & Engineering Chemistry, 56*(12), 40-52. doi:10.1021/ie50660a008

Franz, C. M. (2010). Essential oil research: past, present and future. *Flavour and Fragrance Journal, 25*(3), 112-113.

Franzios, G., Mirotsou, M., Hatziapostolou, E., Kral, J., Scouras, Z. G., & Mavragani-Tsipidou, P. (1997). Insecticidal and Genotoxic Activities of Mint Essential Oils. *Journal of Agricultural and Food Chemistry, 45*(7), 2690-2694. doi:10.1021/jf960685f

Friedman, M., Henika, P. R., & Mandrell, R. E. (2002). Bactericidal activities of plant essential oils and some of their isolated constituents against Campylobacter jejuni, Escherichia coli, Listeria monocytogenes, and Salmonella enterica. *J Food Prot, 65*(10), 1545-1560. doi:10.4315/0362-028x-65.10.1545

Gharsallaoui, A., Roudaut, G., Chambin, O., Voilley, A., & Saurel, R. (2007). Applications of spray-drying in microencapsulation of food ingredients: An overview. *Food Research International, 40*(9), 1107-1121. doi:https://doi.org/10.1016/j.foodres.2007.07.004

Ghorbanzadeh Ahangari, M., Fereidoon, A., Jahanshahi, M., & Sharifi, N. (2014). Effect of nanoparticles on the micromechanical and surface properties of poly(urea–formaldehyde) composite microcapsules. *Composites Part B: Engineering, 56*, 450-455. doi:https://doi.org/10.1016/j.compositesb.2013.08.071

Girardi, N. S., Passone, M. A., García, D., Nesci, A., & Etcheverry, M. (2018). Microencapsulation of Peumus boldus essential oil and its impact on peanut seed quality preservation. *Industrial Crops and Products, 114*, 108-114. doi:https://doi.org/10.1016/j.indcrop.2018.01.036

Girifalco, L. A., & Good, R. J. (1957). A Theory for the Estimation of Surface and Interfacial Energies. I. Derivation and Application to Interfacial Tension. *The Journal of Physical Chemistry, 61*(7), 904-909. doi:10.1021/j150553a013

Goubet, I., Le Quere, J. L., & Voilley, A. J. (1998). Retention of Aroma Compounds by Carbohydrates: Influence of Their Physicochemical Characteristics and of Their Physical State. A Review. *Journal of Agricultural and Food Chemistry, 46*(5), 1981-1990. doi:10.1021/jf970709y

Gouin, S. (2004). Microencapsulation: industrial appraisal of existing technologies and trends. Trends in Food Science & Technology, 15(7), 330-347. doi:https://doi.org/10.1016/j.tifs.2003.10.005

Govender, T., Choonara, Y. E., Kumar, P., Du Toit, L. C., Modi, G., Naidoo, D., & Pillay, V. (2015). A Novel Melt-Dispersion Technique for Simplistic Preparation of Chlorpromazine-Loaded Polycaprolactone Nanocapsules. Polymers, 7(6), 1145-1176. Retrieved from https://www.mdpi.com/2073-4360/7/6/1145

Graebin, C. S., Madeira, M. d. F., Yokoyama-Yasunaka, J. K. U., Miguel, D. C., Uliana, S. R. B., Benitez, D., & Eifler-Lima, V. L. (2010). Synthesis and in vitro activity of limonene derivatives against Leishmania and Trypanosoma. *European Journal of Medicinal Chemistry, 45*(4), 1524-1528. doi:https://doi.org/10.1016/j.ejmech.2009.12.061

Gray, A., Egan, S., Bakalis, S., & Zhang, Z. (2016). Determination of microcapsule physicochemical, structural, and mechanical properties. *Particuology, 24*, 32-43. doi:https://doi.org/10.1016/j.partic.2015.06.002

Green, B. K., & Schleicher, L. (1957). US Patent No. 2,500,457.

Gu, X. L., Zhu, X., Kong, X. Z., & Tan, Y. (2010). Comparisons of simple and complex coacervations for preparation of sprayable insect sex pheromone microcapsules and release control of the encapsulated pheromone molecule. *J Microencapsul, 27*(4), 355-364. doi:10.3109/02652040903221532

Gulão Eda, S., de Souza, C. J., Andrade, C. T., & Garcia-Rojas, E. E. (2016). Complex coacervates obtained from peptide leucine and gum arabic: formation and characterization. Food Chem, 194, 680-686. doi:10.1016/j.foodchem.2015.08.062

Gutzeit, H. O., & Ludwig-Müller, J. (2014). *Plant Natural Products: Synthesis, Biological Functions and Practical Applications*.

Hacura, A., & Zimnicka, B. (2006). An Investigation of Molecular Structure and Dynamics of Crude Beeswax by Vibrational Spectroscopy. *Polish J. Environ. Stud., 15*.

Harkins, W. D., & Feldman, A. (1922). Films. the spreading of liquids and the spreading coefficient. *Journal of the American Chemical Society, 44*(12), 2665-2685. doi:10.1021/ja01433a001

He, J. Y., Zhang, Z. L., Midttun, M., Fonnum, G., Modahl, G. I., Kristiansen, H., & Redford, K. (2008). Size effect on mechanical properties of micron-sized PS–DVB polymer particles. *Polymer, 49*(18), 3993-3999. doi:https://doi.org/10.1016/j.polymer.2008.07.015

He, L., Hu, J., & Deng, W. (2018). Preparation and application of flavor and fragrance capsules. *Polymer Chemistry, 9*(40), 4926-4946. doi:10.1039/C8PY00863A

He, Y., Bowen, J., Andrews, J., Liu, M., Smets, J., & Zhang, Z. (2014). Adhesion of perfume-filled microcapsules to model fabric surfaces. *Journal of Microencapsulation*. doi:10.3109/02652048.2013.871359

He, Y., Yao, S., Hao, J., Wang, H., Zhu, L., Si, T., & Lin, J. (2019). Synthesis of melamine-

formaldehyde microcapsules containing oil-based fragrances via intermediate polyacrylate bridging layers. *Chinese Journal of Chemical Engineering, 27*(10), 2574-2580. doi:https://doi.org/10.1016/j.cjche.2018.10.023

Herrmann, K. M., & Weaver, L. M. (1999). The shikimate pathway. *Annu Rev Plant Physiol Plant Mol Biol, 50*, 473-503. doi:10.1146/annurev.arplant.50.1.473

Hirai, M., Ota, Y., & Ito, M. (2022). Diversity in principal constituents of plants with a lemony scent and the predominance of citral. *J Nat Med, 76*(1), 254-258. doi:10.1007/s11418-021-01553-7

Hofmeister, I., Landfester, K., & Taden, A. (2015). Controlled formation of polymer nanocapsules with high diffusion-barrier properties and prediction of encapsulation efficiency. *Angewandte Chemie International Edition, 54*(1), 327-330. doi:https://doi.org/10.1002/anie.201408393

Hogan, S. A., O'Riordan, E. D., & O'Sullivan, M. (2003). Microencapsulation and oxidative stability of spray-dried fish oil emulsions. *Journal of Microencapsulation, 20*(5), 675-688. doi:10.3109/02652040309178355

Howe, S. (2020). Chapter 1 - Raw materials. In C. Smart (Ed.), *The Craft Brewing Handbook* (pp. 1-46): Woodhead Publishing.

Hu, J., Chen, H.-Q., & Zhang, Z. (2009). Mechanical properties of melamine formaldehyde microcapsules for self-healing materials. *Materials Chemistry and Physics - MATER CHEM PHYS, 118*, 63-70. doi:10.1016/j.matchemphys.2009.07.004

Hu, J., Zhang, X., & Qu, J. (2018). Investigation on the mechanical properties of polyurea (PU)/melamine formaldehyde (MF) microcapsules prepared with different chain extenders. *J Microencapsul, 35*(3), 219-228. doi:10.1080/02652048.2018.1462414

Hwang, J.-S., Kim, J.-N., Wee, Y.-J., Yun, J.-S., Jang, H.-G., Kim, S.-H., & Ryu, H.-W. (2006). Preparation and characterization of melamine-formaldehyde resin microcapsules containing fragrant oil. *Biotechnology and Bioprocess Engineering, 11*(4), 332-336. doi:10.1007/BF03026249

Imran, M., Aslam, M., Alsagaby, S. A., Saeed, F., Ahmad, I., Afzaal, M., & Islam, S. (2022). Therapeutic application of carvacrol: A comprehensive review. *Food Science & Nutrition, 10*(11), 3544-3561. doi:https://doi.org/10.1002/fsn3.2994

Isac-García, J., Dobado, J. A., Calvo-Flores, F. G., & Martínez-García, H. (2016). Chapter 7 - Basic Operation Experiments. In J. Isac-García, J. A. Dobado, F. G. Calvo-Flores, & H. Martínez-García (Eds.), *Experimental Organic Chemistry* (pp. 207-238): Academic Press.

Jańczuk, B., Białopiotrowicz, T., & Wójcik, W. (1989). The components of surface tension of liquids and their usefulness in determinations of surface free energy of solids. *Journal of Colloid and Interface Science, 127*(1), 59-66. doi:https://doi.org/10.1016/0021-9797(89)90007-6

Ji, Z., Liu, H., Yu, L., Duan, Q., Chen, Y., & Chen, L. (2020). pH controlled gelation behavior and morphology of gelatin/hydroxypropylmethylcellulose blend in aqueous solution. *Food Hydrocolloids, 104*, 105733. doi:https://doi.org/10.1016/j.foodhyd.2020.105733

Jridi, M., Hajji, S., Ayed, H. B., Lassoued, I., Mbarek, A., Kammoun, M., . . . Nasri, M. (2014). Physical, structural, antioxidant and antimicrobial properties of gelatin–chitosan composite edible films. *International Journal of Biological Macromolecules, 67*, 373-

379. doi:https://doi.org/10.1016/j.ijbiomac.2014.03.054

Jyothi, N. V., Prasanna, P. M., Sakarkar, S. N., Prabha, K. S., Ramaiah, P. S., & Srawan, G. Y. (2010). Microencapsulation techniques, factors influencing encapsulation efficiency. *J Microencapsul, 27*(3), 187-197. doi:10.3109/02652040903131301

Kelly, T. J., Smith, D. L., & Satola, J. (1999). Emission Rates of Formaldehyde from Materials and Consumer Products Found in California Homes. Environmental Science & Technology, 33(1), 81-88. doi:10.1021/es980592

Khatibi, S. A., Ehsani, A., Nemati, M., & Javadi, A. (2021). Microencapsulation of Zataria multiflora Boiss. essential oil by complex coacervation using gelatin and gum arabic: Characterization, release profile, antimicrobial and antioxidant activities. *Journal of Food Processing and Preservation, 45*(10), e15823. doi:https://doi.org/10.1111/jfpp.15823

Kim, B., Ban, E., & Kim, A. (2021). Gelatin-Alginate Coacervates Optimized by DOE to Improve Delivery of bFGF for Wound Healing. *Pharmaceutics, 13*(12). doi:10.3390/pharmaceutics13122112

Kłosowska, A., Wawrzyńczak, A., & Feliczak-Guzik, A. (2023). Microencapsulation as a route for obtaining encapsulated flavors and fragrances. *Cosmetics, 10*(1), 26. Retrieved from https://www.mdpi.com/2079-9284/10/1/26

Knaebel, A., Rebre, S. R., & Lequeux, F. (1997). Determination of the elastic modulus of superabsorbent gel beads. *Polymer Gels and Networks, 5*(2), 107-121. doi:https://doi.org/10.1016/S0966-7822(96)00034-2

Knowles, A. (2008). Recent developments of safer formulations of agrochemicals. *The Environmentalist, 28*, 35-44.

Kong, X. Z., Gu, X., Zhu, X., & Zhang, Z. (2009). Spreadable dispersion of insect sex pheromone capsules, preparation via complex coacervation and release control of the encapsulated pheromone component molecule. *Biomedical Microdevices, 11*(1), 275-285. doi:10.1007/s10544-008-9234-z

Koo, S. Y., Cha, K. H., Song, D.-G., Chung, D., & Pan, C.-H. (2014). Microencapsulation of peppermint oil in an alginate–pectin matrix using a coaxial electrospray system. *International Journal of Food Science & Technology, 49*(3), 733-739. doi:https://doi.org/10.1111/ijfs.12358

Kralovec, J. A., Zhang, S., Zhang, W., & Barrow, C. J. (2012). A review of the progress in enzymatic concentration and microencapsulation of omega-3 rich oil from fish and microbial sources. *Food Chemistry, 131*(2), 639-644. doi:https://doi.org/10.1016/j.foodchem.2011.08.085

Kumar, P., Mishra, S., Malik, A., & Satya, S. (2014). Preparation and characterization of PEG-Mentha oil nanoparticles for housefly control. *Colloids and Surfaces B: Biointerfaces, 116*, 707-713. doi:https://doi.org/10.1016/j.colsurfb.2013.11.012

Lapczynski, A., Jones, L., McGinty, D., Bhatia, S., Letizia, C. S., & Api, A. M. (2007). Fragrance material review on hexyl salicylate. *Food and Chemical Toxicology, 45*(1, Supplement 1), S410-S417. doi:https://doi.org/10.1016/j.fct.2007.09.045

Lashgari, S., Arabi, H., Mahdavian, A. R., & Ambrogi, V. (2017). Thermal and morphological studies on novel PCM microcapsules containing n-hexadecane as the core in a flexible shell. *Applied Energy, 190*, 612-622.

doi:https://doi.org/10.1016/j.apenergy.2016.12.158
Leitereg, T. J., Guadagni, D. G., Harris, J., Mon, T. R., & Teranishi, R. (1971). Evidence for the Difference between the Odours of the Optical Isomers (+)- and (−)-Carvone. *Nature, 230*(5294), 455-456. doi:10.1038/230455a0
Lemetter, C. Y. G., Meeuse, F. M., & Zuidam, N. J. (2009). Control of the morphology and the size of complex coacervate microcapsules during scale-up. AIChE Journal, 55(6), 1487-1496. doi:https://doi.org/10.1002/aic.11816
Leung, H. W. (2001). Ecotoxicology of glutaraldehyde: review of environmental fate and effects studies. Ecotoxicol Environ Saf, 49(1), 26-39. doi:10.1006/eesa.2000.2031
Li, K., Nam, J. H., Kang, S., Liu, Y., & Lee, J. (2022). Carvone and its eutectic mixtures as novel, biodegradable, and tunable solvents to extract hydrophobic compounds in substitution for volatile toxic solvents. Food Chemistry, 374, 131630. doi:https://doi.org/10.1016/j.foodchem.2021.131630
Lim, S.-J., Lee, J.-H., Kim, J.-H., Choi, G., Cho, N.-J., & Park, B.-J. (2014). Quantitative Analysis of Cinnamaldehyde, Cinnamylalcohol and Salicylaldehyde in Commercial Biopesticides Containing Cinnamon Extract Using Gas Chromatography - Flame Ionization Detector. *Korean Journal of Environmental Agriculture, 33*, 213-219. doi:10.5338/KJEA.2014.33.3.213
Lim, X.-Y., Li, J., Yin, H.-M., He, M., Li, L., & Zhang, T. (2023). Stabilization of Essential Oil: Polysaccharide-Based Drug Delivery System with Plant-like Structure Based on Biomimetic Concept. *Polymers, 15*(16), 3338. Retrieved from https://www.mdpi.com/2073-4360/15/16/3338
Lin, L.-T., Wu, S.-J., & Lin, C.-C. (2013). The Anticancer Properties and Apoptosis-inducing Mechanisms of Cinnamaldehyde and the Herbal Prescription Huang-Lian-Jie-Du-Tang (Huáng Lián Jiě Dú Tang) in Human Hepatoma Cells. *Journal of traditional and complementary medicine, 3*, 227-233. doi:10.4103/2225-4110.119732
Ling, S. D., Geng, Y., Chen, A., Du, Y., & Xu, J. (2020). Enhanced single-cell encapsulation in microfluidic devices: From droplet generation to single-cell analysis. *Biomicrofluidics, 14*(6), 061508. doi:10.1063/5.0018785
Liu, F., Antoniou, J., Li, Y., Majeed, H., Liang, R., Ma, Y., & Zhong, F. (2016). Chitosan/sulfobutylether-β-cyclodextrin nanoparticles as a potential approach for tea polyphenol encapsulation. *Food Hydrocolloids, 57*, 291-300. doi:https://doi.org/10.1016/j.foodhyd.2016.01.024
Liu, J., Shim, Y. Y., Wang, Y., & Reaney, M. J. T. (2015). Intermolecular interaction and complex coacervation between bovine serum albumin and gum from whole flaxseed (Linum usitatissimum L.). Food Hydrocolloids, 49, 95-103. doi:https://doi.org/10.1016/j.foodhyd.2015.02.035
Liu, X.-D., Atarashi, T., Furuta, T., Yoshii, H., Aishima, S., Ohkawara, M., & Linko, P. (2007). Microencapsulation of emulsified hydrophobic flavors by spray drying. *DRYING TECHNOLOGY, 19(7)*, 1361-1374. doi:10.1081/DRT-100105293
Liu, Y., & Jiang, J. (2023). Preparation of β-ionone microcapsules by gelatin/pectin complex coacervation. *Carbohydrate Polymers, 312*, 120839. doi:https://doi.org/10.1016/j.carbpol.2023.120839
Liu, Y., Wang, H., Fu, R., Zhang, L., Liu, M., Cao, W., & Wang, S. (2023). Preparation and

characterization of cinnamon essential oil extracted by deep eutectic solvent and its microencapsulation. *Journal of Food Measurement and Characterization, 17*(1), 664-673. doi:10.1007/s11694-022-01653-2

Liu, Z., Ge, X., Lu, Y., Dong, S., Zhao, Y., & Zeng, M. (2012). Effects of chitosan molecular weight and degree of deacetylation on the properties of gelatine-based films. *Food Hydrocolloids, 26*(1), 311-317. doi:https://doi.org/10.1016/j.foodhyd.2011.06.008

Loksuwan, J. (2007). Characteristics of microencapsulated β-carotene formed by spray drying with modified tapioca starch, native tapioca starch and maltodextrin. *Food Hydrocolloids, 21*(5), 928-935. doi:https://doi.org/10.1016/j.foodhyd.2006.10.011

Long, Y., Vincent, B., York, D., Zhang, Z., & Preece, J. A. (2010). Organic–inorganic double shell composite microcapsules. *Chemical Communications, 46*(10), 1718-1720. doi:10.1039/B911266A

Long, Y., York, D., Zhang, Z., & Preece, J. A. (2009). Microcapsules with low content of formaldehyde: preparation and characterization. *Journal of Materials Chemistry, 19*(37), 6882-6887. doi:10.1039/B902832C

López de Dicastillo, C., Velásquez, E., Rojas, A., Garrido, L., Moreno, M. C., Guarda, A., & Galotto, M. J. (2023). Developing Core/Shell Capsules Based on Hydroxypropyl Methylcellulose and Gelatin through Electrodynamic Atomization for Betalain Encapsulation. *Polymers, 15*(2), 361. Retrieved from https://www.mdpi.com/2073-4360/15/2/361

Loxley, A., & Vincent, B. (1998). Preparation of Poly(methylmethacrylate) Microcapsules with Liquid Cores. *J Colloid Interface Sci, 208*(1), 49-62. doi:10.1006/jcis.1998.5698

Lozano-Vazquez, G., Lobato-Calleros, C., Escalona-Buendia, H., Chavez, G., Alvarez-Ramirez, J., & Vernon-Carter, E. J. (2015). Effect of the weight ratio of alginate-modified tapioca starch on the physicochemical properties and release kinetics of chlorogenic acid containing beads. *Food Hydrocolloids, 48*, 301-311. doi:https://doi.org/10.1016/j.foodhyd.2015.02.032

Luo, S., Gao, M., Pan, X., Wang, Y., He, Y., Zhu, L., & Sun, Y. (2022). Fragrance oil microcapsules with low content of formaldehyde: Preparation and characterization. *Colloids and Surfaces A: Physicochemical and Engineering Aspects, 648*, 129019. doi:https://doi.org/10.1016/j.colsurfa.2022.129019

Luo, S., He, Y., Zhu, L., Si, T., & Sun, Y. (2023). Comprehensive evaluation on the encapsulation performances of melamine-formaldehyde microcapsules affected by core oils. *Colloids and Surfaces A: Physicochemical and Engineering Aspects, 659*, 130794. doi:https://doi.org/10.1016/j.colsurfa.2022.130794

Lv, Y., Yang, F., Li, X., Zhang, X., & Abbas, S. (2014). Formation of heat-resistant nanocapsules of jasmine essential oil via gelatin/gum arabic based complex coacervation. *Food Hydrocolloids, 35*, 305-314. doi:https://doi.org/10.1016/j.foodhyd.2013.06.003

Lv, Y., Zhang, X., Zhang, H., Abbas, S., & Karangwa, E. (2013). The study of pH-dependent complexation between gelatin and gum arabic by morphology evolution and conformational transition. Food Hydrocolloids, 30(1), 323-332. doi:https://doi.org/10.1016/j.foodhyd.2012.06.007

Mączka, W., Duda-Madej, A., Grabarczyk, M., & Wińska, K. (2022). Natural Compounds in

the Battle against Microorganisms—Linalool. *Molecules, 27*(20), 6928. Retrieved from https://www.mdpi.com/1420-3049/27/20/6928

Madene, A., Jacquot, M., Scher, J., & Desobry, S. (2006). Flavour encapsulation and controlled release – a review. *International Journal of Food Science & Technology, 41*(1), 1-21. doi:https://doi.org/10.1111/j.1365-2621.2005.00980.x

Manaf, M., Subuki, I., Jai, J., Raslan, R., & Mustapa, A. (2018). Encapsulation of Volatile Citronella Essential Oil by Coacervation: Efficiency and Release Study. *IOP Conference Series: Materials Science and Engineering, 358*, 012072. doi:10.1088/1757-899X/358/1/012072

Martins Dos Santos, V. A., Leenen, E. J., Rippoll, M. M., van der Sluis, C., van Vliet, T., Tramper, J., & Wijffels, R. H. (1997). Relevance of rheological properties of gel beads for their mechanical stability in bioreactors. *Biotechnol Bioeng, 56*(5), 517-529. doi:10.1002/(sici)1097-0290(19971205)56:5<517::Aid-bit5>3.0.Co;2-l

Martins, I. M., Barreiro, M. F., Coelho, M., & Rodrigues, A. E. (2014). Microencapsulation of essential oils with biodegradable polymeric carriers for cosmetic applications. *Chemical Engineering Journal, 245*, 191-200. doi:https://doi.org/10.1016/j.cej.2014.02.024

Mediratta, P. K., Sharma, K. K., & Singh, S. (2002). Evaluation of immunomodulatory potential of Ocimum sanctum seed oil and its possible mechanism of action. *J Ethnopharmacol, 80*(1), 15-20. doi:10.1016/s0378-8741(01)00373-7

Mehta, N., Kumar, P., Verma, A. K., Umaraw, P., Kumar, Y., Malav, O. P., & Lorenzo, J. M. (2022). Microencapsulation as a Noble Technique for the Application of Bioactive Compounds in the Food Industry: A Comprehensive Review. *Applied Sciences, 12*(3), 1424. Retrieved from https://www.mdpi.com/2076-3417/12/3/1424

Mendes, S., Zille, A., Bezerra, F., & Catarino, A. (2018). *Preparation and characterization of gelatin/arabic gum microcapsules containing methyl salicylate deposited onto a cotton fabric*.

Mendoza-Duarte, M. E., Estrada-Moreno, I. A., López-Martínez, E. I., & Vega-Rios, A. (2023). Effect of the Addition of Different Natural Waxes on the Mechanical and Rheological Behavior of PLA—A Comparative Study. Polymers, 15(2), 305. Retrieved from https://www.mdpi.com/2073-4360/15/2/305

Meneses, A. C., Marques, E. B. P., Leimann, F. V., Gonçalves, O. H., Ineu, R. P., de Araújo, P. H. H., & Sayer, C. (2019). Encapsulation of clove oil in nanostructured lipid carriers from natural waxes: Preparation, characterization and in vitro evaluation of the cholinesterase enzymes. *Colloids and Surfaces A: Physicochemical and Engineering Aspects, 583*, 123879. doi:https://doi.org/10.1016/j.colsurfa.2019.123879

Mercadé-Prieto, R., Allen, R., York, D., Preece, J. A., Goodwin, T. E., & Zhang, Z. (2012a). Determination of the shell permeability of microcapsules with a core of oil-based active ingredient. *Journal of Microencapsulation, 29*(5), 463-474. doi:10.3109/02652048.2012.658444

Mercadé-Prieto, R., Allen, R., Zhang, Z., York, D., Preece, J. A., & Goodwin, T. E. (2012b). Failure of elastic-plastic core–shell microcapsules under compression. *AIChE Journal, 58*(9), 2674-2681. doi:https://doi.org/10.1002/aic.12804

Mercadé-Prieto, R., Nguyen, B., Allen, R., York, D., Preece, J. A., Goodwin, T. E., & Zhang, Z.

(2011). Determination of the elastic properties of single microcapsules using micromanipulation and finite element modeling. *Chemical Engineering Science, 66*(10), 2042-2049. doi:https://doi.org/10.1016/j.ces.2011.01.015

Merkus, H. G. (2009). *Particle size measurements : fundamentals, practice, quality* [1 online resource]. doi:10.1007/978-1-4020-9016-5

Meyer, R. (2005). Delivery system handbook for personal care and cosmetic products: technology. *Application and Formulations, Published in united states by William Andrew, 2006*, 334.

Milanovic, J., Ilic-Sevic, G., Gavrilovic, M., Milosavljević, M., & Bugarski, B. (2017). Blend of natural waxes as a matrix for aroma encapsulation. *Facta universitatis - series: Physics, Chemistry and Technology, 15*, 103-111. doi:10.2298/FUPCT1702103M

Milanovic, J., Levic, S., Manojlovic, V., Nedovic, V., & Branko, B. (2011). Carnauba wax microparticles produced by melt dispersion technique. *Chemical Papers, 65*, 213-220. doi:10.2478/s11696-011-0001-x

Milanovic, J., Manojlovic, V., Levic, S., Rajic, N., Nedovic, V., & Bugarski, B. (2010). Microencapsulation of Flavors in Carnauba Wax. *Sensors, 10*(1), 901-912. Retrieved from https://www.mdpi.com/1424-8220/10/1/901

Mimica-Dukić, N., Bozin, B., Soković, M., Mihajlović, B., & Matavulj, M. (2003). Antimicrobial and antioxidant activities of three Mentha species essential oils. *Planta Med, 69*(5), 413-419. doi:10.1055/s-2003-39704

Mishra, M. (2015). *Handbook of Encapsulation and Controlled Release*: CRC Press.

Mittal, V. (2013). Encapsulation Nanotechnologies.

Mohammed, N. K., Tan, C. P., Manap, Y. A., Muhialdin, B. J., & Hussin, A. S. M. (2020). Spray Drying for the Encapsulation of Oils-A Review. *Molecules, 25*(17). doi:10.3390/molecules25173873

Morcia, C., Tumino, G., Ghizzoni, R., & Terzi, V. (2016). Carvone (Mentha spicata L.) Oils. In (pp. 309-316).

Morgan, J., Townley, S., Kemble, G., & Smith, R. (2002). Measurement of physical and mechanical properties of beeswax. *Materials Science and Technology, 18*, 463-467. doi:10.1179/026708302225001714

Motoki, M., & Seguro, K. (1998). Transglutaminase and its use for food processing. Trends in Food Science and Technology, 9, 204-210.

Muhoza, B., Xia, S., Wang, X., Zhang, X., Li, Y., & Zhang, S. (2022). Microencapsulation of essential oils by complex coacervation method: preparation, thermal stability, release properties and applications. *Critical Reviews in Food Science and Nutrition, 62*(5), 1363-1382. doi:10.1080/10408398.2020.1843132

Muhoza, B., Xia, S., & Zhang, X. (2019). Gelatin and high methyl pectin coacervates crosslinked with tannic acid: The characterization, rheological properties, and application for peppermint oil microencapsulation. *Food Hydrocolloids, 97*, 105174. doi:https://doi.org/10.1016/j.foodhyd.2019.105174

Naigre, R., Kalck, P., Roques, C., Roux, I., & Michel, G. (1996). Comparison of antimicrobial properties of monoterpenes and their carbonylated products. *Planta Med, 62*(3), 275-277. doi:10.1055/s-2006-957877

Najafi, A., Zivdar, M., & Vahabzadeh, F. (2004). Microencapsulation of Orange Oil by

Complex Coacervation and its Release Behavior (REASEARCH NOTE). International Journal of Engineering, 17(4), 333-342. Retrieved from https://www.ije.ir/article_71543_cbc05e361c9166350bdb361c9c0cae03.pdf

Nandy, A., Lee, E., Mandal, A., Saremi, R., & Sharma, S. (2020). Microencapsulation of retinyl palmitate by melt dispersion for cosmetic application. *Journal of Microencapsulation, 37*(3), 205-219. doi:10.1080/02652048.2020.1720029

Napiórkowska, A. & Kurek, M. (2022a). Coacervation as a Novel Method of Microencapsulation of Essential Oils-A Review. *Molecules, 27*(16). doi:10.3390/molecules27165142

Napiórkowska, A, & Kurek, M. (2022b). Microencapsulation of juniper and black pepper essential oil using the coacervation method and its properties after freeze-drying. *Foods*, **2023**, *12*, 4345. https://doi.org/10.3390/foods12234345

Nedovic, V., Kalusevic, A., Manojlovic, V., Levic, S., & Bugarski, B. (2011). An overview of encapsulation technologies for food applications. Procedia Food Science, 1, 1806-1815. doi:https://doi.org/10.1016/j.profoo.2011.09.265

Nelson, G. (2013). 4 - Microencapsulated colourants for technical textile application. In M. L. Gulrajani (Ed.), *Advances in the Dyeing and Finishing of Technical Textiles* (pp. 78-104): Woodhead Publishing.

Nishinari, K., Fang, Y., Guo, S., & Phillips, G. O. (2014). Soy proteins: A review on composition, aggregation and emulsification. *Food Hydrocolloids, 39*, 301-318. doi:https://doi.org/10.1016/j.foodhyd.2014.01.013

Niu, F., Dong, Y., Shen, F., Wang, J., Liu, Y., Su, Y., Yang, Y. (2015). Phase separation behavior and structural analysis of ovalbumin–gum arabic complex coacervation. Food Hydrocolloids, 43, 1-7. doi:https://doi.org/10.1016/j.foodhyd.2014.02.009

Ogilvie-Battersby, J. D., Nagarajan, R., Mosurkal, R., & Orbey, N. (2022). Microencapsulation and controlled release of insect repellent geraniol in gelatin/gum arabic microcapsules. *Colloids and Surfaces A: Physicochemical and Engineering Aspects, 640*, 128494. doi:https://doi.org/10.1016/j.colsurfa.2022.128494

Ohtsubo, T., Tsuda, S., & Tsuji, K. (1991). A study of the physical strength of fenitrothion microcapsules. *Polymer, 32*(13), 2395-2399. doi:https://doi.org/10.1016/0032-3861(91)90080-3

Oliveira, L. C. d., Barbosa, J. R., Ribeiro, S. d. C. A., Vasconcelos, M. A. M. d., Aguiar, B. A. d., Pereira, G. V. d. S., & Lourenço, L. d. F. H. (2019). Improvement of the characteristics of fish gelatin – gum arabic through the formation of the polyelectrolyte complex. *Carbohydrate Polymers, 223*, 115068. doi:https://doi.org/10.1016/j.carbpol.2019.115068

Owens, D. K., & Wendt, R. C. (1969). Estimation of the surface free energy of polymers. *Journal of Applied Polymer Science, 13*(8), 1741-1747. doi:https://doi.org/10.1002/app.1969.070130815

Pakzad, H., Alemzadeh, I., & Kazemii, A. (2013). Encapsulation of Peppermint Oil with Arabic Gum-gelatin by Complex Coacervation Method. *International Journal of Engineering, 26*, 807-814.

Pan, X., Mercadé-Prieto, R., York, D., Preece, J. A., & Zhang, Z. (2013). Structure and Mechanical Properties of Consumer-Friendly PMMA Microcapsules. *Industrial &*

Engineering Chemistry Research, 52(33), 11253-11265. doi:10.1021/ie303451s

Pandey, M. K., Von Suskil, M., Chitren, R., Al-Odat, O., Jonnalagadda, S. C., & Aggarwal, B. B. (2022). Chapter 29 - Cancer on fire: role of inflammation in prevention and treatment. In B. Hernández-Ledesma & C. Martínez-Villaluenga (Eds.), *Current Advances for Development of Functional Foods Modulating Inflammation and Oxidative Stress* (pp. 605-626): Academic Press.

Partanen, R., Ahro, M., Hakala, M., Kallio, H., & Forssell, P. (2002). Microencapsulation of caraway extract in ß-cyclodextrin and modified starches. *European Food Research and Technology, 214*, 242-247. doi:10.1007/s00217-001-0446-1

Pedro Henrique Rodrigues do, A., Patrícia Lopes, A., & Leilane Costa de, C. (2019). Microencapsulation and Its Uses in Food Science and Technology: A Review. In S. Fabien (Ed.), *Microencapsulation* (pp. Ch. 6). Rijeka: IntechOpen.

Peng, C., Zhao, S.-Q., Zhang, J., Huang, G.-Y., Chen, L.-Y., & Zhao, F.-Y. (2014). Chemical composition, antimicrobial property and microencapsulation of Mustard (Sinapis alba) seed essential oil by complex coacervation. *Food Chemistry, 165*, 560-568. doi:https://doi.org/10.1016/j.foodchem.2014.05.126

Pisani, E., Fattal, E., Paris, J., Ringard, C., Rosilio, V., & Tsapis, N. (2008). Surfactant dependent morphology of polymeric capsules of perfluorooctyl bromide: Influence of polymer adsorption at the dichloromethane–water interface. *Journal of Colloid and Interface Science, 326*(1), 66-71. doi:https://doi.org/10.1016/j.jcis.2008.07.013

Plotto, A., Roberts, D. D., & Roberts, R. G. (2003). Evaluation of plant essential oils as natural postharvest disease control of tomato (lycopersicon esculentum). *Acta Horticulturae, 628*, 737-745. doi:10.17660/ActaHortic.2003.628.93

Poncelet, D., & Neufeld, R. J. (1989). Shear breakage of nylon membrane microcapsules in a turbine reactor. *Biotechnol Bioeng, 33*(1), 95-103. doi:10.1002/bit.260330113

Pongpaibul, Y., Price, J. C., & Whitworth, C. W. (1984). Preparation and Evaluation of Controlled Release Indomethacin Microspheres. *Drug Development and Industrial Pharmacy, 10*, 1597-1616.

Prata, A. S., & Grosso, C. R. F. (2015). Influence of the Oil Phase on the Microencapsulation by Complex Coacervation. *Journal of the American Oil Chemists' Society, 92*(7), 1063-1072. doi:10.1007/s11746-015-2670-z

Prata, A. S., Zanin, M. H., Ré, M. I., & Grosso, C. R. (2008). Release properties of chemical and enzymatic crosslinked gelatin-gum Arabic microparticles containing a fluorescent probe plus vetiver essential oil. Colloids Surf B Biointerfaces, 67(2), 171-178. doi:10.1016/j.colsurfb.2008.08.014

Priftis, D., Farina, R., & Tirrell, M. (2012). Interfacial Energy of Polypeptide Complex Coacervates Measured via Capillary Adhesion. *Langmuir, 28*(23), 8721-8729. doi:10.1021/la300769d

PubChem, N. C. f. B. I. (2023a). PubChem Annotation Record for , (D)-LIMONENE, Source: Hazardous Substances Data Bank (HSDB). Retrieved from https://pubchem.ncbi.nlm.nih.gov

PubChem, N. C. f. B. I. (2023b). PubChem Compound Summary for CID 439570, Carvone, (-)-. Retrieved from https://pubchem.ncbi.nlm.nih.gov/compound/5R_-2-methyl-5-prop-1-en-2-ylcyclohex-2-en-1-one.

PubChem, N. C. f. B. I. (2024a). Carvacrol. Retrieved from https://pubchem.ncbi.nlm.nih.gov/compound/Carvacrol

PubChem, N. C. f. B. I. (2024b). Cinnamaldehyde. Retrieved from https://pubchem.ncbi.nlm.nih.gov/compound/Cinnamaldehyde

PubChem, N. C. f. B. I. (2024c). Linalool, (+/-)-. Retrieved from https://pubchem.ncbi.nlm.nih.gov/compound/Linalool

Putievsky, E. (1993). Cultivation and processing of medicinal plants, edited by L. Hornok, John Wiley, Chichester, 1992. No. of pages: 338, price £50.00. ISBN 0–471–923883–4. *Flavour and Fragrance Journal, 8*(2), 125-125. doi:https://doi.org/10.1002/ffj.2730080212

Qin, J., Priftis, D., Farina, R., Perry, S. L., Leon, L., Whitmer, J., & De Pablo, J. J. (2014). Interfacial Tension of Polyelectrolyte Complex Coacervate Phases. *ACS Macro Letters, 3*(6), 565-568. doi:10.1021/mz500190w

Rakhee, Mishra, J., Sharma, R. K., & Misra, K. (2018). Chapter 9 - Characterization Techniques for Herbal Products. In K. Misra, P. Sharma, & A. Bhardwaj (Eds.), *Management of High Altitude Pathophysiology* (pp. 171-202): Academic Press.

Ranjha, N. M., Khan, H., & Naseem, S. (2010). Encapsulation and characterization of controlled release flurbiprofen loaded microspheres using beeswax as an encapsulating agent. *Journal of Materials Science: Materials in Medicine, 21*(5), 1621-1630. doi:10.1007/s10856-010-4034-4

Ravichandran, C., Badgujar, P. C., Gundev, P., & Upadhyay, A. (2018). Review of toxicological assessment of d-limonene, a food and cosmetics additive. *Food Chem Toxicol, 120*, 668-680. doi:10.1016/j.fct.2018.07.052

Reineccius, G. A. (1988). Spray-Drying of Food Flavors. In *Flavor Encapsulation* (Vol. 370, pp. 55-66): American Chemical Society.

Reineccius, G. A. (1989). Flavor encapsulation. *Food Reviews International, 5*(2), 147-176. doi:10.1080/87559128909540848

Reis, D. R., Ambrosi, A., & Luccio, M. D. (2022). Encapsulated essential oils: A perspective in food preservation. *Future Foods, 5*, 100126. doi:https://doi.org/10.1016/j.fufo.2022.100126

Ren, P.-W., Ju, X.-J., Xie, R., & Chu, L.-Y. (2010). Monodisperse alginate microcapsules with oil core generated from a microfluidic device. *Journal of Colloid and Interface Science, 343*(1), 392-395. doi:https://doi.org/10.1016/j.jcis.2009.11.007

Reshna, K. R., Gopi, S., & Balakrishnan, P. (2022). Introduction to Flavor and Fragrance in Food Processing. In *Flavors and Fragrances in Food Processing: Preparation and Characterization Methods* (Vol. 1433, pp. 1-19): American Chemical Society.

Rhim, J. W., & Shellhammer, T. H. (2005). 21 - Lipid-based edible films and coatings. In J. H. Han (Ed.), *Innovations in Food Packaging* (pp. 362-383). London: Academic Press.

Rocha, G. A., Fávaro-Trindade, C. S., & Grosso, C. R. F. (2012). Microencapsulation of lycopene by spray drying: Characterization, stability and application of microcapsules. *Food and Bioproducts Processing, 90*(1), 37-42. doi:https://doi.org/10.1016/j.fbp.2011.01.001

Rodríguez-López, M. I., Mercader-Ros, M. T., Lucas-Abellán, C., Pellicer, J. A., Pérez-Garrido, A., Pérez-Sánchez, H., . . . Núñez-Delicado, E. (2020). Comprehensive

Characterization of Linalool-HP-β-Cyclodextrin Inclusion Complexes. Molecules, 25(21). doi:10.3390/molecules25215069

Rojas-Moreno, S., Cárdenas-Bailón, F., Osorio-Revilla, G., Gallardo-Velázquez, T., & Proal-Nájera, J. (2018). Effects of complex coacervation-spray drying and conventional spray drying on the quality of microencapsulated orange essential oil. *Journal of Food Measurement and Characterization, 12*(1), 650-660. doi:10.1007/s11694-017-9678-z

Rosenberg, M., Kopelman, I. J., & Talmon, Y. (1990). Factors affecting retention in spray-drying microencapsulation of volatile materials. *Journal of Agricultural and Food Chemistry, 38*(5), 1288-1294. doi:10.1021/jf00095a030

Rosenberg, M., & Sheu, T. Y. (1996). Microencapsulation of volatiles by spray-drying in whey protein-based wall systems. *International Dairy Journal, 6*(3), 273-284. doi:https://doi.org/10.1016/0958-6946(95)00020-8

Rousi, Z., Malhiac, C., Fatouros, D. G., & Paraskevopoulou, A. (2019). Complex coacervates formation between gelatin and gum Arabic with different arabinogalactan protein fraction content and their characterization. *Food Hydrocolloids, 96*, 577-588. doi:https://doi.org/10.1016/j.foodhyd.2019.06.009

Rulison, C. (2000). Two-component surface energy characterization as a predictor of wettability and dispersability. *KRUSS Application note AN213*, 1-22.

Rungwasantisuk, A., & Raibhu, S. (2020). Application of encapsulating lavender essential oil in gelatin/gum-arabic complex coacervate and varnish screen-printing in making fragrant gift-wrapping paper. *Progress in Organic Coatings, 149*, 105924. doi:https://doi.org/10.1016/j.porgcoat.2020.105924

Saeed, F., Afzaal, M., Raza, M. A., Rasheed, A., Hussain, M., Nayik, G. A., & Ansari, M. J. (2023). Chapter 4 - Lavender essential oil: Nutritional, compositional, and therapeutic insights. In G. A. Nayik & M. J. Ansari (Eds.), *Essential Oils* (pp. 85-101): Academic Press.

Samakradhamrongthai, R. S., Thakeow Angeli, P., Kopermsub, P., & Utama-ang, N. (2019). Optimization of gelatin and gum arabic capsule infused with pandan flavor for multi-core flavor powder encapsulation. *Carbohydrate Polymers, 226*, 115262. doi:https://doi.org/10.1016/j.carbpol.2019.115262

Sanguansri, L., & Ann Augustin, M. (2010). Microencapsulation in Functional Food Product Development. In *Functional Food Product Development* (pp. 1-23).

Saravacos, G., & Moyer, J. (1968). Volatility of some aroma compounds during vacuum-drying of fruit juices. *Food Technology, 22*(5), 89-+.

Saricaoglu, F. T. (2020). Application of high-pressure homogenization (HPH) to modify functional, structural and rheological properties of lentil (Lens culinaris) proteins. *International Journal of Biological Macromolecules, 144*, 760-769. doi:https://doi.org/10.1016/j.ijbiomac.2019.11.034

Sarika, P. R., Pavithran, A., & James, N. R. (2015). Cationized gelatin/gum arabic polyelectrolyte complex: Study of electrostatic interactions. Food Hydrocolloids, 49, 176-182. doi:https://doi.org/10.1016/j.foodhyd.2015.02.039

Schmitt, C., Aberkane, L., & Sanchez, C. (2009). 16 - Protein–polysaccharide complexes and coacervates. In G. O. Phillips & P. A. Williams (Eds.), Handbook of Hydrocolloids (Second Edition) (pp. 420-476): Woodhead Publishing.

Schubert, M. A., & Müller-Goymann, C. C. (2005). Characterisation of surface-modified solid lipid nanoparticles (SLN): influence of lecithin and nonionic emulsifier. *Eur J Pharm Biopharm, 61*(1-2), 77-86. doi:10.1016/j.ejpb.2005.03.006

Seneca. (2007). CHAPTER 2 - Alkaloid Chemistry. In T. Aniszewski (Ed.), *Alkaloids - Secrets of Life* (pp. 61-139). Amsterdam: Elsevier.

Senoo, S., & White, A. (2017). Analysis and design of wet-steam stages. In (pp. 165-218).

Serfert, Y., Drusch, S., Schmidt-Hansberg, B., Kind, M., & Schwarz, K. (2009). Process engineering parameters and type of n-octenylsuccinate-derivatised starch affect oxidative stability of microencapsulated long chain polyunsaturated fatty acids. *Journal of Food Engineering, 95*(3), 386-392. doi:https://doi.org/10.1016/j.jfoodeng.2009.05.021

Shaddel, R., Hesari, J., Azadmard-Damirchi, S., Hamishehkar, H., Fathi-Achachlouei, B., & Huang, Q. (2018). Use of gelatin and gum Arabic for encapsulation of black raspberry anthocyanins by complex coacervation. *International Journal of Biological Macromolecules, 107*, 1800-1810. doi:https://doi.org/10.1016/j.ijbiomac.2017.10.044

Shahidi, F., & Han, X. Q. (1993). Encapsulation of food ingredients. Crit Rev Food Sci Nutr, 33(6), 501-547. doi:10.1080/10408399309527645

Sharifi-Rad, M., Varoni, E. M., Iriti, M., Martorell, M., Setzer, W. N., Del Mar Contreras, M., . . . Sharifi-Rad, J. (2018). Carvacrol and human health: A comprehensive review. *Phytother Res, 32*(9), 1675-1687. doi:10.1002/ptr.6103

Shekhar, K., Madhu, M., Pradeep, B., & Banji, D. (2010). A review on Microencapsulation. *International Journal of Pharmaceutical Sciences Review and Research, 5*, 58-62.

Sheu, T.-Y., & Rosenberg, M. (1998). Microstructure of Microcapsules Consisting of Whey Proteins and Carbohydrates. *Journal of Food Science, 63*(3), 491-494. doi:https://doi.org/10.1111/j.1365-2621.1998.tb15770.x

Shirin-Abadi, A. R., Khoee, S., Rahim-Abadi, M. M., & Mahdavian, A. R. (2014). Kinetic and thermodynamic correlation for prediction of morphology of nanocapsules with hydrophobic core via miniemulsion polymerization. *Colloids and Surfaces A: Physicochemical and Engineering Aspects, 462*, 18-26. doi:https://doi.org/10.1016/j.colsurfa.2014.08.009

Shirvani, A., Goli, S. A. H., Varshosaz, J., & Sedaghat Doost, A. (2022). Cinnamaldehyde encapsulation within new natural wax-based nanoparticles; formation, optimization and characterization. *Journal of Dispersion Science and Technology*, 1-12. doi:10.1080/01932691.2022.2044843

sigma-Aldrich. (2023a). Carvone Saftey Data Sheet. Retrieved from https://www.sigmaaldrich.com/US/en/sds/ALDRICH/435759

Sigma-Aldrich. (2023b). Cinnamaldehyde. Retrieved from https://www.sigmaaldrich.com/US/en/product/aldrich/w228613#product-documentation

Sigma-Aldrich. (2023c). Hexyl salicylate. Retrieved from https://www.sigmaaldrich.com/US/en/product/sial/61690

sigma-Aldrich. (2023d). Limonene. Retrieved from https://www.sigmaaldrich.com/US/en/product/aldrich/218367

Sigma-Aldrich. (2023e). Linalool. Retrieved from

https://www.sigmaaldrich.com/US/en/product/aldrich/l2602

Silva, G. L., Luft, C., Lunardelli, A., Amaral, R. H., Melo, D. A., Donadio, M. V., & De Oliveira, J. R. (2015). Antioxidant, analgesic and anti-inflammatory effects of lavender essential oil. *An Acad Bras Cienc, 87*(2 Suppl), 1397-1408. Doi:10.1590/0001-3765201520150056

Silva, M. T. S., & Pinto, J. C. (2019). Influence of Encapsulated Aroma Compounds on the Formation and Morphology of Gelatin Microparticles. *Macromolecular Symposia, 383*(1), 1800061. Doi:https://doi.org/10.1002/masy.201800061

Soottitantawat, A., Takayama, K., Okamura, K., Muranaka, D., Yoshii, H., Furuta, T., & Linko, P. (2005). Microencapsulation of l-menthol by spray drying and its release characteristics. *Innovative Food Science & Emerging Technologies, 6*(2), 163-170. doi:https://doi.org/10.1016/j.ifset.2004.11.007

Soottitantawat, A., Yoshii, H., Furuta, T., Ohkawara, M., & Linko, P. (2003). Microencapsulation by Spray Drying: Influence of Emulsion Size on the Retention of Volatile Compounds. *Journal of Food Science, 68*, 2256-2262. doi:10.1111/j.1365-2621.2003.tb05756.x

Sousa, V. I., Parente, J. F., Marques, J. F., Forte, M. A., & Tavares, C. J. (2022). Microencapsulation of Essential Oils: A Review. *Polymers (Basel), 14*(9). doi:10.3390/polym14091730

Spruijt, E., Sprakel, J., Cohen Stuart, M. A., & Van der Gucht, J. (2010). Interfacial tension between a complex coacervate phase and its coexisting aqueous phase. *Soft Matter, 6*(1), 172-178. Doi:10.1039/B911541B

Sri, S., Seethadevi, A., Prabha, K., Muthuprasanna, P., & Pavitra, P. (2012). Microencapsulation: A review. *International Journal of Pharma and Bio Sciences, 3*, P509-P531.

Stauffer, E., Dolan, J. A., & Newman, R. (2008). CHAPTER 8 - Gas Chromatography and Gas Chromatography—Mass Spectrometry. In E. Stauffer, J. A. Dolan, & R. Newman (Eds.), *Fire Debris Analysis* (pp. 235-293). Burlington: Academic Press.

Stojaković, D., Bugarski, B., & Rajić, N. (2012). A kinetic study of the release of vanillin encapsulated in Carnauba wax microcapsules. *Journal of Food Engineering, 109*(3), 640-642. Doi:https://doi.org/10.1016/j.jfoodeng.2011.11.022

Sun, G., & Zhang, Z. (2001). Mechanical properties of melamine-formaldehyde microcapsules. *J Microencapsul, 18*(5), 593-602. Doi :10.1080/02652040010019541

Sundberg, D. C., Casassa, A. P., Pantazopoulos, J., Muscato, M. R., Kronberg, B., & Berg, J. (1990). Morphology development of polymeric microparticles in aqueous dispersions. I. Thermodynamic considerations. *Journal of Applied Polymer Science, 41*(7-8), 1425-1442. Doi:10.1002/app.1990.070410706

Sundberg, E. J., & Sundberg, D. C. (1993). Morphology development for three-component emulsion polymers: Theory and experiments. *Journal of Applied Polymer Science, 47*(7), 1277-1294. Doi:https://doi.org/10.1002/app.1993.070470716

Surewicz, & Mantsch. (1988). New insight into protein secondary structure from resolution-enhanced infrared spectra. *Biochim Biophys Acta, 952*(2), 115-130. Doi:10.1016/0167-4838(88)90107-0

Sutaphanit, P., & Chitprasert, P. (2014). Optimisation of microencapsulation of holy basil

essential oil in gelatin by response surface methodology. *Food Chemistry, 150*, 313-320. Doi:https://doi.org/10.1016/j.foodchem.2013.10.159

Szczotok, A. M., Garrido, I., Carmona, M., Kjøniksen, A.-L., & Rodriguez, J. F. (2018). Predicting microcapsules morphology and encapsulation efficiency by combining the spreading coefficient theory and polar surface energy component. *Colloids and Surfaces A: Physicochemical and Engineering Aspects, 554*, 49-59. Doi:https://doi.org/10.1016/j.colsurfa.2018.06.022

Takigawa, T., & Endo, Y. (2006). Effects of Glutaraldehyde Exposure on Human Health. Journal of Occupational Health, 48(2), 75-87. doi:https://doi.org/10.1539/joh.48.75

Tang, Y., Scher, H. B., & Jeoh, T. (2020). Industrially scalable complex coacervation process to microencapsulate food ingredients. *Innovative Food Science & Emerging Technologies, 59*, 102257. Doi:https://doi.org/10.1016/j.ifset.2019.102257

Tasker, A. L., Hitchcock, J. P., He, L., Baxter, E. A., Biggs, S., & Cayre, O. J. (2016). The effect of surfactant chain length on the morphology of poly(methyl methacrylate) microcapsules for fragrance oil encapsulation. *Journal of Colloid and Interface Science, 484*, 10-16. Doi:https://doi.org/10.1016/j.jcis.2016.08.058

Tekin, R., Bac, N., & Erdogmus, H. (2013). Microencapsulation of Fragrance and Natural Volatile Oils for Application in Cosmetics, and Household Cleaning Products. *Macromolecular Symposia, 333*. Doi:10.1002/masy.201300047

Tello, F., Prata, A. S., Rodrigues, R. A. F., Sartoratto, A., & Grosso, C. R. F. (2016). Improving the performance of transglutaminase-crosslinked microparticles for enteric delivery. *Food Res Int, 88*(Pt A), 153-158. Doi:10.1016/j.foodres.2016.02.020

Teper-bamnolker, P., Dudai, N., Fischer, R., Belausov, E., Zemach, H., Shoseyov, O., & Eshel, D. (2010). Mint essential oil can induce or inhibit potato sprouting by differential alteration of apical meristem. *Planta, 232*, 179-186. Doi:10.1007/s00425-010-1154-5

Thomasin, C., Merkle, H. P., & Gander, B. A. (1997). Physico-chemical parameters governing protein microencapsulation into biodegradable polyesters by coacervation. *International Journal of Pharmaceutics, 147*(2), 173-186. Doi:https://doi.org/10.1016/S0378-5173(96)04810-7

Timilsena, Y. P., Akanbi, T. O., Khalid, N., Adhikari, B., & Barrow, C. J. (2019). Complex coacervation: Principles, mechanisms and applications in microencapsulation. International Journal of Biological Macromolecules, 121, 1276-1286. doi:https://doi.org/10.1016/j.ijbiomac.2018.10.144

Tinto, W. F., Elufioye, T. O., & Roach, J. (2017). Chapter 22 - Waxes. In S. Badal & R. Delgoda (Eds.), *Pharmacognosy* (pp. 443-455). Boston: Academic Press.

Tiwari, D., & Verma, P. (2011). Microencapsulation technique by solvent evaporation method (Study of effect of process variables). *2*, 998-1005.

Tongnuanchan, P., & Benjakul, S. (2014). Essential Oils: Extraction, Bioactivities, and Their Uses for Food Preservation. *Journal of Food Science, 79*(7), R1231-R1249. Doi:https://doi.org/10.1111/1750-3841.12492

Tonon, R., Grosso, C., & Hubinger, M. (2011). *Microencapsulation of flaxseed oil by spray drying: Influence of process conditions and emulsion properties.* Paper presented at the 11th International Congress on Engineering and Food, Athens, Greece.

Torza, S., & Mason, S. G. (1970). Three-phase interactions in shear and electrical fields.

Journal of Colloid and Interface Science, 33(1), 67-83. doi:https://doi.org/10.1016/0021-9797(70)90073-1

Trujillo-Ramírez, D., Reyes, I., Lobato-Calleros, C., Vernon-Carter, E. J., & Alvarez-Ramirez, J. (2022). Chia seed oil-candelilla wax oleogels structural features and viscoelasticity are enhanced by annealing. *LWT, 153*, 112433. doi:https://doi.org/10.1016/j.lwt.2021.112433

Turgeon, S., & Laneuville, S. (2009). Protein + Polysaccharide Coacervates and Complexes. In (pp. 327-363).

Turgeon, S. L., Schmitt, C., & Sanchez, C. (2007). Protein–polysaccharide complexes and coacervates. *Current Opinion in Colloid & Interface Science, 12*(4), 166-178. doi:https://doi.org/10.1016/j.cocis.2007.07.007

Uhlemann, J., Schleifenbaum, B., & Bertram, H. J. (2002). Flavor encapsulation technologies: An overview including recent developments. Perfumer and flavorist, 27, 52-61.

Van der Graaf, S., Schroën, C. G. P. H., van der Sman, R. G. M., & Boom, R. M. (2004). Influence of dynamic interfacial tension on droplet formation during membrane emulsification. *Journal of Colloid and Interface Science, 277*(2), 456-463. doi:https://doi.org/10.1016/j.jcis.2004.04.033

Van Raamsdonk, J. M., & Chang, P. L. (2001). Osmotic pressure test: A simple, quantitative method to assess the mechanical stability of alginate microcapsules. *Journal of Biomedical Materials Research, 54*(2), 264-271. doi:https://doi.org/10.1002/1097-4636(200102)54:2<264::AID-JBM14>3.0.CO;2-7

Van Zyl, A. J. P., Sanderson, R. D., de Wet-Roos, D., & Klumperman, B. (2003). Core/Shell Particles Containing Liquid Cores: Morphology Prediction, Synthesis, and Characterization. *Macromolecules, 36*(23), 8621-8629. doi:10.1021/ma034596x

Vecchiato, M., Gregoris, E., Barbaro, E., Barbante, C., Piazza, R., & Gambaro, A. (2017). Fragrances in the seawater of Terra Nova Bay, Antarctica. *Science of The Total Environment, 593-594*, 375-379. doi:https://doi.org/10.1016/j.scitotenv.2017.03.197

Vilas-Boas, S. M., Pokorný, V., Štejfa, V., Ferreira, O., Pinho, S. P., Růžička, K., & Fulem, M. (2019). Vapor pressure and thermophysical properties of eugenol and (+)-carvone. *Fluid Phase Equilibria, 499*, 112248. doi:https://doi.org/10.1016/j.fluid.2019.112248

Vilstrup, P. (2001). *Microencapsulation of food ingredients*: Woodhead Publishing Limited.

Voci, S., Fresta, M., & Cosco, D. (2021). Gliadins as versatile biomaterials for drug delivery applications. *Journal of Controlled Release, 329*, 385-400. doi:https://doi.org/10.1016/j.jconrel.2020.11.048

Voilley, A. J. (1995). Flavor Encapsulation. In *Encapsulation and Controlled Release of Food Ingredients* (Vol. 590, pp. 169-179): American Chemical Society.

Walter, A., Rehage, H., & Leonhard, H. (2000). Shear-induced deformations of polyamide microcapsules. *Colloid and Polymer Science, 278*(2), 169-175. doi:10.1007/s003960050028

Wang, B., Adhikari, B., & Barrow, C. J. (2014). Optimisation of the microencapsulation of tuna oil in gelatin-sodium hexametaphosphate using complex coacervation. Food Chem, 158, 358-365. doi:10.1016/j.foodchem.2014.02.135

Wang, H.-H, Li, M., Dong, Z., Zhang, T., & Yu, Q. (2021). Preparation and Characterization of Ginger Essential Oil Microcapsule Composite Films. *Foods, 10*, 2268.

doi:10.3390/foods10102268

Wang, H., Zhang, X., Zhu, W., Jiang, Y., & Zhang, Z. (2018). Self-Assembly of Zein-Based Microcarrier System for Colon-Targeted Oral Drug Delivery. *Industrial & Engineering Chemistry Research, 57*(38), 12689-12699. doi:10.1021/acs.iecr.8b02092

Wang, T. H., Hsia, S. M., Wu, C. H., Ko, S. Y., Chen, M. Y., Shih, Y. H., . . . Wu, C. Y. (2016). Evaluation of the Antibacterial Potential of Liquid and Vapor Phase Phenolic Essential Oil Compounds against Oral Microorganisms. PLoS One, 11(9), e0163147. doi:10.1371/journal.pone.0163147

Wang, Z., Zou, W., Liu, L., Wang, M., Li, F., & Shen, W. (2021). Characterization and bacteriostatic effects of β-cyclodextrin/quercetin inclusion compound nanofilms prepared by electrospinning. Food Chem, 338, 127980. doi:10.1016/j.foodchem.2020.127980

Waters, J. A. (1994). Predicting the surface morphology of composite latex particles. *Colloids and Surfaces A: Physicochemical and Engineering Aspects, 83*(2), 167-174. doi:https://doi.org/10.1016/0927-7757(94)80100-2

Weinbreck, F., de Vries, R., Schrooyen, P., & de Kruif, C. G. (2003). Complex Coacervation of Whey Proteins and Gum Arabic. Biomacromolecules, 4(2), 293-303. doi:10.1021/bm025667n

Xiao, Z., Liu, W., Zhu, G., Zhou, R., & Niu, Y. (2014a). A review of the preparation and application of flavour and essential oils microcapsules based on complex coacervation technology. *J Sci Food Agric, 94*(8), 1482-1494. doi:10.1002/jsfa.6491

Xiao, J.-x., Yu, H., & Jian, Y. (2011). Microencapsulation of sweet orange oil by complex coacervation with soybean protein isolate/gum Arabic. *Food Chemistry - FOOD CHEM, 125*, 1267-1272. doi:10.1016/j.foodchem.2010.10.063

Xiao, Z., Li, W., & Zhu, G. (2015). Effect of wall materials and core oil on the formation and properties of styralyl acetate microcapsules prepared by complex coacervation. *Colloid and Polymer Science, 293*(5), 1339-1348. doi:10.1007/s00396-015-3515-x

Xiao, Z., Liu, W., Zhu, G., Zhou, R., & Niu, Y. (2014b). Production and characterization of multinuclear microcapsules encapsulating lavender oil by complex coacervation. *Flavour and Fragrance Journal, 29*(3), 166-172. doi:https://doi.org/10.1002/ffj.3192

Yakimets, I., Wellner, N., Smith, A. C., Wilson, R. H., Farhat, I. A., & Mitchell, J. R. (2005). Mechanical properties with respect to water content of gelatin films in glassy state. *Polymer, 46*, 12577-12585.

Yalkowsky, S. H., He, Y., & Jain, P. (2010). *Handbook of Aqueous Solubility Data*: CRC Press.

Yaman, D. M., Koçak Yanık, D., Elik Demir, A., Uzun Karka, H., Güçlü, G., Selli, S., Göğüş, F. (2023). Effect of Encapsulation Techniques on Aroma Retention of Pistacia terebinthus L. Fruit Oil: Spray Drying, Spray Freeze Drying, and Freeze Drying. Foods, 12(17), 3244. Retrieved from https://www.mdpi.com/2304-8158/12/17/3244

Yan, C., Kim, S. R., Ruiz, D. R., & Farmer, J. R. (2022). Microencapsulation for Food Applications: A Review. *ACS Appl Bio Mater, 5*(12), 5497-5512. doi:10.1021/acsabm.2c00673

Yan, Y., Zhang, Z., Stokes, J. R., Zhou, Q.-Z., Ma, G.-H., & Adams, M. J. (2009). Mechanical characterization of agarose micro-particles with a narrow size distribution. *Powder Technology, 192*(1), 122-130. doi:https://doi.org/10.1016/j.powtec.2008.12.006

Yang, T., Zhu, Y., Shao, C.-Y., Zhang, Y., Shi, J., Lv, H.-P., & Lin, Z. (2016). Enantiomeric analysis of linalool in teas using headspace solid-phase microextraction with chiral gas chromatography. *Industrial Crops and Products, 83*, 17-23. doi:https://doi.org/10.1016/j.indcrop.2015.12.025

Yang, W., Gong, Y., Wang, Y., Wu, C., Zhang, X., Li, J., & Wu, D. (2024). Design of gum Arabic/gelatin composite microcapsules and their cosmetic applications in encapsulating tea tree essential oil. RSC Adv, 14(7), 4880-4889. doi:10.1039/d3ra08526k

Yang, X., Gao, N., Hu, L., Li, J., & Sun, Y. (2015). Development and evaluation of novel microcapsules containing poppy-seed oil using complex coacervation. *Journal of Food Engineering, 161*, 87-93. doi:https://doi.org/10.1016/j.jfoodeng.2015.03.027

Yang, Y., Anvari, M., Pan, C. H., & Chung, D. (2012). Characterisation of interactions between fish gelatin and gum arabic in aqueous solutions. *Food Chem, 135*(2), 555-561. doi:10.1016/j.foodchem.2012.05.018

Yap, S. F., Adams, M. J., Seville, J. P. K., & Zhang, Z. (2008). Single and bulk compression of pharmaceutical excipients: Evaluation of mechanical properties. *Powder Technology, 185*(1), 1-10. doi:https://doi.org/10.1016/j.powtec.2007.09.005

Yilmaztekin, M., Lević, S., Kalušević, A., Cam, M., Bugarski, B., Rakić, V., & Nedović, V. (2019). Characterisation of peppermint (Mentha piperita L.) essential oil encapsulates. *Journal of Microencapsulation, 36*(2), 109-119. doi:10.1080/02652048.2019.1607596

Young, T. (1805). III. An essay on the cohesion of fluids. *Philosophical Transactions of the Royal Society of London, 95*, 65-87. doi:doi:10.1098/rstl.1805.0005

Yu, F., Li, Z., Zhang, T., Wei, Y., Xue, Y., & Xue, C. (2017). Influence of encapsulation techniques on the structure, physical properties, and thermal stability of fish oil microcapsules by spray drying. *Journal of Food Process Engineering, 40*(6), e12576. doi:https://doi.org/10.1111/jfpe.12576

Yu, F., Xue, C., & Zhang, Z. (2021). Mechanical characterization of fish oil microcapsules by a micromanipulation technique. *LWT, 144*, 111194. doi:https://doi.org/10.1016/j.lwt.2021.111194

Yuan, L., Liang, G., Xie, J., Li, L., & Guo, J. (2006). Preparation and characterization of poly (urea-formaldehyde) microcapsules filled with epoxy resins. *Polymer, 47*, 5338-5349. doi:10.1016/j.polymer.2006.05.051

Yun, P., Devahastin, S., & Chiewchan, N. (2021). Microstructures of encapsulates and their relations with encapsulation efficiency and controlled release of bioactive constituents: A review. *Comprehensive Reviews in Food Science and Food Safety, 20*(2), 1768-1799. doi:https://doi.org/10.1111/1541-4337.12701

Zhang, Y., Adams, M. J., Zhang, Z., Vidoni, O., Leuenberger, B. H., & Achkar, J. (2016). Plasticisation of carnauba wax with generally recognised as safe (GRAS) additives. *Polymer, 86*, 208-219. doi:https://doi.org/10.1016/j.polymer.2016.01.033

Zhang, Z.-Q., Pan, C.-H., & Chung, D. (2011). Tannic acid cross-linked gelatin–gum arabic coacervate microspheres for sustained release of allyl isothiocyanate: Characterization and in vitro release study. *Food Research International, 44*(4), 1000-1007. doi:https://doi.org/10.1016/j.foodres.2011.02.044

Zhang, Z. (1999). Mechanical strength of single microcapsules determined by a novel

micromanipulation technique. *Journal of Microencapsulation, 16*(1), 117-124. doi:10.1080/026520499289365

Zhang, Z., Ferenczi, M. A., Lush, A. C., & Thomas, C. R. (1991). A novel micromanipulation technique for measuring the bursting strength of single mammalian cells. *Applied Microbiology and Biotechnology, 36*(2), 208-210. doi:10.1007/BF00164421

Zhang, Z., Ferenczi, M. A., & Thomas, C. R. (1992). A micromanipulation technique with a theoretical cell model for determining mechanical properties of single mammalian cells. *Chemical Engineering Science, 47*, 1347-1354. doi:10.1016/0009-2509(92)80280-p

Zhang, Z., He, Y., & Zhang, Z. (2022). Micromanipulation and Automatic Data Analysis to Determine the Mechanical Strength of Microparticles. *Micromachines, 13*(5), 751. Retrieved from https://www.mdpi.com/2072-666X/13/5/751

Zhang, Z., Saunders, R., & Thomas, C. R. (1999). Mechanical strength of single microcapsules determined by a novel micromanipulation technique. *J Microencapsul, 16*(1), 117-124. doi:10.1080/026520499289365

Zhang, Z., Stenson, J. D., & Thomas, C. R. (2009). Chapter 2 Micromanipulation in Mechanical Characterisation of Single Particles. In J. Li (Ed.), *Advances in Chemical Engineering* (Vol. 37, pp. 29-85): Academic Press.

Zhang, Z., He, Y., & Zhang, Z. (2022). Micromanipulation and Automatic Data Analysis to Determine the Mechanical Strength of Microparticles. *Micromachines (Basel), 13*(5). doi:10.3390/mi13050751

Zhao, H., Fei, X., Liang, C., Xian, Z., Cao, L., & Yang, T. (2021). The evaluation and selection of core materials for microencapsulation: A case study with fragrances. *Flavour and Fragrance Journal, 36*(6), 652-661. doi:https://doi.org/10.1002/ffj.3675

Zhu, G., Xiao, Z., Zhou, R., & Yi, F. (2012). Fragrance and Flavor Microencapsulation Technology. Advanced Materials Research, 535-537, 440 - 445.

Zuanon, L. A. C., Malacrida, C. R., & Telis, V. R. N. (2013). Production of Turmeric Oleoresin Microcapsules by Complex Coacervation with Gelatin–Gum Arabic. *Journal of Food Process Engineering, 36*(3), 364-373. doi:https://doi.org/10.1111/jfpe.12003

Zuidam, N. J., & Shimoni, E. (2010). *Overview of Microencapsulates for Use in Food Products or Processes and Methods to Make Them*.

Appendix A. UV calibration curves of core oils in solvents

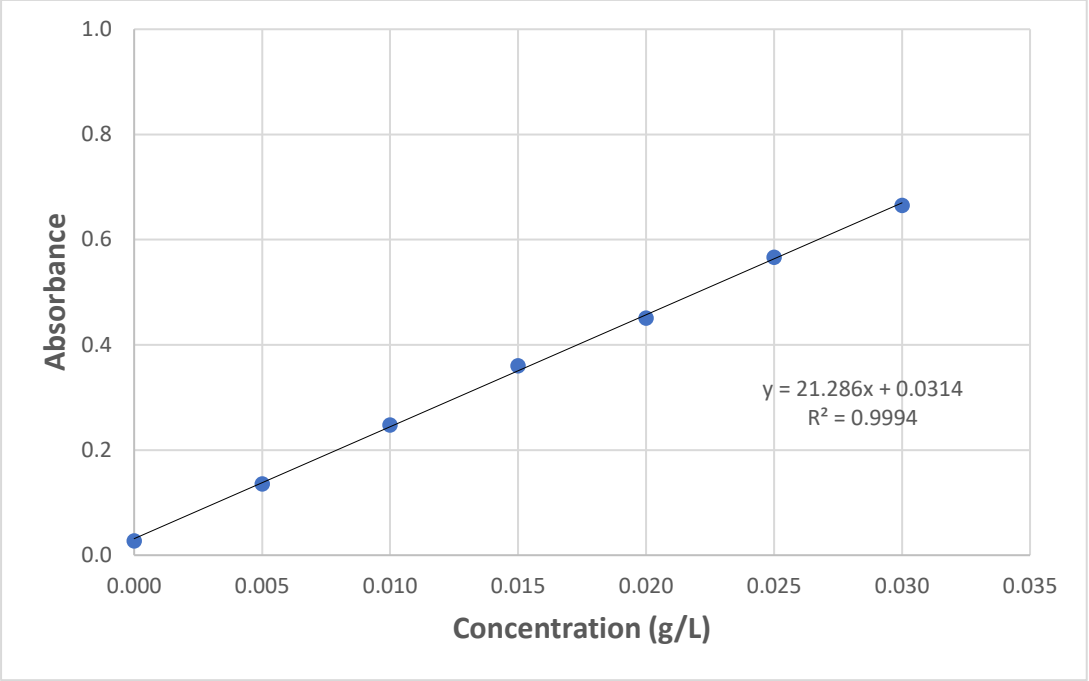

Figure A-1. UV calibration curve of HS in 36% 1-Prapanol

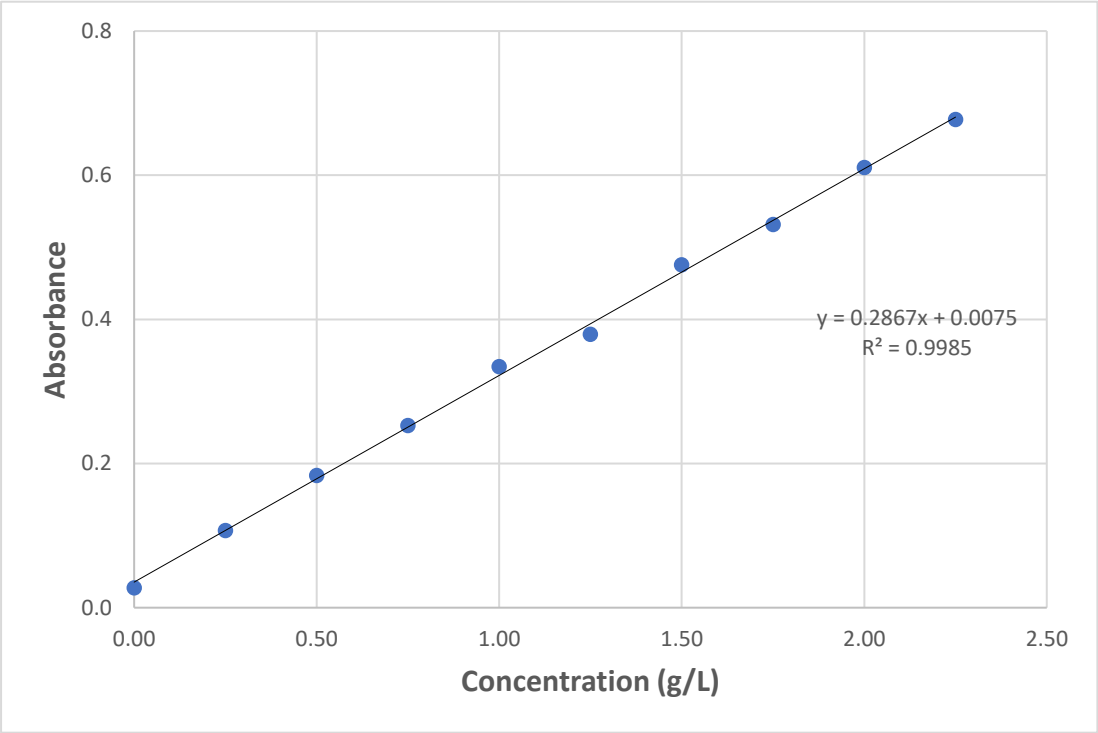

Figure A-2. UV calibration curve with LC in ethanol

Appendix B. GC calibration curves of LC and LM in ethanol

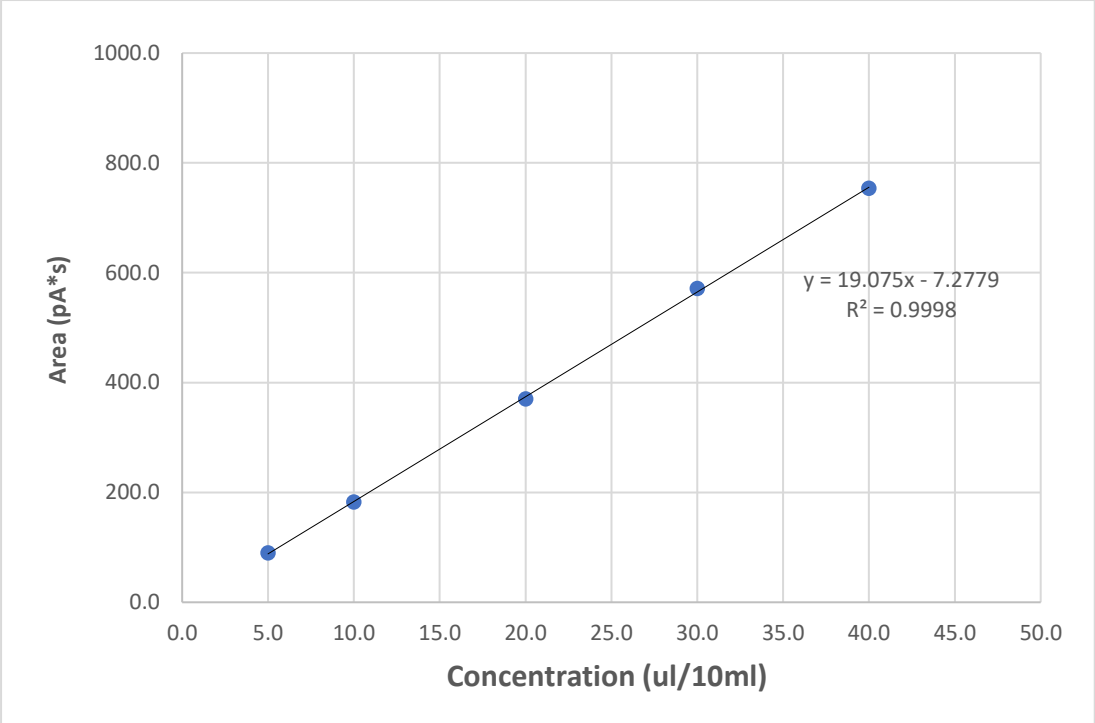

Figure B-1. GC calibration curve with LC in ethanol

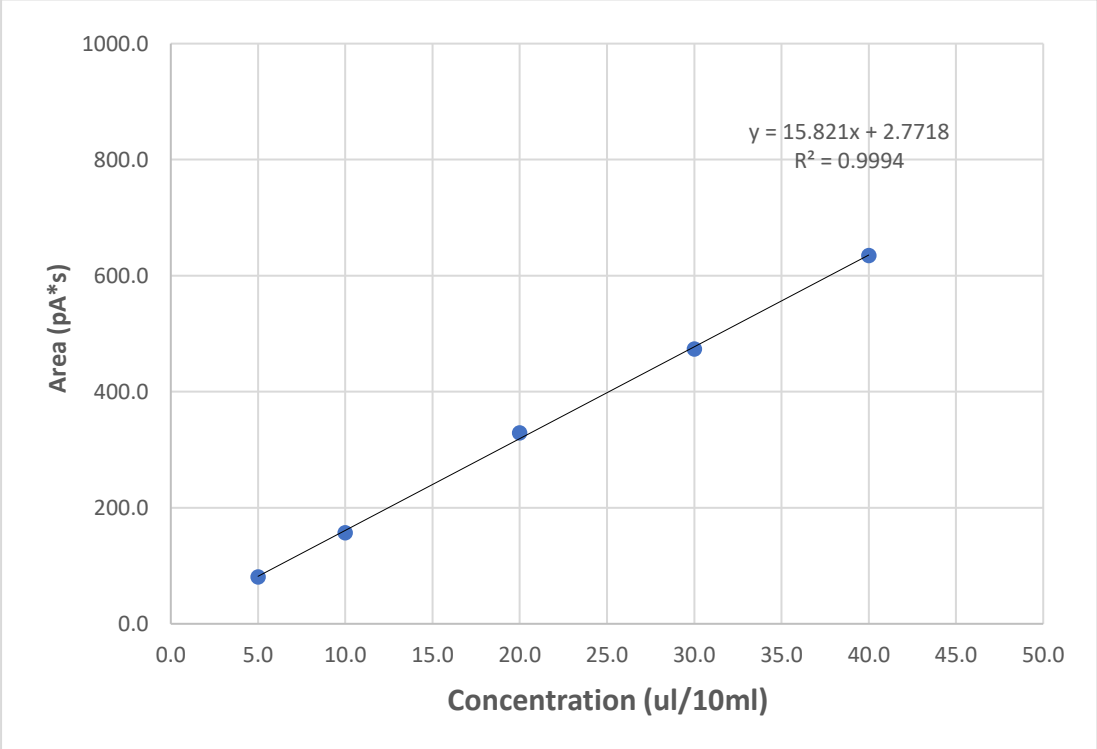

Figure B-2. GC calibration curve with LM in ethanol

Appendix C. GC temperature programs

Table C-1. GC temperature programs for each oil.

Core oil	LM	LC	LL	CV	CD
Initial temperature (° C)	50	100	70	100	100
Temperature increasing rate (°C/min)	10	10	10	10	10
Holding temperature (° C)	180	230	200	240	235
Holding time (min)	2	5	2	5	10
Temperature increasing rate (°C/min)	5	10	5	5	10
Holding temperature (°C)	200	240	220	245	245
Holding time (min)	1	1	1	2	2
Detector temperature (min)	250	250	250	250	250

Appendix D. GC calibration curves of reference oils in solvents

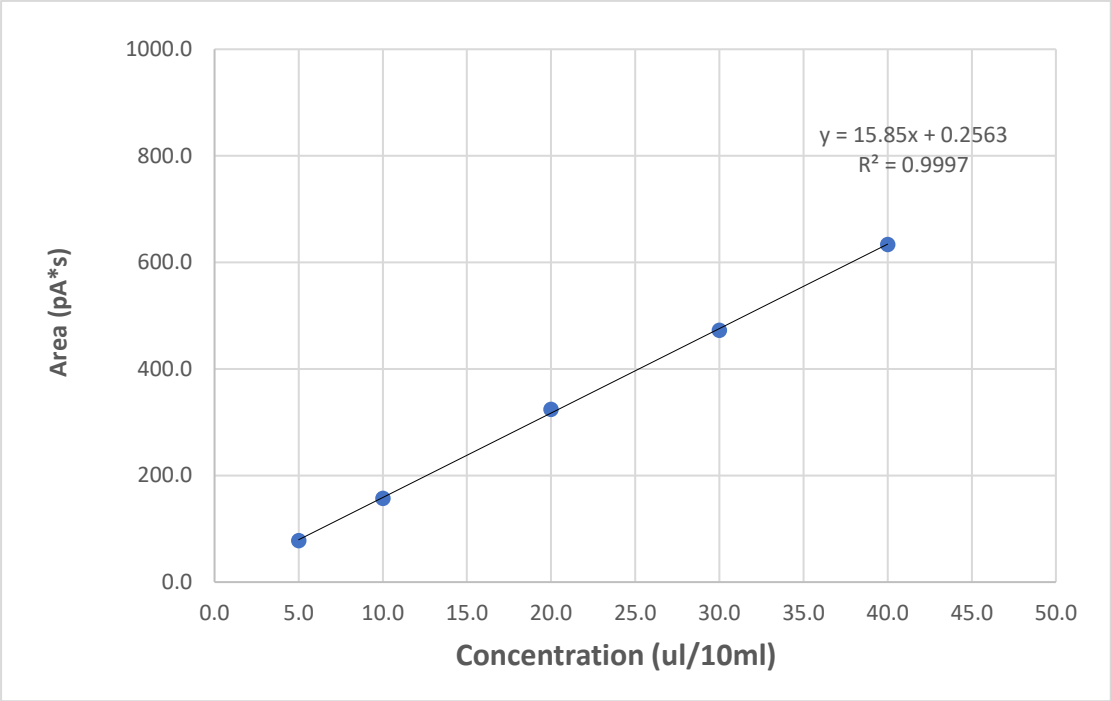

Figure D-1. GC calibration curve with LL in ethanol

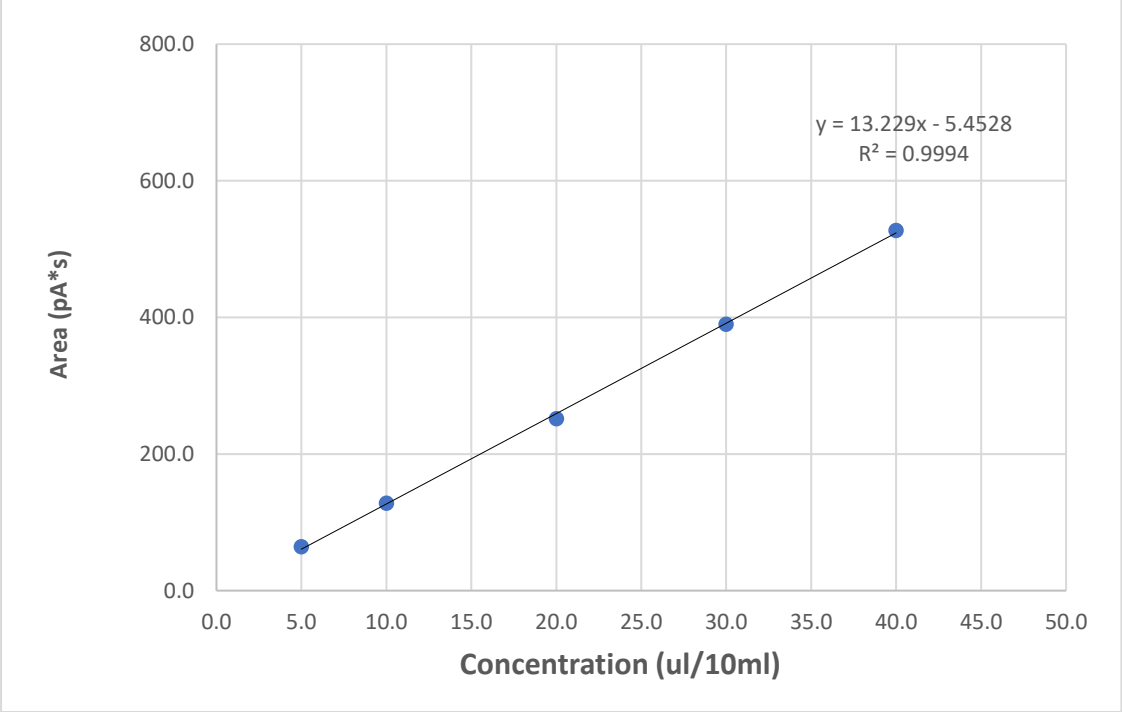

Figure D-2. GC calibration curve with CV in Hexane

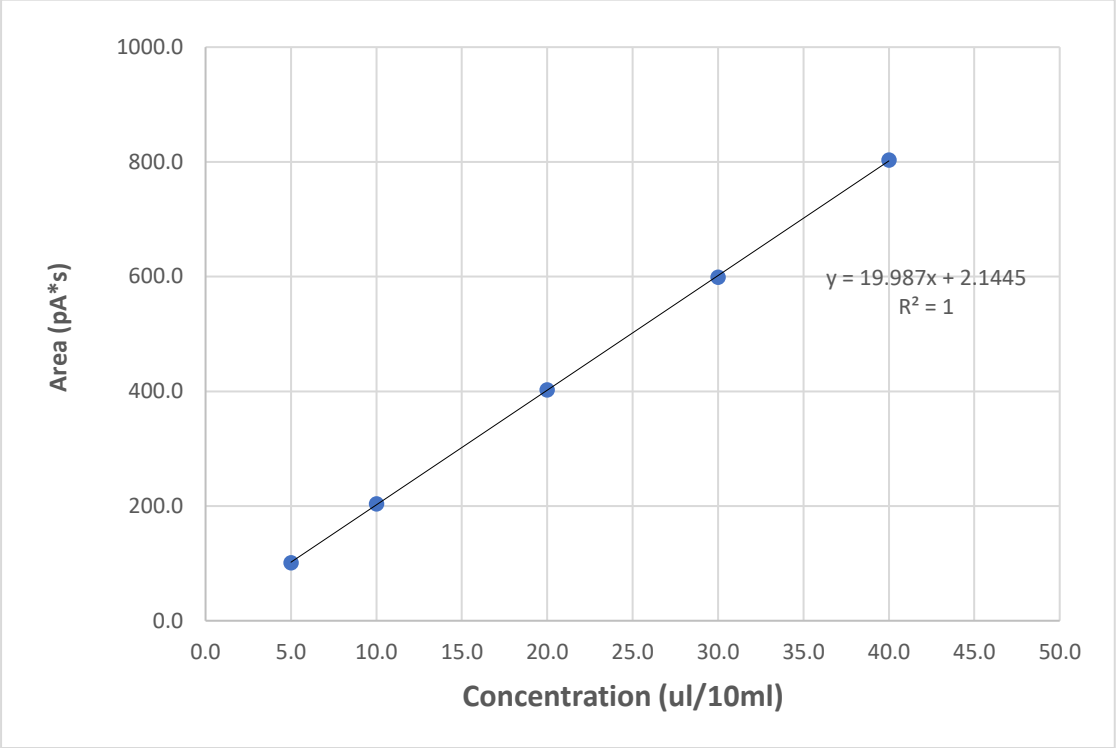

Figure D-3. GC calibration curve with CD in Hexane